UNITED STATES
DEPARTMENT OF THE INTERIOR
GEOLOGICAL SURVEY

DIAGENESIS IN THE MONTEREY FORMATION
EXAMINED LATERALLY ALONG THE COAST NEAR
SANTA BARBARA, CALIFORNIA

———————

By

Caroline M. Isaacs

———————

Open-File Report
80-606

Menlo Park, California
May 1980

TABLE OF CONTENTS

LIST OF FIGURES

ABSTRACT

Lateral differences in Monterey rocks along the Santa Barbara coast indicate that diagenesis is more advanced toward the west, as noted by Bramlette (1946). Silica changes toward the west from biogenic opal-A (in diatom frustules) to diagenetic opal-CT and then to diagenetic quartz. This study describes the original equivalence and the cause of lateral diagenetic differences and then examines lithologic changes and diagenetic processes in laterally equivalent strata.

Continuous exposure for 55 km, simple homoclinal structure, paleogeography, and detailed analysis of 14 stratigraphic sections together show that sediments were laterally equivalent, as originally deposited. Rocks principally contain: biogenic or diagenetic silica (5 to 90 percent), detrital minerals (5 to 70 percent), carbonates (0 to 80 percent), and organic matter (1 to 25 percent). Distinctive stratigraphic differences in rock composition are used to define five informal members, including an uppermost member nearly free of carbonate and four lower carbonate-bearing members. Each member is laterally continuous and shows consistent sedimentary features and compositions. Boundaries between members are also laterally age-constant.

Original equivalence indicates that lateral diagenetic differences were caused by postdepositional conditions. Overburden thicknesses (post-Luisian strata thicken, east to west, from 300 to 1850 m) and temperature-sensitive characteristics of kerogen (O/C atomic ratios decrease, east to west, from >0.2 to <0.1) show that increased temperature and burial caused the westward increase in diagenesis.

Lateral examination of equivalent strata showed that both silica phase transformations were accompanied by large reductions in porosity, which averages 60 percent in diatomaceous rocks, 35 percent in opal-CT rocks, and 15 percent in quartz rocks. Lithologic character changed mainly during opal-CT formation, resulting in greatly increased hardness, brittleness, bulk density, and cohesiveness. Much less increase in these properties accompanied quartz formation, and quartz rocks are practically indistinguishable from opal-CT rocks in the field. Among both quartz and opal-CT rocks, hardness, brittleness, bulk density, and luster all vary markedly with the silica/detrital ratio, which is ≥ 3.0 in cherty (vitreous) rocks, 0.75 to 4.0 in porcelanous (matte) rocks, and ≤ 1.0 in siliceous mudstones.

At each stratigraphic level, diagenetic changes typically occurred in a distinctive sequence. As temperature and burial increased: opal-CT formed first in cherts and cherty porcelanites, then in porcelanites, and finally in siliceous mudstones; subsequently, quartz formed first in siliceous mudstones, then in porcelanites, and finally in cherty porcelanites and cherts. Two diagenetic changes in carbonate-bearing rocks--formation of disseminated dolomite and of unusual quartz cherts--were not consistently produced by increased temperature and are not related to timing of silica diagenesis in typical rocks.

The timing sequence is related to the silica/detrital ratio in individual beds. As the ratio decreased, opal-CT formed later, initial "ordering" of opal-CT was higher, and quartz subsequently formed earlier. Carbonates did not significantly affect rates of silica diagenesis, as timing was nearly identical in associated

calcareous, dolomitic, and carbonate-free rocks with equal silica/

detrital ratios. Exceptions were carbonate-bearing rocks with silica/

detrital ratios ≥ 8, in which some quartz formed early in diagenesis,

probably before opal-CT formation.

Timing differences show that diagenetic changes occurred indepen-

dently in each layer of rock (down to the scale of beds ≤ 2 mm thick).

Independence, petrologic characteristics, and lateral similarity

of compositional ranges together indicate that formation of neither

opal-CT nor quartz involved appreciable transfer of silica between

beds. Timing differences also provide evidence that porosity changes

resulted directly from silica phase transformations, not from generally

increased temperature and burial; and changes in strata thickness show

that porosity decreased by rapid compaction, not by simple cementation.

Both silica phase transformations thus occurred by rapid, nearly

in situ, solution-precipitation of silica accompanied by appreciable

compaction.

ACKNOWLEDGEMENTS

Many persons have contributed to this report and I extend my grateful acknowledgement to each of them. Mitchell W. Reynolds, formerly at U. C. Berkeley and now with the U.S. Geological Survey at Reston, first stimulated my curiosity about the Monterey Formation in the Berkeley Hills and introduced me to the work of M. N. Bramlette. Robert R. Compton's and James C. Ingle's knowledge and enthusiasm for the Monterey Formation fostered my interest, and Larry A. Beyer and Robert E. Garrison encouraged and supported the research from the beginning.

Assistance in research was provided by many persons. I particularly thank my mother, Mary Carol Isaacs, for her companionship and support during a number of field trips exploring diatomaceous deposits in Oregon, California, and Nevada and for her encouragement and assistance in field work along the Santa Barbara coast. Great thanks are given to Larry A. Beyer of the U.S. Geological Survey, Menlo Park, through whose interest and substantial support many instruments (including pycnometers and X-ray diffraction apparatus) and services (including chemical analyses) were made available to me. Special thanks are also given to Robert R. Compton of Stanford University for field assistance, section measurement, and collection of many extremely fresh rocks from the field area. B. E. Felber of Mobil Research and Development Corporation's Field Research Laboratory in Dallas, Texas, generously arranged for an supervised X-ray diffraction analyses of

CHAPTER 1

INTRODUCTION

The origin and paleoenvironmental significance of siliceous rocks
has been debated for decades. Chemical, biologic, and volcanic
origins have all been proposed and a wide variety of paleoenvironments
suggested for various siliceous rocks (e.g., Bailey and others, 1964;
Banks, 1970; Chipping, 1971; Gibson and Towe, 1971, 1975; Surdam and
others, 1972; Weaver and Wise, 1974, 1975). Criteria for determining
genesis, however, are nearly always debatable, and in practice
paleoenvironments are usually inferred from surrounding strata. The
significance of petrologic features in siliceous rocks *per se* has
remained surprisingly obscure, as illustrated by the modern debate
over abyssal versus supratidal deposition of novaculites (McBride and
Thomson, 1970; Folk, 1973; Folk and McBride, 1976).

A major cause of obscurity is the profound diagenetic changes
in siliceous sediments which take place at low temperature yet are
essentially metamorphic. Highly diatomaceous sediments, for example,
are evidently altered to quartz cherts, after two complete solution-
precipitations of silica, at temperatures of less than 100°C, or
less than 2000 m of burial (Murata and Larson, 1975). By contrast,
calcite in most nannofossil sediments is only partially recrystallized
at 2000 m, and major changes in clay shales do not usually occur until
shales are buried much more deeply (Meade, 1964; Scholle, 1977).

1

Interpreting features of siliceous rocks is particularly difficult due to poor understanding of the natural processes accompanying major diagenetic changes. Knowledge of silica diagenesis (diagenetic changes in silica minerals) has advanced greatly in recent decades, but lithologic changes and important associated processes have remained unclear. Do significant amounts of silica move between beds during diagenesis? How is porosity lost? Are marked differences in lithologic characteristics solely diagenetic, or do they also reflect original differences in the sediments? Which features are primary sedimentary features and which are secondary?

These questions are difficult to answer by examining most Mesozoic and Paleozoic siliceous rocks because of the absence of diagenetically altered precursors. Where relatively unaltered biogenous sections can be examined, among younger siliceous rocks, recent studies have focussed on diagenesis in stratigraphic sequences (e.g., Murata and Larson, 1975; Mitsui and Taguchi, 1977). Stratigraphic sequences, however, generally involve variations in age, sediment composition, and depositional environment. As a result, effects of diagenesis may be ambiguous, and distinguishing precursors of specific types of rocks and determining the diagenetic processes involved in their formation may be impossible.

The purpose of the present study was to examine natural diagenetic processes in an area where: (1) diatomaceous rocks are laterally continuous with and sedimentologically equivalent to diagenetically altered rock; and (2) lateral differences in diagenesis are due only to postdepositional differences in temperature and burial depth. In such an area, precursors of specific (and unusual) types of

diagenetically altered rocks are clear, and effects of different variables on diagenesis are easily distinguished.

Laterally equivalent diatomaceous and porcelanous strata have been described in several localities in the Monterey Formation, but in most places exposed strata are of limited extent (Bramlette, 1946). Along the coast near Santa Barbara, however, between Goleta and Point Conception, laterally equivalent diatomaceous and porcelanous strata form a continuous exposure nearly 55 km long. Previous work showed that these rocks consist of a distinctive compositional sequence that includes abundant calcite-rich siliceous rocks and organic phosphatic shales as well as clay-bearing siliceous rocks typical of the Monterey in other parts of California (Bramlette, 1946; Dibblee, 1966). The area also contains, from east to west, diatomaceous, opal-CT, and quartz sections--the same sequence of silica phases observed widely, both experimentally and in the field, with increasing diagenesis.

This study, then, concerns diagenesis in the Monterey Formation examined laterally along the Santa Barbara coast (fig. 1). Three principal questions are addressed. First, were the sediments that are now laterally different originally similar? The answer is approached by examination of the geologic setting, paleogeography, and structural history of the area and by lateral examination of sedimentary features, rock compositions, and distinctive strati-graphic units within the Monterey Formation. Second, what caused lateral differences in diagenesis? In addition to original differences in the sediment, lateral differences in thermal and burial history are examined. Third, and most important, what lithologic changes and

Fig. 1—Location of sections studied in the Monterey
Formation along the coast west of Santa Barbara.

what processes were involved in diagenesis? This question is answered through detailed petrologic study of lateral sets of stratigraphically equivalent rocks, focussing on the distribution and range of bulk chemical compositions, porosity values, physical properties, and silica phases.

CHAPTER 2

GEOLOGIC SETTING

A preliminary part of the study was to determine whether lateral
diagenetic differences are related to structural displacements or
paleogeographic variations. Literature was examined on late Paleogene
and Neogene stratigraphy, Miocene paleogeography, and structural history.
Each of these topics is now summarized for the immediate area in which
the Monterey Formation was studied along the Santa Barbara coast.
Overall significance to diagenesis is then evaluated.

Stratigraphy and Paleoenvironment

This study covers the Monterey Formation extending for 55 km along
the Santa Barbara coast, from Point Conception to Elwood Beach near
Goleta (fig. 1). The rocks are exposed in the south-dipping homocline
on the south flank of the southwestern Santa Ynez Range, in the Trans-
verse Ranges of southern California (fig. 2).

In the area studied, the Monterey Formation is part of a thick
section of sediments which record nearly continuous marine deposition
from Late Cretaceous to early Pliocene time (Dibblee, 1950, 1966; Weaver,
1965). The one major stratigraphic discontinuity, in mid-Oligocene
time, is marked by an angular unconformity within the marine section
in the western part of the area. In the eastern part of the area,
late Eocene and early Oligocene marine strata grade laterally into
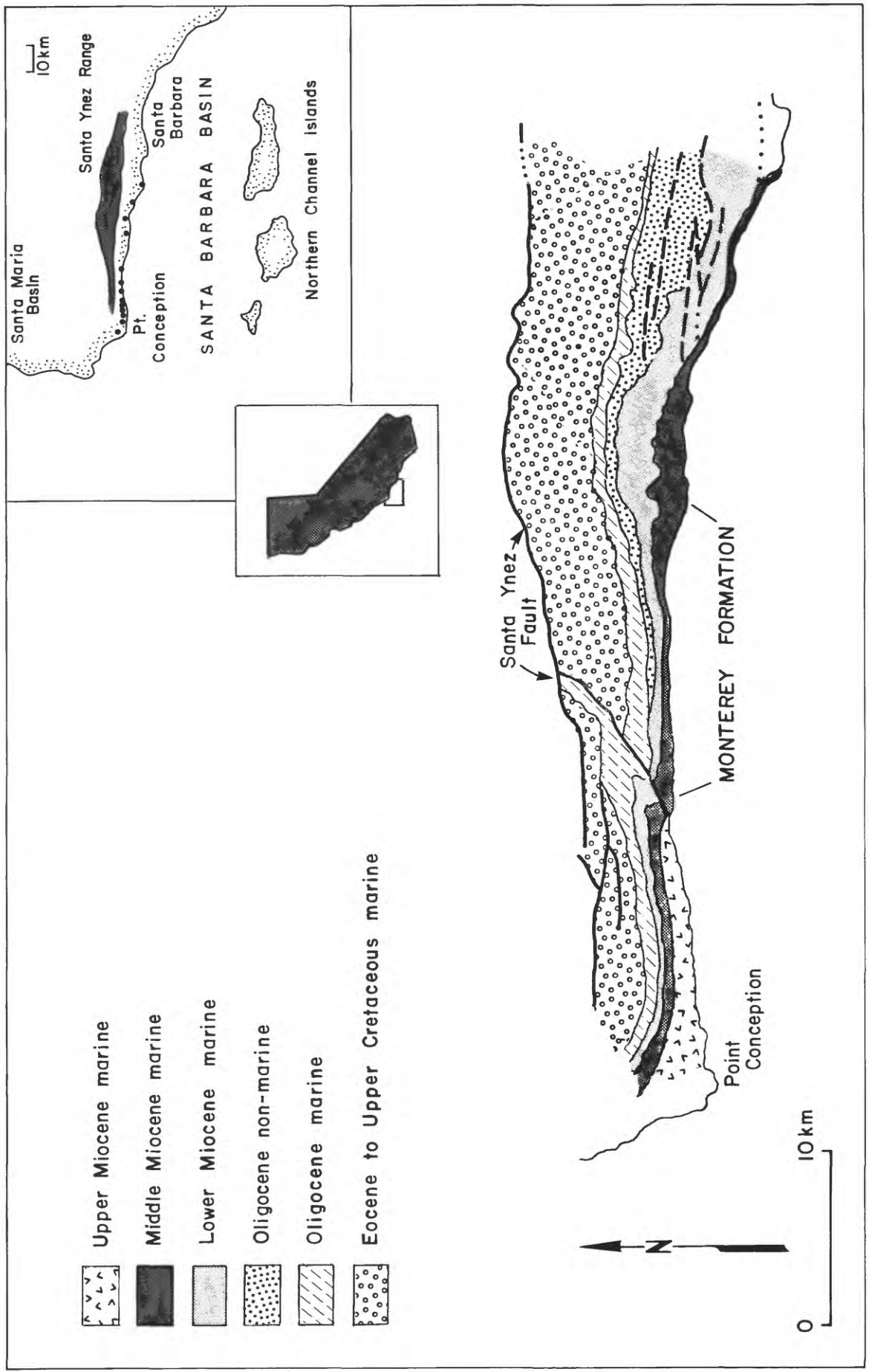
Fig. 2--Geologic setting of the Monterey Formation along the coast west of Santa Barbara, between Goleta and Point Conception. Adapted from Jennings (1959) and Jennings and Strand (1969).

continental red beds which thicken eastward to more than 1,000 m
near Goleta.

Overlying this stratigraphic break is the Vaqueros Formation,
a coarse strandline or sandy bank-top deposit (Corey, 1965; Ingle,
in press). Ranging from 10 to 150 m in thickness, the Vaqueros Forma-
tion marks the initiation of subsidence in late Oligocene (Zemorrian)
time (Dibblee, 1950, 1966; Ingle, in press). Overlying the Vaqueros
is the Rincon Shale, which is latest Oligocene (latest Zemorrian)
to early Miocene (latest Saucesian) in age (Weaver, 1965). The Rincon
Shale is a slope deposit, about 500 m thick, consisting of mudstone
with sparse foraminifera and occasional dolomite concretions (Dibblee,
1950, 1966; Ingle, in press). Water depths increased rapidly to
1,000 m during Rincon deposition and pelletal phosphorite probably
indicates intersection of the slope with the oxygen minimum zone (Ingle,
in press). Stratigraphically above the Rincon Shale is a bentonite or
tuff, up to 25 m thick, which is considered part of the Tranquillon
Volcanics (Dibblee, 1950). The tuff marks the base of Monterey strata,
which are early Miocene (latest Saucesian) to late Miocene (late
Mohnian) in age. The Monterey Formation, which is about 400 m thick,
consists of carbonate-bearing siliceous rock near the base, calcareous
organic shale in the middle, and carbonate-free siliceous rock at the
top, with occasional sands and conglomerates in uppermost strata.
These Monterey rocks were apparently deposited in water depths of
1,000 to 1,500 m, within silled anaerobic basins (Ingle, in press).

Overlying the Monterey Formation, except where locally eroded, is
the Sisquoc Formation, a siliceous mudstone and siliceous shale unit.
Of late Miocene and Pliocene (late Mohnian and Delmontian) age, Sisquoc

strata were deposited in somewhat shallower bathyal depths than Monterey strata (Ingle, in press). Although the top of the Sisquoc is nowhere exposed, the formation is more than 1,100 m thick at Point Conception. East of the study area, Pliocene siltstones and sandstones are locally exposed lying unconformably over the Sisquoc Formation (Dibblee, 1966). Offshore from Gaviota, near the Hondo Field, the Monterey Formation is covered by Delmontian and younger Pliocene beds that are more than 2,000 m thick (U.S. Geological Survey, 1974).

Paleogeography

Structurally, the study area is located in the Santa Ynez block of the western Transverse Ranges Province, where east-west tectonic alignment was complete by late Oligocene or early Miocene time (Fischer, 1976). During the Neogene, the Santa Ynez block was part of the Santa Barbara Basin area, which is the seaward extension of the Ventura Basin (Fischer, 1976).

Because most of the Neogene Santa Barbara Basin is offshore, information about the area is limited. In addition, available offshore data may be irrelevant due to structural displacements after middle Miocene time. Study of bathymetry patterns has concentrated on the area immediately to the northwest and south of the Channel Islands (Arnal, 1976). Between this area and the Santa Barbara coast lies the East Santa Cruz Basin fault system, with postulated lateral movement of several hundred kilometers since middle Miocene time (Howell, 1975). Monterey rocks now located near the northwestern Channel Islands, therefore, may have been deposited several hundred kilometers south

of rocks now exposed along the Santa Barbara coast and paleogeographies
of the two areas not closely related.

Paleogeography during Monterey deposition can be inferred to some
extent from evidence in deposits now onshore. Vaqueros strata were
deposited throughout the modern coastal area and to the north as far
as the Vaqueros strandline, located parallel to and about 20 km north
of the modern coastline (Fischer, 1976). A few kilometers north of
the study location was a lower Miocene offshore bank, which extended
from near Point Conception east as far as Refugio (Corey, 1965).
Between Gaviota and Goleta the Vaqueros Formation thickens from 10 to
150 m, apparently as a result of lees of calm water on the southeast
side of this bank (Dibblee, 1950, 1966; Corey, 1965).

Rapid subsidence occurred during deposition of the lower Miocene
Rincon Shale with formation of an east-west basin. Based on paleodepths
inferred from foraminifera in the Rincon Shale, the deepest part of
this basin extended along or slightly to the south of the modern
coastline in late Zemorrian and Saucesian time (Edwards, 1971, p. 222-
223; Fischer, 1976). The strandline paralleled the modern
coastline about 20 km to the north (Fischer, 1976). Although the
southern limit of the Miocene basin is speculative, the strandline did
trend east-northeast from near Ventura in the modern onshore and may
have continued westward north of the Channel Islands (Fischer, 1976).

Monterey deposition was much more widely distributed than either
Vaqueros or Rincon deposition, apparently due to widespread subsidence
(Ingle, in press). To the north, the entire Santa Maria Basin was
submerged at this time so that the northern strandline was located
30 to 60 km from the study location (fig. 3). Scant data bear directly
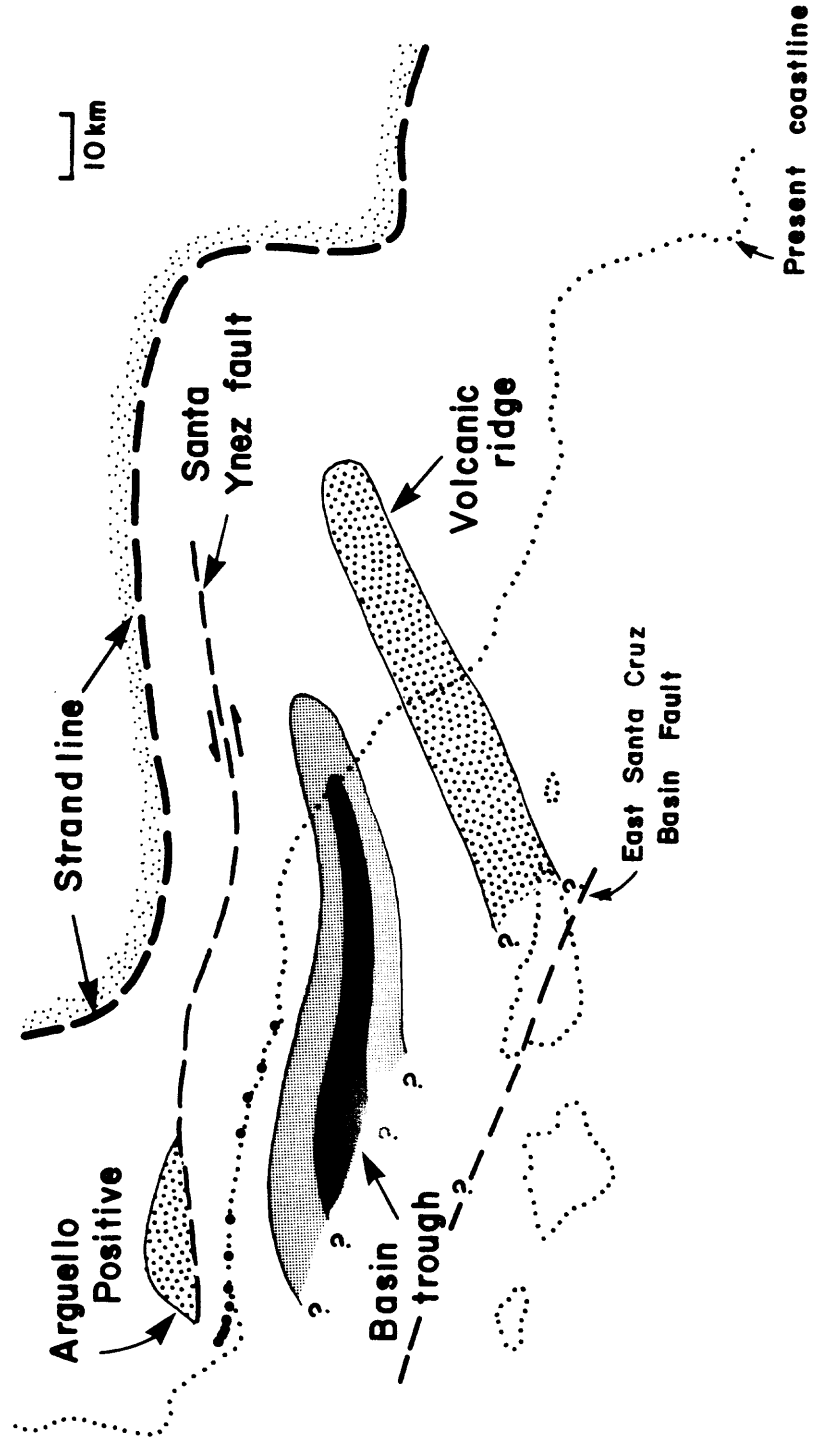
Fig. 3—Miocene paleogeography of the Santa Barbara Basin. Adapted from Corey (1965), Edwards (1971), Fischer (1976) and Ingle (in press).

on bathymetric patterns within the Monterey Formation. However, those areas bordering the basin which were positive before and after Monterey deposition were also relatively positive during Monterey deposition, even though at much greater water depths (Fischer, 1976). In addition, studies of Pliocene and early Pleistocene paleogeography indicate that the basinal trend at that time was similar to the trend during earlier deposition of the Rincon Shale (Fischer, 1976). These relationships strongly suggest that the Rincon basinal trend persisted during Monterey deposition.

Paleogeography of onshore Miocene deposits suggests, then, that all Monterey rocks in this study were probably deposited in a single elongate east-west basin whose axis was more or less parallel with the present coastline. To the north this basin was partly protected from terrigenous debris by a submerged positive area only a few kilometers distant. Conditions to the south, although largely speculative, suggest a parallel submarine ridge, possibly north of the northern Channel Islands.

Monterey sedimentation may have varied laterally to some extent due to differences in protection from terrigenous debris. Whereas the western part of the basin was 60 km or more distant from the Miocene strandline and protected to the north by the Arguello positive, east of Gaviota the basin was closer to the strandline and possibly unprotected to the north. Although these features could have caused significant lateral variation in terrigenous input, rapid deepening prior to Monterey deposition probably minimized the variation. Deep basins deficient in terrigenous sediment sources characterize middle Miocene geography all around the Pacific margin (Ingle, in press).

Most sediment first deposited in these basins was derived from biogenic detritus with terrigenous debris insignificant until later stages of basin filling.

Structure

In the area studied along the Santa Barbara coast, most tectonic structures are mid-Pleistocene in age (Vedder and others, 1969). The homocline formed at this time as well as numerous smaller folds and faults, mainly east of Gaviota.

A major earlier structure is the Santa Ynez fault, which bounds the southern Santa Ynez Range to the north. Total estimated offset includes 3,500 m of relative vertical displacement (south side up), mainly east of the study area, and slight left-lateral movement. The fault splits near Gaviota Pass into two faults with relatively little displacement. One split crosses the study area and both apparently die out about 8 km west of the pass.

Although the exact time when faulting started is not known, most displacement is post-Miocene. Mild structural deformation in the modern offshore area began in early Pliocene time (Vedder and others, 1969) and some uplift of the Santa Ynez Range, presumably associated with vertical displacement along the Santa Ynez fault, began in early to middle Pliocene time (Dibblee, 1966).

Significance to Diagenetic Variation

Lateral diagenetic variations are apparently not attributable to major differences in depositional environment or structural dislocations. The Monterey Formation studied is part of a thick section of sediments,

mainly marine, now exposed in the south-dipping homocline along the Santa Barbara coast. The formation is continuous throughout the area and was apparently unaffected by major structural displacements.

Miocene paleogeography suggests that Monterey rocks in all sections studied were deposited along the axis of a single anaerobic silled basin. Sediment composition in this silled basin was not necessarily laterally uniform, and protection from terrigenous debris may have increased westward. However, the impact of this difference was probably minimized both by distance from the shoreline and by rapid transgression and deepening immediately prior to Monterey deposition.

CHAPTER 3

METHODS AND TERMS

Most methods used in this study are described fully in the appen-
dices. In this section, methods are briefly mentioned and usage of
important terms described.

Methods of Study

Investigation of Montery rocks along the Santa Barbara coast
concentrated on both primary sedimentary features and major diagenetic
processes. Study therefore included lateral lithologic correlation,
lateral age correlation, and examination of thermally produced changes
in organic matter as well as detailed petrology.

Stratigraphic Techniques

Lithologic correlations were based on field examination guided
by preliminary study of relationships between analytical data and
field characteristics (see p. 34-54). Most sections were taped and
parts of some sections measured in detail (see Appendix F). Age
dates are based on microfossil identifications listed in Appendix H.

Petrologic Techniques

Petrologic investigation concentrated on bulk characteristics of
rocks--particularly bulk chemical and mineralogical composition,
porosity, and field properties. The mineral composition was determined

by interrelating X-ray diffraction and chemical analyses (see Appendix B).
Complete chemical analyses and semiquantitative trace element contents
are listed in Appendix A and mineral abundances of samples in Appendix G.
Methods of analysis of thermally produced differences in organic matter
are described in Appendix C.

Porosity values were derived from bulk density and grain density
measurements (see Appendix E) made on oven-dried samples matched with
powder splits used for determination of mineral abundances. A variety
of field characteristics (color, gross hardness, fracture and impact
properties, surface texture, and weathering features) was used to
integrate the analytical results with field occurrences. Some
permeability measurements were also made (see Appendix E), as well
as petrographic and SEM study.

Silica phases were determined by X-ray diffraction and, in the
case of diatomaceous rocks, checked by macroscopic or microscopic
examination. Measurement of opal-CT d-spacings is described fully
in Appendix D.

Terms

This section describes terms that are used throughout the study
with a special sense. The terms are grouped as follows: (1) rock
names; (2) minerals and materials in rocks; (3) terms used to compare
rocks.

Rock Names

Names of siliceous rocks have historically been based on differences
in surface texture and physical properties assumed to represent bulk

compositional differences. Chert, as used by Bramlette (1946),

refers to both composition and surface texture, regardless of silica

mineralogy:

> The name chert is applied to the relatively pure silica rocks
> of the Monterey Formation that are dense and vitreous, regard-
> less of whether they consist mainly of opal or mainly of
> chalcedony * * * (p. 16).

Similarly, the term "porcelanite" refers to rocks with surface textures

resembling unglazed porcelain (Bramlette, 1946, p. 15).

In recent years, terms for siliceous rocks have become confused

with terms for silica minerals. In this usage, a chert is a rock

composed mainly of diagenetic quartz and a porcelanite is a rock with

abundant opal-CT. This terminology is impractical and misleading.

The term "chert" is ineradicably associated with dense smooth-surfaced

rocks, many of which contain only minor amounts of quartz entirely

as detrital material. Conversely, in the Monterey Formation many

rocks containing diagenetic silica only as quartz have a grainy or

matte surface indistinguishable from that of opal-CT porcelanites.

Reliable identification of the silica phase requires X-ray diffraction.

The restriction of rock names to silica phases is also misleading

because siliceous rocks nearly always contain other materials.

Moderate amounts of some materials greatly affect the appearance and

diagenesis of rocks. In fact, the characteristic properties of

porcelanites may be caused as much by the detrital clays as by silica

minerals.

Rock names used in this study are descriptive terms based on

identifiable field or hand specimen characteristics, irrespective of

silica phase or any other feature determined solely by laboratory

techniques. Field characteristics reflect mineral composition
to some degree, as will be described, but rock names are not defined
by mineral abundances. Similar definitions are used by several
other authors (e.g., Murata and Nakata, 1974; Keene, 1975).

Chert: an aphanitic rock with a smooth or sometimes vitreous
surface, considerable hardness (>5), toughness, and brittleness.
When fractured, cherts always break into angular fragments, usually
across bedding planes, and may fracture conchoidally.

Porcelanite: an aphanitic rock with a rough or somewhat grainy,
matte surface. Compared to a nonsiliceous mudstone or shale, it is
tough, brittle, and hard--but less so than a chert. Porcelanites
have hardnesses of 3 or less and, even where laminated or well bedded,
fracture irregularly with a rough splintery surface.

Siliceous mudstone (or siliceous shale): less distinctly sili-
ceous rocks which are massive (or finely layered) and free of carbonate.
Siliceous mudstones and siliceous shales have grainy surfaces, are
not brittle, and dent when impacted. They are, however, usually
harder and tougher than nonsiliceous mudstones and shales.

Mudstone (or shale): massive (or finely layered) fine-grained
rocks which do not have the characteristics of the rock types just
described. The term is not meant to imply high detrital content and is
generally used with descriptive modifiers--for example, calcareous or
diatomaceous.

Terms for carbonate-bearing rocks: A large proportion of the
rocks in this study contain some carbonate. Many of the rocks, whose
bulk compositions fall near the center of a carbonate-clay-silica
diagram, have no well-accepted nomenclature, and some suggested composi-

tional names are misleading. "Cherty limestone," for example, does

not accurately describe an opal-CT-bearing coccolith-rich rock with

45 percent porosity. For this reason, and because most of the

calcareous (or dolomitic) rocks are macroscopically indistinguishable

from one another, they are usually described as calcareous (or

dolomitic) shales or mudstones. The exceptions are calcareous (or

dolomitic) cherts and occasionally calcareous (or dolomitic) porcelanites.

These terms are used for calcite-bearing (or dolomite-bearing) rocks

whenever applicable.

Minerals and Materials in Rocks

Silica, or silica component: all minerals (and mineraloids)

composed of silica or hydrated silica which is either biogenic or

derived from biogenic silica. The term includes amorphous opal,

opal-CT, and diagenetic quartz and excludes detrital quartz.

Amorphous opal: opal-A, as defined by Jones and Segnit (1971).

The term refers to the hydrated silica mineraloid composing siliceous

microfossil tests and frustules.

Opal-CT: a disordered, diagenetic silica mineral, as defined

by Jones and Segnit (1971), presumed to be composed of both α-cristo-

balite and α-tridymite. Opal-CT is often called cristobalite and has

many other names in the literature, as summarized by Wise and Weaver

(1974).

Opal-CT d-spacing: the spacing of the principal XRD peak of

opal-CT at 21.5° to 22.0° (Cu Kα 2θ). This term has the same meaning

as "d-101 spacing of cristobalite," as used by some authors (e.g.,

Murata and Larson, 1975).

"Order" of opal-CT: the structural state of opal-CT indicated by the d-spacing of opal-CT. "Disordered" opal-CT has relatively high d-spacing values, "ordered" opal-CT has relatively low d-spacing values, and "order" increases as d-spacing values decrease. "Ordering" is synonomous with "order" or indicates an increase in "order." The terms are used with quotation marks because differences in the structure of opal-CT may not be due to ordering (see p. 151-158).

Detrital minerals: detrital grains that are not biogenic. The term excludes detrital biogenic debris (siliceous tests, calcareous shells, and organic matter), closely related diagenetic minerals (opal-CT, diagenetic quartz, and dolomite), as well as pyrite. Silt and clay grains derived from arenaceous foraminiferal tests are, however, included in detrital minerals.

Aluminosilicates: all detrital minerals except detrital quartz.

Organic matter: materials which are organic in the geochemical sense—including all carbon compounds except oxides and carbonates (Krauskopf, 1967, p. 283). The term excludes biogenic carbonate and silica minerals.

Rock Comparisons

Component composition: the composition of a rock as expressed by specific groups of minerals and materials (components)—namely, carbonate minerals, detrital minerals, organic matter, apatite, and silica.

Bulk composition: the chemical composition of the whole rock. Rocks equivalent in bulk composition are also equivalent in component composition except among carbonate-bearing rocks, where calcareous

and dolomitic rocks with similar component compositions do not have similar bulk compositions.

Relative detrital content: the percentage of detrital minerals in the sum of detrital minerals + silica. Thus the relative detrital content is the detrital content normalized to a basis free of carbonate, apatite, organic matter, etc.

Relative silica content: the percentage of silica in the sum of detrital minerals + silica.

Lithology: "physical character of a rock, generally as determined megascopically or with the aid of a low-power magnifier" (American Geological Institute, 1962). As used here, diatomites are different in lithology from porcelanites or cherts.

Laterally equivalent: closely similar in component composition, age, and primary sedimentary features such as internal layering and bedding. Lateral equivalents may be different in lithology due to the presence of different silica or carbonate phases.

Laminated: characterized by very thin layering. "Regularly" laminated rocks are marked by distinct, continuous laminations, usually 0.05 to 0.2 mm in thickness. While having prominent planar fabric, "irregularly" laminated rocks (generally described as "finely layered") have comparatively few continuous laminations, usually 3 to 10 mm apart.

CHAPTER 4

STRATIGRAPHY

An important step in the study was to determine whether lateral diagenetic differences are related to variations in age. For this purpose, the lithostratigraphic sequence was informally divided into five members based on simple compositional and sedimentary differences. Microfossil ages of member boundaries were then determined as a framework for identifying lateral age differences.

Lithologic Members

The Monterey Formation studied along the Santa Barbara coast contains a distinctive stratigraphic sequence. Compared to many Monterey sections, it is unusual in having a thick carbonate-rich base and a thick organic-rich, apatite-bearing shale in the middle of the section (Bramlette, 1946; Dibblee, 1950). A similar lithostratigraphic sequence is also present in the Santa Maria Basin to the north (Canfield, 1939).

Along the Santa Barbara coast, five lithologic members with broad compositional differences are here defined and used informally (fig. 4). Because virtually all rocks in the lower four members contain calcite, these members together comprise the "calcareous members." The uppermost, or siliceous, member is calcite-free.

In the following descriptions, rocks are outlined only for the central part of the area, between San Augustine and Gaviota Canyons,
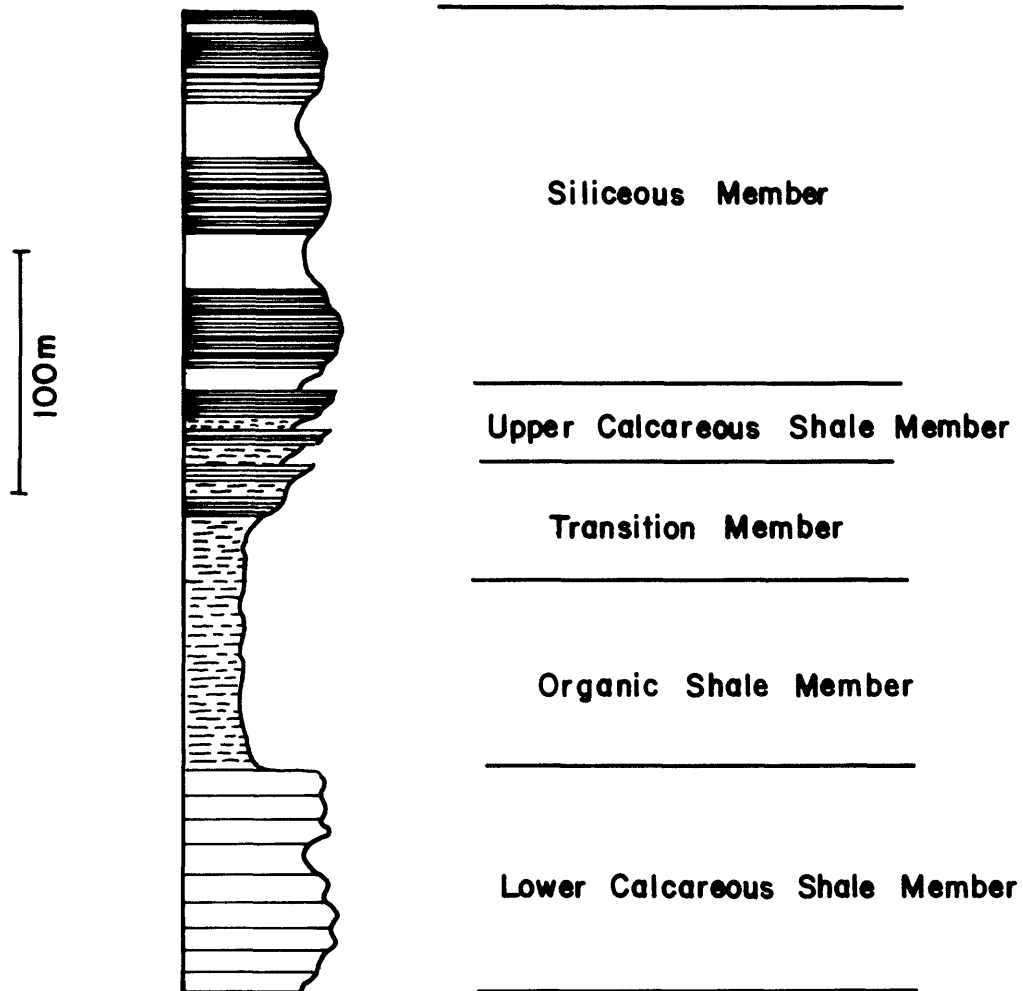
22

Fig. 4--Lithologic members and
        generalized lithologic
        column of the Monterey
        Formation between San
        Augustine and Gaviota
        Canyons. Regularly
        laminated rocks are
        cherts and porcelanites
        (most resistant). Thin-
bedded rocks are carbonate-bearing shales (least
resistant). Massive rocks include siliceous mudstones
in the siliceous member and calcareous cherts and
mudstones in the lower calcareous shale member.

and stratigraphic thicknesses are taken from the San Augustine section. Members, including bedding features characteristic of different rocks, are more fully described in the next chapter (p. 54-73).

Siliceous Member

This uppermost member consists mainly of porcelanites and siliceous mudstones, with some cherty porcelanites and a few cherts and siliceous shales. Thin (<3 mm) sand layers are common in parts of the member, and some thicker (>5 cm) sand beds and conglomerates occur locally. Except for occasional nodular dolomites, generally in mudstone layers, no carbonate is present. The member is relatively resistant to erosion. Thickness is about 155 m.

Upper Calcareous Shale Member

Underlying the siliceous member is the upper calcareous shale member, in which all rocks contain calcite (or, in a few cases, dolomite). Rocks are mainly calcareous cherty porcelanites and hard calcareous shales, with some calcareous porcelanites and a few organic-rich phosphatic shales. The member is moderately resistant to erosion and is about 25 m thick.

Transition Member

The transition member contains a mixture of the lithologies dominating the overlying upper calcareous shale member and the underlying organic shale member. Less than half of the section consists of the soft blebby calcareous shale characteristic of the organic shale member while the rest is calcareous cherty porcelanites

and hard calcareous shales. The member is about 40 m in thickness.

Organic Shale Member

Underlying the transition member is the organic shale member, which is dominantly composed of soft, easily weathered, organic-rich calcareous shales bearing apatite blebs. The organic shale member is the most poorly exposed member and least resistant to erosion. Thickness is about 80 m, of which less than 15 percent is hard calcareous shales or calcareous cherts.

Lower Calcareous Shale Member

This basal unit, which immediately overlies the bentonite or tuff of the Tranquillon Volcanics, is composed mainly of hard blocky calcareous (and in part dolomitic) mudstones and shales, with occasional calcareous cherts. The member is relatively resistant to erosion. Thickness is about 95 m.

Age Correlation

Bramlette (1946, pl. 2) published two foraminiferally dated sections along the Santa Barbara coast, at Naples and Point Conception. Both sections include upper strata now included in the Sisquoc Formation (Dibblee, 1950, 1966). The Naples section is partly described in Kleinpell (1938, table IV, fig. 6) and included by Wornhardt (1972, fig. 17) in his revised biostratigraphy of the late Miocene and early Pliocene. The lower part of Bramlette's (1946) Point Conception section was almost certainly measured in Wood Canyon and

so provides some information on stage boundaries in that section,
although no faunal lists or sampling localities were published.

In this study, foraminiferal stage boundaries were not precisely
located within sections. Rather, most microfossil sample localities
were placed as closely as possible to boundaries between lithologic
members in order to identify lateral age variation. Samples were
examined for benthonic and planktonic foraminifera, calcareous nanno-
fossils, and diatoms (for complete faunal lists, see Appendix H).
Most ages are based on Kleinpell's (1938) benthonic foraminiferal
zones and Wornhardt's (1972) revision of these zones. Some determina-
tions are based solely on Schrader's (1973) diatom zones as modified
by Barron (1976).

Due to facies control of benthonic fauna, benthonic foraminiferal
zones may be somewhat time-transgressive (Bukry and others, 1977;
Ingle, in press). Thus time equivalence cannot be precisely evaluated
from these microfossil age determinations. Problems of faunal time-
transgression, however, are probably minimized by the fact that Monterey
sediments studied along the Santa Barbara coast were deposited in
a single basin and extend a distance of only 55 km.

Using the biostratigraphic framework based on benthonic foramini-
feral zones, microfossil age determinations show that the Monterey
Formation ranges in age from latest Saucesian to mid or late Mohnian
throughout the area studied. Member boundaries in the lower calcite-
rich part of the section also appear to be laterally constant in
age (fig. 5).

The upper boundary of the Monterey Formation, however, is
probably not age-constant. The siliceous member is barren of fossils
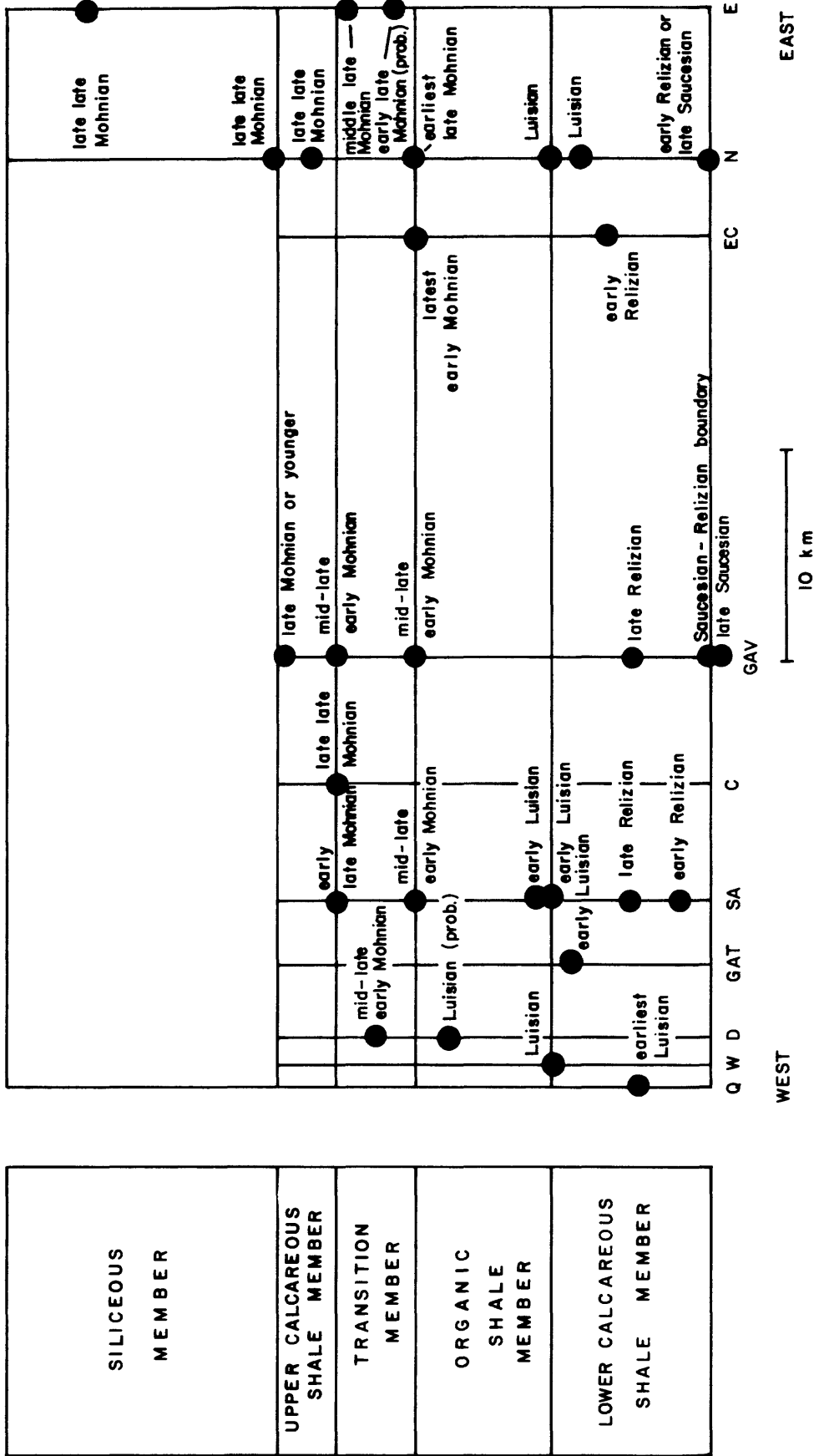
Fig. 5--Ages of lithologic members, indicating the lateral and stratigraphic position of each microfossil date. (Q = Quail; W = Wood; D = Damsite; GAT = Gato; SA = San Augustine; C = Coyote; GAV = Gaviota; EC = El Capitan; N = Naples; E = Elwood).

other than diatoms and arenaceous foraminifera, and its upper boundary
was approximately dated in this study only at the Elwood Beach
section. Judged from its age at Elwood Beach and at Naples Beach
(Kleinpell, 1938), the top of the siliceous member is latest Mohnian
in the eastern sections. In the west, however, the same lithologic
boundary is overlain by 500 m of Mohnian strata (Bramlette, 1946;
Appendix F, sec. 12). This relationship suggests that the top of the
siliceous member is younger in the eastern sections than in the western
sections.

Significance to Diagenesis

As shown by microfossil correlations, boundaries of most lithologic
members of the Monterey Formation in the study area are approximately
age-constant. One exception is the upper boundary of the Monterey
Formation, at the top of the siliceous member, which is probably
older in the western sections than in the eastern sections. As the
base of the siliceous member is approximately age-constant, however,
rock samples were obtained from the lower part of the siliceous member,
whenever possible, and can be considered age-equivalent. In sample
sets within each member, therefore, lateral diagenetic variations
are unrelated to age differences.

CHAPTER 5

PETROLOGY

A preliminary aspect of the study was to characterize the lithology

in order to evaluate original lateral similarities and differences.

In addition, a major aspect was to examine lithologic changes due to

increasing diagenesis. Most Monterey rocks along the Santa Barbara

Coast are aphanitic and contain few sedimentary structures. The

majority of contained minerals and materials are either cryptocrystal-

line or amorphous. It was necessary, therefore, to recognize lithologic

features that could be used to discriminate among rocks which are

similar in appearance. A second important step was to identify features

that indicate prediagenetic similarities among rocks which may be

quite different in appearance. For these purposes, bulk chemical

composition, primary sedimentary features, and diagenetic changes in

mineralogy and physical properties were examined.

In this part of the thesis, results of petrologic investigation

are described as follows: (1) minerals and other materials in rocks;

(2) characteristics of rocks, emphasizing the limits of discrimination

between rocks of different bulk composition or with different silica

phases; and (3) lithologic correlation of members and evaluation of

original lateral similarities and differences. Progressive changes

in lithology due to increasing diagenesis are described in the next

chapter.

Minerals and Materials in the Rocks

Minerals and materials in Monterey rocks along the Santa Barbara coast are grouped into the following principal components (for definitions, see p. 19): silica, detrital minerals, carbonate minerals, apatite, and organic matter. Other minor minerals include pyrite and zeolite.

The abundance of the principal components in specific rocks was determined by X-ray diffraction and chemical analysis (Appendix B). In the descriptions that follow, hand specimen and petrographic characteristics are emphasized.

Silica

Silica is either biogenic (amorphous opal) or diagenetic (opal-CT and quartz). Silica is generally present in amounts ranging from 10 to 95 percent, but only a few percent in some dolomites.

Biogenic silica occurs as diatom frustules (including broken debris) and as much less abundant silicoflagellate tests and sponge spicules. Where present in amounts greater than about 20 percent, diatom frustules are easily observed along bedding planes in hand specimen, and very small amounts of diatom debris are detectable in strew slides.

Opal-CT is mainly cryptocrystalline, although rare microcrystalline aggregates can be observed in thin section. In large amounts opal-CT can be differentiated from diagenetic quartz by its low refractive index, but opal-CT was routinely identified by X-ray diffraction. In the rocks studied, all opal-CT is inferred to derive from biogenic silica, for thick stratigraphic sections of diatomaceous rocks are laterally

equivalent to thick sections of opal-CT rocks. Mineralogically, opal-CT
rocks differ from diatomaceous rocks with the same bulk chemical com-
position only by the presence of opal-CT and the absence of diatom
frustules.

Diagenetic quartz is mainly cryptocrystalline except in some cherts
in the calcareous members and was routinely identified by X-ray
diffraction. Diagenetic quartz is inferred to be derived from biogenic
silica because thick sections of opal-CT rocks are laterally equivalent
to thick sections of rocks bearing diagenetic quartz.

Detrital Minerals

Detrital minerals are present in amounts generally ranging from
5 to 70 percent. In hand specimen, detrital minerals are most obvious
as flattened tests of arenaceous foraminifera, present as white pods
2 to 4 mm long with detailed coiled structures visible on bedding
surfaces. Where detrital minerals are abundant, micaceous grains are
also visible parallel to bedding.

Petrographically recognizable silt and large clay-sized particles
consist mainly of quartz, with plagioclase, K-feldspar, and occasional
colorless (or, rarely, brown pleochroic) mica. Silt-sized grains
may be scattered throughout the rock or concentrated in tests of arena-
ceous foraminifera. Clays occur as barely visible particles of moderate
refringence which are optically length-slow. In laminated rocks,
clays produce mass extinction parallel and perpendicular to bedding
but in massive rocks clays are more randomly oriented.

X-ray diffraction analysis showed that the principal mineral in
the detrital fraction is mixed-layer illite-montmorillonite, with

40 to 60 percent illite layers. Quartz, plagioclase, and K-feldspar were also detected by X-ray diffraction, as well as small amounts of mica and chlorite in the more detrital-rich rocks.

The mineralogical and chemical compositions of the detrital fraction are apparently similar in all rocks, whether they contain large or small amounts of detrital minerals (see Appendix B). Abundances of trace elements, present mainly in detrital minerals, are given in Appendix A.

Carbonate Minerals

Two carbonate minerals, calcite and dolomite, are present in the rocks studied. Calcite, in amounts ranging from 2 to 80 percent, is most obvious as foraminiferal tests but is probably mainly contained in coccoliths. Judging from d-104 spacing measurements made on a variety of samples, the calcite is low-magnesian (Goldsmith and Graf, 1958). This composition is characteristic of the calcareous microfossils present (Milliman, 1974).

Dolomite occurs in amounts ranging from 2 to 90 percent. Dolomite is not visible in hand specimen but is usually obvious in thin section as small colorless crystals, often with rhombohedral form. Because many calcareous rocks contain a few percent dolomite and because lateral equivalents of calcareous cherts and shales with a wide range of bulk compositions contain dolomite as the only carbonate mineral, most dolomite is inferred to be a replacement of calcite. Dolomite is also present in relatively pure concretions, nodules, and layers. Judging from three analyses of calcite-free dolomitic rocks, the mineral is actually proto-dolomite, with a considerable excess of calcium. Dolomite

is also high in strontium, probably inherited from calcite, and contains some iron and manganese (see Appendix A).

Organic Matter

Unweathered samples contain 1 to 16 weight percent organic carbon, equivalent to about 0.5 to 24 percent organic matter. Because of its relatively low density, this amount of organic matter represents a larger volume percentage—as high as 45 percent—so that in some rocks organic matter is the predominant component by volume.

The presence of organic matter is indicated by the dark color of many rocks and their bituminous smell when fractured or cut. Organic matter is not easy to identify, however, either in hand specimen or thin section. In addition, darkness is not always a reliable indication of abundance, as some dark rocks contain only small amounts while pale rocks may contain much more abundant organic matter (see p. 55).

Most organic matter is in the form of kerogen, a solid mineraloid whose structure is difficult to characterize. All of the organic matter is thermally immature and contains little extractable hydrocarbon which is highly asphaltic (see Appendix C).

Apatite

Apatite, in amounts from 1 to 20 percent, occurs as bone fragments, pure nodules, and as disseminated nodular bodies. In hand specimen, apatite is most obvious as white, cream, or slightly rose-colored blebs which are usually somewhat more resistant to weathering than the organic shales in which they occur. In rocks where the apatite is less concentrated, it is sometimes detectable as white flecks. Apatite

is sometimes detrital, as pellets in sandstones, but more commonly
occurs in nodules or disseminated nodular bodies surrounded by frag-
ments of partially replaced foraminifera tests.

Other Minerals

Small amounts of pyrite occur in nearly all unweathered rocks, as
small round or cubic grains, sometimes with a framboidal form. Amounts
of pyrite in a variety of rocks were estimated by comparison of iron,
sulfur, and organic carbon contents combined with petrographic estimates.
Most rocks probably contain less than 0.5 percent pyrite, although
a few contain as much as 2 percent. Pyrite undoubtedly formed after
deposition, at least in some rocks, as it occurs inside some foramini-
fera tests.

Small amounts of zeolite, detected by X-ray diffraction, are present
in a few rocks in the lower calcareous and organic shale members of the
eastern area. Only the most detrital-rich rocks contain any zeolite,
which is probably clinoptilolite. Association with volcanic glass is
suggested by its distribution in the lower two members in the eastern
sections, where there are several thin beds of fresh volcanic glass.
No shards, however, were detected in the zeolite-bearing rocks.

Rocks

Monterey rocks along the Santa Barbara coast are naturally divided
into two main compositional groups: siliceous (carbonate-free) rocks,
present only in the siliceous member, and carbonate-bearing rocks,
present only (except for nodular dolomites) in the lower four carbonate-
bearing members. A third group, the organic shales, has been distinguished

from other carbonate-bearing rocks because of its abundance in the organic shale member and its restricted range of chemical compositions.

In this part of the study, field and analytical properties of typical rocks are described, with emphasis on macroscopic characteristics. Since these characteristics are affected as much by diagenetic mineral changes as by chemical composition, all diatomaceous rocks are treated separately and distinctive properties of dolomitic rocks delineated after calcareous rocks. A rare rock type, "unusual" quartz chert, is described in the next chapter (p. 136). Rock names are defined on pages 16-19.

Diatomaceous Rocks

Rocks with moderate to high diatom contents are very distinctive even when they contain abundant calcite, apatite, or organic matter. Common characteristics include softness (<2), low resistance to erosion, friability, and low bulk density. Compared to rocks of similar bulk composition containing diagenetic opal-CT or quartz, diatomaceous rocks are easily distinguished petrographically by the presence of diatom debris. Also, arenaceous and calcareous microfossils are usually less compacted in diatomaceous rocks.

Among moderately to highly diatomaceous rocks, variations in silica content have only slight effect on field properties. Darkness, irrespective of organic matter content, and bulk density both increase with detrital content. In the field, however, small variations in water content may mask both differences. Thus the term "diatomaceous shale" covers a wide range of bulk compositions.

Sparsely diatomaceous rocks are easily distinguished in the field from other diatomaceous rocks by their greater density, smaller

friability, and darker color. Some sparsely diatomaceous rocks are difficult to identify as diatomaceous, however, as diatom frustules in small quantities cannot be reliably detected in the field. Because detection is only impractical below about 20 percent frustules (W. W. Wornhardt, pers. commun., 1976), even the most detrital diatomaceous rocks in the siliceous member are identifiable. However, diatoms are difficult to detect in many calcareous diatomaceous rocks—particularly those in the organic shale member. In addition, the latter rocks are not easily distinguished, by physical characteristics, from rocks of similar bulk composition containing small amounts of silica entirely as opal-CT or quartz.

Siliceous Rocks

The main components of siliceous (carbonate-free) rocks are biogenic or diagenetic silica and detrital minerals. Also present are 1 to 10 percent organic matter and small amounts of pyrite (<2 percent). Petrographically, the rocks appear to be largely isotropic, whether the silica is contained in diatoms, opal-CT, or quartz. Recognizable particles are mainly silt and large clay-sized detrital minerals, often in arenaceous foraminifera tests, and some barely visible clay particles.

Differences in analytical characteristics generally distinguish siliceous rock types defined by field properties. Among opal-CT rocks, average detrital content increases progressively from cherts or cherty porcelanites, to porcelanites, and then to siliceous mudstones or shales. Total compositional ranges of these rock types, however, overlap to some extent (fig. 6A). Siliceous rock types also vary in
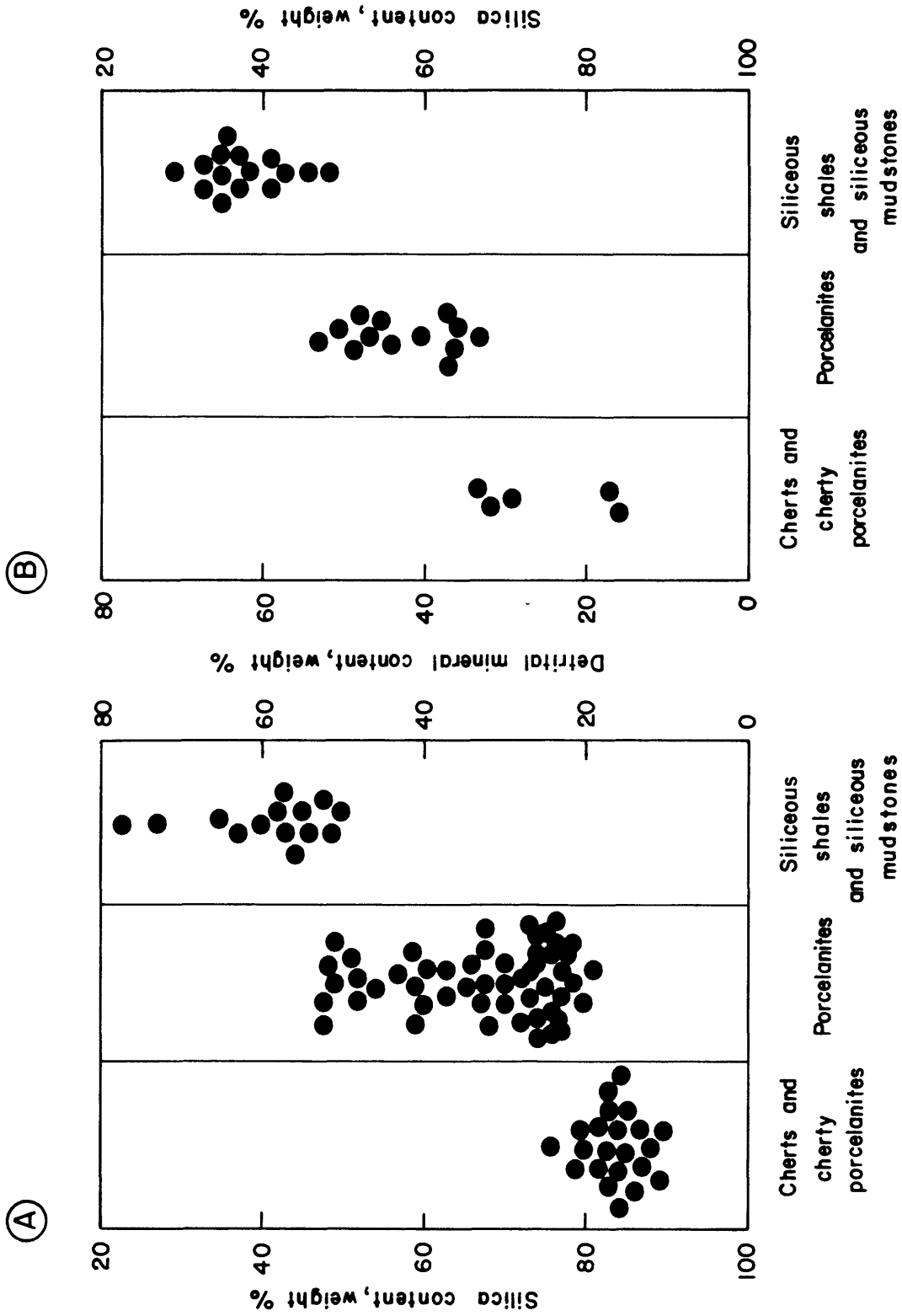
Fig. 6—Silica and detrital contents of cherts, porcelanites, and siliceous mudstones from the siliceous member. (Values on organic-free basis.) (A) Opal-CT rocks. (B) Quartz rocks.

average bulk density. Compared to values of porcelanites (1.39 to 1.51 g/cc), bulk densities are slightly greater among siliceous shales and mudstones (1.49 to 1.66 g/cc) and distinctly greater among cherts and cherty porcelanites (1.55 to 1.83 g/cc).

Considering their distinct field properties, opal-CT cherts are surprisingly similar in analytical characteristics to some opal-CT porcelanites. Most cherts and cherty porcelanites, for example, are only slightly more detrital than the most siliceous porcelanites. In addition, even though they are distinctly denser than opal-CT porcelanites, opal-CT cherts are not as dense as might be inferred from their smooth, sometimes vitreous surface. Although usually assumed to reflect pore-filling, cherty texture may actually be due to crystal habit, and this possibility is discussed later (see p. 158).

As with opal-CT rocks, the average detrital content among quartz rocks also increases progressively from cherts to porcelanites and then to siliceous mudstones and shales (fig. 6B). In contrast to opal-CT rocks, however, bulk densities of quartz porcelanites do not tend to be smaller than values of more detrital rocks. In fact, although data are sparse, bulk densities seem to increase with increasing silica content from siliceous shales and mudstones (1.75 to 1.97 g/cc) to porcelanites (1.93 to 2.03 g/cc) to cherts (2.05 to 2.30 g/cc).

Among opal-CT and quartz rocks, physical differences related to chemical composition are pronounced in the field. In addition to hardness, toughness, properties of fracturing, and surface textures (see description of rock names, p. 18), weathering characteristics also differ among siliceous rocks. The most important distinguishing feature is resistance to erosion, which increases with silica content.

Weathering products also vary. In weathered exposures, the more siliceous rocks are commonly stained with orange limonite while the more detrital rocks are stained with yellow jarosite. In addition, although most rocks are brown or black where fresh, weathered surfaces differ in color. Lightness usually increases with silica content so that the most siliceous rocks are typically white. Some opal-CT and quartz cherts, however, may be black, even where deeply weathered.

Differences between opal-CT rocks and quartz rocks are much less pronounced and distinction is ordinarily impractical in the field. Quartz rocks are denser and usually darker, but weathering and water saturation obscure these differences. Surface textures in hand specimens, fracturing and weathering characteristics are similar (fig. 7). Quartz porcelanites, when licked, adhere to the tongue less commonly than opal-CT porcelanites. This, however, is not a reliable diagnostic characteristic because: water saturation eliminates this property in all rocks; detrital-rich opal-CT porcelanites are not adherent, even when dry; and some quartz porcelanites are adherent, especially when weathered.

Calcareous Rocks

Component compositions of calcareous rocks from the upper and lower calcareous shale and transition members vary considerably (fig. 8A). Many calcareous rocks are essentially calcite-bearing siliceous rocks, with calcite contents averaging 10 to 30 percent and the silica component over 50 percent. Only a few samples contain more than 60 percent calcite.

Fig. 7--Outcrop comparison of opal-CT porcelanites (above) and quartz porcelanites (below). Note similarities in bedding, flagginess, and matte surface texture. Gaviota Beach (above) and Black Canyon (below).
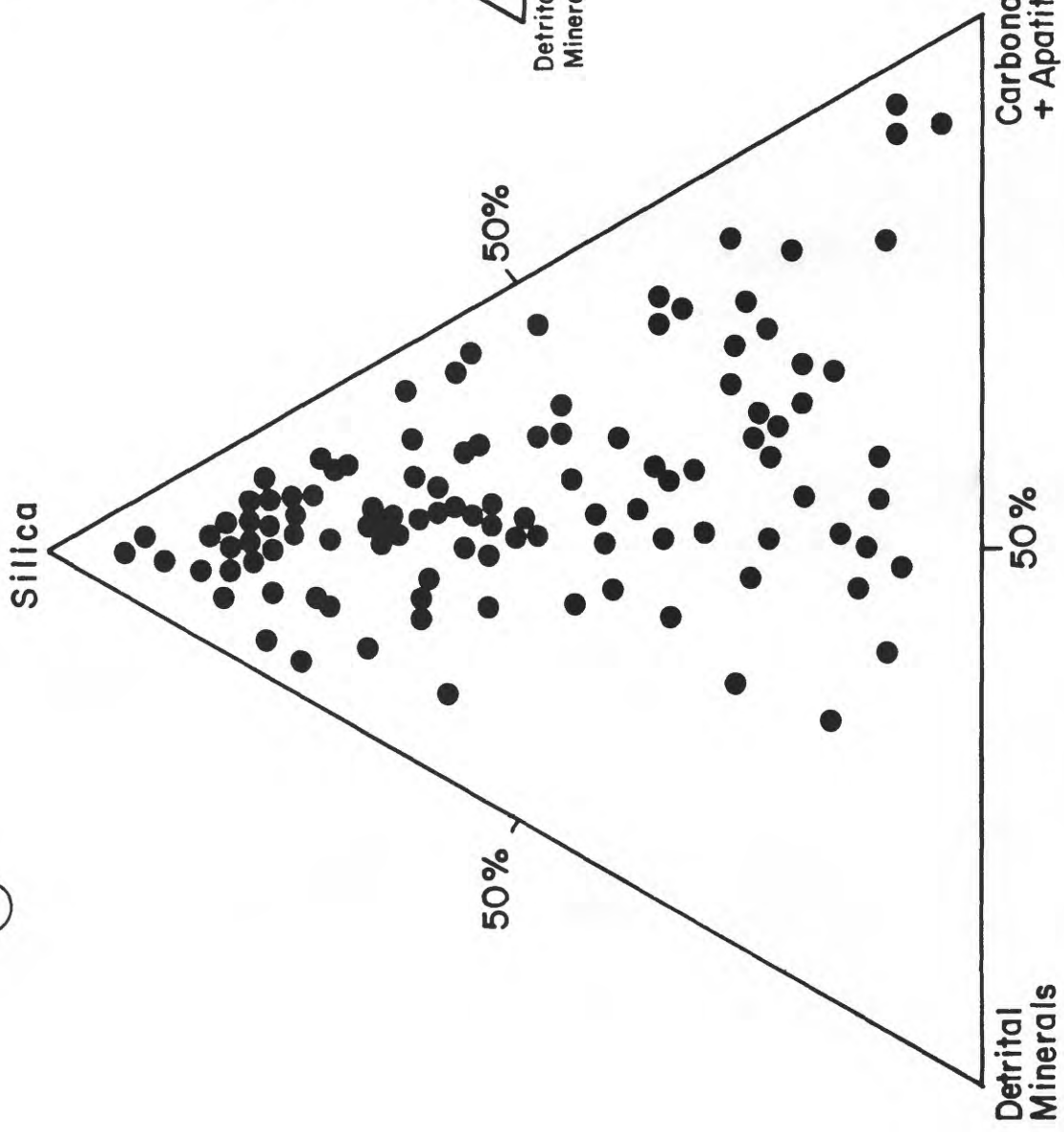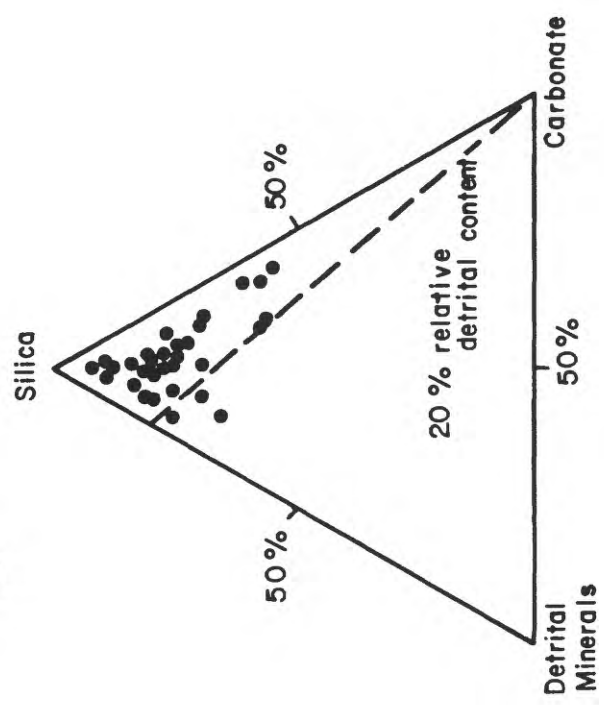
Fig. 8--Component compositions of calcareous rocks (in weight percent, organic-free basis). (A) All calcareous rocks except those in the organic shale member, including rocks with carbonate partly (<50%) dolomite. (B) Cherty rocks, including dolomite-bearing cherty rocks.

Petrographically, the calcareous rocks are generally similar to the siliceous rocks. They appear to be mainly isotropic except for foraminiferal tests, silt grains, and arenaceous foraminiferal pods. In addition, most rocks contain fine-grained calcite which may be difficult to distinguish from clay minerals. A few calcareous rocks contain abundant foraminiferal tests but most rocks are sparsely foraminiferal, and some rocks contain no foraminifera at all. Point counts of several typical samples analyzed for carbonate show that less than 10 percent of the calcite is contained in foraminiferal fragments. Additional calcite fills some foraminifera tests, most commonly in low-aluminum rocks with high calcite contents, but this represents only a small proportion of calcite. Most calcite is probably contained in coccoliths, which are present in all calcareous rocks examined by SEM (fig. 9A). Occasional coccospheres are detectable petrographically. In one calcareous chert with layers of abundant highly refringent minute spheres, SEM photographs showed numerous preserved coccospheres (fig. 9B).

The field characteristics and physical properties of the calcareous rocks distinguish these rocks from the carbonate-free siliceous rocks. Calcareous rocks, which when fresh have a grey-green hue (5Y/1), weather to a buff or slightly yellow color. The more siliceous of the calcareous rocks become distinctively mottled in pink and yellow whereas carbonate-free siliceous rocks all weather to a homogeneous pink or brownish-pink color. Calcareous rocks are also somewhat denser, though not necessarily less porous, than carbonate-free rocks with the same silica phase. Few calcareous opal-CT rocks have the characteristic lightness of opal-CT porcelanites.

1 μm
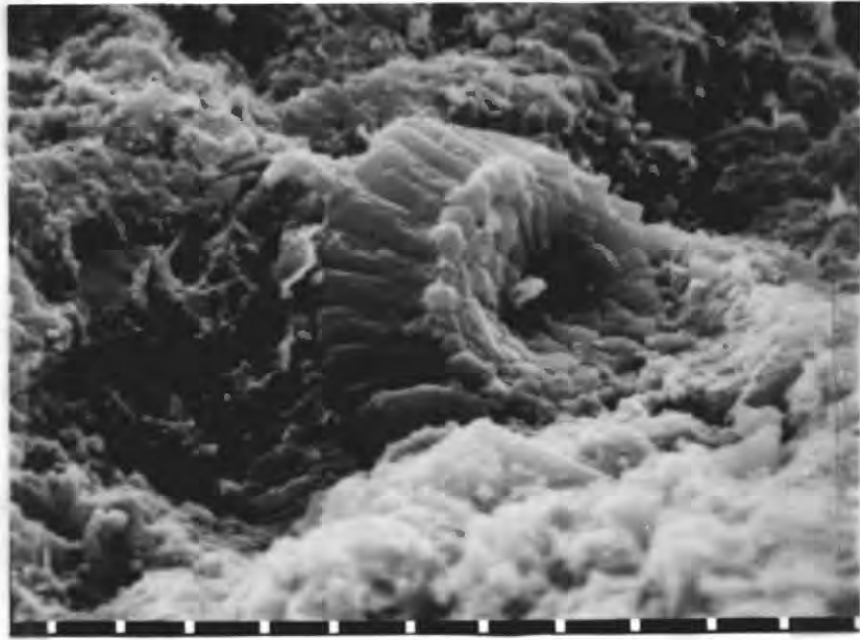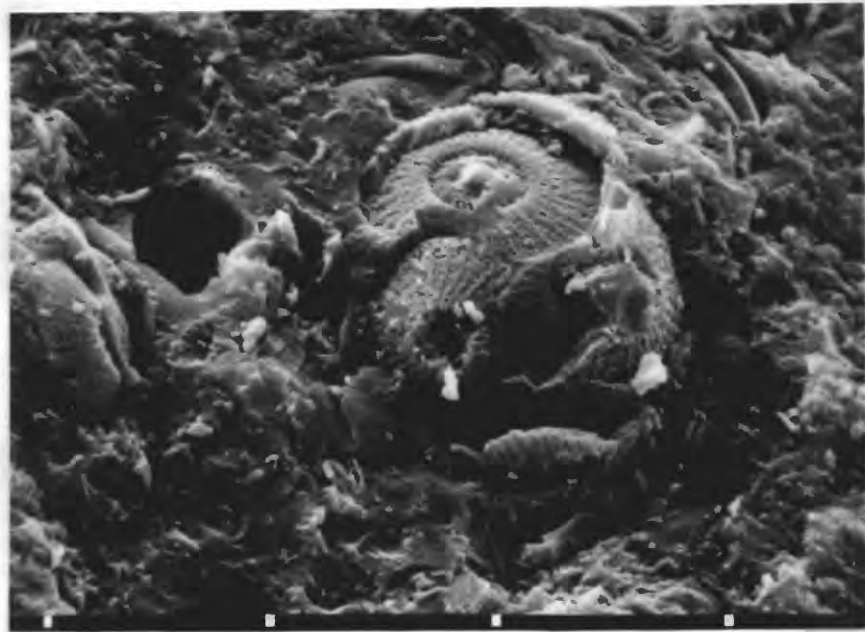
10 μm

Fig. 9--Nannofossils in calcareous rocks. (A) Coccolith in clay-poor
calcareous rock, Refugio Beach. (B) Coccosphere in calcareous
chert, Elwood Beach.

Among calcareous rocks, the most distinctive are the cherts and cherty porcelanites, which are similar in field and hand specimen characteristics to noncalcareous cherts and cherty porcelanites. One difference, in addition to mottling on weathered surfaces, is the presence of foraminiferal tests, which are usually obvious in calcareous rocks. Analytically, cherts are characterized by high proportions of diagenetic silica to detrital minerals rather than by high total diagenetic silica contents (fig. 8B).

Except for cherts, most calcareous rocks are not obviously siliceous in the field. In the lower part of the lower calcareous shale member, where most rocks are massive, the surface texture of all rocks except cherts is similarly grainy and resembles the texture of siliceous mudstones (fig. 10). Where rocks are only slightly weathered, one distinctive feature is surface color, which tends to be lighter with increasing silica content (cf. fig. 18). Bulk composition is most reliably indicated, however, by toughness, cohesiveness, and resistance to erosion, all of which increase with silica content (fig. 11). By contrast, toughness and cohesiveness tend to decrease with calcite content, suggesting that most calcite is in the form of microfossils rather than cement. Many rocks previously described as limestones are actually highly siliceous rocks--or sometimes dolomites.

In the upper calcareous shale member, rocks are more similar to the siliceous (carbonate-free) rocks, and both cherts and porcelanites are distinguishable. Many calcareous shales, however, contain more than 50 percent silica (or 70 percent silica on a calcite-free basis). Compared to rock type, therefore, toughness is a more reliable test of relative silica content. In addition to calcite content, density,

Fig. 10--Typical carbonate-bearing mudstone in the lower calcareous shale member, showing matte surface texture, thick bedding, and absence of laminations. Beach 3.5 km east of Gaviota pier.
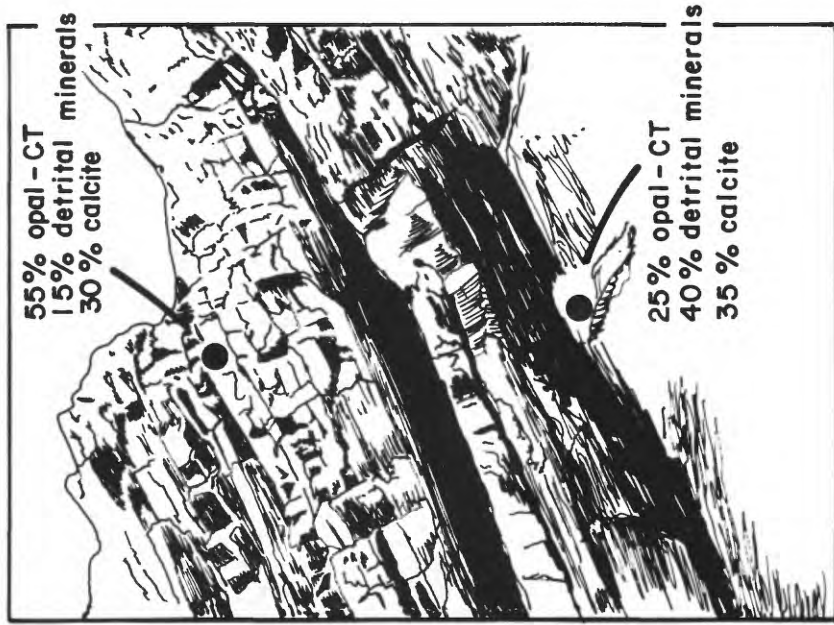
Fig. 11--Resistance to erosion varying with mineral composition. The more resistant bed with the lighter surface color is the more silica-rich. Lower calcareous shale member, Refugio Beach.

and weathering characteristics, two minor features distinguish these rocks from the overlying siliceous rocks. Calcareous shales contain tiny white flecks of apatite absent in siliceous shales; and calcareous cherts are more vitreous (and less detrital) than noncalcareous cherts.

Most calcareous quartz rocks are indistinguishable in the field from calcareous opal-CT rocks. Quartz rocks are denser and tend to be darker than opal-CT rocks of equivalent bulk composition. These differences are not sharply diagnostic, however, because bulk density and color vary considerably within both groups. Surface textures, fracturing, and weathering characteristics of quartz rocks are nearly always similar to those of opal-CT rocks (cf. fig. 24). An exception is quartz cherts, which are usually black even on highly weathered surfaces, while opal-CT cherts tend to be bleached white.

Dolomitic Rocks

Many of the calcareous rocks contain a small percentage of dolomite, and lateral equivalents of calcareous shales with a wide range of silica and detrital mineral contents contain dolomite as the principal carbonate mineral (fig. 12A). Petrographically, dolomite usually occurs as tiny grains scattered throughout the matrix of rocks.

The presence of dolomite affects some field characteristics and physical properties. Even in minor amounts, dolomite is often apparent by an ochre or yellow-brown tone of weathered rocks. Dolomitic rocks are also denser, although not necessarily less porous, than compositionally similar calcareous rocks. In areas where some of the rocks are dolomitic, the field recognition of lithologies is somewhat compli-
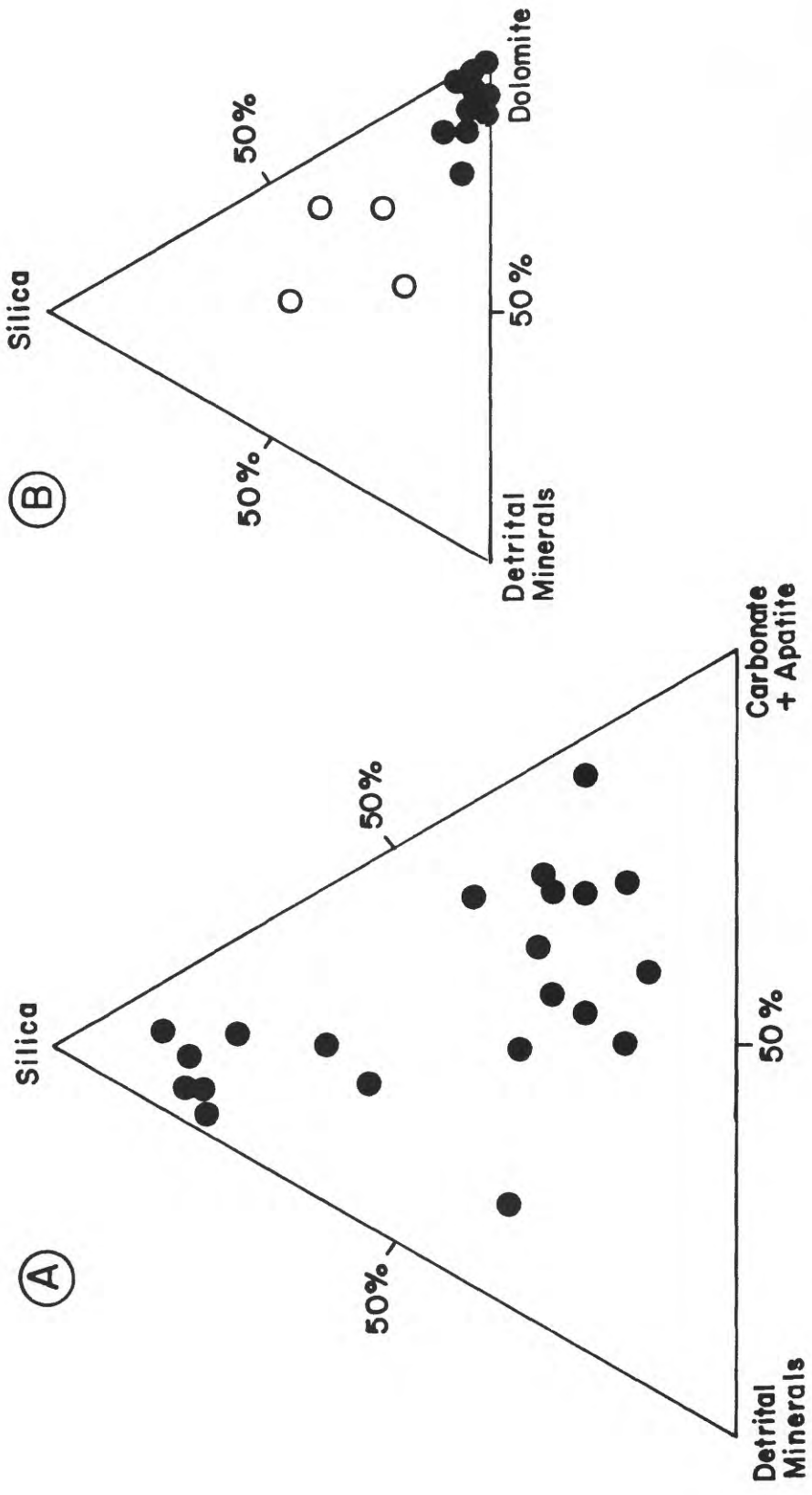
Fig. 12--Component compositions of dolomitic rocks (in weight percent, organic-free basis). (A) Shales, porcelanites, and cherts. (B) Nodular and pure bedded dolomites from the siliceous member (o) and from the calcareous members (•).

cated by the extra toughness, cohesiveness, and resistance to weathering of silica-poor dolomitic rocks. Since silica content increases these properties much more than dolomite, however, field properties of moderately and highly siliceous rocks are practically unaffected by dolomitization.

In addition to dolomitic rocks which are laterally equivalent to calcareous rocks, some purer dolomitic rocks occur in nodules, concretions, and beds. These rocks are not abundant but are conspicuous in the field because of their resistance to weathering. The purest dolomitic rocks have a sugary texture, are dark-brown where fresh, and ochre where weathered. Both silica and detrital mineral contents are usually low in sugary dolomites. Other nodular or bedded dolomites may contain as much as 40 percent silica, either quartz or opal-CT, or up to 25 percent detrital minerals (fig. 12B).

Organic Shales

The organic shales characteristic of the organic shale and transition members are similar in bulk composition to the most silica-poor calcareous rocks. They are generally low in biogenic or diagenetic silica, and moderately rich in detrital minerals and calcite. These shales are considered separately, partly because of their considerable thickness in the organic shale member, and also because they contain more abundant apatite and organic matter than other rocks in the area. Organic shales are also notable because they contain no dolomite.

Organic shales appear to have a limestone composition on a triangular plot of (organic-free) weight percentages of calcite + apatite, detrital minerals, and silica (fig. 13A). All organic
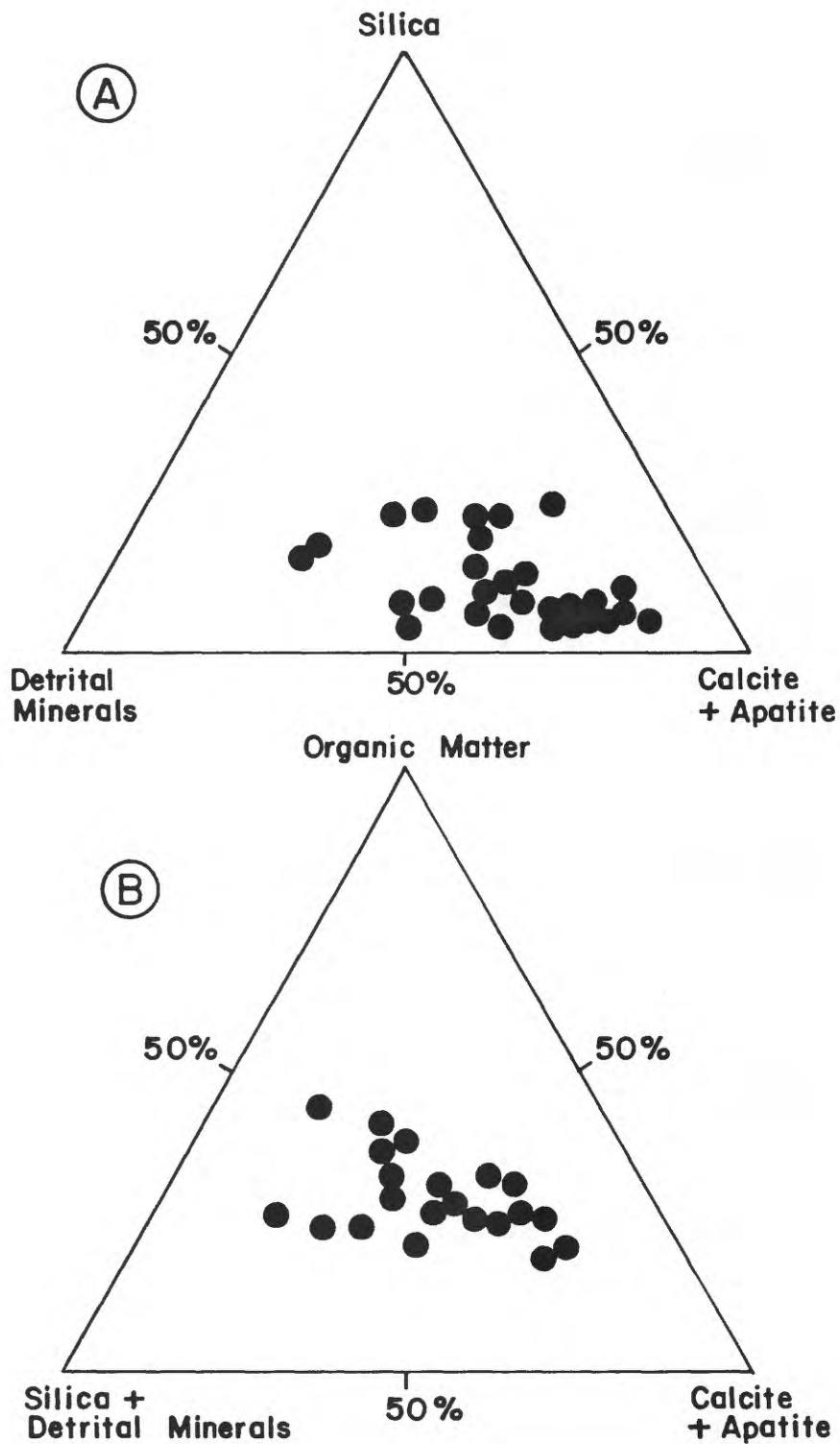
Fig. 13--Component compositions of organic shales from the organic
shale member. (A) In weight percent, organic-free basis.
(B) In volume percent, with organic matter as a separate
component; silica is combined with detrital minerals.

shales, however, are characterized by relatively abundant organic matter, as much as 24 percent. Since organic matter has a low specific density, the volume percentage of organic matter is as high as 45 percent. Figure 13B shows a triangular plot of the volume percentage of silica + detritals, calcite + apatite, and organic matter. On this basis, only a few samples are mainly composed of calcite and apatite; and in several samples organic matter is the largest single component.

The field characteristics of organic shales follow from their low silica and high organic matter contents. The rocks are very dark in color, soft, relatively unresistant to erosion, and poorly exposed. Since organic matter represents such a large volume percentage, weathering readily destroys the cohesiveness of the rocks which become punky, friable and pale-brownish-pink in color (fig. 14). Because of these characteristics, the organic shale member has previously been described as diatomaceous even in places where the silica is entirely opal-CT or quartz.

Summary

Rocks can be divided into two main compositional groups: (1) siliceous rocks, composed largely of biogenic or diagenetic silica and detrital minerals, with small amounts of organic matter (2-10 percent) and minor (<2 percent) pyrite and apatite; (2) carbonate-rich rocks, with compositions similar to those of the siliceous rocks except for the addition of calcite and/or dolomite, usually in small to moderate amounts (5-35 percent). A third group, the organic shales, is distinguished from other carbonate-rich rocks because of its abundance in

Fig. 14--Weathering in organic shale member at sea cliff, Naples
Beach. Note difference in color and in parting of shale
between base and top of exposure, a distance of 2 m.

the organic shale member. Organic shales are composed of small to moderate amounts (5-25%) of biogenic or diagenetic silica, moderate amounts (10-25%) of organic matter, and moderate to large amounts (10-60%) of detrital minerals and calcite.

Field characteristics and physical properties of these rocks depend mainly on the dominant silica phase and the chemical composition of the rock. In terms of silica phase, field characteristics differ most between diatomaceous rocks and rocks bearing diagenetic silica (either opal-CT or quartz), while field characteristics of opal-CT rocks differ only slightly from those of quartz rocks. Compared to diatomaceous rocks, most rocks bearing diagenetic silica are much harder, denser, much more cohesive and brittle, and much more resistant to erosion; as a result, physical characteristics alone generally distinguish these two groups of rocks in the field. By contrast, quartz rocks broadly differ from opal-CT rocks mainly in their greater bulk density so that differentiation between the two groups is usually impractical in the field. Another important effect of silica phase is that field characteristics of all diatomaceous rocks are relatively similar, irrespective of chemical composition, while distinct physical differences exist among rocks bearing diagenetic silica. For this reason, field discrimination between various diatomaceous rocks is much more difficult than between various rocks bearing abundant diagenetic silica.

In terms of chemical composition, field characteristics of opal-CT and quartz rocks are mainly influenced by the proportion of detrital minerals to silica. As this proportion increases, cohesiveness, hardness, and brittleness all decrease. Relative detrital content affects

bulk density in a more complex way. Among opal-CT rocks, detrital-rich
and detrital-poor rocks are denser, while rocks with moderate detrital
contents are lighter. Among quartz rocks, bulk densities tend simply
to increase with silica content.

Carbonate also affects field characteristics, but to a lesser
extent. All carbonate-bearing rocks, for example, are somewhat denser
than carbonate-free rocks of similar composition and silica phase.
In addition, except in cherts, both cohesiveness and gross hardness
tend to decrease with calcite content, while cohesiveness increases
somewhat with dolomite content.

Lateral Lithologic Correlation

This part of the study examines members in relation to original
sedimentary characteristics. Diagenetic changes in silica minerals
had sufficient impact on physical properties that rock names, which
are based on field characteristics, differ between rocks with identical
chemical compositions. Thus lithology--in a strict sense--is not
laterally constant along the Santa Barbara coast, even within each
member. By disregarding silica mineral phases, however--and, in addi-
tion, substitution of dolomite for calcite--original lateral similarities
become apparent.

In the following sections, lateral similarities and differences
are evaluated by examining the range of component compositions and the
primary sedimentary features typical of rocks in each member. First,
however, it is necessary to consider bias due to sampling strategy.

Sampling Bias

Several sources of sampling bias are likely to affect comparisons of component compositions between different sections. Generally, samples were collected either because of their apparent freshness or to provide information on silica phases in rocks of the widest possible range of compositions. Sample sets therefore were not specially designed as random sets and do not always accurately represent median compositions.

Two sources of bias particularly affect comparison of diatomaceous sections with sections containing abundant diagenetic silica. First, all diatomaceous rocks have relatively similar field characteristics. In the easternmost sections, therefore, highly siliceous rocks are less likely to have been collected because they are not distinguished by high resistance to erosion as they are in the central sections.

The second source of bias derives from the presumption made during sampling that darker rocks are fresher. Comparison of bulk darkness (color value) with organic analyses and component compositions subsequently showed that darkness may be more affected by other rock properties than by freshness. Darkness mainly increases with sample translucence--probably because of greater light absorption with deeper penetration--and also with clay content. Among diatomaceous rocks, then, where most sample surfaces are quite opaque, detrital-poor rocks may be pale grey even with large amounts of organic matter. Since darkness increases mainly with detrital content, sampling of diatomaceous rocks was biased towards detrital-rich samples.

Siliceous Member

This member contains mainly siliceous (carbonate-free) rocks.
Other rock types include occasional nodular dolomites and sandstone
beds, and scarce conglomerates.

Rocks in the siliceous member are usually divided into units,
1 to 3 m thick, which are alternately laminated and massive. Laminated
units consist mainly of moderately to highly siliceous rocks, while
massive units consist of detrital-rich mudstones (figs. 4, 15).
Thin (1-2 mm) sand layers are locally common in laminated rock.
Dolomites, on the other hand, are typically large (0.5-1 m long) strati-
form nodules in mudstone units. Layering and bedding are similar
throughout the area, irrespective of the silica phase present (fig. 16).

The siliceous member can be distinguished from the overlying
Sisquoc Formation by several features. Where both are nondiatomaceous,
the Sisquoc is ordinarily recognized by its higher average detrital
content, much greater proportion of mudstone to laminated or fissile
rock, pencilly weathering of porcelanite, and the grey (rather than
brown) tone of fresh mudstone. Even where both the Sisquoc and the
siliceous member are partly or entirely diatomaceous, the Sisquoc can
be distinguished by its higher proportion of mudstones and comparatively
poor bedding.

Compositions of siliceous rocks are quite similar laterally,
except that detrital content appears to be somewhat high in the eastern
sections (fig. 17). Although partly due to sampling bias, as described,
this relationship may also reflect a small lateral difference in the
original average sediment composition.

Fig. 15--Typical bedding in the siliceous member. Unit of siliceous
     mudstone (black) interlayered with units of more resistant
     porcelanite (white, red brown). Gaviota Beach.
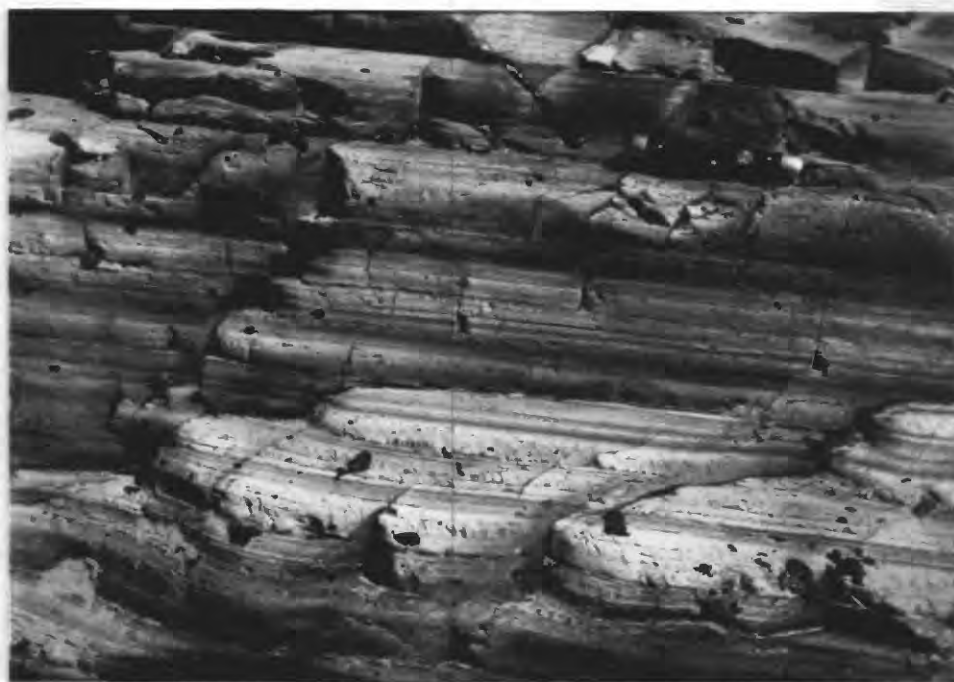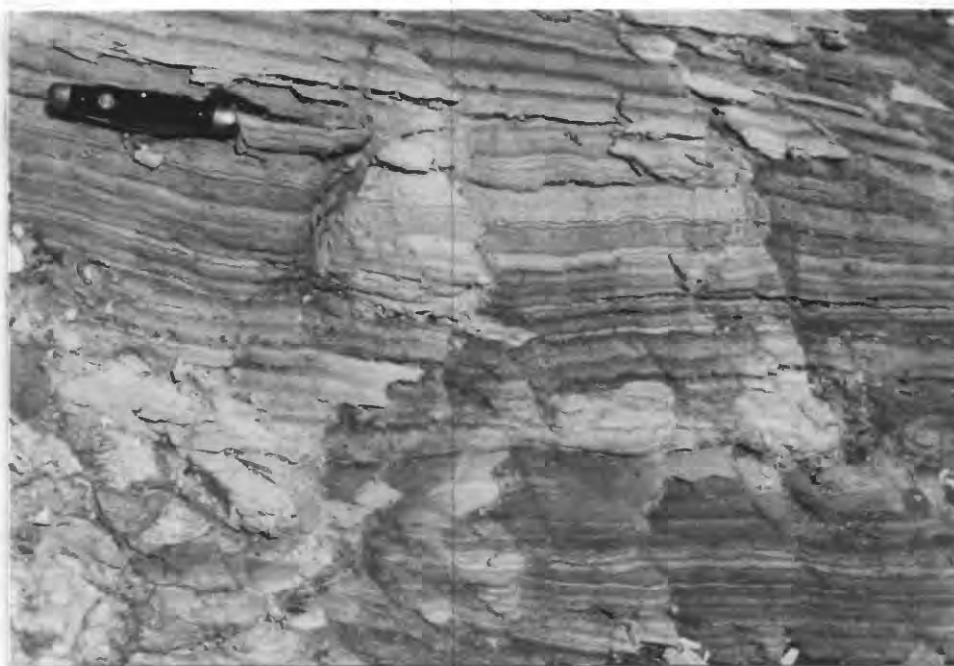
Fig. 16--Similarity of laminations in diatomaceous shales (above, Elwood Beach) and opal-CT porcelanites (below, Gaviota Beach), siliceous member.
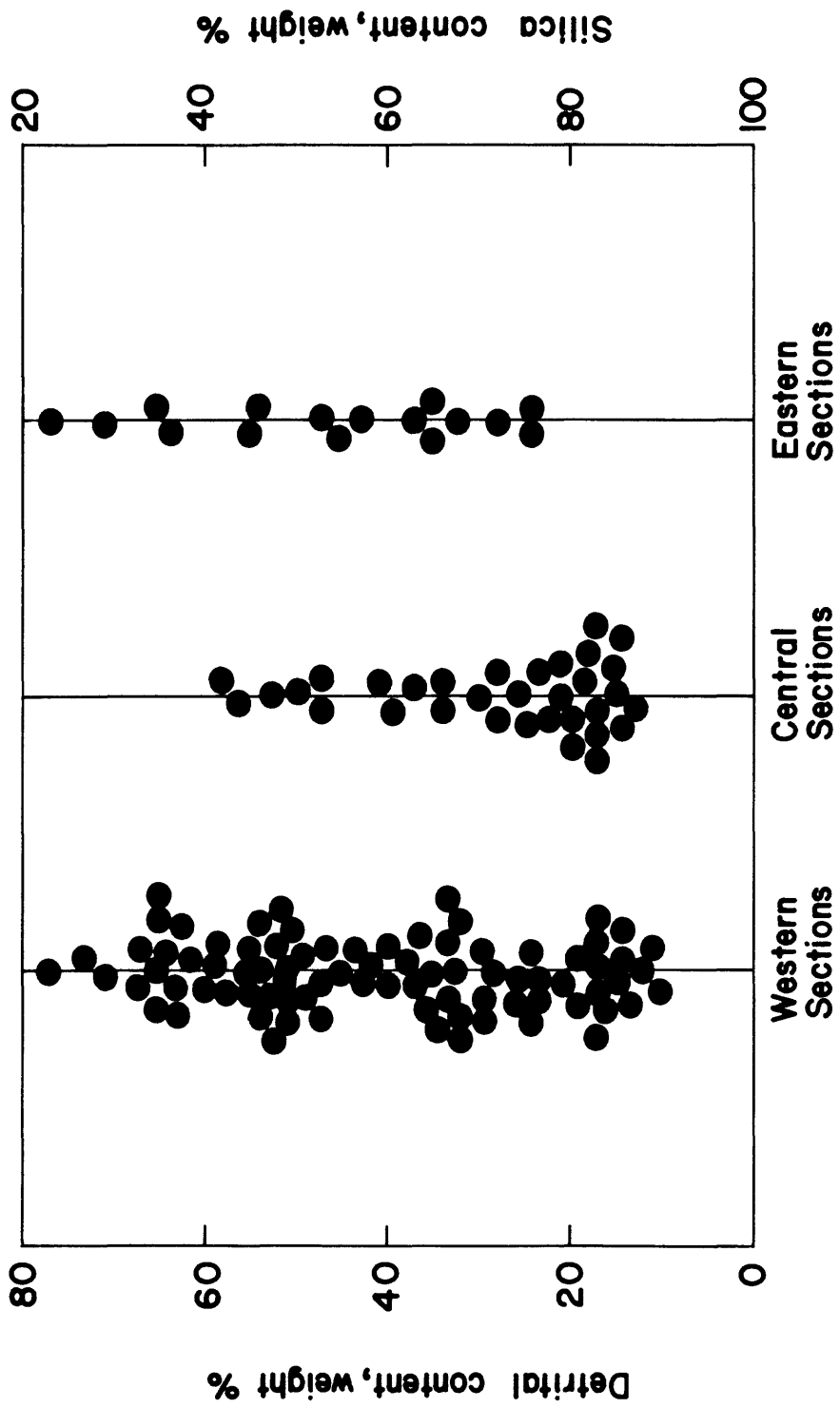
Fig. 17--Lateral comparison of detrital contents in the siliceous member. (Values on organic-free basis.)

Upper Calcareous Shale Member

This member consists mainly of calcareous and dolomitic rocks. Other rock types include organic shale (5 percent or less) and occasional unusual quartz cherts with sparse or no carbonate and very minor detrital mineral content.

Rocks in the upper calcareous shale frequently occur in units, 1 to 2 m thick, which tend to grade downward from highly siliceous, sometimes cherty, rock through moderately siliceous rock to detrital-rich shales (fig. 4, 18A). Downward grading, however, is not always apparent and some units tend to be divided into an upper silica-rich part and a lower detrital-rich part (fig. 18B). In either case, thin (about 3 mm) beds of contrasting composition are frequently interspersed throughout the units. All rocks are finely layered, but the most siliceous rocks are the most distinctly and regularly laminated. Layering and bedding are similar throughout the area, irrespective of the silica or carbonate phases present (fig. 19).

The upper boundary of the upper calcareous shale member is easily distinguished in most sections by the absence of disseminated carbonate in the siliceous member. Only where outcrops are extremely weathered, or where the upper calcareous shale member contains carbonate mainly as disseminated dolomite, does differentiation from the siliceous member require careful field examination. Two additional distinctive characteristics of the upper calcareous shale member (where nondiatomaceous) are mottled weathering and abundance of very cherty rocks.

Compositions of rocks in the upper calcareous shale member are quite similar laterally (fig. 20), except for the presence of a few unusual quartz cherts low in both carbonate and detrital minerals in

Fig. 18--Typical bedding in the upper calcareous shale member. (A)
single unit grading downward from thinly laminated calcareous
cherty rock (light-colored rock with jagged surface) to
silica-rich carbonate-bearing rock (light-colored rock with
rounded edges, just above hammer butt) to moderately
siliceous carbonate-bearing shale (dark rock, beneath and to
the left of hammer); beach 0.7 km west of Gaviota pier.
(B) Alternating units of silica-rich dolomitic rock (dark,
orange-stained) and moderately siliceous dolomitic rock
(light, pinkish); Jalama Canyon.

Fig. 19--Outcrops illustrating lateral similarity of rocks in the upper calcareous shale member. Note thin bedding, lateral continuity, and intimate interlayering of different types of rock. At left, creek exposure of dolomitic shales (black) with silica as quartz and of dolomitic porcelanites and cherts (light) with silica as opal-CT. At right, beach exposure of partly dolomitic shales (darker, less resistant) and of calcareous porcelanites and cherts (lighter, more resistant) with silica in all rocks as opal-CT. Left, Damsite Canyon; right, beach 0.7 km west of Gaviota pier.

Fig. 20--Lateral comparison of
component compositions
in the upper calcareous
shale member. (Components
in weight percent,
organic-free basis.)
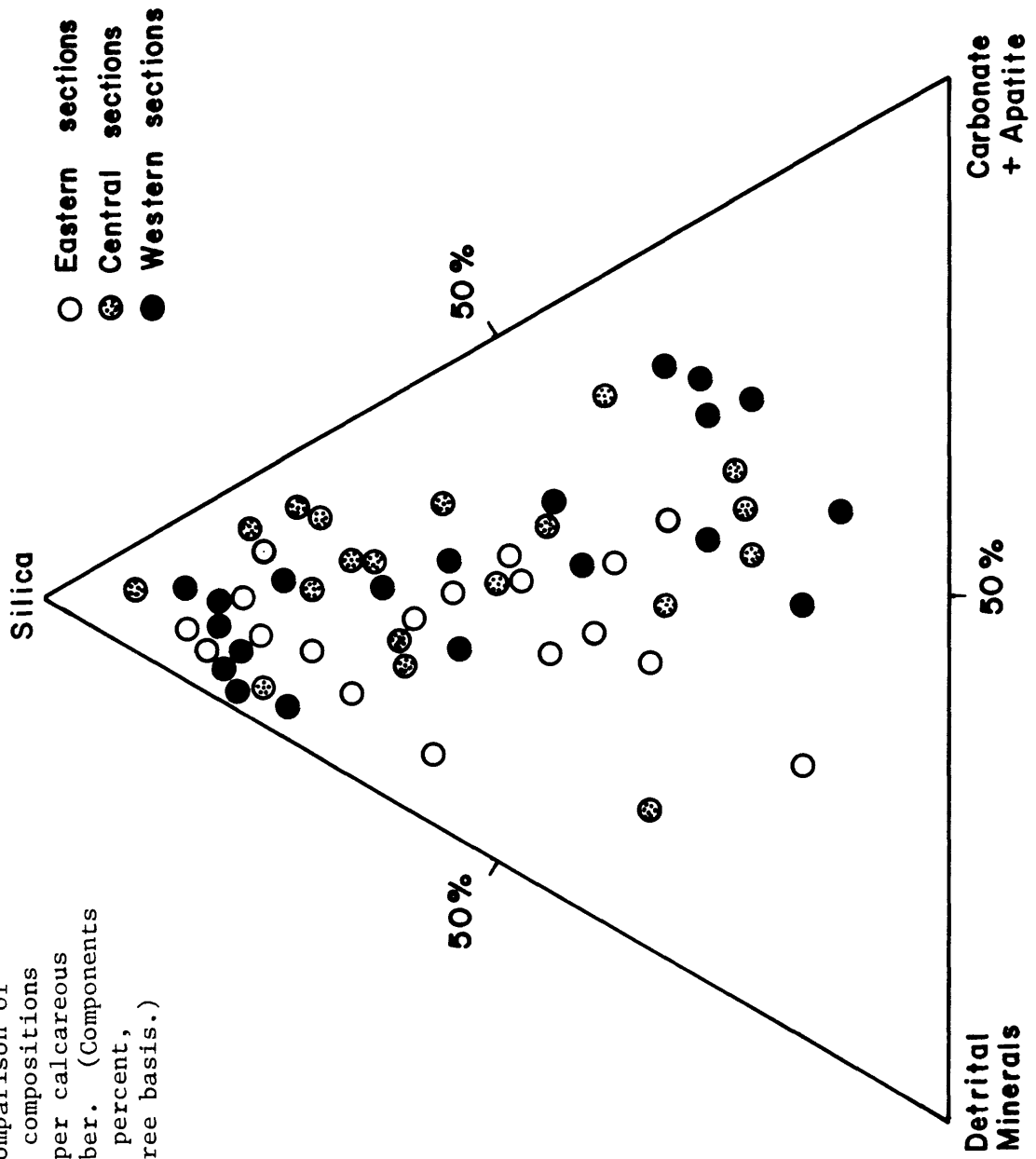
some of the westernmost sections. These rocks are apparently not lateral equivalents of any rocks further east.

Transition Member

The transition member contains a mixture of the lithologies characteristic of the member immediately overlying and the member immediately underlying. Calcareous and dolomitic rock represents about 70 to 75 percent of the section and organic shale represents about 25 to 30 percent of the section.

These two lithologic types are not usually intimately inter-layered. Sets of more siliceous calcareous beds without organic shales may be 3 m thick while some sequences of organic shale are as much as 6 m thick. Layering in the organic shales is similar throughout the area, whether silica is amorphous opal, opal-CT, or quartz (fig. 21).

The boundary between the upper calcareous shale member and the transition member is marked by an abrupt downward increase in the abundance of organic shale, which changes from 5 percent or less above to 25 to 30 percent below the boundary. In addition, the abundance of highly siliceous rock decreases gradually from about 40 percent to about 15 percent below the boundary. In nondiatomaceous sections, the downward decrease in abundance of carbonate-bearing cherts and porcelanites is quite distinctive in the field. In partly or entirely diatomaceous sections, where field characteristics do not vary as markedly with composition, this boundary is difficult to distinguish and was placed only approximately.

Compositions of rocks have a greater range in the transition member than in any other member. For this reason, and because only
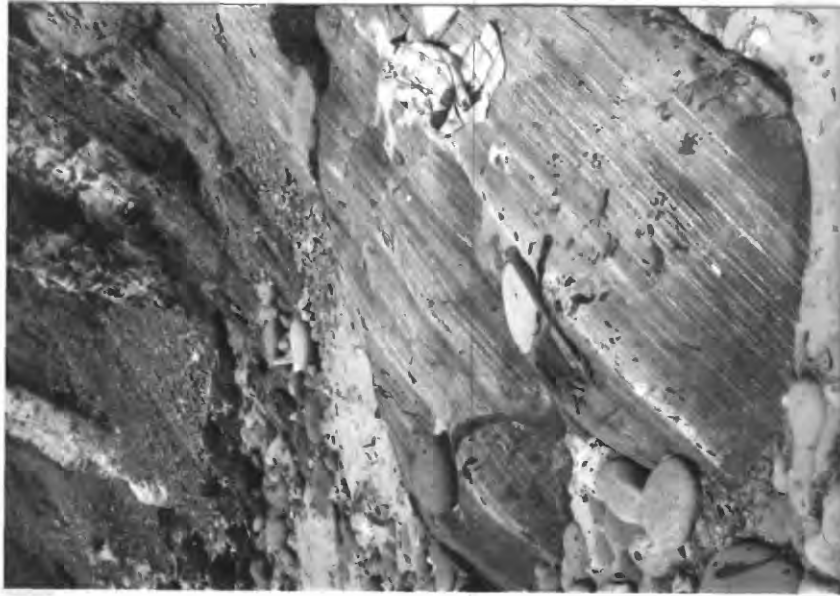
Fig. 21--Outcrops illustrating lateral similarity of organic shales. White layers are apatite. Silica is quartz in the left photograph (Wood Canyon), opal-CT in the middle photograph (El Capitan Beach), and opal-A in the right photograph (beach near mouth of Eagle Canyon, between Naples Beach and Elwood Beach).

a few samples were analyzed from this member, its lateral variability is not examined in detail.

Organic Shale Member

This member consists mainly of organic shales. Other rock types include about 10 percent calcareous rock, occasional unusual quartz chert, and scarce dolomite. In addition, some volcanic ash beds are present in the section at Naples and thin montmorillonite-rich beds in the section at Gaviota.

The organic shale member is the most homogeneous member, forming a nearly continuous sequence with infrequent distinct beds. The rocks are not regularly laminated, but they are fissile and typically contain thin layers or nodules of apatite (fig. 22). The member also contains some disturbed zones (fig. 21, right).

Where exposed, the boundary with the overlying transition member is relatively easy to recognize in all sections. In nondiatomaceous sections, less than 10 percent of the organic shale member is represented by rocks relatively resistant to weathering, whereas about 30 percent of rocks in the transition member are relatively resistant to weathering even near its base. In partly or entirely diatomaceous sections, the boundary can be distinguished by an abrupt downward decrease in variability of sediments and in abundance of regularly laminated rocks.

Compositions of rocks in the organic shale member are quite similar laterally (fig. 23), except for the presence of a few unusual quartz cherts in the central part of the area.
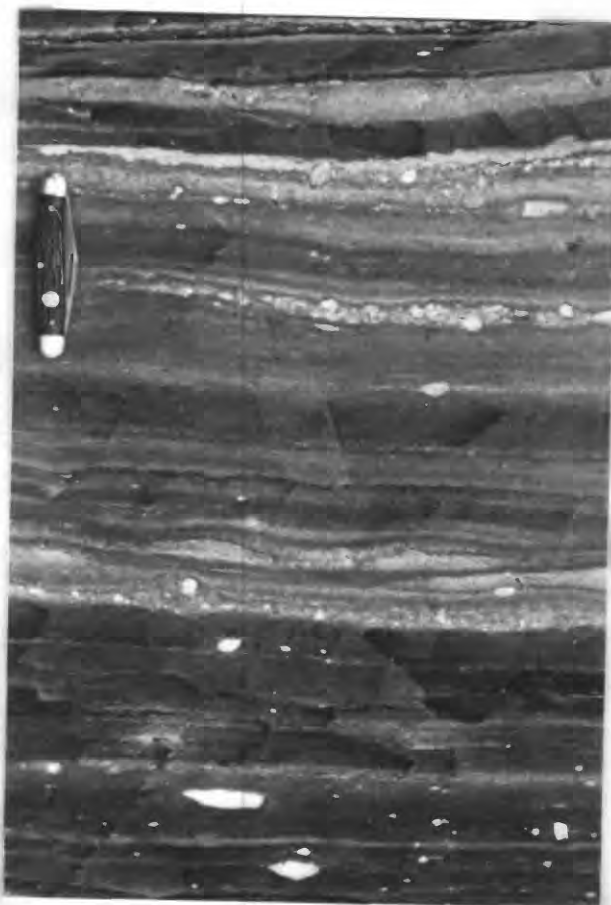
Fig. 22--Layering in organic shale, with white nodules of apatite
and white layers of disseminated apatite. El Capitan
Beach.

Fig. 23—Lateral comparison of
component compositions of
organic shales from the
organic shale member.
(Components in weight
percent, organic-free
basis.)
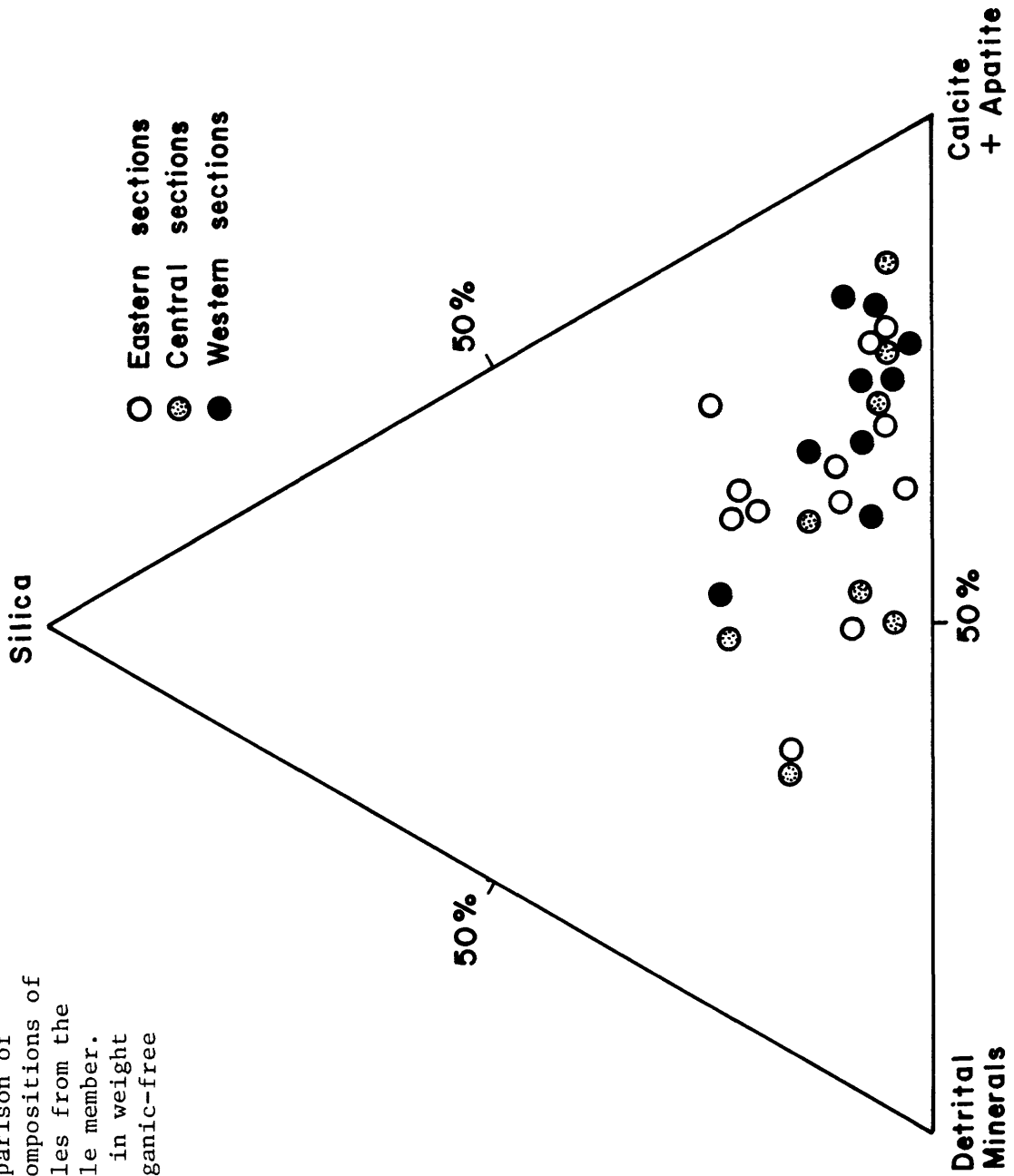
Silica

Calcite
+ Apatite

Detrital
Minerals

50%

50%

50%

O Eastern sections
⊛ Central sections
● Western sections

Lower Calcareous Shale Member

This member consists mainly of calcareous and dolomitic rocks. Other rock types include minor organic shale (less than 5 percent), occasional unusual quartz cherts and bedded dolomites, scarce intraformational breccias, and sandstones.

Rocks in the lower calcareous shale member are, as a whole, relatively resistant to weathering. The upper part of the member is usually shaly, containing fissile or finely layered, but not laminated, rock. Beds of shale as much as 6 m thick are also present in some sections even near the base, but the great majority of rocks are well-bedded mudstones without distinct fine-scale layering. Bedding in the lower calcareous shale member is similar throughout the area (fig. 24).

The boundary with the overlying organic shale member is relatively easy to distinguish. Even though usually fissile and sometimes containing thin layers of white apatite nodules, uppermost rocks in the lower calcareous shale member are distinctly more siliceous than rocks in the organic shale member. In nondiatomaceous sections, the boundary is marked by an abrupt downward increase in resistance to weathering, decreased organic matter, and increased silica content. At Naples, where this boundary occurs in diatomaceous rocks, it is marked by an abrupt downward decrease in bulk density and resistance to weathering, and a decrease in darkness of fresh rock.

Where the underlying tuff or bentonite is well exposed, the lower boundary of the lower calcareous shale member is easy to recognize. West from Cojo Canyon, the tuff and associated tuffaceous sediments are quite thick—as much as 20 m—and unmistakable. East from Gaviota

Fig. 24--Outcrops illustrating lateral similarity of rocks in the lower calcareous shale member. Bedding is generally thicker in these rocks than in rocks of other members, and beds have no obvious internal layering. Silica is quartz in the left photograph (Damsite Canyon), opal-CT in the middle photograph (beach 2.5 km east of Gaviota pier), and opal-CT also in the right photograph (Refugio Beach).

Canyon, a bentonite bed, sometimes only 25 cm thick, lies near the base of all sections. Between Cojo and Gaviota Canyons, however, no tuff or bentonite was detected, and the lower boundary was placed at the top of the Rincon Shale. In contrast to well-bedded carbonate-rich rocks of the lower calcareous shale, the Rincon Shale consists mainly of massive mudstones with little carbonate. In addition, the Rincon is rich in swelling clay, is poorly exposed, and is readily eroded, forming slopes with many large landslides. These characteristics provide a close approximation of the boundary between the Monterey Formation and the Rincon Shale, even where it is unexposed.

Laterally, compositions of rocks in the lower calcareous shale member are similar (fig. 25). One difference not apparent from component compositions is the presence of small amounts (to 5 or 10 percent) of zeolite at the Naples and El Capitan sections. Zeolite occurs only in the most detrital rocks.

Summary and Conclusions

Monterey members exposed along the Santa Barbara coast are distinguished by rocks of specific component compositions with characteristic primary sedimentary features. The siliceous member contains mainly siliceous rocks and, except for nodular dolomites, virtually no carbonate. Rocks occur in units (1-3 m thick) consisting of alternate sets of laminated rock, which is more siliceous, and massive rock, which is more detrital. The upper calcareous shale member consists mainly of calcareous and/or dolomitic rocks, all laminated or finely layered, and commonly occurring in units (1-2 m thick) in which silica content tends to decrease downward. The transition
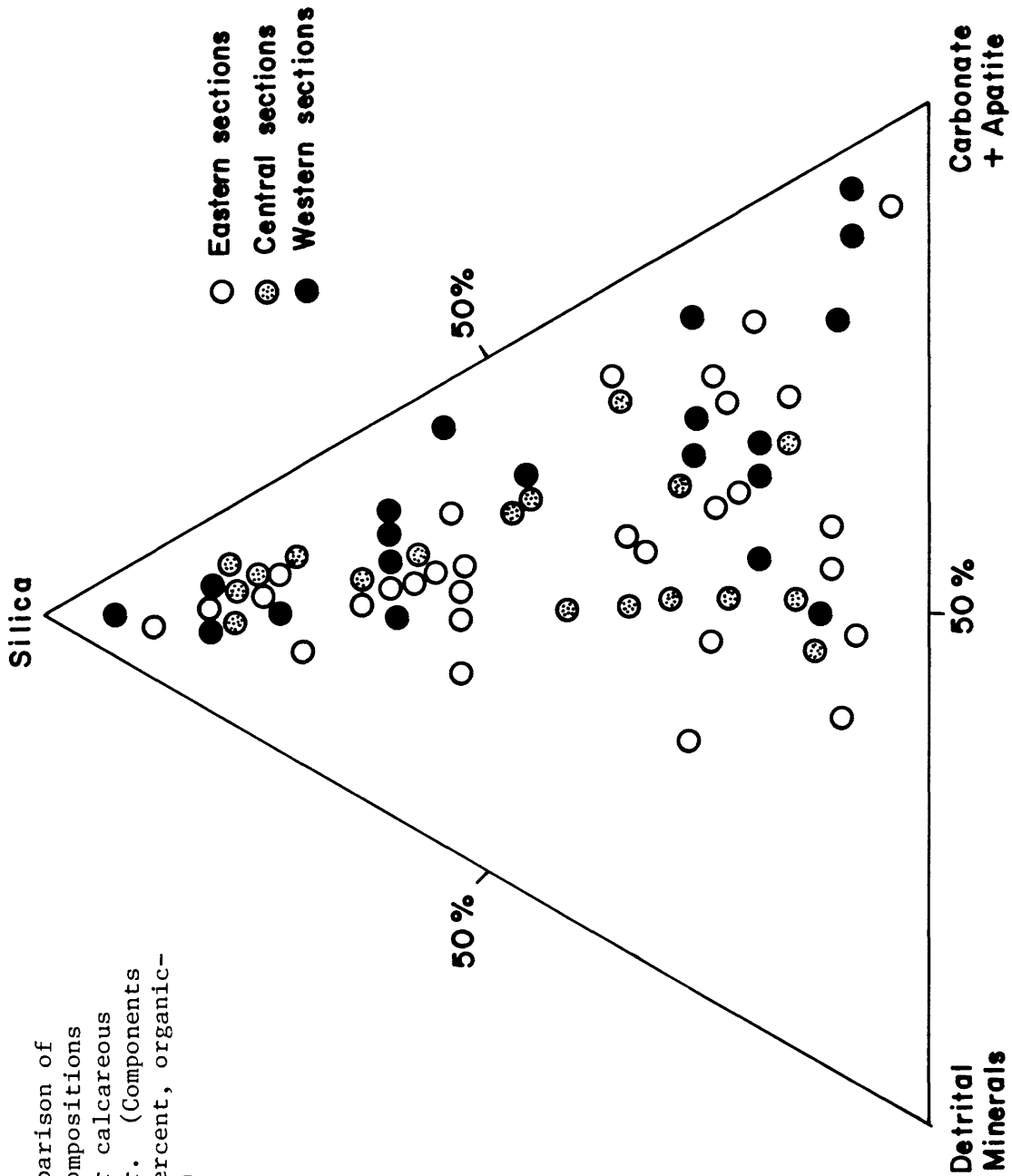
Fig. 25--Lateral comparison of
component compositions
in the lower calcareous
shale member. (Components
in weight percent, organic-
free basis.)

member contains both calcareous and/or dolomitic rocks and organic shales, frequently in thick (2-6 m) alternating sets. The organic shale member consists mainly of organic shale--fissile but not regularly laminated--in a homogeneous sequence with infrequent distinct beds. The lower calcareous shale member mainly contains calcareous and/or dolomitic rocks. Although fissile near the top of the member, most rocks are well-bedded mudstones without fine layering.

Lateral comparisons show that the range of component compositions as well as primary sedimentary features of rocks in each member are, in general, laterally constant. One difference suggested by lateral comparison of compositions is that rocks in the siliceous member seem to be somewhat more detrital-rich in the eastern part of the area, but this difference is partly due to sampling bias. Another difference is indicated by unusual quartz cherts--locally present in the calcareous members--which apparently do not have lateral equivalents. With these minor exceptions, however, lateral comparisons show the original similarity of Monterey sections examined along the Santa Barbara coast.

CHAPTER 6

DIAGENESIS

Paleogeography, structure, and lithologic correlation all suggest

that the sections of Monterey rocks along the Santa Barbara coast

examined in this study were originally similar when deposited. Present

lateral differences between sections are therefore due to differences

in postdepositional changes, or diagenesis.

This part of the thesis examines the lateral diagenetic changes

and evaluates the processes involved in diagenesis. Topics are dis-

cussed as follows: (1) previous work on diagenesis of diatomaceous

rocks and background material on factors promoting diagenesis; (2) cause

of lateral diagenetic differences along the Santa Barbara coast;

(3) lateral diagenetic changes, including (a) progressive changes

in lithology, silica minerals, and porosity for rocks of each member;

(b) evidence concerning effects of compositional variables on timing

of diagenetic changes; and (c) lateral irregularities; and (4) diagenetic

processes—including solution, precipitation, movement of silica,

compaction, cementation, and solid-state changes.

Background on Diagenesis of Diatomaceous Rocks

What is known about the diagenesis of diatomaceous rocks? Most

information concerns silica diagenesis, or changes of the silica

phases in the rocks. General results on silica diagenesis from field

studies of diatomaceous rocks will therefore be presented first,

74

together with some results from experimental studies and from work on the chemistry and structure of silica minerals. Information on lithologic changes--which are comparatively poorly known and which have not, in general, been studied comprehensively--is then summarized.

Silica Diagenesis in Diatomaceous Rocks

The amorphous opal (opal-A) in diatom frustules is both unstable and quite soluble under near-surface conditions. After slight burial, however, little silica seems to dissolve from frustules, and thick sequences of buried diatomaceous sediments and rocks show that abundant amorphous opal can resist dissolution near the top of the sediment column. As diagenesis increases, however, the silica in opal-A changes to another metastable silica mineral--opal-CT--before forming quartz, which is the stable silica phase under conditions of moderate burial (Murata and Larson, 1975; Mitsui and Taguchi, 1977). Opal-CT also usually forms from silica dissolved from diatom frustules in low-temperature experiments (Kastner and others, 1977).

In diatomaceous rocks, the transformation of amorphous opal to opal-CT ordinarily involves both solution and precipitation. This conclusion can be inferred from the fact that opal-CT naturally occurs in forms--sometimes, as in lepispheres, quite distinctive forms-- which are completely different from diatom frustules (Weaver and Wise, 1972; Flörke and others, 1975; Hein and others, 1978). A solution-precipitation mechanism is also shown by changes in isotope ratios and in porosity which are associated with the transformation (Murata and Larson, 1975).

Why, if it is not stable, does opal-CT form at all? Metastable formation of opal-CT is usually attributed to low energy during crystallization and to high silica concentrations in solution. According to Jones and Segnit (1972), silica tetrahedra tend to polymerize in saturated solution and may link together to form six-membered rings of particularly low energy; coalescence of these rings, because of their geometry, then results in either a cristobalite or tridymite structure depending on differences in one-dimensional stacking order. Apparently quartz does not ordinarily form from the solution of amorphous opal because silica is excessively saturated with respect to quartz (Kastner and others, 1977). Precipitation of a silica phase is apparently not favored unless the concentration of silica in solution is only slightly over-saturated with respect to that particular phase (Murata and Larson, 1975; Kastner and others, 1977). Since the solubility of opal-CT is intermediate between that of amorphous opal (higher) and that of quartz (lower), opal-CT forms much more easily than quartz (Fournier, 1973; Murata and Larson, 1975). Incorporation of extraneous ions into the mineral structure may also stabilize opal-CT, as suggested by Lancelot (1973).

Since opal-CT forms metastably, conditions favoring its formation are difficult to predict. Empirical observations, however, indicate that temperature is a major factor in promoting the transformation in diatomaceous rocks (Murata and Larson, 1975; Hein and others, 1978). Many other factors—including time, sediment composition, and permeability—have been suggested as influencing the reaction rate (see Kastner and others, 1977). Experimental work at low temperature indicates that crystallization rates rather than solution rates govern

the reaction (Kastner and others, 1977). For this reason, formation of opal-CT in silica-rich sediments is not necessarily enhanced by the introduction of dissolved silica, which is abundant and easily available once opal-CT nucleates. Experiments also suggest that foraminiferal calcite promotes, and clay retards, crystallization (Kastner and others, 1977).

Once opal-CT has formed from silica in diatomaceous rocks, its transformation to quartz can be considered a function of kinetics. Conditions which are likely to promote the change thus include: higher temperature (due to greater burial depth or greater heat flow), longer time, greater surface area, greater permeability, and faster fluid flow. In addition, the transformation may be affected by the chemical environment or the presence of other minerals, although these factors have not been studied in rocks of diatomaceous origin. In radiolarian rocks, however, calcite is thought to promote the formation of quartz from opal-CT (Keene, 1975; Robertson, 1977).

The mechanism of the transformation of opal-CT to quartz is disputed. On the basis of experimental work at 300° to 500°C by Ernst and Calvert (1969), the transformation has been widely stated to occur by solid-solid reaction. However, reinterpretation of these experimental data (Stein and Kirkpatrick, 1976), other experimental studies (Mizutani, 1977), and recent field studies (Murata and Larson, 1975) all show that solution-precipitation is the more probable mechanism in rocks of diatomaceous origin. In addition, growing evidence suggests that the transformation of opal-CT to quartz is either aided by, or requires, the "ordering" of opal-CT (Murata and Nakata, 1974; Murata and Larson, 1975; Mizutani, 1977). This relationship has been explained by

differences in solubility among opal-CTs with different structures. "Disordered" opal-CT, like amorphous opal, dissolves to form solutions with silica concentrations which are apparently excessively over-saturated with respect to quartz for precipitation of quartz to occur (Murata and Larson, 1975; Kastner and others, 1977). "Ordered" opal-CT, however, is inferred to be less soluble than "disordered" opal-CT so that quartz is favored for precipitation from solutions in equilibrium with opal-CT once it is "ordered" (Fournier, 1973; Murata and Larson, 1975; Kastner and others, 1977).

Lithologic Changes of Diatomaceous Rocks

Comparatively little is known about diagenesis in diatomaceous rocks other than silica phase changes. In terms of lithology, rocks generally change with increasing diagenesis from diatomites and diatomaceous shales and mudstones to opal-CT porcelanites and then to denser quartz porcelanites (Murata and Nakata, 1974; Murata and Larson, 1975). The most siliceous diatomites, however, are inferred to change to opal-CT cherts and then to quartz cherts (Murata and Nakata, 1974; Murata and Larson, 1975).

Many specific lithologic characteristics are also altered during diagenesis of diatomaceous rocks--particularly porosity, bulk density, permeability, and ultra-structure. Of these, bulk density has received most attention. Hamilton (1976), who measured bulk densities and rebound of deep-sea sediments, shows progressive compaction in diatomaceous ooze as burial depth increases from 0 to 500 m. With greater burial--in thick stratigraphic sequences progressing downward through diatomaceous, opal-CT, and into quartz rocks--a general increase in

bulk density with burial depth is also shown by Mitsui and Taguchi
(1977) in well cores and by Murata and Larson (1975) in surface
samples. In addition, both porosity and bulk density have been studied
in conjunction with bulk chemical composition of diatomaceous and
opal-CT rocks from well cores in the San Joaquin Valley (Isaacs and
Beyer, in prep.). That study shows that porosity abruptly decreased
during formation of opal-CT and documents reductions, within 50
stratigraphic meters, of as much as 20 porosity percent in rocks of
equivalent composition. Published data on permeability are few,
but indicate ranges in diatomaceous rocks (Stosur and David, 1976).

Cause of Lateral Diagenetic Differences

Lateral diagenetic differences in the Monterey rocks studied
along the Santa Barbara coast are almost certainly due to lateral
differences in temperature and burial depth. This conclusion can be
drawn from two sets of direct evidence--thickness of late Monterey
and post-Monterey strata; and composition of organic matter within
the Monterey.

The original total thickness of overburden cannot be measured
directly. Erosion, due to exposure resulting from mid-Pleistocene
deformation, has removed part of the strata originally lying above
the Monterey. Differences in maximum burial depth, however, can be
inferred from late Miocene sediment thicknesses in two sections
exposed at the extreme ends of the study area. In the syncline at
Point Conception (west end), Mohnian strata are 800 m thick and
tentative Delmontian strata 550 m thick; by comparison, at Naples
(east end), Mohnian strata are only 140 m thick and Delmontian strata

only 150 m thick (Bramlette, 1946, pl. 2). Adjusted to a level of
compaction comparable to that at Naples, strata at Point Conception
(with average porosity 35 percent) would measure 1000 m for the
Mohnian (at 50 percent porosity) and 850 m for the Delmontian (at
60 percent porosity) (fig. 26A). Thus the weight of Mohnian and
Delmontian strata at Point Conception was over six times that of
age-equivalent strata at Naples.

In areas with average geothermal gradients, widespread opal-CT
generally forms at 600 to 700 m and quartz at about 2000 m (Murata
and Larson, 1975; Hein and others, 1978). High geothermal gradients
offshore Point Conception (McCulloh and Beyer, 1979) suggest, however,
that phase transformations may have occurred at somewhat shallower
burial depths (500 m and 1550 m) along the Santa Barbara coast. Based
on porosity-depth relationships in diatomaceous sequences (Hamilton,
1976; Murata and Larson, 1975), actual post-Luisian overburden at
the end of Delmontian time was probably about 1600 m at Point Conception
and 450 m at Naples. Assuming modest post-Delmontian sedimentation,
therefore, lateral differences in overburden thickness easily account
for lateral differences in silica mineral phases.

Thermal diagenesis of organic matter provides further evidence
of postdepositional differences. Monterey rocks along the Santa
Barbara coast apparently did not experience burial temperatures high
enough to generate abundant hydrocarbons, which form only above
100°C (Phillipi, 1965). Some immature hydrocarbon is present in the
western part of the area, but most organic matter consists of kerogen,
a solid mineraloid substance predominant at low temperatures.
Elemental analysis of the kerogen shows that atomic oxygen/carbon
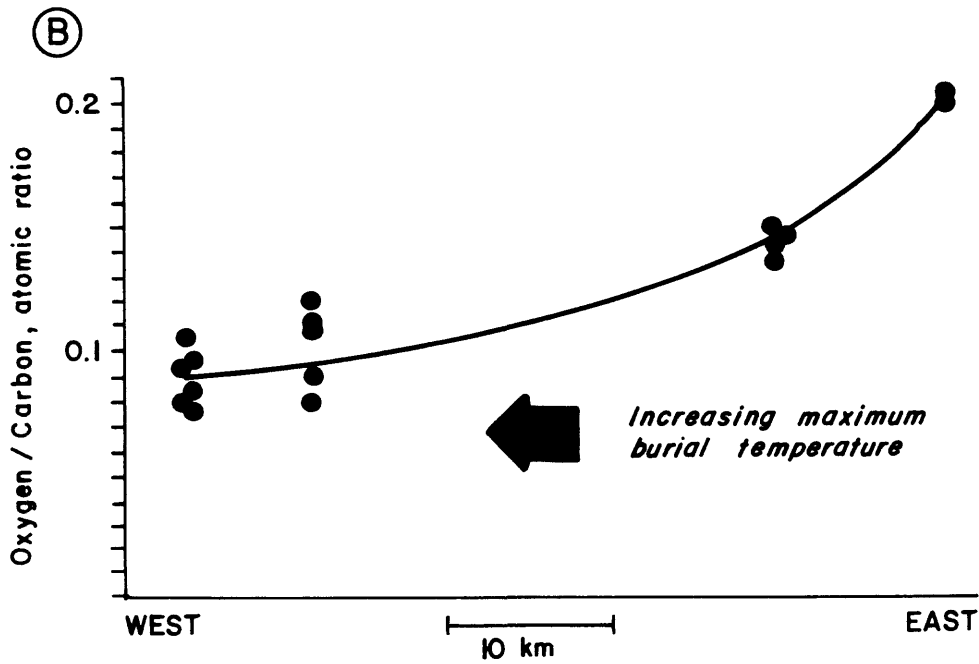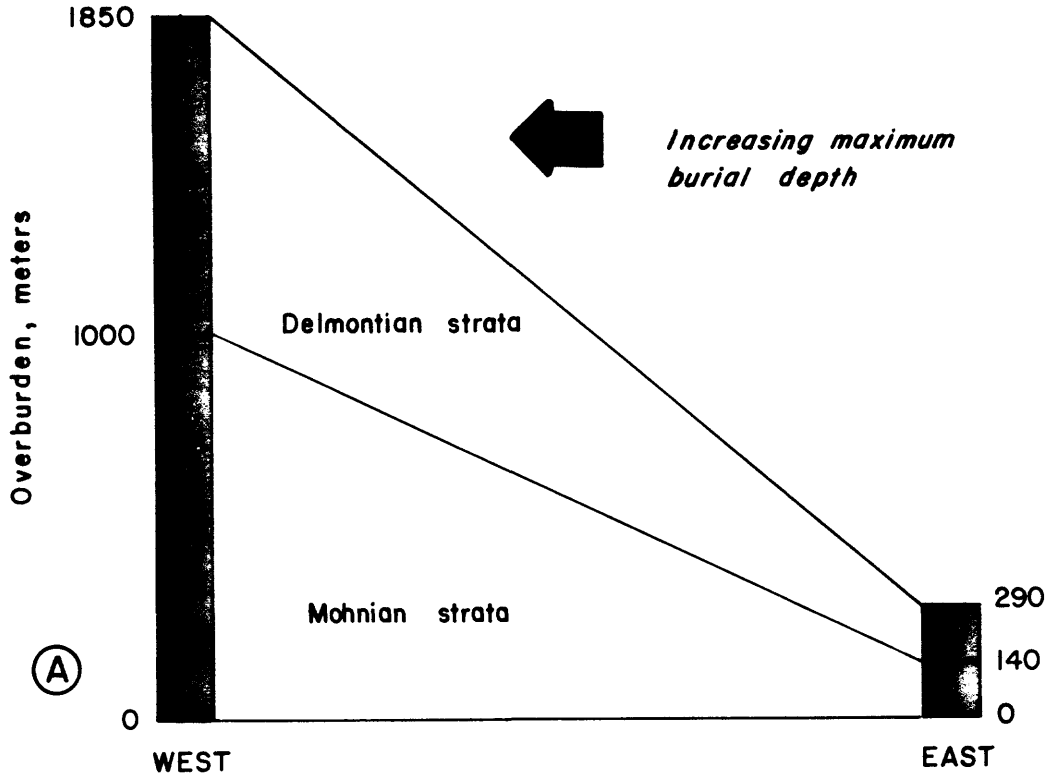
Fig. 26--Lateral differences in maximum temperature and depth during
    burial.   (A) Westward increase in thickness of Mohnian and
    Delmontian strata.   Based on data in Bramlette (1946).
    (B) Lateral change in the oxygen/carbon ratio of kerogen,
    showing westward increase in maximum burial temperature.
    Based on data in Appendix C from lower strata of the
    calcareous members.

ratios decrease westward (fig. 26B) while atomic hydrogen/carbon
ratios, with a median value of 1.36, do not consistently change along
the Santa Barbara coast. This pattern is characteristic of changes
in organic matter which is derived from mixed continental and algal
sources and is subjected to increased temperature (Tissot and others,
1974). The pattern of elemental ratios therefore indicates westward
increase in maximum burial temperature.

On the basis of east-west differences in composition of organic
matter and overburden thickness, then, lateral diagenetic differences
can be attributed to increased temperature and depth of burial towards
the west. Since maximum overburden thickness cannot be measured at
every section, temperature and burial depth are assumed to have
increased progressively westward.

<u>Lateral Relationships</u>

<u>Diagenetic Changes in Lithology</u>

A major purpose of the study was to examine progressive lithologic
changes due to increased diagenesis. Because originally similar rocks
experienced increasing temperature and burial towards the west, sections
of Monterey rocks along the Santa Barbara coast could be viewed
laterally as a series of diagenetic time-frames. In this view,
the easternmost section represents the earliest stage of diagenesis
considered and each more westerly section delineates a subsequent
stage of diagenesis at each stratigraphic level.

Diagenetic changes in lithology and silica phase, summarized in
figure 27, are related in complex ways to stratigraphic and lateral
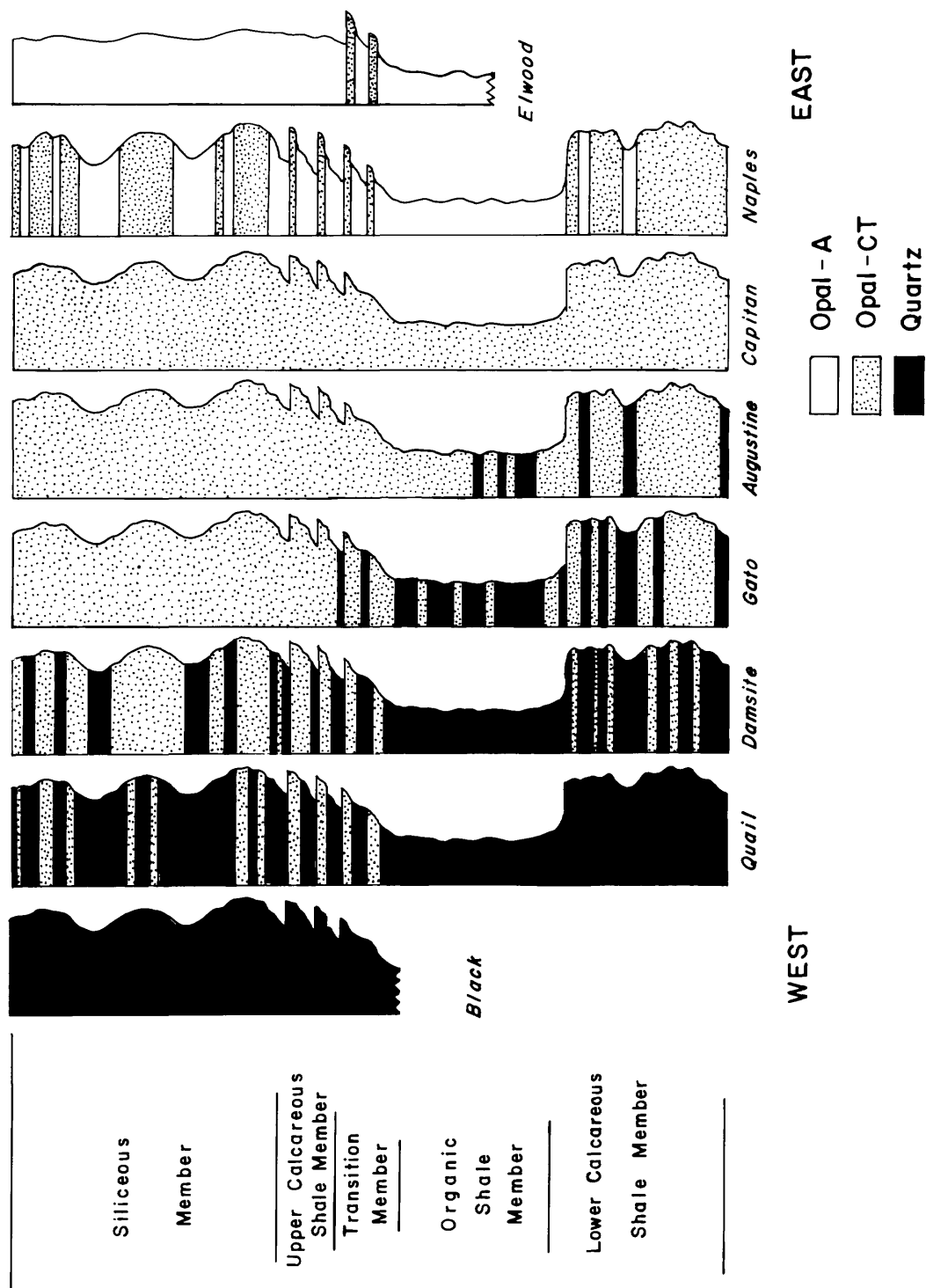
Fig. 27--Pattern of lateral changes in lithology and in principal silica phase for all lithologic members. For most sections, rock types are explained in figure 4; lateral equivalents are shown for the Naples and Elwood sections. The presence of unusual quartz cherts (banded, veined, massive, and lensoid types) is not indicated.

position. In this part of the thesis, therefore, lithology is described separately for each member, except for the upper calcareous shale and transition members which are described together. Silica phases and values of bulk density and porosity are also presented.

Siliceous member. Overall lateral changes in the lithology of the siliceous member are striking. In the east, rocks are almost entirely diatomaceous, with average porosity 60 percent or more. In the central part of the area, the member consists of cherts, porcelanites, and siliceous mudstones--all bearing abundant opal-CT and averaging 35 percent porosity. In the extreme west, cherts, porcelanites, and siliceous mudstones all bear diagenetic quartz and average porosity is only 15 percent. In the following description, each step of these changes is described from east to west (see fig. 27).

The easternmost section of the siliceous member, at Elwood Beach, consists of 70 m of laminated diatomites interbedded with massive diatomaceous mudstones. Nearly all rocks are diatomaceous, with low bulk densities (0.7-0.85 g/cc) and high porosities (60-70 percent). The only exceptions are rare opal-CT chert nodules, averaging 2 mm in thickness and 1 cm in length, which represent less than 0.1 percent of the total section. Seven kilometers west of Elwood Beach, at Naples Beach, most laminated rocks contain opal-CT while detrital-rich siliceous shales and massive siliceous mudstones remain friable, punky, and contain abundant diatom frustules. In outcrop, the siliceous rocks at Naples have large variations in hardness, toughness, and resistance to erosion, and the field aspect of the section differs greatly from that at Elwood Beach, where rocks have little variation in these properties. In detail, however,

sedimentary features show equivalence of the two sections and rocks
at both sections are similarly interbedded in alternating groups of
silica-rich laminated rock and massive detrital-rich rock.

West of Naples, all of the siliceous rocks are harder, tougher,
and more resistant than the diatomaceous shales at Elwood and Naples.
From El Capitan Beach through Gato Canyon (42 km) the siliceous rocks
tend to occur in alternating groups (1-2 m thick) of massive detrital-
rich siliceous mudstones and laminated porcelanites, cherty porcelanites,
and cherts. Bulk densities range from 1.39 to 1.66 g/cc in most rocks
and as high as 1.83 g/cc in cherts. All siliceous rocks as far west
as Gato Canyon contain opal-CT as the principal silica mineral.
At Gato Canyon, however, some siliceous mudstones contain minor quartz
inferred to be diagenetic.

West of Gato Canyon--in Damsite, Wells, Wood, Quail, Black, and
several unnamed canyons north of Black Canyon--the siliceous rocks
have a slightly different field aspect. Toward the west, first
siliceous mudstones and then porcelanous rocks are denser, even though
still flaggy and having matte or grainy surface textures. These denser
rocks contain abundant diagenetic quartz and little to no opal-CT.

Where they first occur, in Damsite, Wells, and Wood Canyons,
quartz rocks are interbedded with opal-CT rocks containing little
diagenetic quartz. Near the base of the siliceous member at Damsite
Canyon, 3.5 km west of Gato Canyon, some siliceous shales and mudstones
are completely quartzose, with bulk densities of 1.90 to 2.00 g/cc
and porosities only 18 to 22 percent. Other siliceous rocks contain
at least a few percent diagenetic quartz, and bulk densities of rocks
with significant amounts range from 1.76 to 1.90 g/cc. In the middle

part of the siliceous member at Wood Canyon, 2 km west of Damsite

Canyon, all siliceous shales and mudstones are apparently completely

quartzose, with bulk densities typical of quartz rocks (1.90-2.0

g/cc). Porcelanites and cherts at Wood Canyon, however, contain only

small amounts of diagenetic quartz, with bulk densities (1.54-1.72

g/cc) more typical of opal-CT rocks.

At the base of the siliceous member in Quail Canyon, 0.5 km west

of Wood Canyon, all rocks contain quartz except cherts and cherty

porcelanites. Near the top of the section in the same canyon, abundant

opal-CT occurs in cherts, porcelanites, and some siliceous mudstones

and shales. In Black Canyon, 1 km northwest of Quail Canyon, no rocks

containing opal-CT were found anywhere in the siliceous member and

quartz is the only silica mineral even in cherts. Bulk densities

range from 1.9 to 2.3 g/cc, with porosities from 0 to 20 percent.

Opal-CT is abundant, however, in the overlying Sisquoc Formation.

Upper calcareous shale and transition members. The lithology

of the upper calcareous shale and transition members varies con-

siderably along the Santa Barbara coast. In the east, diatomaceous rocks

are interbedded with opal-CT cherts; in the middle of the area are

shales, porcelanites, and cherts--all containing abundant opal-CT;

while in the east, cherts, porcelanites, and shales all contain

diagenetic quartz. Another variation is in carbonate minerals--for

while all rocks contain carbonate, only calcite is present in some

sections and disseminated dolomite is widely distributed in others.

Locally, unusual nodular or replacement quartz cherts are also present.

In the following description, the distribution of these features is

described from east to west (see fig. 27).

The easternmost section, at Elwood Beach, contains mainly calcareous diatomites and diatomaceous shales, with low bulk densities (0.8-1.1 g/cc) and high porosities (50-60 percent). In the upper 40 m of strata are rare stratiform chert nodules about 2 mm thick and up to 4 cm long. In the lower strata (transition member), calcareous diatomaceous shales are interlayered with numerous bedded calcareous cherts, usually in groups about 1 m thick. Many of these cherts are quite vitreous, dense (1.9-2.0 g/cc), and all contain opal-CT as the main diagenetic silica mineral. At Naples, also, most strata are diatomaceous while interbedded calcareous cherts contain opal-CT as the principal silica mineral.

West of Naples, however, all of the calcareous rocks in these members are relatively hard and none has the friable punkiness characteristic of the diatomaceous rocks at Elwood and Naples. From El Capitan Beach through San Augustine Canyon the members consist of interbedded calcareous cherts, porcelanites, and shales in which nearly all diagenetic silica is opal-CT. Bulk densities range from 1.37 to 1.80 g/cc (as high as 1.92 g/cc in cherts) and porosities range from 25 to 36 percent (as low as 15 percent in cherts). Scarce bedded dolomites are present, usually near the top of the member, and at Gaviota a few of the uppermost shales contain only dolomite as a carbonate mineral.

West from Gato Canyon the upper calcareous shale member becomes more prominently exposed and west from Cojo Canyon it is the most resistant member. Detailed study of the member east and west of this area shows that lithologies are similar and similarly interbedded-- except that to the west a large proportion of carbonate is dolomite

and the member contains a few pure dolomitic rocks. Also, west from Cojo Canyon there is a prominent (and extremely resistant) massive quartz chert bed, 40 to 80 cm thick, near the top of the members.

At Gato Canyon, and immediately west at Cojo Canyon, no calcite was found in the upper calcareous shale member or, where it is exposed, in the transition member. Dolomite is present in every rock examined-- cherts, porcelanites, and shales. A few beds of pure dolomite are also prominent due to their resistance but represent only 1 to 2 m of section. Opal-CT is nonetheless the principal silica mineral in most rocks at Gato Canyon, except in a few shales which contain only quartz.

At Damsite Canyon, and immediately west in Wells Canyon, most of the rocks are also dolomitic. At least at Damsite, however, calcite is common near the base of the upper calcareous shale member and in the transition member below. Here quartz occurs as the only silica mineral in some dolomitic shales, and most rocks contain a few percent diagenetic quartz. At Wood Canyon, in contrast to exposures in adjacent canyons to the east and west, nearly all the rocks in the upper shale contain calcite as the predominant carbonate mineral. In addition, there are occasional lensoid quartz cherts, usually bearing calcite but occasionally dolomite. Only bedded cherts and cherty porcelanites contain opal-CT. At Quail Canyon, the upper calcareous shale contains carbonate only as dolomite, and several beds of pure dolomite are present. All rocks contain abundant diagenetic quartz except for cherts and cherty porcelanites which predominantly bear opal-CT. A few lensoid and massive quartz cherts, however, are also present. At Black Canyon, all rocks contain diagenetic quartz without opal-CT;

dolomite predominates in the upper calcareous shale member, and calcite predominates in the transition member.

Organic shale member. The organic shale member shows little lateral variation in the field. Shales are everywhere relatively punky and friable, especially where exposed to surface weathering, and the member is everywhere the least resistant of the members (see fig. 27). Siliceous interbeds occur widely but they are a minor fraction of the section. As far as can be determined there is no dolomite in any of the shales or more siliceous rocks in the member, although a few pure dolomite beds are present.

At Naples, the most eastern exposure examined of the organic shale, the member consists of 90 m of punky, dark, unresistant strata, which are mainly diatomaceous. Bulk densities are low (0.9-1.1 g/cc) and porosities high (50-60 percent). At El Capitan Beach, typical shales are friable and punky but rocks chip when fractured and the member is slightly more resistant than at Naples. Typical shales are denser (1.2-1.4 g/cc) and less porous (39-44 percent) than at Naples. These differences are due to formation of opal-CT--every sample examined at El Capitan Beach contains opal-CT without diatom frustules. At Gaviota, where the member is only moderately exposed, both opal-CT and quartz are present.

Unusual quartz cherts, a striking feature in the organic shale member, occur in three adjacent canyons (Agujas, Bulito, and San Augustine Canyons) in the central part of the area west of Gaviota. These quartz cherts occur either as massive beds, up to 0.5 m thick, or as veined cores of highly siliceous opal-CT rocks. Although prominent in the field because of their resistance to erosion and because they

are quite black even when weathered, unusual quartz cherts represent only a small proportion of the section and are unevenly distributed. In San Augustine Canyon, where they are most abundant, unusual quartz cherts total only 3 m and all beds lie between 25 and 40 m below the top of the member.

In other respects the organic shale member at San Augustine Canyon is typical—the shale itself is relatively soft and easily weathered. Some analyzed samples contain opal-CT but a few contain only quartz. All bulk densities seem to be greater (1.54-1.62 g/cc) than at El Capitan and porosities are smaller (26-33 percent). West of San Augustine Canyon the member is poorly exposed except at Wood Canyon. A few shales analyzed from Damsite Canyon are quartzose. At Wood Canyon all samples contain only quartz and all samples are denser (1.75-1.97 g/cc) and less porous (22-27 percent) than at San Augustine.

Lower calcareous shale member. Laterally, the lower part of the lower calcareous shale member varies only slightly in the field (fig. 24). Everywhere the rocks are variably resistant mudstones which are in part dolomitic. Opal-CT is the principal diagenetic silica mineral in the east, quartz in the west, while both phases are present in the central part of the area. Lithologic variation is more pronounced in the upper part of the member, which differs from the lower part in containing more abundant shale and also in containing mainly diatomaceous rocks in the Naples section. In other sections, however, silica phases are similar in both the upper and lower parts of the member (see fig. 27).

The easternmost exposure examined, at Naples, consists largely of calcareous mudstones with different proportions of opal-CT and detrital minerals, producing more and less resistant beds. Many of these mudstones contain a few percent dolomite and some are quite dolomitic, especially near the base of the member. In the middle of the lower calcareous shale at Naples is an intraformational breccia described by Bramlette (1946). Rocks above the breccia are less massive and more finely layered and calcareous diatomaceous shales predominate in this part of the member.

West of Naples, the upper part of the lower calcareous shale is more resistant than at Naples and rocks in the lower part are everywhere hard and tough. No diatom frustules were detected in any sample. At El Capitan and Refugio Beaches all mudstones and shales contain opal-CT as the only diagenetic silica mineral. Typical rocks have bulk densities ranging from 1.38 to 1.64 g/cc, with porosities of 32 to 43 percent. Fourteen kilometers west at Gaviota, most rocks contain a few percent diagenetic quartz and some mudstones and shales contain diagenetic silica only as quartz. The latter rocks are distinctly denser (1.74-1.95 g/cc) and less porous (23-31 percent) than opal-CT rocks farther east.

West of Gaviota, the abundance of finely layered rock increases somewhat, although the member still consists mainly of blocky calcareous and partly dolomitic mudstones. At San Augustine Canyon all rocks contain some opal-CT but some shales have formed small amounts of diagenetic quartz.

West of San Augustine Canyon, the basal part of the lower calcareous shale, where exposed, tends to be more dolomitic than it is further

east. At Gato Canyon, some mudstones and shales contain diagenetic

silica only as quartz, all mudstones and shales contain at least some

diagenetic quartz, while porcelanites and cherts contain only opal-CT.

Farther west at Cojo Canyon, where the lower calcareous shale is

poorly exposed, a sandstone occurs near the base of the member.

Offshore, this horizon is also sandy (U.S. Geological Survey, 1974).

At Damsite Canyon, most of the basal shales and mudstones are

dolomitic while the upper rocks are calcareous. Opal-CT dominates

in cherts and cherty porcelanites although some quartz has formed

in all rocks. Several irregularly veined, banded quartz cherts are

present in opal-CT chert beds. Calcareous opal-CT rocks persist to

Wells Canyon, immediately west of Damsite Canyon.

In Wood Canyon, however, no opal-CT is apparently present anywhere

in the lower calcareous shale member. As in the upper calcareous

shale at the same canyon, lensoid quartz cherts occur discontinuously

in certain layers. At Quail Canyon, only 20 m of strata in the lower

calcareous shale are exposed. Here the basal rocks are not dolomitic

but are dark calcareous shales with quartz as the only silica mineral.

There are, however, no unusual types of quartz chert.

Conclusions. Lateral relationships in the different members of

the Monterey Formation along the Santa Barbara coast indicate that

most diagenetic changes consistently occurred in a simple sequence

as temperature increased to the west. The sequence, which is marked

by formation of silica phases at different times in different types

of rock, can be outlined by the following stages:

1. diatomites + diatomaceous shales and diatomaceous mudstones

2. opal-CT cherts + diatomaceous shales and diatomaceous mudstones

3. opal-CT cherts + opal-CT porcelanites + diatomaceous shales and diatomaceous mudstones

4. opal-CT cherts + opal-CT porcelanites + opal-CT siliceous shales and opal-CT siliceous mudstones

5. opal-CT cherts + opal-CT porcelanites + quartz siliceous shales and quartz siliceous mudstones

6. opal-CT cherts + quartz porcelanites + quartz siliceous shales and quartz siliceous mudstones

7. quartz cherts + quartz porcelanites + quartz siliceous shales and quartz siliceous mudstones.

Differences in timing are important because they show that silica phase changes took place independently in each layer of rock and did not result simply from massive influxes of meteoric water.

Porosity changes also took place independently in each layer of rock. Interbedded rocks with different silica phases generally have distinctly different bulk densities and porosities, while values are generally similar in rocks of the same type with the same silica phase from different localities. These relationships show that most porosity changes were closely associated with silica phase changes rather than with specific conditions of temperature and burial depth. Exceptions are organic shales, in which porosity values decrease gradually westward, apparently irrespectively of silica phase changes.

Lateral relationships in the calcareous members indicate that some diagenetic changes were not consistently produced by increased temperature and burial depth. For this reason, dolomitization and formation of unusual (banded, veined, massive, and lensoid) quartz cherts are not included in the typical diagenetic stages outlined.

Effects of Bulk Composition on Timing of Silica Phase Changes

In this part of the thesis, evidence is examined which relates timing of silica phase changes to compositional variables. First, effects due to detrital minerals will be considered in rocks of the siliceous member. Results are then compared with timing in calcareous and dolomitic rocks--particularly rocks in the upper calcareous shale member which are close in stratigraphic position to rocks in the siliceous member. Finally, effects of organic matter are examined, by comparing timing of silica phase changes in rocks of the organic shale member with timing in overlying and underlying rocks.

Detrital minerals. Sets of rocks sampled in the siliceous member are similar in age, and each set was collected within less than 35 stratigraphic meters. Any variation in silica phase within sets, therefore, should be due only to differences in bulk composition-- mainly in relative abundances of silica and detrital minerals.

Timing of silica phase changes is closely related to detrital content (fig. 28). Lateral distribution suggests that opal-CT formed progressively later as detrital content increased and that the most detrital-rich rocks retained diatom frustules the longest. Quartz, by contrast, formed progressively earlier as detrital content increased. Differences in timing of complete quartzification are not due simply to the lesser abundance of opal-CT in detrital rocks. Greater actual amounts of diagenetic quartz formed earlier in detrital-rich rocks (fig. 29).

D-spacings of opal-CT are also affected by detrital content and values at each locality vary with a range of about 0.02 $\overset{\circ}{A}$, decreasing with relative detrital content (fig. 30). Laterally, values in rocks
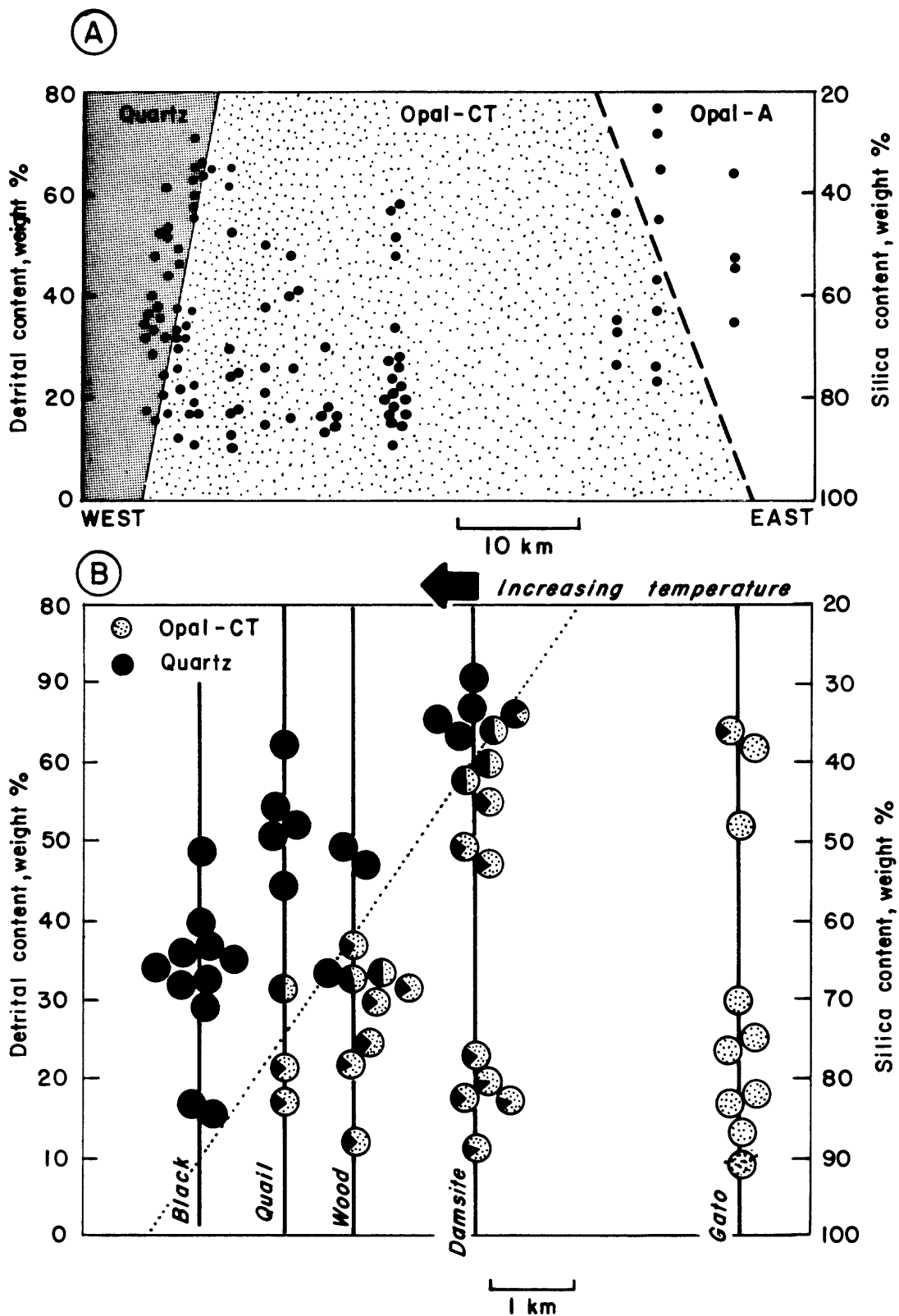
Fig. 28--Overall lateral relation between detrital content and timing
of silica phase transformations in the siliceous member. Each
lateral position is represented by closely associated samples,
and sample sets are stratigraphically equivalent. (Silica and
detrital contents on organic-free basis.) (A) Overall pattern,
with sample positions (•) indicated. (B) Detail between Gato
and Black Canyons, indicating silica phase of each sample.
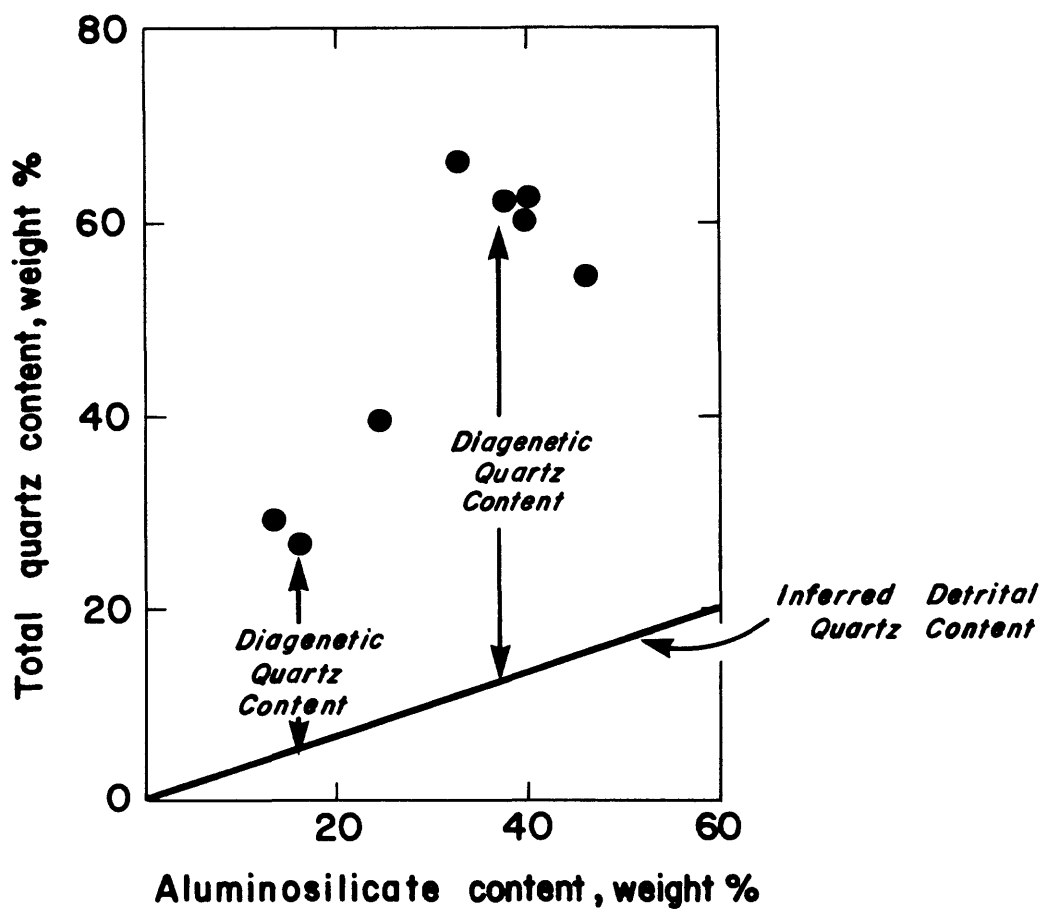
Fig. 29--Abundance of quartz in closely associated rocks during a
middle stage of quartz formation. Note the high abundance
of diagenetic quartz in detrital-rich rocks. Samples are
from the lower part of the siliceous member, Quail Canyon.
(Values on organic-free basis; for derivation of detrital
quartz contents, see Appendix B.)
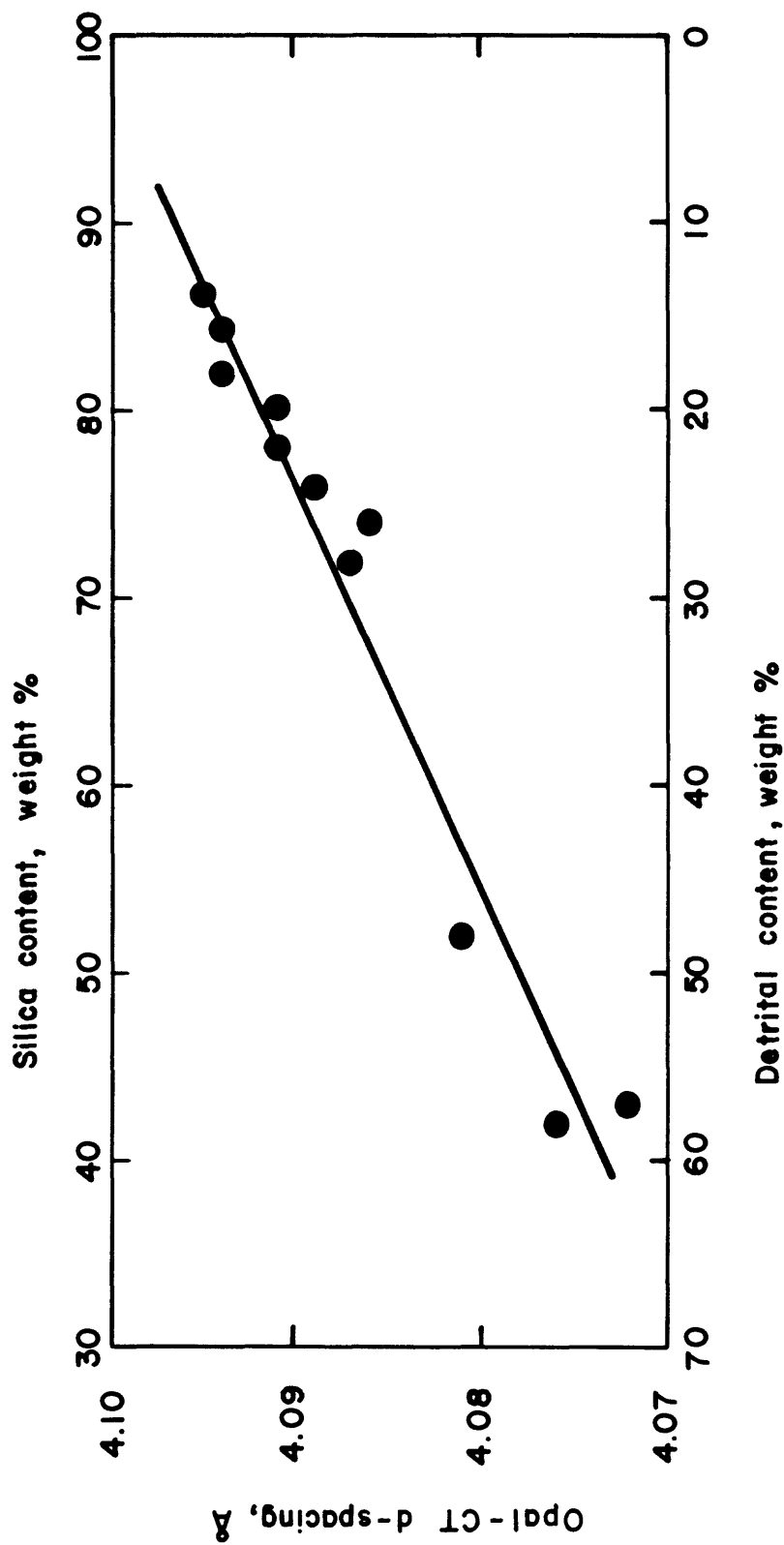
Fig. 30--Correlation between opal-CT d-spacings and detrital content in closely associated rocks from the siliceous member, Gaviota Beach. Values are from samples within 20 stratigraphic meters. (Silica and detrital contents on organic-free basis.)

of each composition generally decrease westward (with increasing

temperature and burial), in accord with lateral changes in silica

phases. In addition, quartz formed in rocks of each composition only

where opal-CT with a d-spacing of 4.07 $\overset{o}{A}$ or less was subjected to greater

temperature and burial (fig. 31). Differences in timing of diagenetic

quartz formation therefore empirically relate to differences in opal-CT

"ordering."

Carbonate minerals. Rocks of the siliceous and upper calcareous

shale members are similar in age, and most sample sets in the two

members are separated by less than 60 stratigraphic meters. Rocks

from these two members in the same section, then, experienced similar

(although not identical) temperature and burial depth. Comparison

of silica phases in the two members should therefore indicate any

major effect due to the presence of carbonate.

In general, results show that carbonate had little effect on

silica diagenesis, as indicated by comparison of lithologies in the

siliceous member and in the upper calcareous shale member (fig. 27).

Overall comparisons of analytical data include, in some sections,

samples from the somewhat older and more deeply buried transition

member. Taking this into account, analytical data show that timing

of silica phase changes did not significantly differ in carbonate-

bearing rocks and in carbonate-free rocks with equal relative detrital

contents (fig. 32). In addition, the pattern of opal-CT d-spacings

is similar in both groups of rocks (fig. 33, cf. fig. 31).

Because calcite is widely thought to affect silica diagenesis

(e.g., Lancelot, 1973; Robertson, 1977), detailed evidence on timing

is presented relative to the presence and also to the amount of
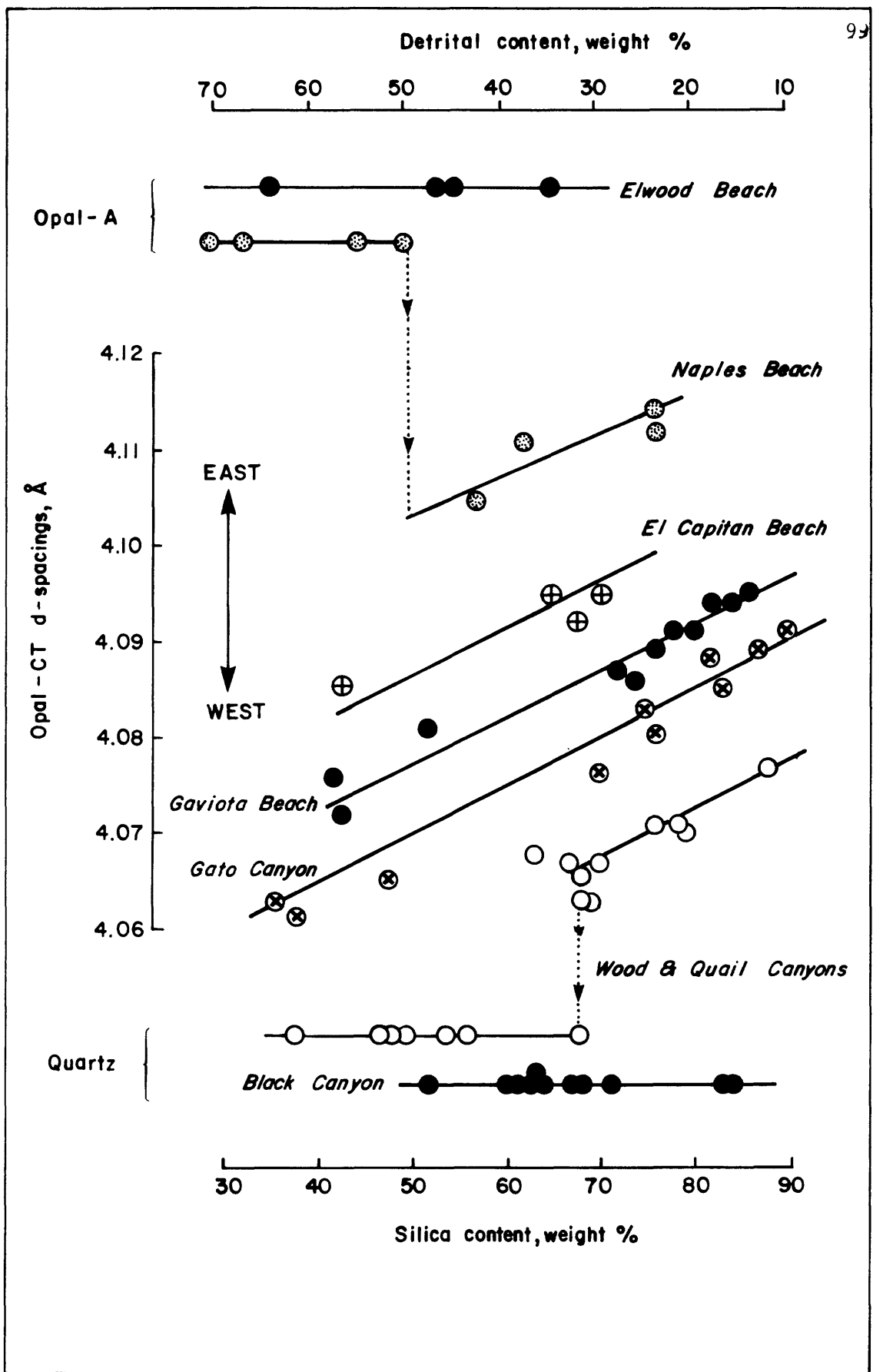
Fig. 31--Lateral pattern of changes in opal-CT d-spacings for rocks in the siliceous member. Each section is represented by closely associated samples, and sample sets are stratigraphically equivalent. (Silica and detrital contents on organic-free basis.)
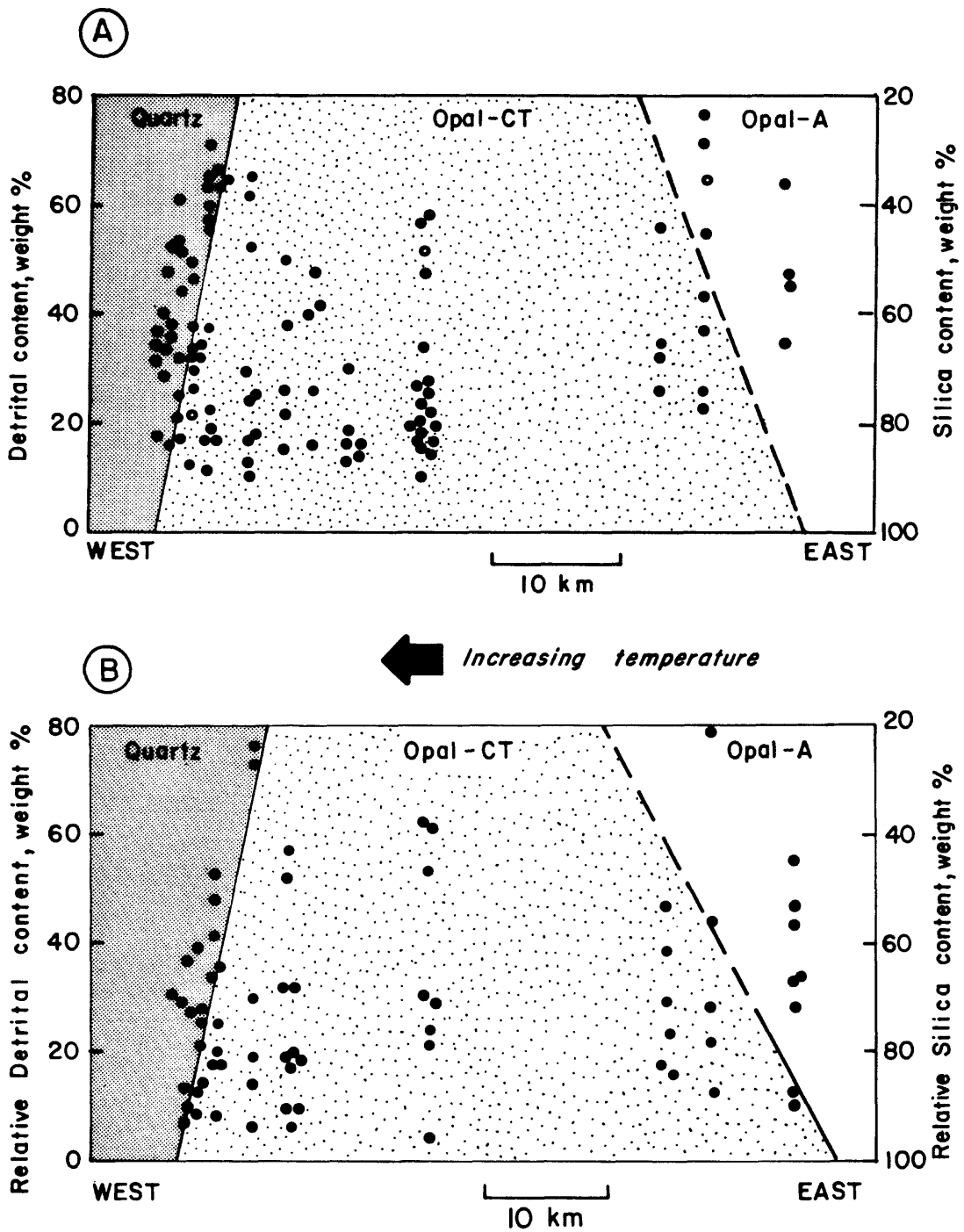
Fig. 32--Comparison of timing of silica phase transformations in
associated carbonate-bearing and carbonate-free rocks.
(A) Rocks from the lower part of the siliceous member (as
on fig. 28A). (B) Rocks from the transition and upper
calcareous shale members.
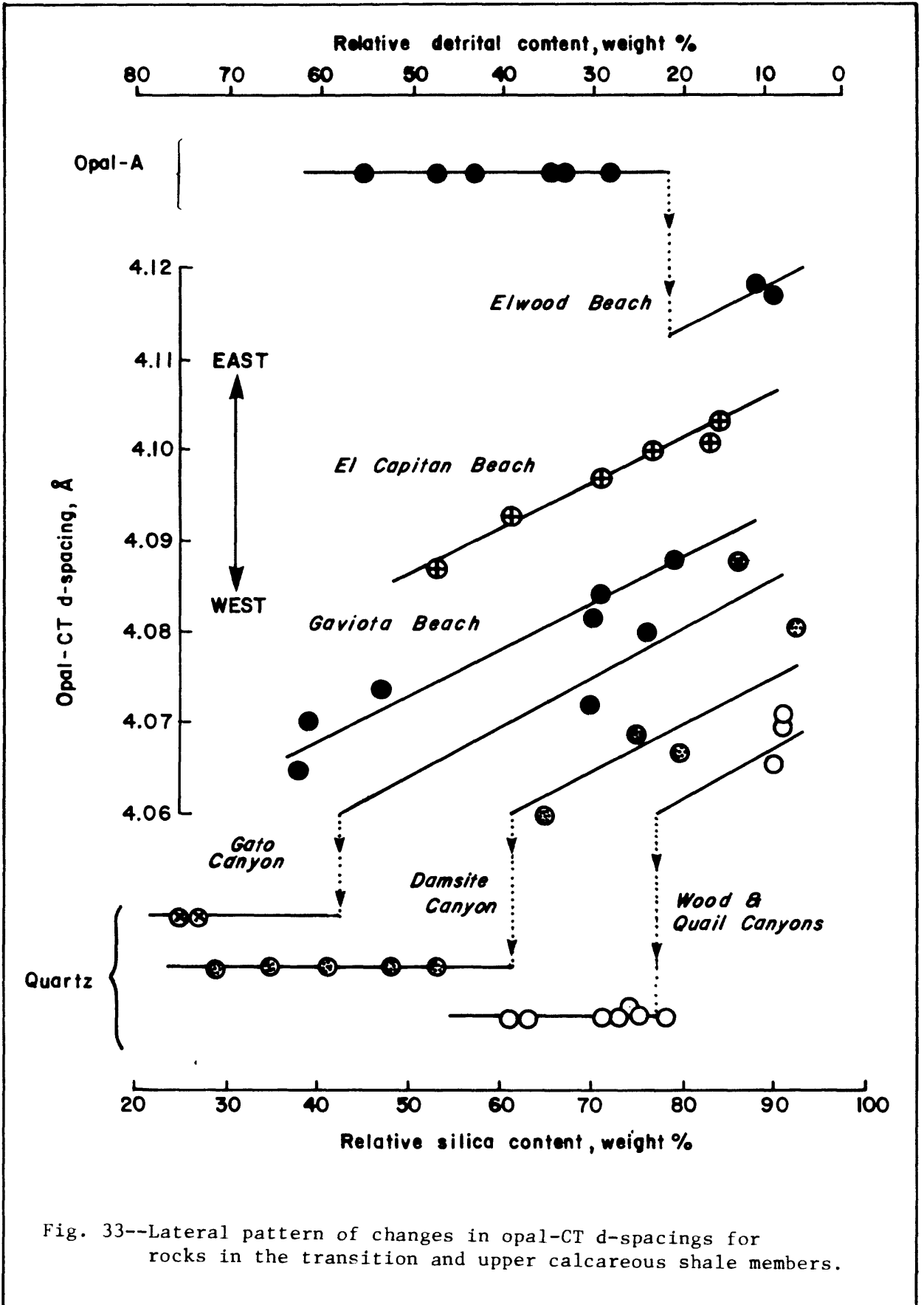
Fig. 33--Lateral pattern of changes in opal-CT d-spacings for
rocks in the transition and upper calcareous shale members.

carbonate. Two sets of data are considered: comparisons between rocks in the upper calcareous shale and siliceous members; and relationships among compositional variables of rocks in the lower calcareous shale member. Data are described for each silica phase change, in order of its occurrence with increasing temperature and burial depth.

Early quartz formation. Although carbonate generally had no effect on the nature and timing of silica phase changes, one exception is apparent early in diagenesis. Quartz contents of carbonate-free siliceous rocks with "disordered" opal-CT are more or less proportional to Al_2O_3 content. Compared to this proportion of quartz, which is considered to be entirely detrital, some calcareous rocks in which the main silica phase is "disordered" opal-CT contain excess quartz inferred to be diagenetic (fig. 34). This "early" diagenetic quartz is restricted to rocks with relatively high silica and low detrital contents (diagenetic silica/detrital minerals $\geq$ 8) and is unrelated to the abundance of calcite. Early diagenetic quartz is petrographically apparent mainly as fillings of foraminiferal tests, in a few cases as microlenses.

The exact time of formation of this quartz, relative to opal-CT formation, cannot be determined from available evidence, since diatomaceous equivalents of these rocks are not present. Early quartz did form prior to widespread formation of opal-CT, however, as quartz occurs in calcareous opal-CT cherts from both the Elwood and Naples sections, where most rocks are diatomaceous.

Timing of opal-CT formation. Most silica dissolved from diatom frustules formed opal-CT, and timing of opal-CT formation
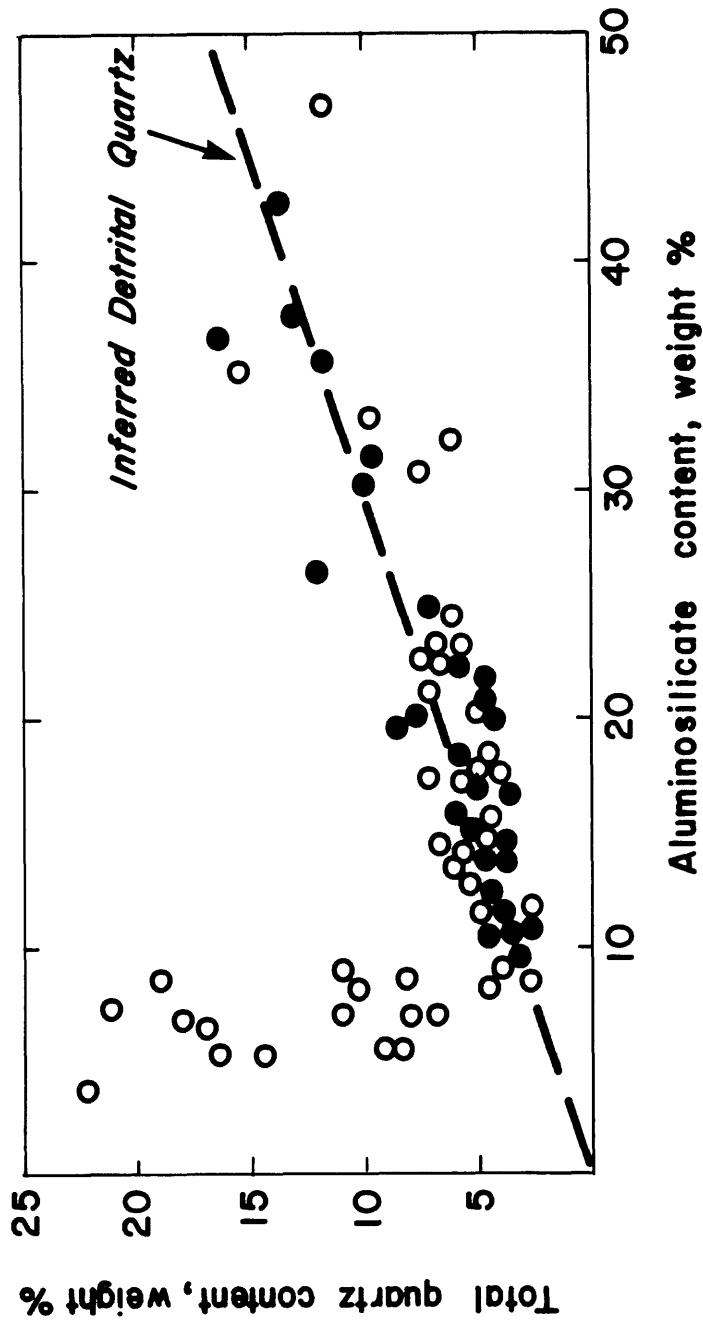
Fig. 34—Relation between quartz content and aluminosilicate content in opal-CT rocks, showing early quartz formation in calcareous rocks with low detrital contents. Values are from rocks with opal-CT d-spacings $\geq$4.080 Å east of Gato Canyon. (Quartz content and aluminosilicate content are given as a percent of the sum of silica + detrital minerals.)

does not appear to have been greatly affected by the presence of calcite. As a general result, this conclusion is based on field relationships, by comparison of lithologies in the three eastern sections (fig. 27). At Elwood Beach, the easternmost section, nearly all rocks are diatomaceous in both the siliceous member and the upper calcareous shale member, while bedded opal-CT rocks are not present stratigraphically above the transition member. Seven kilometers west, in the Naples section, both the siliceous and upper calcareous shale members contain bedded opal-CT rocks, as well as detrital-rich shales and mudstones which are diatomaceous. Farther west, at El Capitan Beach, all rocks in the two members contain opal-CT. Opal-CT therefore formed at approximately the same time in rocks with similar relative detrital contents, irrespective of the presence of calcite.

In general, analytical data from the Elwood and Naples sections support this conclusion. In the transition member at the Elwood section, for example, opal-CT is present in bedded cherts, and comparison of bulk compositions with silica phases suggests that opal-CT formed where relative detrital contents were less than about 20 percent rather than where calcite was abundant (fig. 35A). Calcite therefore did not generally promote formation of extensive opal-CT. Some evidence suggests, however, that calcite may have slightly retarded formation of opal-CT. In the siliceous member at Naples, only those rocks with 40 percent or more detrital minerals still retain diatom frustules and more detrital-rich rocks usually contain some opal-CT; in contrast, calcite-bearing rocks with 40 percent or higher relative detrital contents contain abundant diatom frustules (and no opal-CT)
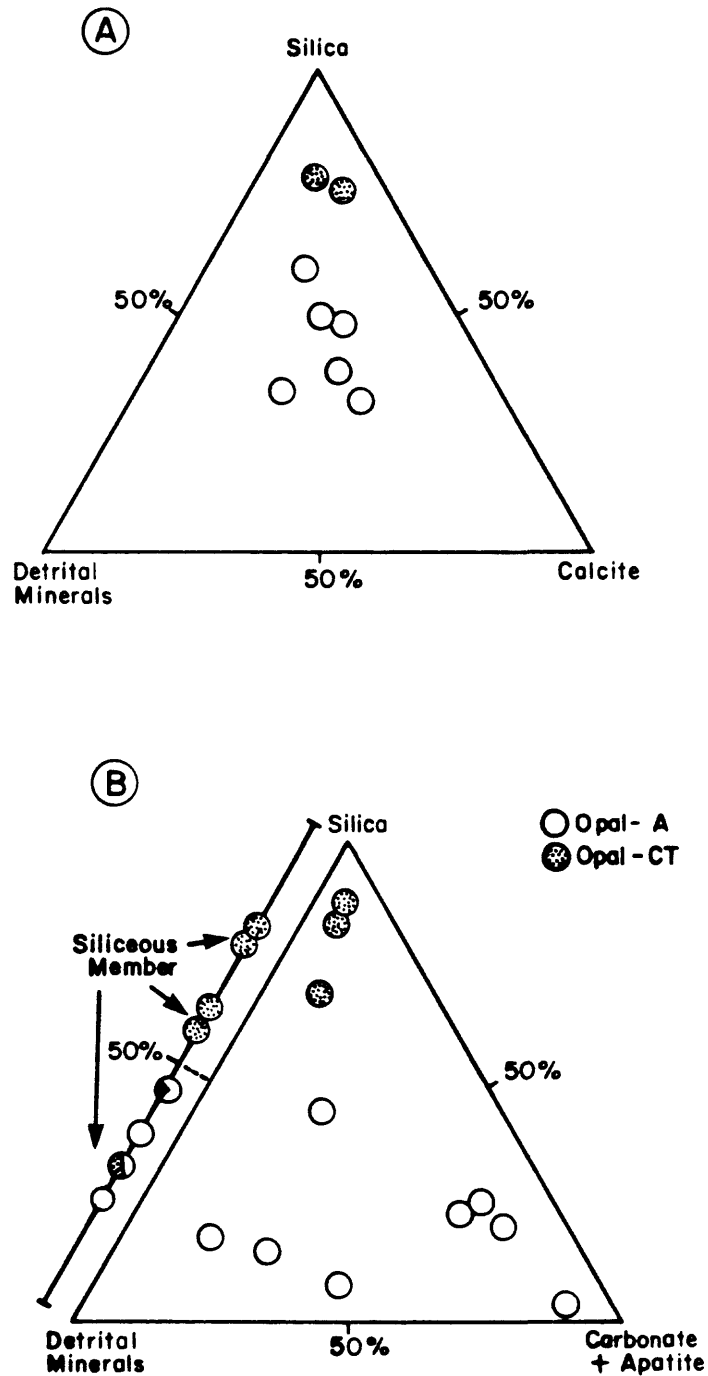
Fig. 35--(A) Correlation between timing of opal-CT formation and
relative detrital content in closely associated calcareous
rocks, transition member, Elwood Beach. (Components in
weight percent, organic-free basis.) (B) Comparison of
timing of opal-CT formation in associated calcareous and
carbonate-free rocks, Naples Beach. Along bar at left,
rocks from the siliceous member; in triangular diagram,
post-Relizian calcareous rocks underlying the siliceous
member. (Components in weight percent, organic-free basis.)

as much as 180 m stratigraphically below the siliceous member (fig. 35B).
Since the calcareous diatomaceous rocks at Naples are older (as old
as early Luisian) as well as more deeply buried than rocks in the
siliceous member, calcite appears to have slightly retarded opal-CT
formation. The effect is not large, however, and data are too sparse
for a firm conclusion.

Values of opal-CT d-spacings. D-spacings of opal-CT
were apparently not affected by either calcite or dolomite. At El
Capitan Beach, for example, opal-CT rocks from the upper calcareous
shale member, 40 m below the siliceous rocks analyzed, all contain
calcite. When rocks of equal relative detrital content are compared,
however, d-spacings of opal-CT in the calcareous rocks are similar
to those in the noncalcareous rocks of the siliceous member (fig. 36).
In addition, at Gaviota, several samples analyzed from the upper
calcareous shale member, within 40 m of the siliceous rocks analyzed,
contain dolomite. Comparison between component compositions and
opal-CT d-spacings indicates that neither the presence nor amount
of either carbonate mineral affected the d-spacing (fig. 37).

Timing of quartz formation. Timing of quartz formation,
except in special cases early in diagenesis, was not generally affected
by calcite or dolomite. In Damsite Canyon, for example, both the
upper calcareous shale member and the lower part of the siliceous
member consist of interbedded rocks with different silica phases,
from predominantly opal-CT to predominantly diagenetic quartz.
Carbonate-bearing rocks contain somewhat more diagenetic quartz than
carbonate-free rocks of similar relative detrital content (fig. 38A),
but the sample sets were located 70 stratigraphic meters apart. Two
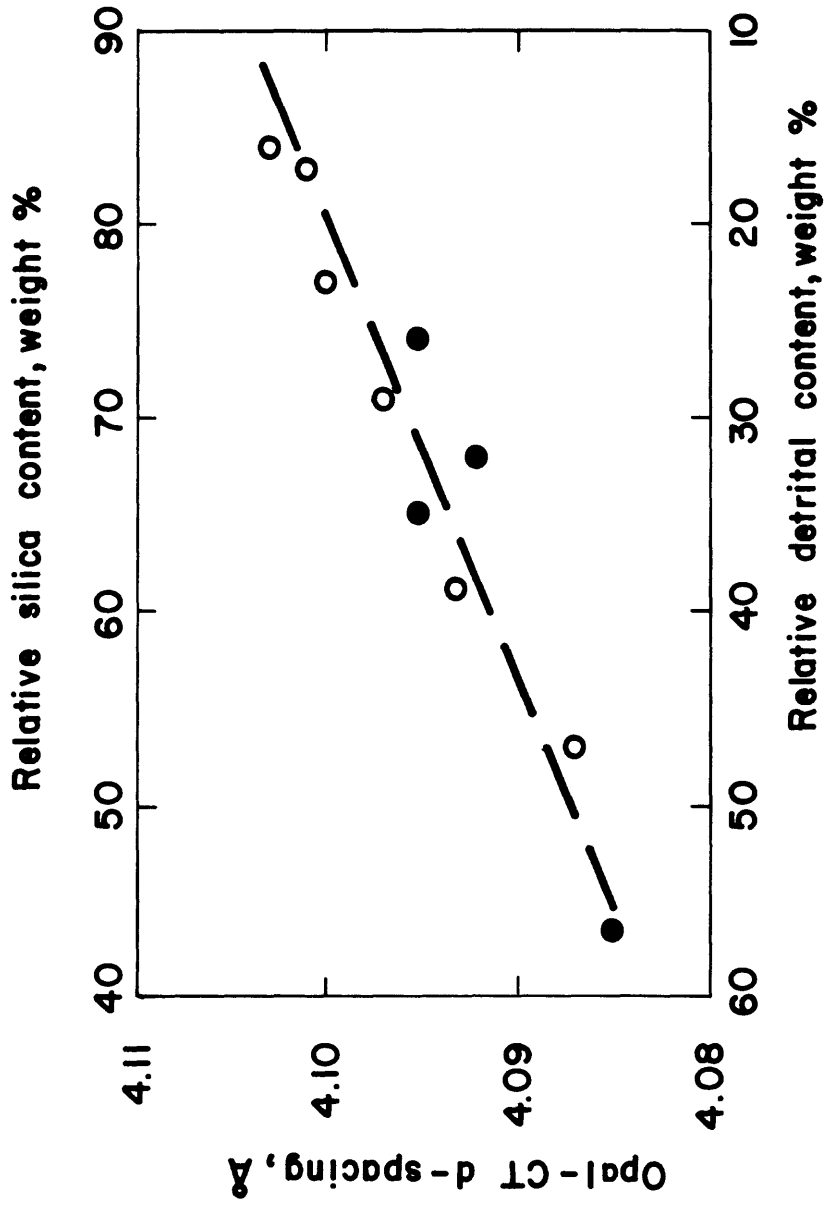
Fig. 36--Comparison of opal-CT d-spacings in closely associated calcareous (o) and carbonate-free (●) rocks. Values are from samples within about 40 stratigraphic meters, siliceous member and upper calcareous shale member, El Capitan Beach.
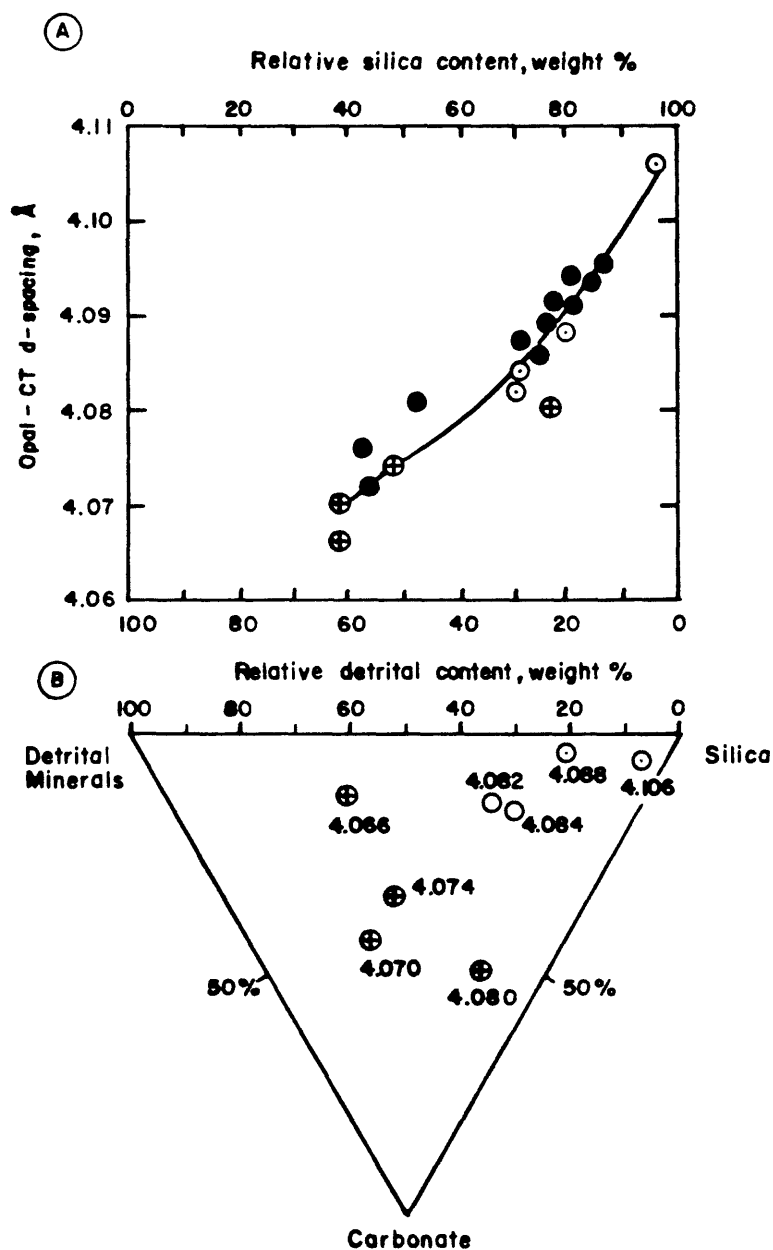
Fig. 37—Comparison of opal-CT d-spacings in closely associated
calcareous (o), dolomitic (⊕), and carbonate-free (•)
rocks, Gaviota Beach. (A) Correlation between opal-CT
d-spacings and relative detrital content, upper calcareous
shale and siliceous members. (B) Relation between opal-CT
d-spacings (in A) and component compositions (in weight percent,
organic-free basis), upper calcareous shale member.
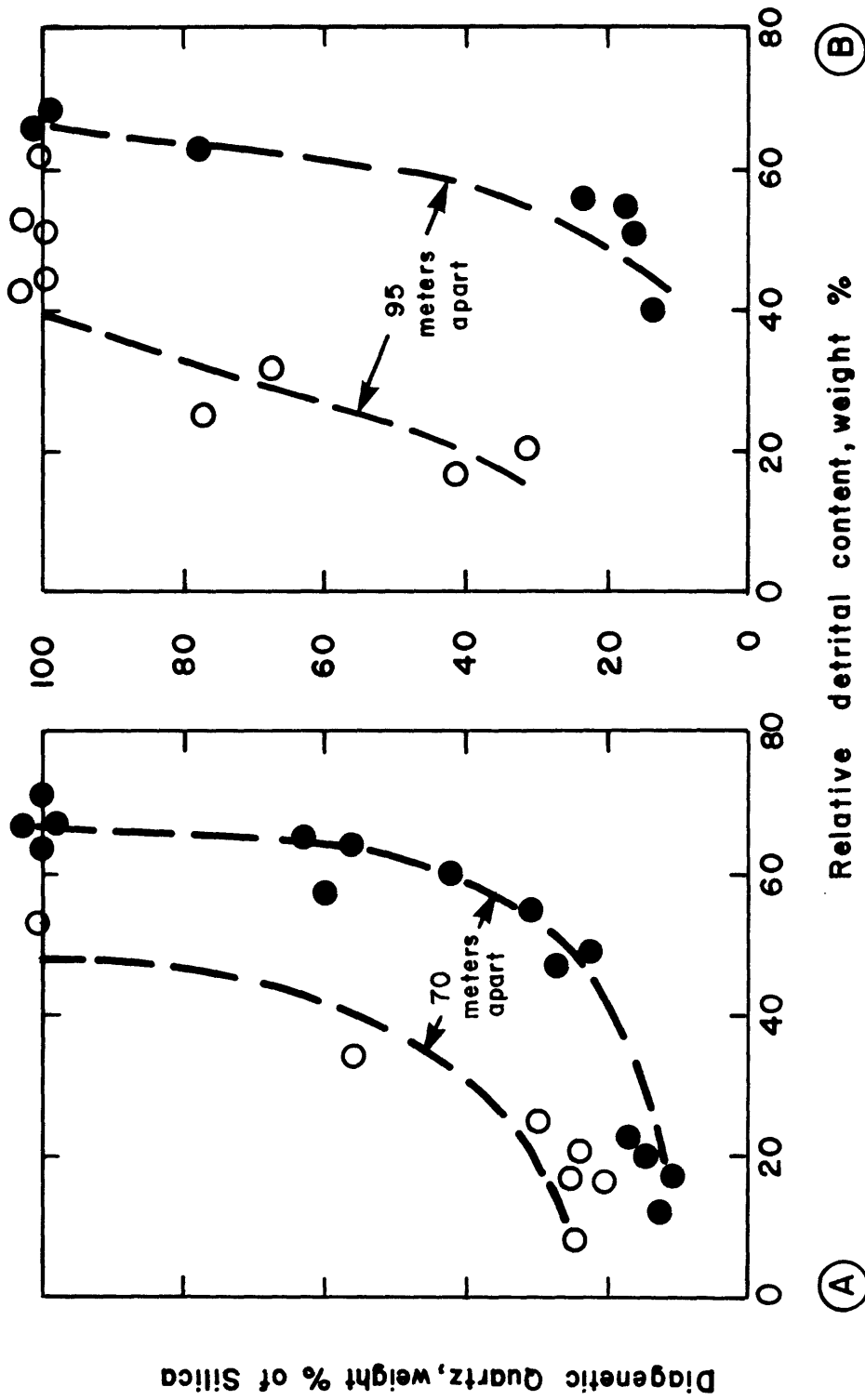
Fig. 38—Comparison of timing of quartz formation in associated carbonate-bearing and carbonate-free rocks. (A) Changes in quartz content between a set of carbonate-free rocks (●) and a set of carbonate-bearing rocks (o) sampled 70 stratigraphic meters apart; siliceous and upper calcareous shale members, Damsite Canyon. (B) Changes in quartz content between two sets of carbonate-free rocks sampled 95 stratigraphic meters apart; middle (●) and base (o) of the siliceous member, Quail Canyon.

sample sets entirely within the siliceous member at Quail Canyon

that are separated by 95 stratigraphic meters show comparable differences

in proportions of diagenetic silica found as quartz (fig. 38B). Car-

bonate therefore apparently had little effect on the timing of quartz

formation.

This conclusion is supported by analytical data from the lower

calcareous shale member, in which abundant quartz formed earliest in

rocks with high relative detrital contents, whether bearing calcite

or dolomite. At Gaviota dolomite, calcite, opal-CT, and quartz all

occur in typical mudstones, but the quartz rocks all have greater

relative detrital contents than the opal-CT rocks (fig. 39).

Surprisingly, the effect of detrital content persists even in rocks

which are highly calcareous. In the lower calcareous shale at Gato

Canyon some rocks contain so much calcite that insoluble residues must

be prepared to identify opal-CT, which has a high threshold of

detectability by X-ray diffraction. In such rocks small analytical

errors in chemical analysis also decrease the precision of estimates

of relative detrital contents. Nonetheless quartz is the only

silica mineral in rocks with high relative detrital contents and

opal-CT persists in rocks, with as much as 85 percent calcite, having

low relative detrital contents (fig. 40).

Organic matter. Since organic matter contents broadly correlate

with detrital mineral contents, the effects of these two variables

are, in general, difficult to separate. In the organic shale member,

however, organic matter contents are generally two to three times

as great as values in rocks of comparable organic-free component

compositions in the other calcareous members. Evidence on the effect
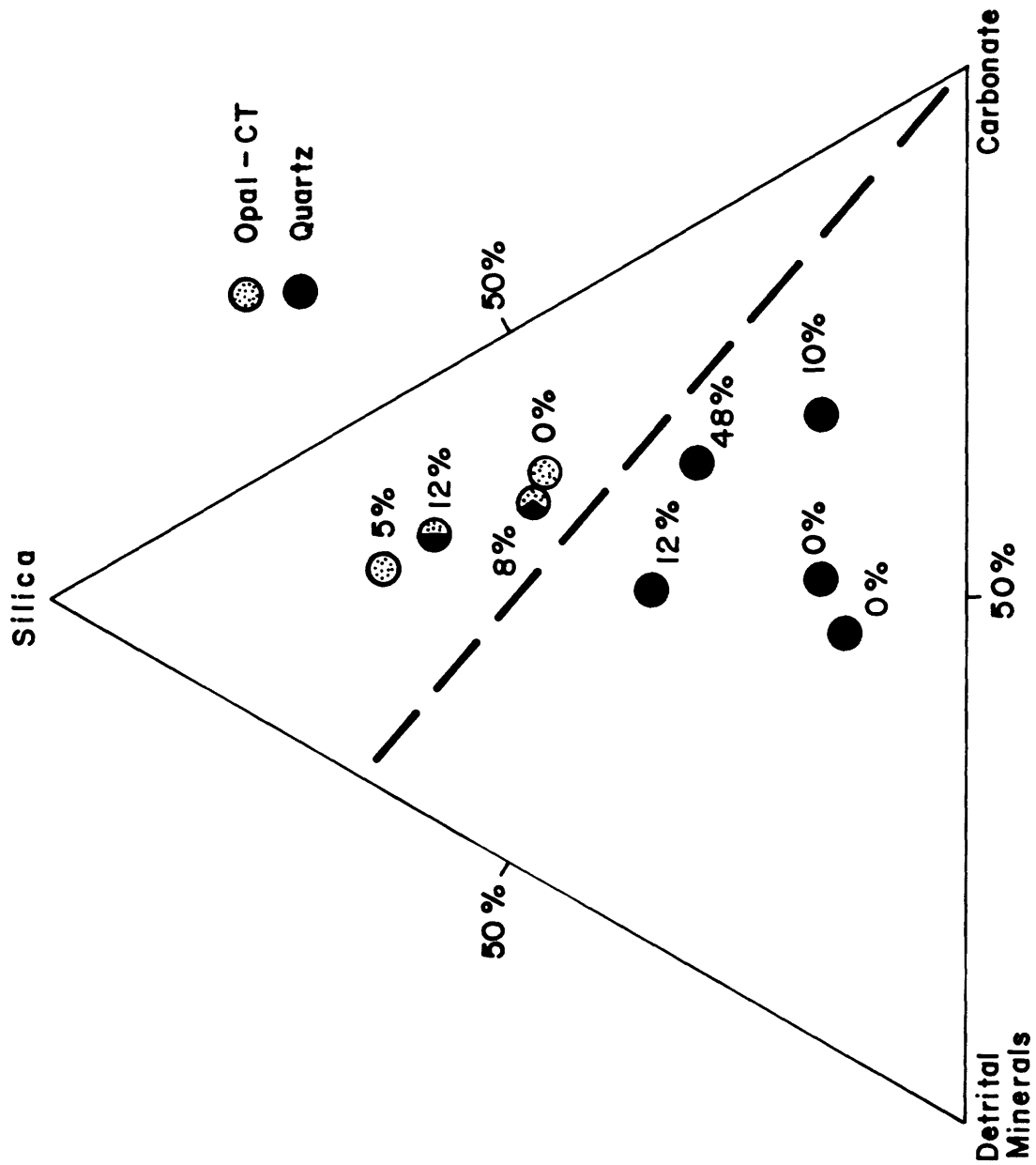
Fig. 39--Correlation between timing of quartz formation and relative detrital content in closely associated carbonate-bearing rocks, lower calcareous shale member, Gaviota Canyon. The figure next to each sample indicates the percent of carbonate minerals in dolomite. (Components in weight percent, organic-free basis.)

112
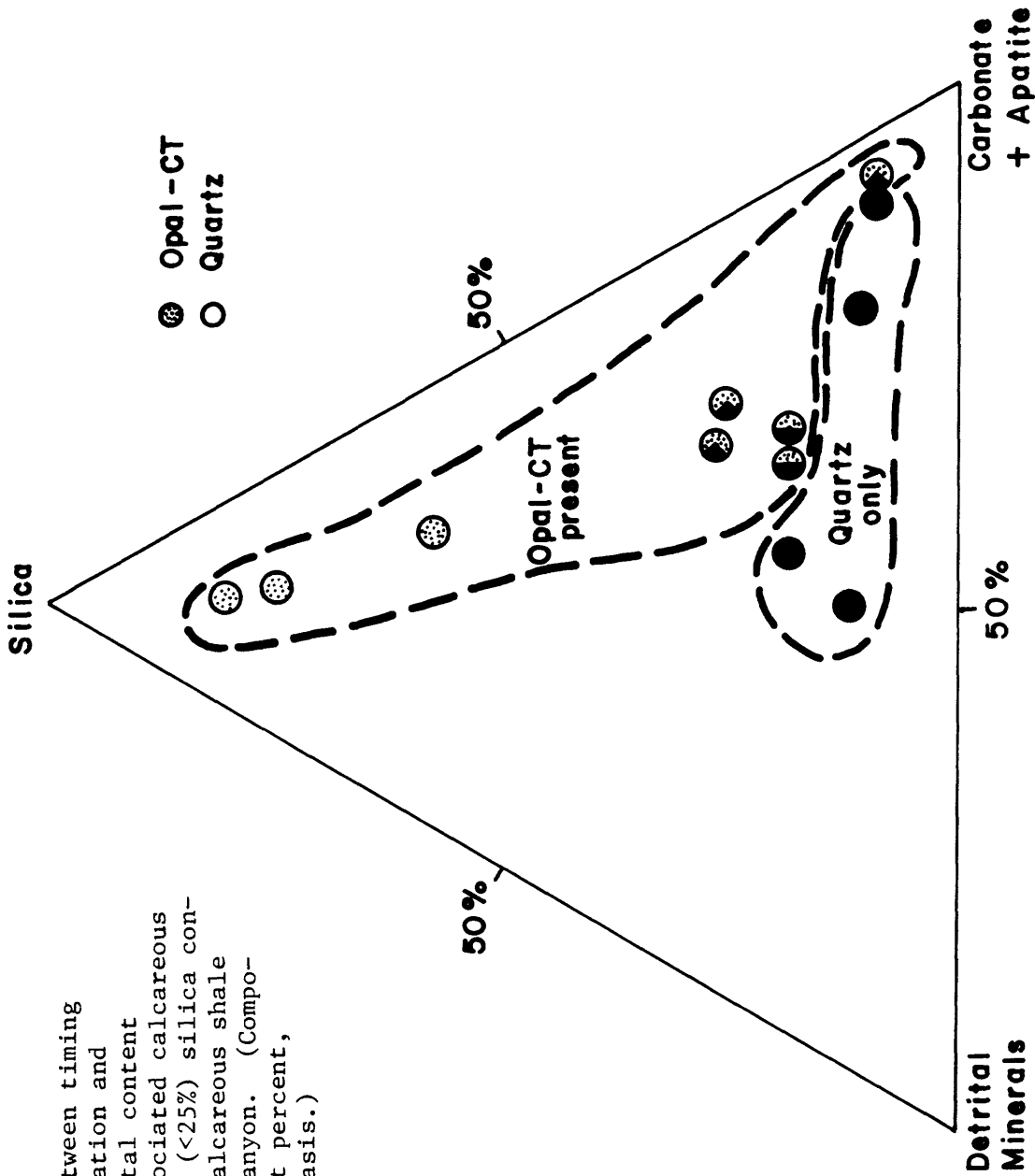
Fig. 40--Correlation between timing of quartz formation and relative detrital content in closely associated calcareous rocks with low (<25%) silica contents, lower calcareous shale member, Gato Canyon. (Components in weight percent, organic-free basis.)

of organic matter is therefore drawn from comparison of rocks in the organic shale member with rocks in the overlying and underlying members.

Silica phases in the organic shale member are related to relative detrital contents, as in other members (fig. 41). In addition, the distribution of silica phases suggests that diagenesis in each section of the organic shale member was intermediate between that in the overlying upper calcareous shale and transition members and that in the underlying lower calcareous shale member. Because of age differences between these members, this relationship does not rule out small effects of organic matter, but large effects are unlikely.

Opal-CT d-spacings are unreliable in most organic shales because of high relative detrital contents (Appendix D). At El Capitan, however, opal-CT d-spacings of two rocks with moderate relative detrital contents were measured and compared with values in calcareous rocks with one-third as much organic matter. Values are quite similar (fig. 42), suggesting that organic matter had little effect on opal-CT d-spacings.

Lateral Irregularities

Although silica phases generally progress westward from amorphous opal to opal-CT to quartz, an exception to this pattern is observed in the lower calcareous shale at Gaviota and San Augustine Canyons (fig. 43). An exception is also observed to the westward decrease of opal-CT d-spacings in rocks from the siliceous member at Coyote Canyon, where d-spacings are higher than farther east (at Gaviota) or farther west (at San Augustine Canyon) (fig. 44).
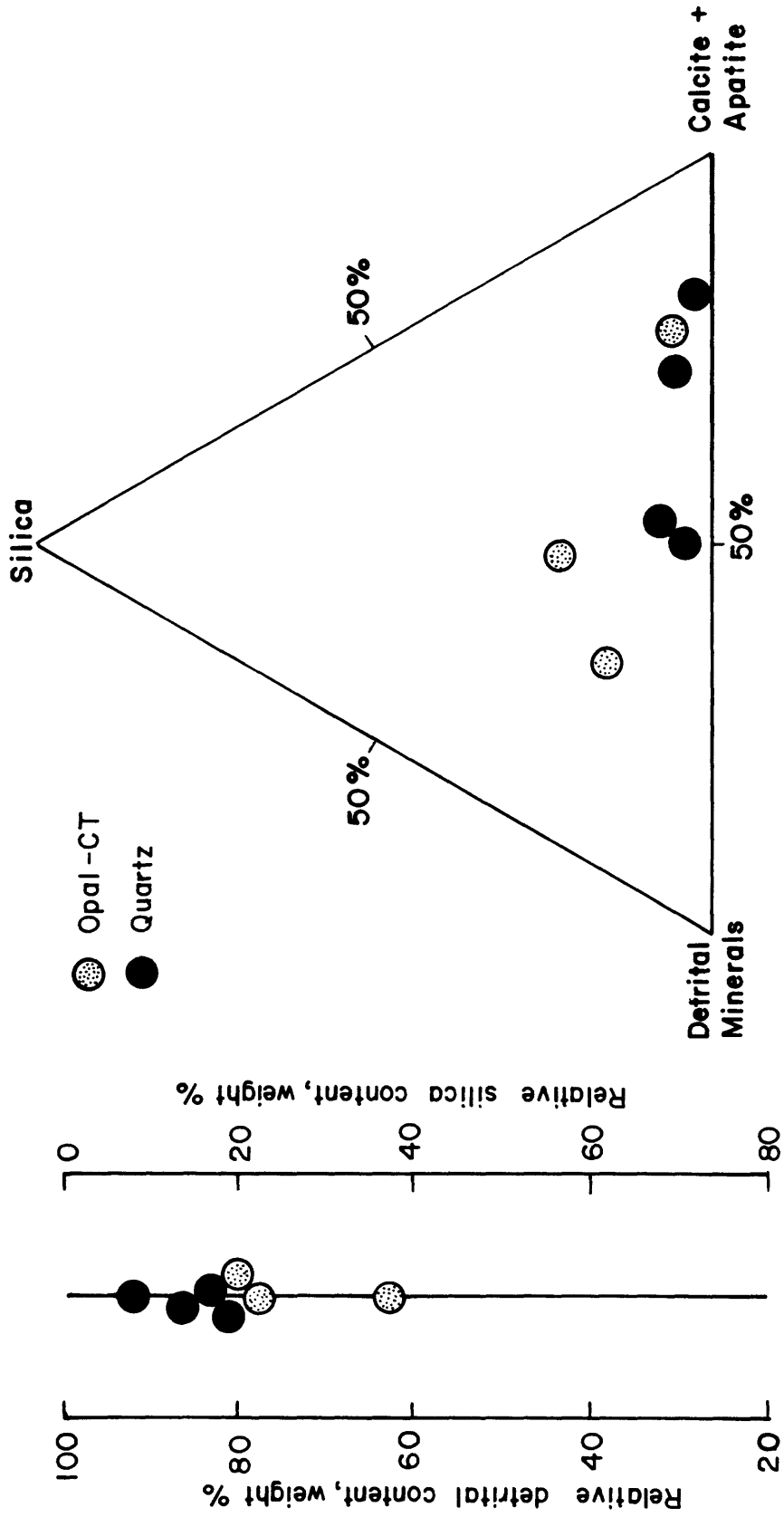
Fig. 41--Correlation between timing of quartz formation and relative detrital content in closely associated organic shales, organic shale member, San Augustine Canyon. (Components in weight percent, organic-free basis.)
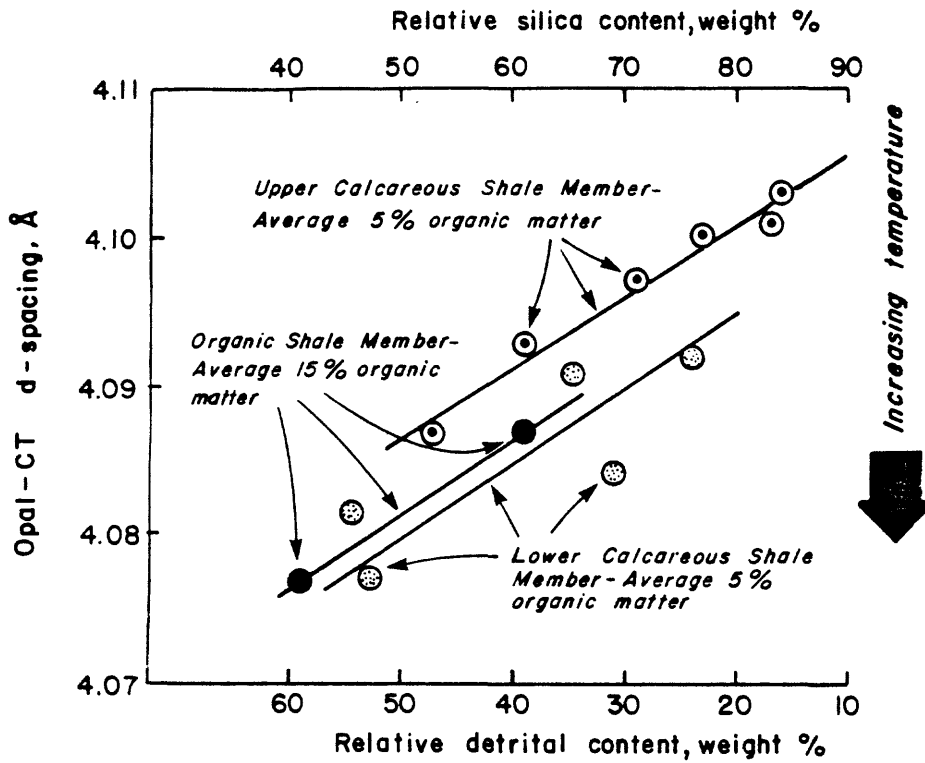
Fig. 42--Comparison of opal-CT d-spacings in associated organic
shales and calcareous rocks. Samples are from the upper
calcareous shale, organic shale, and lower calcareous
shale members, El Capitan Beach.
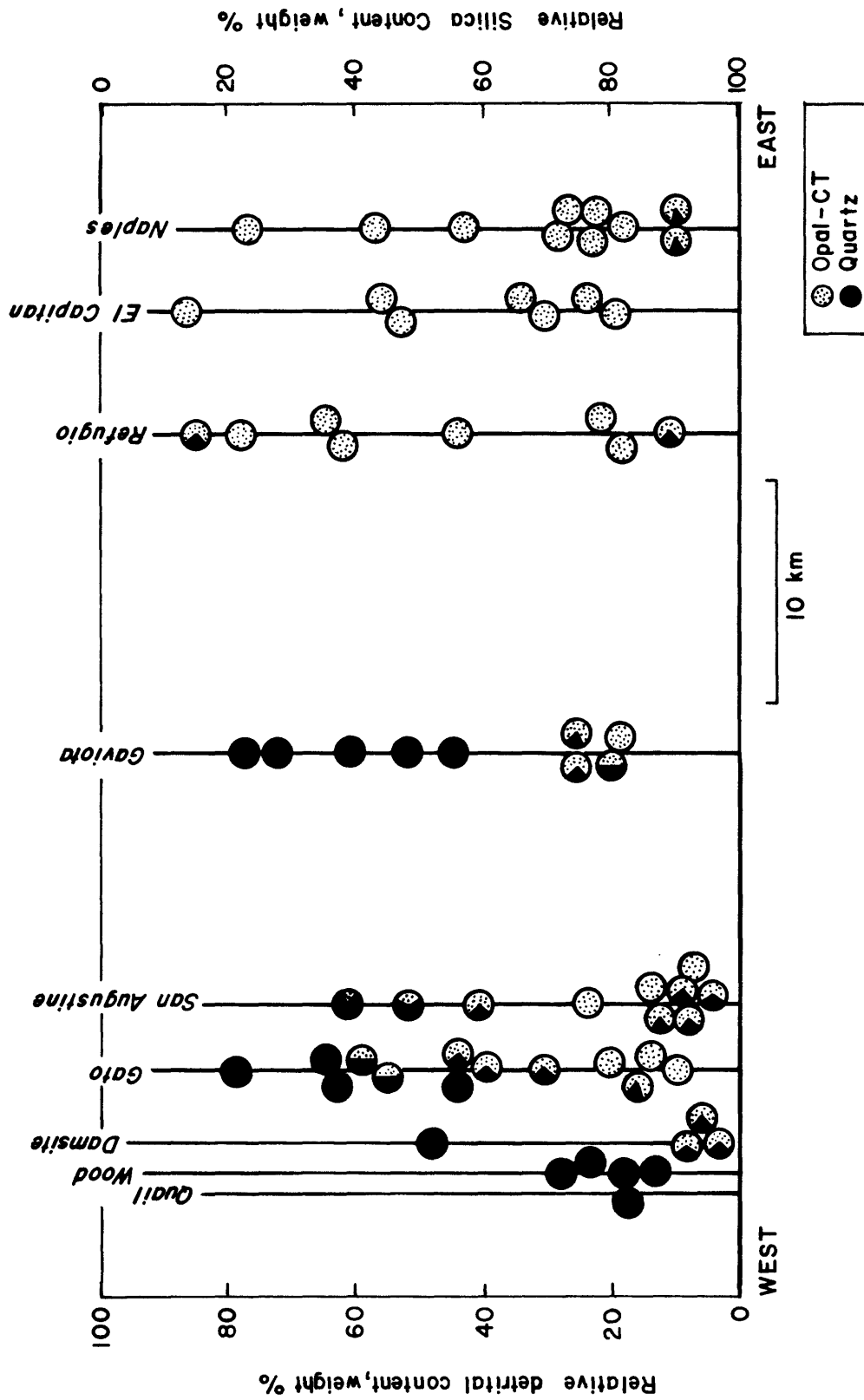
Fig. 43--Overall lateral relation between relative detrital content and timing of silica phase transformations in the lower calcareous shale member. (Excludes samples from uppermost strata in the member at Naples Beach.)
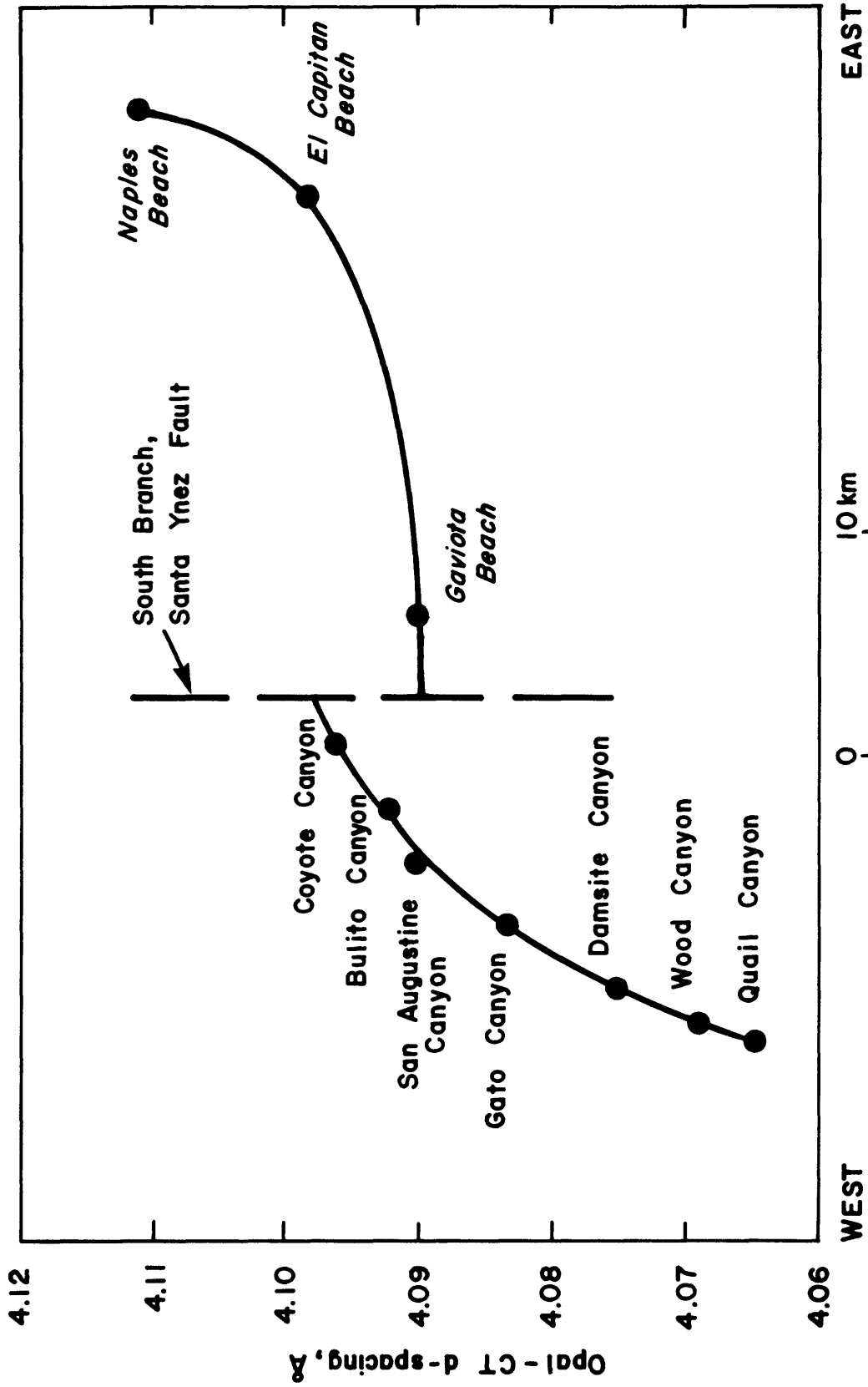
Fig. 44—Irregularity in lateral changes in opal-CT d-spacings across the south branch of the Santa Ynez Fault. D-spacings are given for stratigraphically equivalent rocks (from the lower part of the siliceous member) with similar chemical compositions (75% relative silica content).

These exceptions conflict either with the pattern determined for changes in silica phases as temperature and burial depth increased or with the inference that temperature and burial depth increased progressively westward along the Santa Barbara coast. Since the south branch of the Santa Ynez fault crosses the Monterey between Gaviota and Coyote Canyons, the most reasonable explanation is that movement along this fault caused an irregularity in the progressive increase of temperature and burial depth. Because they are observed in the same stratigraphic horizon, diagenetic irregularities could not be caused merely by vertical displacement after maximum burial. Fault movements consistent with the pattern of irregularity, therefore, are vertical motion (up on the west side) during burial, to cause thinning of overburden, or possibly lateral motion.

The geologic evidence is inconclusive. According to Dibblee (1950), vertical displacement along this branch of the fault is small, and movement was generally up on the east side. However, reverse motion (up on the west side) is indicated in the area where the branch crosses the Monterey sections examined (Dibblee, 1950). In addition, left-lateral motion probably occurred along the fault (Dibblee, 1950). Thinning and thickening of Pliocene sediments across structures parallel to the coast, suggest north-south differences in post-Miocene overburden (U.S. Geological Survey, 1974). Subsequent left-lateral motion along the fault might therefore have juxtaposed sections with somewhat different burial histories.

The exact history of fault motion is thus ambiguous, but probable fault movement could easily have caused an abrupt westward decrease (across the fault branch) in the maximum temperature and burial depth

experienced by rocks in each stratigraphic horizon. For this reason, lateral irregularities in the diagenetic pattern are tentatively attributed to faulting and the sections between Gaviota and San Augustine Canyons regarded as a lateral repetition of the diagenetic sequence.

Diagenetic Processes

A major purpose of the study was to determine the diagenetic processes, such as solution and compaction, which affected Monterey rocks as temperature and burial depth increased. Lateral relations show that the timing of diagenetic changes was influenced by the composition of individual beds. The nature of major changes in silica phases and porosity, however, was similar in rocks of nearly all compositions, and this part of the study focusses on these major diagenetic changes. Because of lateral equivalence, rocks can essentially be examined both before and after each major change and diagenetic processes therefore interpreted with considerable control.

Processes are mainly discussed in their usual diagenetic order as temperature and burial depth increased. However, the distribution and sedimentary relationships of disseminated dolomite and some quartz cherts in the calcareous members show that these rocks are not con- sistently produced by increased temperature and burial depth. For this reason, the formation of unusual quartz cherts and dolomitization are considered separately, at the end of the section.

Mechanism of Opal-CT Formation

Field relations in the Monterey sections at Elwood, Naples, and El Capitan Beaches show that rocks in these three sections were originally similar. In the siliceous member, each section contains massive, moderately diatomaceous mudstone units, 1 m or more thick, interbedded with units of laminated, more highly siliceous rock, also 1 m or more thick (cf. fig. 15). At Elwood nearly all siliceous rocks contain abundant diatoms, at Naples only the mudstones are diatomaceous and most laminated units contain abundant opal-CT, while at El Capitan all rocks contain opal-CT. All three sections also contain the same distinctive sequence of calcareous members, with rocks similarly layered and interbedded. At Elwood and Naples, however, most rocks in the upper calcareous shale, transition, and organic shale members contain diatom frustules, whereas all rocks sampled in the same members at El Capitan contain opal-CT with no diatom frustules. At Naples the upper part of the lower calcareous shale member is also mainly diatomaceous, but at El Capitan contains silica only as opal-CT.

The formation of opal-CT in these rocks clearly involves solution of diatom frustules and precipitation of opal-CT. Evidence for this conclusion is: (1) diatom frustules are abundant and opal-CT is rarely present in diatomaceous rocks; (2) opal-CT is abundant and diatom frustules are rarely present in opal-CT rocks; and (3) opal-CT rocks are much less porous than diatomaceous rocks of equivalent bulk composition. Considering the lateral equivalence of diatomaceous rocks at Elwood with opal-CT rocks at Naples and El Capitan, the absence of diatom frustules indicates that they dissolved at the last two localities. Similarly, the large porosity reduction shows

that the rocks were either compacted or cemented during formation of opal-CT. Solid-solid transformation, as postulated on experimental grounds by Mizutani (1977), would not involve these changes. A solution-precipitation mechanism is supported by oxygen isotope ratios in silica from similar rocks in the San Joaquin Valley, where an abrupt change in values between diatomaceous rocks and closely underlying opal-CT rocks shows that oxygen isotopes equilibrated with pore water during the formation of opal-CT (Murata and others, 1977).

Silica Transfer During Opal-CT Formation

In general, field relations suggest that opal-CT formed with little movement of silica. In the siliceous member, for example, the solid volume of rock at Elwood, at Naples, and at El Capitan is nearly the same, suggesting that the silica in opal-CT at Naples and El Capitan was derived from diatom frustules entirely within the member. Field relations also indicate that silica rarely moved between beds during opal-CT formation. At Naples, for example, diatomaceous and opal-CT strata are interlayered and individual beds are uniform, continuous, and distinct, with no evidence of discontinuities or irregular boundaries of "silicification."

Locally, unusual features suggest that silica moved between beds in rare instances. In the siliceous and upper calcareous shale members at Elwood, a few nodular cherts developed along certain stratigraphic horizons in the more siliceous diatomaceous layers. Although thin (2-8 mm perpendicular to bedding), these cherts are very irregularly shaped, resembling elaborate pretzels as much as

10 cm across. Such nodular cherts are not apparent at other localities in the siliceous member but do occur within calcareous opal-CT rocks west of the Elwood section. This distribution suggests that nodule formation is unusual in carbonate-free rocks but may be typical of calcareous rocks. Even at Elwood, however, nodules represent much less than 0.1 percent of the section and contain a negligible proportion of silica. Similar nodules observed in other Monterey sections have been attributed to local silica "precipitation-and-concentration" (Murata and Larson, 1975).

Another rare example of silica movement is apparent in the uppermost part of the lower calcareous shale member and in the organic shale member at El Capitan, where several cherty beds end abruptly in silica-poor calcareous shale (fig. 45). Cut surfaces of one of these cherts show diffuse cementation which crosses bedding, suggesting impregnation. Quartz also formed in the matrix, filled foraminiferal cavities and partly replaced foraminiferal walls. These features are very unusual. In fact, quartz replacement of foraminiferal tests was observed in only one other opal-CT rock sampled along the Santa Barbara coast.

Although obvious examples of silica transfer are rare, silica might have concentrated by widespread diffusion before or during opal-CT formation. Systematic local movement of calcite during recrystallization has been postulated to explain "rhythmic" layering in some calcareous rocks (Hallam, 1964; Scholle, 1977). An analogous process, which would concentrate silica in already silica-rich rocks and deplete silica in already silica-poor rocks, may be an attractive

Fig. 45--Unusual opal-CT cherts, abruptly ending
in shale, at El Capitan Beach. Right,
chert bed (white, 15 cm thick) in upper
right with sharp fractured edges extends
into smooth-weathering shale (black)
in lower center. Left, similar feature
in center left.
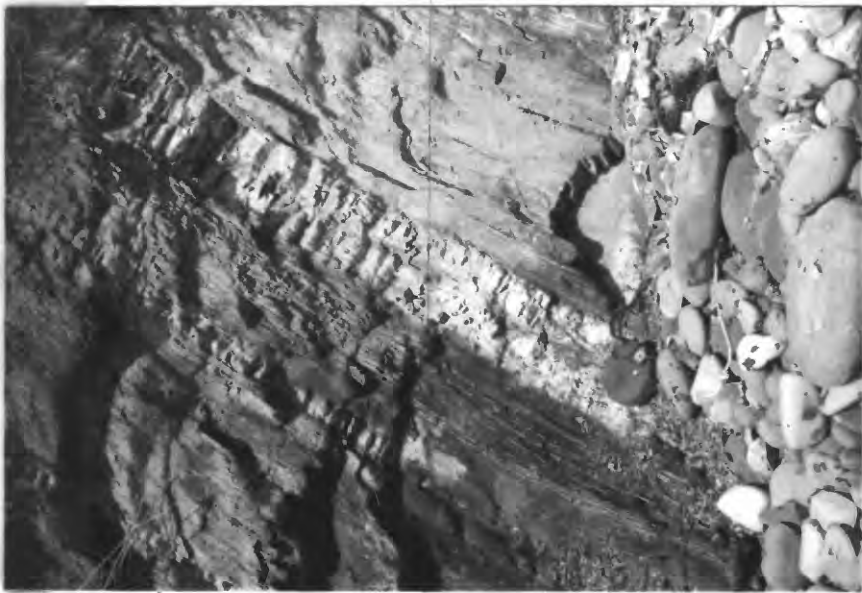
hypothesis to explain "rhythmic" layering in some siliceous rocks, such as the Franciscan cherts.

Systematic local movement of silica, however, does not seem to have occurred in most Monterey rocks. This conclusion is based on two interpretive principles. First, significant concentration of silica due to transfer between beds can be ruled out where diagenetic silica is absent, as in most diatomaceous rocks. This principle derives from the fact that dissolved silica does not crystallize in the intricate form of diatom frustules. Second, generation of highly siliceous beds by silica transfer between beds is detectable by the distribution of bulk compositions before and after opal-CT formation. To "silicify" a diatomite with 80 percent silica to an opal-CT rock with 90 percent silica, more silica must be added to the diatomite than is already present; in fact, "silicification" of the diatomite would require all the silica in two beds of equal weight containing 50 percent diatom frustules. The composition of "recipient" beds is scarcely affected, but "donor" beds must become noticeably silica deficient.

Along the Santa Barbara coast, systematic concentration of large amounts of silica prior to widespread formation of opal-CT can be ruled out by the virtual absence of diagenetic silica in rocks of the siliceous and upper calcareous shale members at Elwood Beach. After opal-CT formation, at Naples and El Capitan Beaches, all rocks in the same members contain as much silica as do diatomaceous rocks. In fact, nonsiliceous clay-rich beds were not observed in the Monterey Formation along the Santa Barbara coast (except for rare beds, 0.2-4 cm thick, which occur at Gaviota and more eastern sections mainly

in the organic shale member and which almost certainly derived from glassy tuffs). In addition, silica-poor clay-rich beds are present only in parts of the section where diatomaceous rocks are also silica-poor. "Silica-donor" beds should be common in opal-CT strata, however, if significant amounts of silica are moved to more siliceous layers during opal-CT formation.

Silica transfer during opal-CT formation has also been evaluated in Monterey rocks from the San Joaquin Valley by comparing compositional ranges before and after opal-CT formation (Isaacs and Beyer, in prep.). In that study, partial chemical analyses were made of 60 core samples within 200 stratigraphic meters. The upper 100 m contains only diatomaceous rocks without opal-CT and SEM study showed little dissolution of frustules except in the lowest samples. The lower 100 m contains only opal-CT rocks without diatom frustules. The range of chemical compositions (SiO_2, Al_2O_3, organic carbon), however, is similar in the diatomaceous rocks and in the opal-CT rocks. This relationship strongly suggests that systematic transfer of silica did not occur during opal-CT formation.

Porosity Reduction During Opal-CT Formation

In Monterey rocks along the Santa Barbara coast, reduction of porosity resulted directly from formation of opal-CT. This conclusion is inferred from the fact that diatomaceous rocks are generally much more porous than opal-CT rocks of equivalent composition--even diatomaceous rocks interbedded with opal-CT rocks. Porosity therefore decreased mainly during the silica phase transformation rather than during gradual increase of overburden.

The porosity reduction accompanying opal-CT formation is remarkable because it is a large change and seems to have occurred rapidly. The mechanism of this change has been obscured by the common practice of describing opal-CT rocks as "silicified," probably because of their toughness. The term implies that opal-CT rocks form by the addition of silica and that the associated porosity reduction is due to simple cementation. Silica addition is unnecessary, however, to form a siliceous rock from a diatomite, and simple cementation does not explain the disappearance of diatom frustules during opal-CT formation.

What mechanism does explain the reduction in porosity? First, it is helpful to review general mechanisms of porosity reduction in marine sediments.

Mechanisms of porosity reduction in marine sediments and rocks. Porosity in sediments ordinarily decreases by compaction (volume reduction of solid sediment), by simple cementation (porosity reduction due to precipitation, without volume reduction), or by a combination of these processes. Recent work has shown that cementation, which is common in near-shore sediments, is relatively rare in deep-sea sediments. Porosity reduction during early burial is mainly due to compaction (Hamilton, 1976; Scholle, 1977). Most deep-sea sediments—calcareous and siliceous oozes as well as clay muds—have porosities at deposition of 70 to 90 percent, which decrease with burial by compaction due to water expulsion under increasing load (Meade, 1964; Hamilton, 1976). In the case of clay-bearing sediments, the expelled water is not just pore water in the obvious sense but also includes tightly bound adsorbed water (Meade, 1964) which for practical purposes is part of the clay mineral (Bush and Jenkins, 1970).

Cementation is most common in sandstones or near-shore sediments. Near-shore sediments may become cemented where hydrologic conditions encourage fluid circulation. Sandstones are susceptible to cementation because they are extremely permeable to fluids, even when partly cemented, compared to most rocks (Blatt and others, 1972, p. 347). In the San Joaquin Valley, Miocene sandstones, even after burial to 2000 m, ordinarily retain permeabilities of about 1000 millidarcies (mD) (Zieglar and Spotts, 1978). By comparison, diatomites--despite their high porosity--have permeabilities on the order of 0.1 to 10 mD (Stosur and David, 1976; also Appendix E). Similarly low values (1-15 mD) characterize deep-sea chalks, even where porosities are as high as 30 to 50 percent (Scholle, 1977).

Porosity may also decrease by compaction associated with partial recrystallization due to increasing load. This process may even affect rocks in which grains are geochemically stable. In contrast to near-shore calcareous sediments, for example, many chalks are composed of low-magnesian calcite, which is highly stable under surface conditions and relatively unsusceptible to solution (Scholle, 1977). In response to increased burial load, however, even calcite in chalks slowly dissolves and forms increments of recrystallized calcite (Scholle, 1977).

Proposed mechanism of porosity reduction during opal-CT formation. As in chalks, porosity reduction during opal-CT formation involves compaction associated with dissolution and crystallization. In diatomaceous rocks, however, compaction probably results from dissolution promoted by factors other than load. For in contrast to low-

magnesian calcite, the amorphous opal contained in diatom frustules is not stable under near-surface conditions.

During early burial of diatomaceous sediments, the instability of amorphous opal does not necessarily have a large effect on diagenetic changes. Once buried, high concentrations of amorphous opal persist to burial depths of 500 m or more (Murata and Larson, 1975; Hein and others, 1978) supporting a structure with 75 percent or more porosity (Hamilton, 1976). This large porosity—which is much higher than that found in typical chalks or clay-rich sediments at the same depth (Hamilton, 1976)—suggests that diatomites are ordinarily remarkably resistant to pressure solution or cementation. In fact, Hein and others (1978) have shown that moderately diatomaceous sediments undergo little solution, once buried, until the formation of opal-CT. Since experimental studies indicate that the rate of opal-CT formation depends on opal-CT precipitation (Kastner and others, 1977), extensive dissolution is probably prevented by lack of crystallization.

Until opal-CT begins to form, therefore, diatomaceous rocks retain unusually high porosities despite the instability of amorphous opal. Once nucleation of opal-CT begins, however, dissolution of amorphous opal is promoted and may proceed rapidly. Since the highly porous framework of diatomaceous rocks is undoubtedly supported by frustules, this framework must collapse during the process of dissolution. Porosity reduction is therefore probably the result of rapid compaction.

Evidence of compaction during opal-CT formation. Along the Santa Barbara coast, compaction during opal-CT formation is shown by thicknesses of laminations in the more siliceous rocks of the siliceous member. Lamination pairs (pairs of light and dark layers) in diatoma-

ceous rocks at Elwood Beach average 0.32 mm in thickness while lamination pairs in laterally equivalent opal-CT rocks at Naples and Gaviota average 0.17 mm in thickness. These average thickness values correspond well with observed porosity differences. Using an average 65 percent porosity for the diatomaceous rocks, compaction to typical values in the opal-CT rocks (35 percent porosity) would reduce the thickness of lamination pairs to 0.17 mm, the exact value observed. All porosity reduction during opal-CT formation is therefore concluded to be the result of compaction.

Compaction during opal-CT formation is also shown by differences in thicknesses of the siliceous member along the Santa Barbara coast. Generally, sediment volumes tend to increase westward, in a pattern consistent with westward increase of sedimentation rates during late Mohnian time. Present member thicknesses, however, decrease westward between the diatomaceous section at Elwood (68 m) and the opal-CT section at El Capitan (43 m). Assuming average porosities based on measurements and field observation of lithologic distribution, sediment volumes are nearly constant across the diagenetic boundary: 27 m at Elwood (60 percent porosity), 24 m at Naples (40 percent porosity), and 29 m at El Capitan (32 percent porosity). These similarities suggest that sediment thicknesses were originally the same and that present differences were caused by compaction accompanying opal-CT formation.

"Ordering" of Opal-CT

In the calcareous members, the initial "order" of opal-CT can be determined on rocks with a wide range of bulk compositions.

Because all rocks (except cherts) in the upper calcareous shale, transition, organic shale, and upper part of the lower calcareous shale members are diatomaceous at Naples Beach, opal-CT in all rocks (except cherts) at El Capitan Beach is inferred to have formed just prior to uplift. Values of opal-CT d-spacings at El Capitan Beach therefore represent initial values at formation.

Opal-CT apparently formed initially with different degrees of "order" in rocks of different bulk compositions. Opal-CT d-spacings at El Capitan Beach vary from 4.077 to 4.097 Å, with d-spacings in cherts as great as 4.104 Å, and values decrease with the proportion of opal-CT to detrital minerals. Newly formed opal-CT was thus most highly "disordered" in the most highly siliceous rocks.

Since initial differences in the d-spacing of opal-CT persist with increased temperature and burial depth, the d-spacing is not a simple temperature indicator. Moreover, the "order" of newly formed opal-CT may be a function of bulk composition rather than of temperature. Evidence of temperature dependence is not entirely convincing. Murata and Larson (1975) suggest that lower values of d-spacings in porcelanites, compared to cherts, are due to relatively later formation of opal-CT, equilibrated to greater temperature. However, if the d-spacing difference was due simply to increased temperature and d-spacing values maintained equilibrium with temperature, then opal-CT in all rocks from the same place should have the same d-spacing. The "ordering" of opal-CT in cherts should have been re-equilibrated by the time opal-CT formed in porcelanites. Since the d-spacing of opal-CT varies considerably in rocks necessarily at the same temperature, equilibrium with temperature was not maintained.

Changes in the "order" of opal-CT with increased temperature

and burial depth were probably solid-state reactions not involving

solution. For one thing, the lateral reduction in d-spacing of opal-CT

was not accompanied by significant porosity reduction in most rocks.

In addition, although values of opal-CT d-spacings at any one locality

differ considerably among different rocks, values in rocks of each

composition generally vary equal amounts between different localities.

Lack of large porosity reduction and independence of "ordering"

rate from bulk composition both suggest that opal-CT "ordering"

does not involve solution or recrystallization. This suggestion is

strongly supported by the invariance of oxygen isotope ratios in

opal-CT, ranging from 4.11 to 4.04 Å, in cherts from the San Joaquin

Valley (Murata and others, 1977).

Porosity Reduction During "Ordering" of Opal-CT

In most opal-CT rocks, porosity does not vary with lateral

position, showing that porosity reduction was not ordinarily associated

with opal-CT "ordering." Estimates at other Monterey localities

indicate that the opal-CT "zone" lies approximately between burial

depths of 700 and 2000 m (Murata and Larson, 1975), and high heat

flows near Point Conception (McCulloh and Beyer, 1979) suggest that

the "zone" may lie between about 500 and 1550 m in that area.

According to porosity-depth curves in McCulloh (1967), compaction in

clay rocks over either interval might cause a loss of about 10

porosity percent. Because of lateral differences in burial load,

then, some reduction in porosity is reasonable to expect during opal-CT

"ordering." Absence of lateral porosity reduction within the opal-CT

"zone" therefore indicates, in addition to absence of recrystallization, rigidity of the silica framework in opal-CT rocks and considerable resistance to compaction.

This conclusion is supported by the fact that porosity values of carbonate-bearing rocks with low opal-CT contents are exceptions to the typical pattern and tend to decrease laterally throughout the opal-CT zone (fig. 46). Lateral porosity reduction in these carbonate-bearing rocks may possibly have been due to compaction permitted by solution-precipitation of calcite, as coccoliths commonly recrystallize at comparable depths (Scholle, 1977). Compaction seems to have occurred only because of the absence of a rigid opal-CT framework, however, because rocks which experienced lateral porosity reduction in the opal-CT "zone" are distinguished mainly by their low silica content rather than by high calcite or clay content.

Mechanism of Quartz Formation

Field relations and sedimentary features in the Monterey Formation between San Augustine and Black Canyons show that rocks in these sections were originally similar. At Black Canyon, however, all rocks now contain diagenetic quartz with no opal-CT while at San Augustine Canyon nearly all rocks contain opal-CT with no diagenetic quartz. Between the two canyons, opal-CT rocks and quartz rocks are both present.

The formation of quartz in these rocks almost always involved solution of opal-CT and precipitation of quartz. This conclusion is based on the fact that nearly all quartz rocks are similar in bulk chemical composition to opal-CT rocks, while quartz rocks are denser.
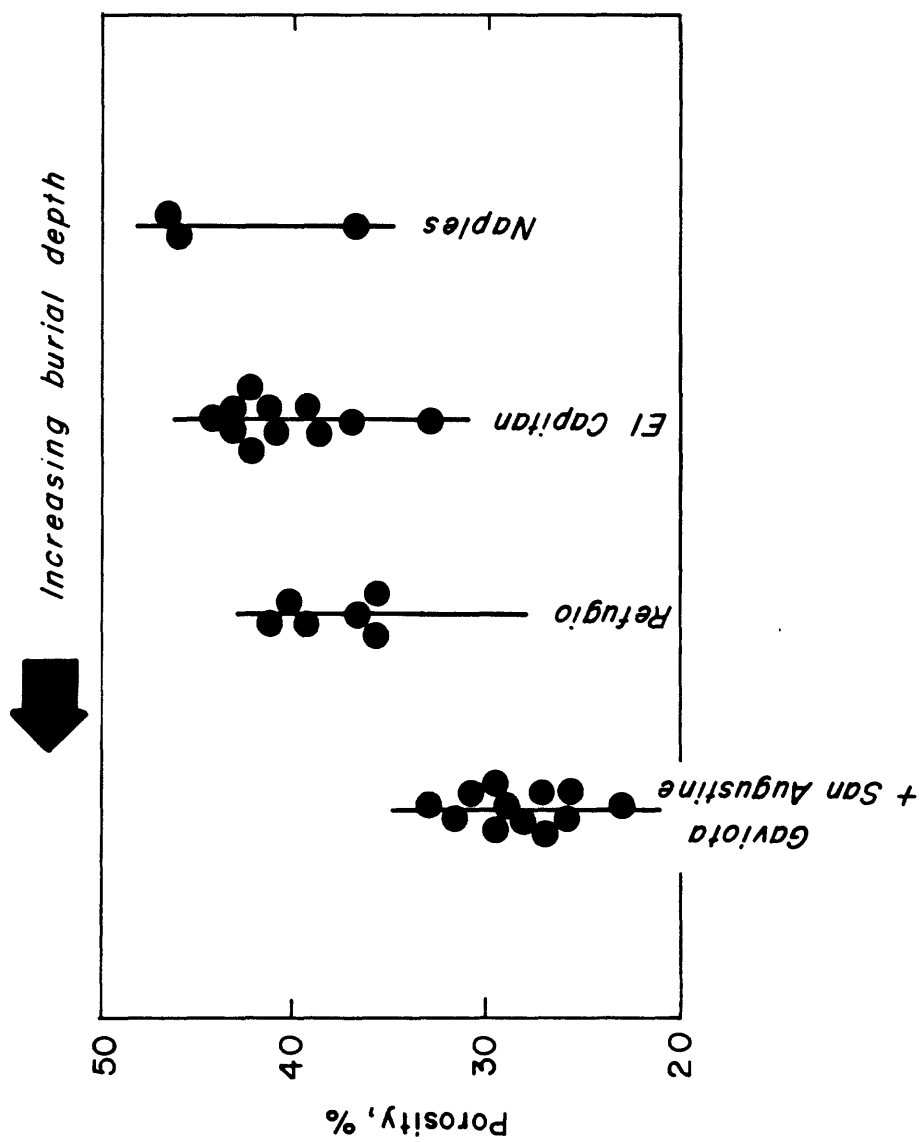
Fig. 46—Decrease in porosity during "ordering" of opal-CT in carbonate-bearing rocks with <50% silica content. Each lateral position includes samples from all calcareous members.

Porosity reduction shows that quartz formation did not occur by solid-solid transformation, as this process would increase the porosity due to the greater density of quartz. A solution-precipitation mechanism is also supported by oxygen isotope ratios in silica from Monterey rocks in the San Joaquin Valley, where values change abruptly between opal-CT rocks and immediately underlying quartz rocks (Murata and others, 1977).

Under special circumstances, quartz may also have formed by precipitation of silica dissolved from diatom frustules. Field relations show that small to moderate amounts of diagenetic quartz had formed in calcareous rocks with high relative silica contents prior to widespread opal-CT formation. Although rocks containing early diagenetic quartz are opal-CT rocks and do not contain diatom frustules, at Elwood and Naples the rocks are interbedded with diatomaceous rocks and the opal-CT thus inferred to be newly formed. Early diagenetic quartz might, therefore, have derived directly from silica dissolved from diatom frustules. A solution-precipitation mechanism is indicated by the presence of most early diagenetic quartz as foraminiferal fillings.

In all other siliceous and calcareous rocks, the "ordering" of opal-CT appears to be a precondition for the formation of quartz, as suggested by Murata and Larson (1975). In fact, in Monterey rocks along the Santa Barbara coast, where opal-CT d-spacings depend on relative detrital content as well as on lateral position, diagenetic quartz also occurs as a function of relative detrital content as well as of lateral position (fig. 31). Formation of quartz therefore

depends, at least empirically, on the "ordering" of opal-CT; and, like opal-CT d-spacings, quartz formation is not a simple temperature indicator.

Silica Transfer During Quartz Formation

Along the Santa Barbara coast, field relations in the Monterey Formation suggest that quartz ordinarily formed without large-scale transfer of silica. Because of differences in timing of quartz formation, rocks containing only quartz as diagenetic silica are interbedded with more siliceous opal-CT rocks in parts of all sections from Gato Canyon west to Quail Canyon. Except for unusual quartz cherts in the calcareous members, there is no evidence of irregular "silicification" and all beds are discrete and laterally continuous (fig. 16).

Textural features support in-situ recrystallization of silica. Diagenetic quartz is usually cryptocrystalline, sometimes micro-crystalline, and the vast majority of quartz rocks are porcelanites or shales, with matte or grainy surface texture. Except for unusual quartz cherts in the calcareous members, all quartz rocks have detailed layering and internal features identical to those in opal-CT rocks.

Analytical data also suggest that little silica moves between beds during formation of quartz. For example, the range of component compositions of rocks in each member shows little change between sections where silica is entirely opal-CT and sections where silica is mainly quartz. In addition, low permeabilities suggest that movement of silica was unlikely. Permeabilities of opal-CT rocks are generally

less than 0.05 mD parallel to bedding and even smaller perpendicular
to bedding (see Appendix E).

Porosity Reduction During Quartz Formation

In most Monterey rocks along the Santa Barbara coast, reduction
of porosity resulted directly from quartz formation rather than from
generally increased burial depth. Evidence for this conclusion is:
(1) all quartz rocks are less porous than opal-CT rocks of equivalent
composition; (2) rocks with moderate amounts of diagenetic quartz
are less porous than typical opal-CT rocks even when both types are
interbedded; and (3) rocks with diagenetic silica only as opal-CT
have porosities typical of opal-CT rocks even when interbedded with
rocks with diagenetic silica only as quartz (fig. 47).

As during opal-CT formation, reduction of porosity during quartz
formation probably resulted from compaction during solution and
recrystallization of silica rather than from simple cementation.
In the first place, simple cementation does not explain the complete
dissolution of opal-CT. At the same time, compaction is indicated
by reduction in porosity without movement of silica between beds.
Compaction is also suggested by the alignment of clays which is much
more pronounced in quartz rocks than in opal-CT rocks.

Formation of Unusual Quartz Cherts

Some quartz cherts in the calcareous members have unusual
features indicating a diagenetic history quite different from most
Monterey rocks along the Santa Barbara coast. These unusual quartz
cherts also have an irregular distribution not simply related to
probable temperature or burial depth. Three kinds are
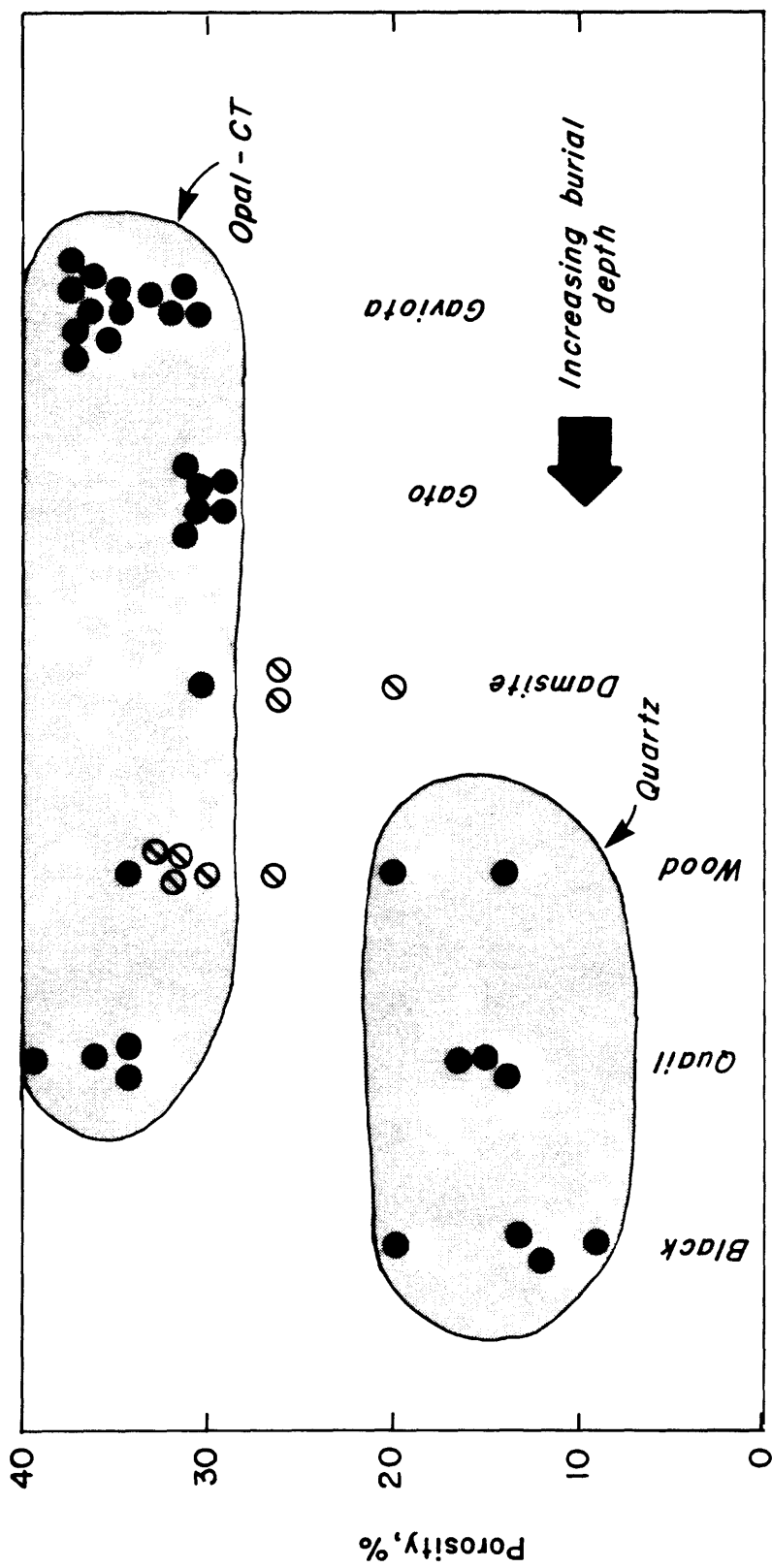
Fig. 47—Synchronous timing of quartz formation and porosity reduction in siliceous rocks from the siliceous member, Gato to Black Canyons. (Excludes samples with detrital contents >50%; ⊘ = samples with both opal-CT and diagenetic quartz.)

distinguishable: lensoid cherts with irregular diffuse boundaries, usually about 6 cm thick and 20 cm or more long; irregularly banded and veined quartz cores of opal-CT cherts; and massive, thick (15-60 cm) quartz chert beds, usually continuous but greatly contorted.

Most lensoid quartz cherts occur at Wood Canyon, in all of the calcareous members except the organic shale member. Some lensoid cherts are also present in the upper calcareous shale member at Quail Canyon. Laminae, although continuous, bulge out within these cherts (fig. 48). Thicknesses between laminae show that adjacent rocks compacted after formation of the quartz cherts to nearly 50 percent of their thickness. Assuming that present porosities are 10 to 20 percent, the difference in thickness indicates that porosities were 55 to 60 percent at the time of chert formation. Lensoid quartz cherts therefore almost certainly formed prior to opal-CT formation.

Irregularly banded and veined quartz cores of opal-CT cherts, although also rare, are the most common and widely distributed of the types of unusual quartz cherts (fig. 49). In the central part of the area, several veined cores are associated with massive quartz cherts in the organic shale member. In the western part of the area, several veined quartz cores occur in opal-CT chert beds in the upper calcareous shale at Gato and Cojo Canyons and in both the upper and lower calcareous shales at Damsite Canyon. Absence of pronounced differential compaction between veined quartz cherts and surrounding opal-CT cherts suggest that quartz formed after opal-CT formation. Since opal-CT formed relatively early in highly siliceous cherts, however, quartz veins and cores may have formed prior to widespread formation of opal-CT. In some places, they had certainly formed soon
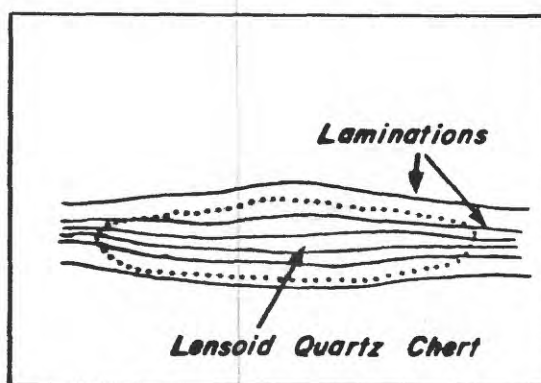
Fig. 48--Lensoid quartz chert in the upper calcareous shale member, Wood Canyon. Note that laminae spread apart within the chert body. Compaction around the lens suggests early formation.
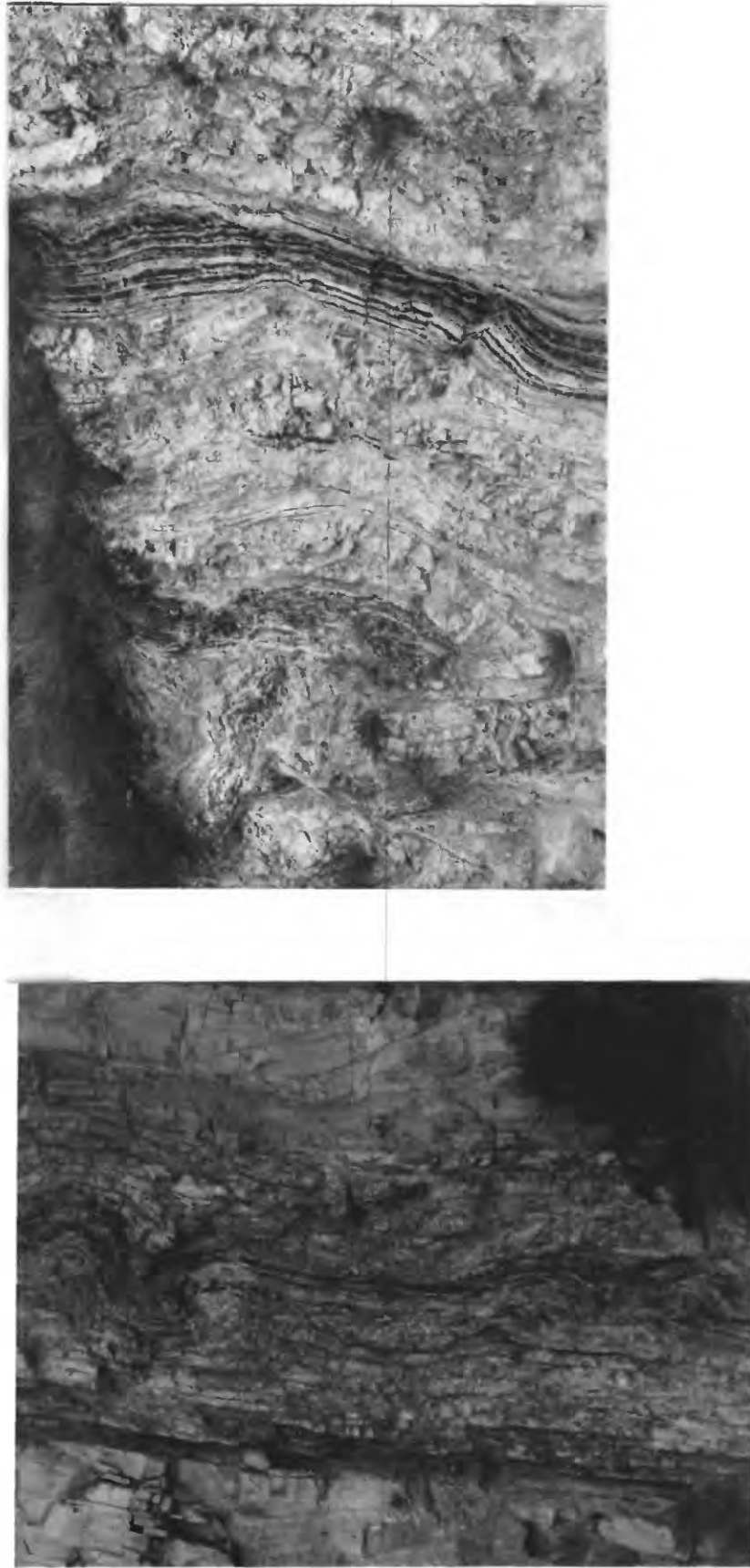
Fig. 49--Irregular quartz cherts in the upper calcareous shale member, Jalama Canyon. At left, veined quartz (black) core of dolomitic opal-CT porcelanite and chert unit (thin-bedded area, 1.2 m thick). At right, banded quartz cherts; in such cherts, white layers are often opal-CT (sometimes quartz) and black layers are quartz.

after opal-CT formation for veined quartz cores are relatively common at Jalama--slightly north of the area studied--where opal-CT d-spacings suggest maximum temperature and burial depths equivalent to the El Capitan section.

Massive quartz cherts, although much more rare, are distributed very much like veined quartzose cores. In the central part of the area, there are several massive quartz chert beds in the organic shale member. Farther west, one massive quartz chert is exposed near the top of the upper calcareous shale in Gato, Cojo, Damsite, and Wells Canyons and several beds occur in the same member at Quail and Black Canyons as well as at Jalama. The similarity in distribution--as well as in general appearance and lithologic relationships--suggests that massive quartz cherts are completely quartzified analogues of veined quartzose cores. Their presence at Jalama, however, shows that in some places massive quartz cherts may have formed as early as veined quartz cores and had certainly also formed soon after widespread opal-CT formation. Further evidence of relatively early formation is indicated by compactional deformation of sediments adjacent to contorted massive quartz cherts (fig. 50).

The distribution and occurrence of all types of unusual quartz cherts in the calcareous members show, therefore, that these rocks were not consistently produced by increased temperature and burial depth and apparently formed early in diagenesis--either when most sediments were still diatomaceous or soon after widespread formation of opal-CT. Early formation is also supported by the abundance of rounded cobbles of the unusual types of Monterey quartz cherts in the conglomerate at Gaviota Beach, of upper Mohnian age.

Fig. 50--Massive quartz chert in the upper calcareous shale member,
Damsite Canyon. Note compactional deformation of under-
lying sediments.

Unusual types of quartz cherts appear to have formed in calcareous rocks with high silica and low clay contents, by a process involving both calcite replacement and pore-filling. Original compositions are indicated by adjacent or surrounding rocks. Lensoid quartz cherts are not only laterally continuous with calcareous quartz rocks of low clay contents but are also absent in clay-rich strata. Veined quartzose cores always occur within highly siliceous opal-CT cherts and, by association, massive quartz cherts probably formed in equally siliceous strata. Evidence of calcite replacement is widespread-- particularly in lensoid cherts, where calcareous laminae are easily traced into the quartz body. Some veined quartz cores also show ghosts of foraminiferal tests. Calcite replacement is also suggested by the sparsity of calcite which, in the unusual types of quartz cherts, usually averages less than 5 percent and is sometimes present only in traces, compared to contents of 15 to 40 percent in typical calcareous rocks. Pore-filling also accompanied the formation of lensoid cherts, judged from differential compaction, and probably occurred during the formation of other types of unusual quartz cherts as well.

The cause of formation of these quartz cherts is unclear. Early formation of quartz has been frequently observed in clay-poor calcareous rocks, possibly due to the combination of low silica solubility under low temperature conditions and alkalinity produced by calcite (Kastner and others, 1977). Along the Santa Barbara coast, however, unusual types of quartz cherts did not follow a pattern of formation predictable by age, burial history, or composition. Local conditions seem to have been more important. In some places, unusual quartz cherts

seem to relate to faulting--as at Jalama, where banded and veined

cherts are most common near the Pacifico fault, in the trend of the

north branch of the Santa Ynez fault. Similar types of cherts are

also reported from Las Cruces, 4 km north of Gaviota, near the branching

of the Santa Ynez fault (Stanford Geological Survey, unpubl. field

reports, 1948). Local tectonics, then, possibly related to unusual

fluid movement, may have influenced the formation of unusual types of

quartz cherts.

Dolomitization

Pure nodular and bedded dolomites, typical of the Monterey Formation,

probably formed early in diagenesis. Highly cemented dolomites, in

places very irregular in thickness, occur in diatomaceous parts of

the Elwood and Naples sections. In opal-CT and quartz rocks, nodular

dolomites are most common in mudstones and, judged from differential

compaction, clearly formed prior to opal-CT formation. Isotope data

on this type of dolomite from other areas in the Monterey suggest

that dolomite formation involved exchange with carbon from methane

production (Murata and others, 1972).

Dolomite disseminated in shales, porcelanites, and cherts is not

widespread in the Monterey Formation generally. The distribution along

the Santa Barbara coast shows that this type of dolomite is mainly

a replacement of calcite. Dolomitic rocks are laterally equivalent

only to calcareous rocks and contain similar amounts of carbonate.

Different types of dolomitic rocks (cherts, shales, and porcelanites)

are also intimately interlayered, just as are different types of

calcareous rocks (fig. 19). The absence of disseminated dolomite in

the Monterey Formation in other areas, then, is undoubtedly due to the original absence of calcareous sediments.

The origin of dolomite in these shales and cherts is not known. No well-accepted theory of dolomitization explains their occurrence (e.g., Blatt and others, 1972; Davies and Supko, 1973, p. 212). Abundant carbonate was available in the calcareous rocks, as well as some excess carbon from methane production in organic matter. As described by Manheim and Sayles (1974), however, the amount of magnesium from pore waters in buried sediments is far too small to produce significant amounts of dolomite. Further, magnesium is not abundant in these rocks. Most rocks contain less than 1.0 percent MgO and only a few, except for dolomitic rocks, contain as much as 2.5 percent. These abundances are much lower than average pelagic sediments (El Wakeel and Riley, 1961).

The presence of dolomite is not related simply either to silica diagenesis or to inferred temperature and burial depth. Although dolomite is more common in the westernmost sections where quartz has formed, the distribution of dolomite there is complex. At Gato and Cojo Canyons, the only carbonate mineral in shales, porcelanites, and cherts in the upper calcareous shale member is dolomite and some dolomite is present in the lower part of the calcareous shale member. The distribution is similar in Damsite Canyon, farther west, except that calcite is common near the base of the upper calcareous shale. However, except in one part of the section, few shales or cherts contain dolomite anywhere in Wood Canyon. The exception is the lower part of the lower calcareous shale member which, farther west at Quail Canyon, contains little dolomite. However, at Quail Canyon,

in contrast to Wood Canyon, carbonate occurs only as dolomite in the upper calcareous shale member where calcite is again present farther west in Black Canyon.

Dolomite is also abundant in the section at Jalama, slightly north of the area studied. At Jalama, rocks equivalent to the upper calcareous member are extensively folded so that the unit is repeatedly exposed. All rocks examined contain dolomite and most rocks—except sucrose dolomites and black quartz cherts—contain "disordered" opal-CT. D-spacings of the opal-CT, averaging 4.092 Å in fairly siliceous porcelanites and 4.103 Å in cherts, suggest that this section experienced maximum postdepositional conditions similar to those in the El Capitan section. Near the study area, then, complete dolomitization of calcite is associated with rocks exposed to temperatures and burial depths much smaller than those which produced widespread quartz rocks.

Dolomite might have formed during Pleistocene uplift due to influx of meteoric waters. However, this possibility seems even more unlikely than formation during burial diagenesis. Little dolomite is present in the eastern part of the area where the rocks are relatively permeable. In the western part of the area, where dolomite is much more abundant, most rocks have permeabilities of less than 0.01 mD (see Appendix E).

Summary

This study examined lateral diagenetic differences in Monterey rocks exposed continuously for 55 km along the coast west of Santa Barbara. Investigation of the paleogeography, structure, stratigraphy,

and lithologic sequence of these rocks shows that the sections studied were laterally similar in original depositional setting, age, and compositional range. Lateral differences in late Miocene sedimentation rates and thermal diagenesis of organic matter in Monterey rocks indicate that lateral diagenetic differences are mainly due to post-depositional differences in temperature and burial depth, which both generally increased from east to west.

Diagenetic differences in Monterey rocks were examined laterally as sequential changes due only to increasing temperature and burial depth. In general, silica minerals progressed from amorphous opal in diatom frustules to "disordered" opal-CT, to "ordered" opal-CT, to microcrystalline or cryptocrystalline quartz. Porosity decreased significantly during initial formation of opal-CT and to a lesser extent during quartz formation. Field characteristics changed mainly during opal-CT formation, resulting in increased hardness, toughness, bulk density, and resistance to weathering. Although some increase in these properties also accompanied quartz formation, most quartz rocks are remarkably similar to opal-CT rocks. Only a minor proportion of quartz rocks (as well as a minor proportion of opal-CT rocks) developed the hardness, brittleness, and smooth, vitreous surface texture characteristic of cherts.

Diagenetic changes occurred at different times even in closely associated rocks. Lateral comparison at each stratigraphic level indicates that a distinctive sequence was consistently followed with increased temperature and burial depth. Opal-CT crystallized first to form cherts and cherty porcelanites, while surrounding rock remained diatomaceous. Opal-CT then formed in porcelanites, and finally

in siliceous mudstones. Subsequently quartz formed first in siliceous

mudstones, while silica in surrounding rock remained as opal-CT.

Quartz then formed in porcelanites, and finally in cherts and cherty

porcelanites. Rocks with contrasting silica phases may be intimately

interlayered, showing that phases changed independently in individual

beds, down to the scale of very thin (<2 mm) beds. In nearly all

rocks, reduction in porosity and changes in field characteristics

were synchronous with—and thus directly resulted from—silica phase

transformations.

Timing differences are empirically related to differences in the

bulk composition of individual beds, and the most important compositional

parameter is the silica/detrital ratio (fig. 51). As this ratio decreased,

opal-CT formed later, the initial "order" of opal-CT was higher, and

quartz (subsequently) formed earlier. Timing differences in most

carbonate-bearing rocks are empirically related to the silica/detrital

ratio in the same pattern. In addition, silica phase changes occurred

at nearly identical times in closely associated calcareous, dolomitic,

and carbonate-free rocks with equal silica/detrital ratios. Carbonate

minerals thus had little effect on rates of silica diagenesis. Effects

of carbonate are apparent only in carbonate-bearing rocks where silica

is eight or more times as abundant as detrital minerals; in such rocks,

small amounts of diagenetic quartz formed early in diagenesis, possibly

prior to widespread formation of opal-CT. Differences in the abundance

of organic matter (between 5 and 15 percent) evidently had no effect

on timing of diagenetic changes.

Major diagenetic processes were inferred from lateral comparison

of stratigraphically equivalent rocks. Detailed lateral equivalence
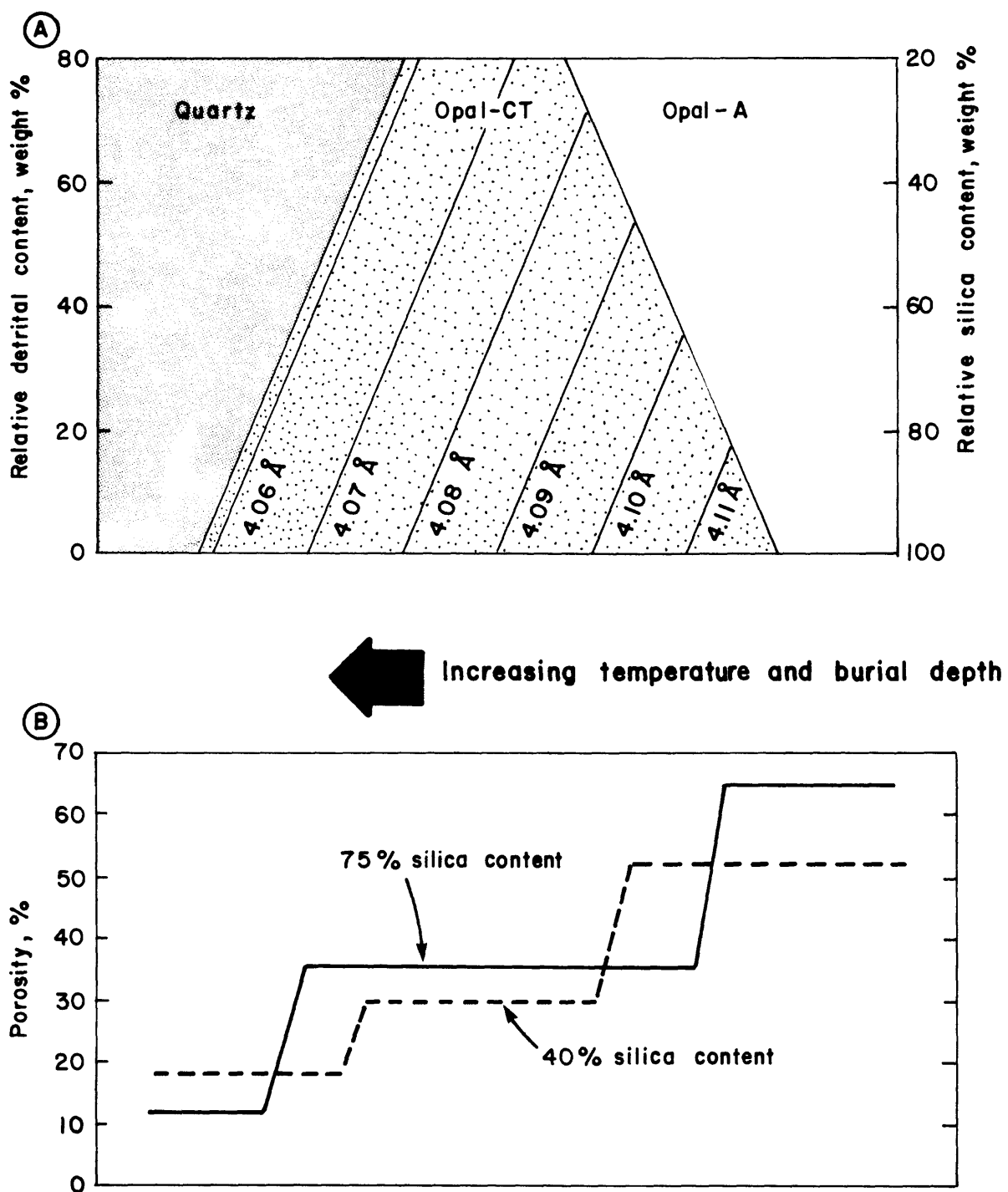
Fig. 51--Summary of differences in timing of diagenetic changes
associated with differences in relative detrital content.
(A) Changes in silica phase. (B) Changes in porosity
(for carbonate-free rocks).

of diatomaceous and opal-CT strata combined with porosity differences shows that opal-CT formed by precipitation of silica dissolved from diatom frustules. Except in rare instances, the change involved transfer of little silica between beds but was accompanied by considerable compaction. As temperature increased, opal-CT "ordered," evidently without solution or precipitation. During "ordering," porosity decreased only in rocks with low (<50 percent) silica contents, probably due to compaction in the absence of a rigid silica framework. Except for small amounts of early diagenetic quartz formed in calcareous rocks, diagenetic quartz formed only after the d-spacing of opal-CT was about 4.07 Å. Detailed lateral equivalence of opal-CT and quartz strata combined with porosity differences shows that quartz typically formed by the precipitation of silica dissolved from opal-CT. The change involved transfer of little silica between beds and was accompanied by compaction.

A few diagenetic changes are atypical in not consistently occurring with increased temperature and burial depth. These atypical changes include the formation of disseminated dolomite and of unusual quartz cherts. Disseminated dolomite evidently replaced calcite in rocks with a considerable range of compositions, but its origin is unclear. Formation of unusual quartz cherts, which may be coarsely crystalline, involved silica replacement of calcite and pore-filling. Such cherts seem to have formed mainly in detrital-poor rocks. Relations with adjacent rocks and spatial distribution suggest that unusual quartz cherts may have formed prior to widespread opal-CT formation, possibly even in diatomaceous rocks.

CHAPTER 7

COMMENTS

This section comments on a few special topics raised by study
of Monterey rocks along the Santa Barbara coast. First, effects of
detrital minerals on silica diagenesis are evaluated and the
crystallographic meaning of opal-CT "ordering" considered. Then,
cherty (vitreous) rocks are compared with porcelanous (matte) rocks
and the origin and significance of differences explored. Finally,
conclusions from other studies about calcite's effect on silica
diagenesis are contrasted with results from the Santa Barbara coast,
and factors are considered (other than temperature and rock composition)
which may influence diagenetic processes.

Impact of Detrital Minerals on "Ordering" of Opal-CT

Along the Santa Barbara coast, opal-CT formed later and with
more "order," and quartz formed earlier, as the proportion of detrital
minerals to silica increased. Is there evidence that these relation-
ships are characteristic of diatomaceous rocks? What explains the
relationships? This section considers these questions, dealing
briefly with timing of opal-CT and quartz formation and then exploring
in more detail the cause of differences in "ordering" of opal-CT.

Timing of Opal-CT Formation and Quartz Formation

Evidence in several studies suggests that clay widely affects
timing of opal-CT formation, as along the Santa Barbara coast.

151

Previous work has shown that formation of opal-CT was retarded by greater clay content in highly detrital diatomaceous cores from the Bering Sea and by even small amounts of montmorillonite in low-temperature experiments with diatom frustules (Kastner and others, 1977; Hein and others, 1978). In addition, although the difference was not specifically related to detrital content, opal-CT in highly siliceous Monterey rocks from California was observed to have formed earlier in cherty rocks than in porcelanites (Murata and Nakata, 1974; Murata and Larson, 1975). Clay minerals probably retard formation of opal-CT because opal-CT competes for its centers of nucleation with montmorillonite, as described by Kastner and others (1977).

Effects of detrital content on timing of quartz formation have not been previously noted in diatomaceous rocks. The relationships observed along the Santa Barbara coast are consistent, however, with results of experimental and field studies which have shown that quartz ordinarily forms only after opal-CT is "ordered" (Murata and Larson, 1975; Mizutani, 1977). Along the Santa Barbara coast, the initial "order" of opal-CT varied with composition, and initial differences persisted because "order" increased at approximately the same rate in all rocks. Differences in timing of quartz formation were therefore apparently due to differences in the initial "order" of opal-CT, and detrital minerals probably did not affect the actual precipitation of quartz.

Background on "Ordering" of Opal-CT

Differences in initial "ordering" of opal-CT have not been previously related to detrital content. Reported d-spacings of

opal-CT inferred to be newly formed, however, are much lower in highly

detrital Bering Sea sediments than in highly siliceous Monterey

rocks (Murata and Larson, 1975; Hein and others, 1978). This evidence

suggests that differences in initial "ordering" of opal-CT may widely

relate to detrital content, as along the Santa Barbara coast.

Imperfect understanding of the structure of opal-CT obscures

the cause of variations in "ordering." Although frequently described

as sheets of silica tetrahedra with both cristobalitic and tridymitic

stacking in random unidimensional disorder, the actual structure of

opal-CT has been debated and at least one quite different alternative

proposed (Wilson and others, 1974). In addition, the validity of

tridymite as a pure phase of SiO_2 has long been in some doubt (Eitel,

1957).

Another difficulty in evaluating variations in d-spacings of

opal-CT is that existing knowledge of the opal-CT structure is

based mainly on samples which have undergone little thermal diagenesis.

Several previous studies have shown that the structure of naturally

occurring opal-CT changes with increased temperature (Murata and

Nakata, 1974; Murata and Larson, 1975; Mitsui and Taguchi, 1977).

However, detailed mineralogical investigation, capable of resolving

these structural changes, has not been made.

Several features could, therefore, be the cause of variations

in opal-CT d-spacings. Differences in grain or domain size are

suggested by the increased sharpness of X-ray diffraction lines with

decreased d-spacing. Alternately, d-spacings may vary with the

proportion of tridymitic to cristobalitic stacking—or with simpler

stacking imperfections, as suggested by the term "order." Finally,

d-spacings could relate to special characteristics of crystal habit, which have been proposed as the cause of the "disordered" X-ray diffraction pattern of opal-CT (Flörke and others, 1975).

Changes in the XRD Pattern of Opal-CT Associated with "Ordering"

Evidence from Monterey rocks suggests that d-spacing differences represent true structural differences in opal-CT. In rocks along the Santa Barbara coast, X-ray diffraction characteristics of opal-CT change with thermal "ordering" in the same pattern illustrated by Murata and Larson (1975) for rocks from the San Joaquin Valley. The main characteristics of the diffractograms (using CuKα radiation) is the presence of two peaks, near 22° and 36° 2θ, which are close to the principal diffraction peaks of both α-cristobalite and α-tridymite. In highly "disordered" opal-CT (d-spacing $\geq$ 4.10 Å), the peak near 22° 2θ is much the stronger, and its average center is close to the value characteristic of α-tridymite at 21.6° 2θ. In addition, a third weaker peak (or, more properly, bulge) is present at about 20.5° 2θ, a diffraction peak characteristic of α-tridymite but not of α-cristobalite. As the d-spacing decreases: (1) the peak near 22° 2θ tends toward the value characteristic of α-cristobalite at 22.0° 2θ; and (2) the bulge near 20.5° 2θ (characteristic of α-tridymite) seems to become less prominent (once quartz begins to form, however, the bulge is obscured by interference from the minor quartz peak at 20.8° 2θ). Finally, highly "ordered" opal-CT (d-spacing $\leq$ 4.06 Å) displays sharper peaks near 22° and 36° 2θ and in addition two weaker peaks characteristic of α-cristobalite (but not of α-tridymite) near 28.4° and 31.4° 2θ.

Despite broad diffraction lines, then, "disordered" opal-CT

produces an X-ray diffraction pattern similar to that of α-tridymite

while "ordered" opal-CT produces an X-ray diffraction pattern similar

to that of α-cristobalite. Changes in grain or domain size alone

are unlikely to cause all the observed differences in XRD patterns,

and absence of significant solution during "ordering" (p. 131)

suggests that changes in crystal habit could not be responsible.

D-spacing variations therefore appear to represent differences in the

proportion of tridymitic and cristobalitic stacking, with tridymitic

stacking predominant in "disordered" opal-CT and cristobalitic

stacking predominant in "ordered" opal-CT.

The "ordering" differences produced by thermal diagenesis do

not necessarily have the same structural basis as initial "ordering"

differences related to variations in detrital content. Details of

opal-CT X-ray diffraction patterns are obscured in detrital-rich

rocks by low peak intensity and by interfering peaks of feldspar and

quartz. Minor peaks characteristic of thermally "ordered" opal-CT,

in particular, are not detectable in detrital-rich rocks. Neverthe-

less, along the Santa Barbara coast, quartz began to form in each

rock soon after the d-spacing of opal-CT reached 4.07 Å, irrespective

of whether the inferred initial value was 4.08 Å or 4.115 Å. This

empirical relation suggests that thermal "ordering" is identical to

the initial "ordering" associated with increased detrital content.

Cause of "Ordering" Differences

"Disorder" of opal-CT is usually attributed to the presence of

impurities, or ions--particularly aluminum--"foreign" to the pure

silica structure (e.g., Kastner and others, 1977; Robertson, 1977).

This explanation, which also helps account for the metastable formation

of opal-CT, is based partly on the fact that a much greater proportion

of "foreign" ions can be incorporated in the α-cristobalite structure

than in the quartz structure (Frondel, 1962). However, no reliable

data suggest that opal-CT actually does contain significant amounts

of "foreign" ions nor that such ions cause the characteristic "disorder"

(cf. Frondel, 1962, p. 293).

In fact, Monterey rocks along the Santa Barbara coast, where

"ordering" of opal-CT increases with detrital content, suggest that

"foreign" ions readily available from detrital minerals have just the

opposite effect and actually promote "order." Although possible, this

effect seems unlikely if initial "ordering" related to detrital content

is identical to thermal "ordering." As temperature increased,

"ordering" of opal-CT would then require—and quartz formation then

depend upon—the continuous incorporation of extraneous ions into the

opal-CT structure.

As suggested by Kastner and others (1977) in explanation of

differences between calcareous and non-calcareous rocks, another

possible cause of initial structural variations in opal-CT is

differences in amounts of silica in solution during crystallization.

"Disordered" opal-CT is more soluble than "ordered" opal-CT (Fournier,

1973; Murata and Larson, 1975), so that if detrital minerals reduce

silica solubility under natural conditions, "ordered" opal-CT would

be more likely to form. In experimental studies, however, mont-

morillonite does not seem to affect silica solubility, only nucleation

of opal-CT (Kastner and others, 1977). The mechanism cannot,

therefore, account for differences in "order" due to detrital content alone.

A more plausible cause of structural differences in opal-CT is initial incorporation of water molecules, hydrogen, or hydroxide ions. Opal (including opal-CT) is usually described as hydrous silica (Segnit and others, 1965). Although most water is loosely attached to the crystal structure, either adsorbed or capillary, some water and hydronium ions are probably present in interstitial positions, and both water and hydroxide may also substitute for oxygen in the structure, causing "disorder" (Frondel, 1962; Segnit and others, 1965).

Water and/or hydroxyls are almost certainly incorporated into the structure of opal-CT during crystallization. According to the model suggested by Jones and Segnit (1972), opal-CT forms by coalescence of six-membered rings of "silica tetrahedra," each of which actually contains two hydroxyls. Polarized water molecules are also attached to most surfaces during crystallization (Segnit and others, 1965). Both hydroxyls and water molecules could easily, therefore, be incorporated into the opal-CT structure. The hypothesis seems to be confirmed by hydrogen isotope ratios of water extracted from opal-CT which suggest that the water in high temperature fractions is derived from hydroxyl groups in the silica (Knauth and Epstein, 1975).

Although no evidence firmly shows that incorporation of water or hydroxyls is the cause of "disorder" in opal-CT, the hypothesis provides a plausible explanation for observed "ordering" differences in newly formed opal-CT. Since both water and hydroxyls are probably more available to silica in montmorillonite-poor environments, opal-CT

could be expected to be initially more "disordered" in silica-rich

rocks if incorporation of water and/or hydroxyls cause "disorder."

Changes in "ordering" might then be due to expulsion of water or

hydroxyls from the structure.

Conclusions

Neither the structural significance nor the empirical cause of

"ordering" differences is actually known. Evidence from opal-CT

in Monterey rocks indicates that d-spacing variations represent

differences in the proportion of tridymitic and cristobalitic stacking

rather than differences in grain size or crystal habit. Detailed

mineralogical study of natural thermally "ordered" opal-CT should

be undertaken, however, to resolve uncertainty about structural

changes.

The inverse relationship between "disorder" and abundance of clay

minerals suggests that "foreign" ions from clay minerals do not cause

"disorder." Incorporation of water and hydroxyls deserves more atten-

tion as a possible cause of "disorder."

Origin and Significance of Differences Between Cherts and Porcelanites

Macroscopic physical properties of rocks are important in geologic

investigation because they are so easily observed. Most useful

properties of coarse-grained rocks, such as grain size and shape,

are not useful in examining siliceous rocks. Siliceous rocks, however,

have many distinctive properties, easily observed in the field,

which could be extremely informative if their significance were

determined.

Differences between cherts and porcelanites are now considered

from this perspective. Field and analytical differences are described,

and ideas postulated to explain these differences. The intention is

not to provide a conclusive explanation but rather to re-evaluate

the role of silica impregnation and pore-filling, generally assumed

to be the main mechanism of chert formation, and to suggest alternate

mechanisms. Comments concentrate on opal-CT rocks but similar ideas

may apply to quartz rocks.

Field and Analytical Differences

Hand specimen and field characteristics of opal-CT cherts and

porcelanites, although sometimes gradational, are nevertheless quite

distinctive. Cherts have a glassy luster and a smooth surface texture

whereas porcelanites have an earthy luster and a matte, or grainy,

surface texture. Cherts are also brittle and break into glassy chips

whereas porcelanites fracture irregularly into splintery fragments.

In addition, cherts are much tougher and have gross hardnesses of

4 or more while porcelanites have hardnesses of 3 or less.

Analytical data suggest reasons for these differences. In the

first place, comparisons of detrital content show that cherts, as a

group, are not merely "denser porcelanites." Among carbonate-free

rocks, compositional ranges overlap somewhat, but the range in cherts

is quite small compared to the range in porcelanites, and all cherts

contain relatively large amounts of diagenetic silica (fig. 6A).

Cherts cannot, however, be characterized simply by high total silica

content. For example, some calcareous cherts contain less than

60 percent diagenetic silica (fig. 8B), while carbonate-free rocks

with only 60 percent silica are detrital-rich porcelanites with completely different lithologic characteristics. Chertiness therefore apparently relates to the proportion of opal-CT to detrital minerals rather than to the total amount of opal-CT.

Cherts and porcelanites also differ in mass properties. Among carbonate-free opal-CT rocks, bulk densities average 1.45 g/cc in porcelanites compared to 1.67 g/cc in cherts and cherty porcelanites, while porosities average 36 percent in porcelanites and 27 percent in cherts and cherty porcelanites. Importantly, differences are not always great—and may be as little as 0.05 g/cc bulk density or 2 porosity percent. Also significant is the fact that quartz porcelanites are denser, and less porous, than almost all opal-CT cherts. These relationships show that the characteristic glassy surface of cherts is not due merely to reduced pore space.

Differences in porosity suggest, however, that chertiness relates to the pore structure—or alternately, to the configuration of silica crystals. Rocks containing abundant opal-CT are characterized by a combination of high porosity, low permeability (less than 0.05 mD parallel to bedding), and extremely high surface area (as much as 45 m^2/g, a value comparable to many clay minerals). These properties together show that pore structure is represented by innumerable small voids intricately incorporated into the configuration of precipitated silica—for example, in lepispheres—rather than by large voids between large solid silica crystals. The principal difference suggested by porosity variations, then, is that opal-CT is more densely aggregated in cherts than in porcelanites.

Impregnation Mechanisms

Why is the silica aggregate denser in cherts? Their smooth glassy surfaces may seem to suggest, intuitively, that cherts formed by silica impregnation and pore-filling. Cherts may, in fact, sometimes form by these processes and locally along the Santa Barbara coast, unusual characteristics of opal-CT cherts suggest silica impregnation (fig. 45). Neither glassy luster nor reduced porosity, however, is prima facie evidence of silica impregnation. Both features simply suggest a pore structure in cherts different from that in porcelanites.

Evidence from rocks along the Santa Barbara coast shows that silica impregnation, by itself, is not a plausible mechanism for formation of opal-CT cherts. If cherts had formed mainly by silica impregnation of diatomaceous rocks, cherts should show comparatively little compaction and pairs of laminations in opal-CT cherts should be twice as thick as in porcelanites. Lamination thicknesses, however, have similar values in opal-CT porcelanites and opal-CT cherts, showing that both types of rocks compacted similar amounts during opal-CT formation. In addition, opal-CT cherts do not contain significant amounts of diatom debris. The amounts of diatom debris expected from silica impregnation can be estimated by comparison of typical values of porosity and composition of opal-CT cherts with values for diatomaceous rocks just prior to chert formation (as in the siliceous member at Elwood Beach). Possible precursors of opal-CT cherts, if the latter were formed by silica impregnation alone, are restricted to diatomaceous rocks with 30 percent or less detrital

minerals, and 40 percent or more of the silica in resulting cherts must be in diatom frustules (fig. 52).

Another impregnation mechanism that might account for the observed compaction and absence of diatom debris involves diffusion of dissolved silica into early centers of opal-CT nucleation. Because opal-CT formed in rocks with low relative detrital contents first, when surrounding rock was comparatively permeable and dissolved silica highly concentrated in pore water, silica might have diffused from adjacent beds into the nucleation centers. Compaction and dissolution of diatom frustules would then be accompanied by some addition of silica. If this process were significant, however, beds adjacent to opal-CT cherts should be particularly silica-deficient (see p. 124), a relation which was not observed. In addition, although permitting some silica transfer, the process does not actually explain pore structure differences. Why should silica dissolved from adjacent beds crystallize more densely than indigenous silica? In fact, since all silica undergoes solution-precipitation and cementation could presumably eliminate all pore space, why is so much pore space consistently retained?

Plausible Mechanisms

The most plausible explanation is that clay minerals interfere, during crystal growth, with the formation of a dense, tightly interlocked opal-CT aggregate. Little is known about the ultra-structure of opal-CT except in rather pure silica samples, but some evidence suggests that the presence of clays decreases the structure's density. For example, (rock) opals, which evidently contain very
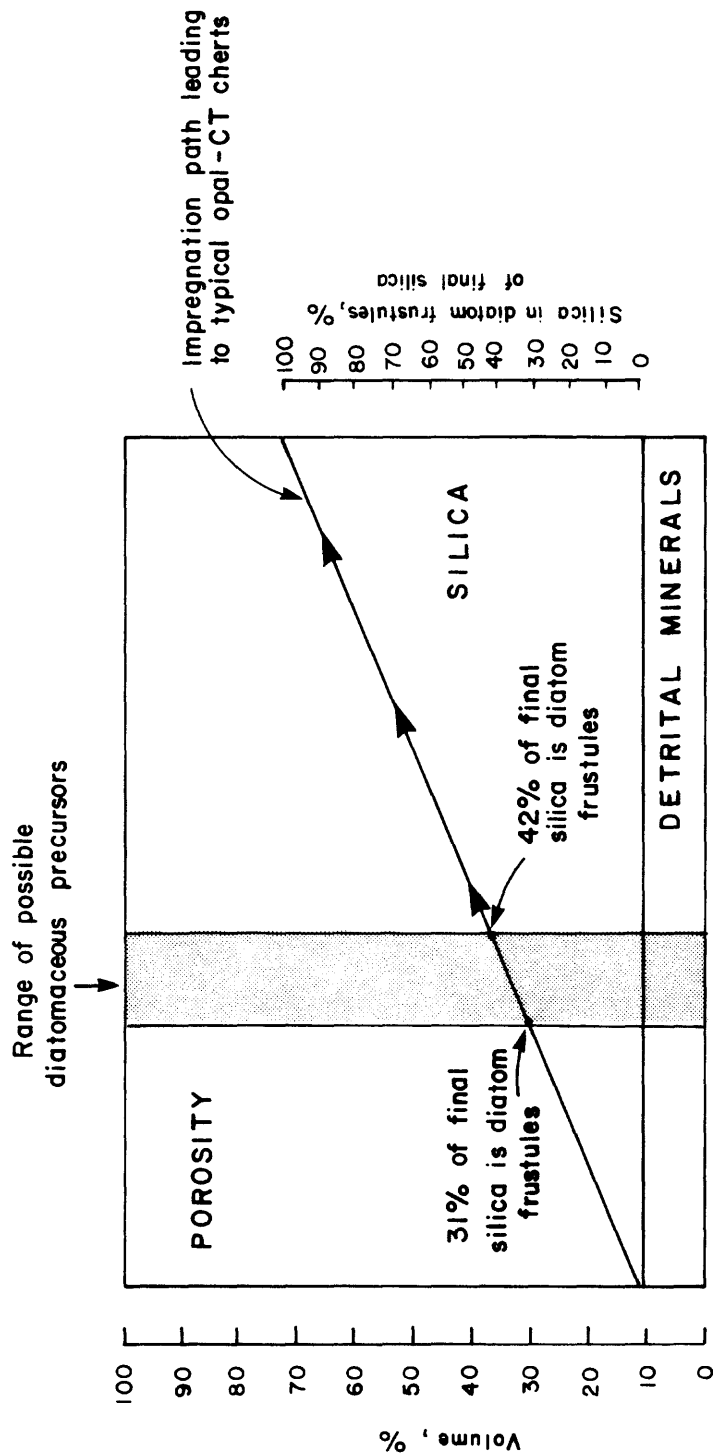
Fig. 52—Hypothetical silica impregnation path, showing the bulk composition
and porosity of possible diatomaceous precursors of opal-CT cherts.
Represents the replacement of porosity in diatomaceous rocks by silica,
on a path leading to typical opal-CT cherts. Scale on right corres-
ponds to starting positions on the impregnation path.

minor clay content, are much denser (Frondel, 1962) than typical opal-CT rocks from the Monterey Formation. Along the Santa Barbara coast, (carbonate-free) opal-CT rocks with lowest values of porosity tend to have either high or low silica/detrital ratios, while opal-CT rocks with highest porosities have intermediate silica/detrital ratios (fig. 53). Assuming that porosity is retained mainly in the silica framework, this unusual porosity pattern indicates that opal-CT incorporates an increasing proportion of voids as the silica/detrital ratio decreases. In addition to containing less opal-CT, then, rocks with higher detrital contents may also contain a more porous--and certainly less interlocking--opal-CT framework.

If differences between cherts and porcelanites are due to the impact of clays on the crystal growth of opal-CT, these differences derive from primary sedimentary variations which are lithologically striking only after the formation of opal-CT. Surface textures may change from porcelanous to cherty due to the rapid increase in silica/ detrital ratios (from 4:1 to 9:1) as relative silica contents increase from 80 to 90 percent. Overlap in compositional ranges could be due to variability in the distribution of clay content, since diatomaceous rocks with small concentrated clay layers might form cherts while rocks with similar amounts of clay more uniformly distributed would form porcelanites.

The mechanism is consistent with several other lithologic relations puzzling in the context of silica impregnation or diffusion. In Monterey rocks along the Santa Barbara coast, for example: (1) sandstones interbedded with opal-CT rocks are typically friable and poorly cemented; (2) cherty layers may be surprisingly thin (2 mm) and
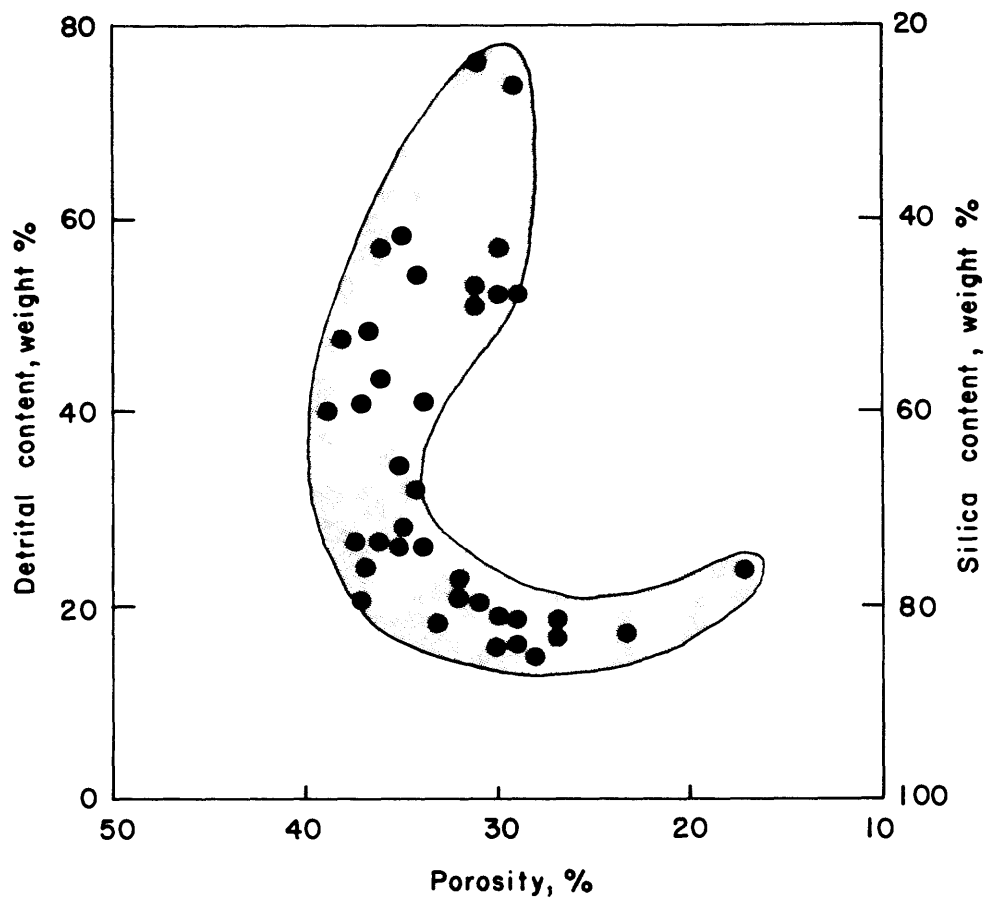
Fig. 53--Relation between porosity and detrital content in opal-CT
rocks from the siliceous member. Note that highest
porosities are in rocks with intermediate detrital
contents. (Silica and detrital contents on organic-free
basis.)

continuous; and (3) cherty texture tends to be present in carbonate-bearing rocks characterized by high silica/detrital ratios rather than by high total silica contents. In addition, opal-CT cherts have several distinctive characteristics which seem to have primary significance. In thinly layered members, for example, opal-CT cherts are distinguished from most other rocks by their very thin (<0.1 mm) continuous laminations. Opal-CT cherts also differ from opal-CT porcelanites in having virtually no apatite and in having organic matter contents which are never high (>6 percent) and typically rather low (<3 percent).

Another possible explanation of differences between cherts and porcelanites is that the crystal habit of opal-CT is affected by precipitation rates. In cherts, opal-CT evidently formed somewhat earlier--and at somewhat lower temperatures--than in porcelanites. Slower crystallization might promote a denser, more interlocked aggregate even without the addition of silica. A relation along the Santa Barbara coast supporting this suggestion is that opal-CT cherts tend to be most cherty in the eastern part of the area, where burial rates were about one-sixth the rates in the western part of the area.

Summary

Physical differences between opal-CT porcelanites and opal-CT cherts seem to arise from differences in the configuration of pore structure in the rocks. In the Monterey Formation along the Santa Barbara coast, these differences were evidently not caused primarily by silica transfer. Silica infilling of diatomaceous rocks, although

intuitively attractive, fails to account for compaction and absence of abundant diatom debris in cherts. Silica diffusion from adjacent rocks during formation of opal-CT is a somewhat more likely mechanism, but adjacent rocks are not silica-deficient. In any case, silica diffusion does not explain differences in pore structure, which is apparently a diagenetic product of crystal habit.

The most plausible explanation of differences between cherts and porcelanites is that clay minerals interfere, during crystal growth, with the formation of a dense, tightly interlocked opal-CT aggregate. If so, lithologic differences result from original sedimentary differences which are striking only after formation of opal-CT. The mechanism is consistent with general porosity patterns, bulk compositions, and sedimentary characteristics of Monterey rocks along the Santa Barbara coast. Another possible explanation of lithologic differences is that crystal habit is affected by precipitation rates.

Factors Influencing Diagenetic Processes in Siliceous Rocks

Many studies have shown that the silica in biogenous siliceous sediments typically changes from opal-A to opal-CT to quartz and that increased temperature promotes these transformations (Ernst and Calvert, 1969; Mizutani, 1970; Murata and Larson, 1975; Mitsui and Taguchi, 1977). As pointed out by Kastner and others (1977), however, exceptions to the usual "maturation sequence" of silica phases are numerous, suggesting that factors other than temperature also influence diagenesis.

Study along the Santa Barbara coast focused on rocks closely associated in terms of depositional and burial environments. Relative

effects of only two variables could be distinguished and separately examined: (1) temperature (combined with burial depth); and (2) rock composition. Other variables--such as age and burial rate--have a comparatively limited range along the Santa Barbara coast, and the effect of large differences in these variables could not be determined.

Which of these variables may have influenced the character of diagenetic processes in Monterey rocks along the Santa Barbara coast? Answers to this question are explored by considering some calcareous-siliceous rocks which: (1) were deposited and buried under conditions quite different from those along the Santa Barbara coast; and (2) evidently also followed a somewhat different diagenetic pattern as temperature and burial increased. First, however, details will be examined of contrasting diagenetic patterns in calcite-bearing rocks.

Comparison of Results on the Effect of Calcite

In many studies of silica diagenesis, considerable importance has been ascribed to the presence or absence of calcite (Lancelot, 1973; Greenwood, 1973; Keene, 1975; Kastner and others, 1977; Robertson, 1977; von Rad and others, 1977). Specific effects attributed to calcite in these studies were in part, however, inferred from comparison of calcite-bearing siliceous rocks with clay-bearing siliceous rocks. Along the Santa Barbara coast, rates of silica phase changes were mainly controlled by the relative detrital abundance, even in calcareous rocks. Diagenetic differences observed between calcite-bearing and clay-bearing siliceous rocks may therefore be due as much to differences in clay content as to the presence or absence of calcite.

Is there evidence suggesting that clay generally affects silica diagenesis in calcareous rocks? Kastner and others (1977) demonstrated experimentally that small amounts of montmorillonite greatly retard formation of opal-CT from frustules, even in the presence of abundant calcite. Different silica phases associated with different clay contents have also been noted in calcite-bearing rocks of Cretaceous age from both Great Britain and the Pacific (Keene, 1975; Scholle, quoted in Kastner and others, 1977). Thus clay content may well affect silica diagenesis in calcareous rocks. Is there evidence that calcite also affects silica diagenesis in clay-bearing rocks? The absence of quantitative data comparing calcareous and noncalcareous rocks of equal clay contents makes it impossible to judge.

Only for clay-poor calcareous rocks do results in other studies clearly contrast with results from Monterey rocks along the Santa Barbara coast. Kastner and others (1977) have shown that calcite increases the rate of opal-CT formation in pure (clay-free) diatomaceous oozes studied experimentally. From analysis of radiolarian sediments in the Pacific, Keene (1975) concluded that quartz with an opal-CT precursor, as well as early quartz, formed much more rapidly in clay-poor calcareous rocks than in clay-rich noncalcareous rocks. A similar rate relationship was shown by von Rad and others (1977) and by Robertson (1977), who also inferred from morphological evidence that the quartz present in calcareous rocks was derived from opal-CT.

Rapid formation of quartz derived from opal-CT suggests that calcite produces one or more of the following effects on silica diagenesis: (1) earlier formation of opal-CT; (2) higher initial "order" of opal-CT; (3) higher rate of "ordering" in opal-CT; and/or

(4) formation of quartz from relatively "disordered" opal-CT. All

of these alternatives, however, conflict with relationships found

along the Santa Barbara coast. Despite some early quartz precipitation,

the majority of silica dissolved from diatom frustules in this area

precipitated as highly "disordered" opal-CT even in calcareous rocks

with as little as 4 percent clay. This opal-CT formed at about the

same time and, once formed, "ordered" at the same rate as opal-CT

in carbonate-free rocks. In addition, nearly all quartz formed from

"ordered" opal-CT at the same time in clay-poor calcareous rocks as

in clay-poor noncalcareous rocks. The final result was that along the

Santa Barbara coast the silica in clay-rich carbonate-free rocks

became completely quartzose before (not after) the silica in clay-poor

calcareous rocks.

The contrast in results suggests that factors other than composi-

tion and temperature may have been important in determining diagenetic

patterns. What other factors are most significant?

Factors Other than Temperature and Rock Composition

A major factor which may influence silica diagenesis is burial

rate. Sedimentation rates in marginal Miocene basins were high compared

to those in many pelagic deposits. Overburden (as presently compacted)

apparently increased at the rate of 1 to 6 mm/thousand years in

Cretaceous rocks studied by Keene (1975) while strata overlying the

Monterey (as presently compacted) near Point Conception probably

increased at about 350 mm/thousand years. The top of the Cretaceous

section in the North Pacific therefore reached burial of 100 m

in 65 million years, while Monterey rocks near Point Conception reached

the same depth in only 300,000 years. This difference could affect silica diagenesis profoundly. Slow reactions and reactions favored by high permeability, in particular, are more likely to occur during slow shallow burial of sediment. In fact, pore filling, replacement, and nodule formation--which were relatively rare in Monterey rocks-- were quite common in pelagic calcareous-siliceous rocks (Keene, 1975). Low temperature (shallow) conditions may also affect chemical reactions, possibly promoting, for example, formation of quartz directly from biogenic silica in calcareous rocks (Kastner and others, 1977).

Differences in siliceous microfossils may also contribute to differences in silica diagenesis. Radiolarian tests, which are the main source of diagenetic silica in rocks described by Keene (1975) and Robertson (1977), differ from diatom frustules in a number of ways. Radiolarian tests are usually much larger; more equidimensional than platy; less susceptible to solution; and, individually, more variable in solubility (Riedel, 1959; Johnson, 1974). These differences suggest the possibility that radiolarian sediments may be more permeable than diatomaceous sediments or may have lower concentrations of dissolved silica at near-surface conditions, or that silica phase changes in radiolarian sediments may be more gradual. Ultimately, diagenesis certainly produces significant differences since crystallized radiolarian tests frequently persist even under moderate metamorphic conditions, whereas most diatom frustules are completely obliterated during moderate diagenesis.

Another variable which may be important in calcareous rocks and sediments is the kind of calcareous microfossil. Most calcite in Monterey rocks along the Santa Barbara coast is contained in coccoliths

whereas foraminiferal tests were used by Kastner and others (1977)

in experimental work. Keene (1975) noted that more quartz formed

directly (without intermediate opal-CT) in calcareous rocks with

high ratios of foraminifera to nannofossils. Although he attributed

this relationship to higher permeability in foraminiferal oozes,

in rocks along the Santa Barbara coast early quartz also precipitated

mainly in foraminiferal tests, even though too few were present to

affect the bulk permeability. Foraminiferal tests may therefore affect

silica differently than coccoliths, possibly because of the large

isolated void absent in coccoliths.

Differences in abundance of organic matter may also affect

diagenesis. Although absent in experimental charges and sparse in

pelagic sediments, organic matter is generally abundant in Monterey

rocks. Along the Santa Barbara coast, where organic matter contents

average 4 to 10 percent by weight, differences in organic content

do not seem to affect silica diagenesis. However, its ubiquitous

presence could widely influence interstitial water chemistry (e.g.,

Emery and Rittenberg, 1952).

Time (or age), which contributes to effects on diagenesis related

to burial rate, may also influence the timing sequence of silica

phase changes in strata of diverse compositions. Experimental results

suggest that time as well as temperature should promote each of the

two silica phase transformations (Ernst and Calvert, 1969; Mizutani,

1970). Increased time may, therefore, produce a diagenetic sequence

identical to that produced by increased temperature. Time could,

however, affect individual steps in silica phase changes differently

than does temperature. Although entirely speculative, two possible

differences might be that opal-CT initially forms with higher "order" under prolonged low temperature conditions or that "order" changes much more rapidly with time than with temperature. If so, silica phase changes in slowly buried sediments may have consistently occurred in a timing sequence different from that observed along the Santa Barbara coast.

Conclusions

Many factors besides temperature and composition probably have impacts on the diagenesis of siliceous rocks. Siliceous-calcareous Monterey rocks along the Santa Barbara coast differ from siliceous-calcareous rocks with contrasting diagenetic patterns in terms of: sedimentation and burial rates, type of siliceous microfossil (diatom frustules versus radiolarian tests), type of calcareous microfossil, abundance of organic matter, and age. Other factors which may influence diagenesis include: influx of meteoric waters, permeability, types of clay minerals, geothermal gradient, and rates of pore water movement through adjacent sediments.

In addition to affecting rates of silica phase changes, each of these factors may also affect lithologic changes and diagenetic processes—for example, transfer of silica between beds and rapid compaction during silica phase transformations. Diagenetic processes inferred for Monterey rocks along the Santa Barbara coast may not apply, therefore, to rocks deposited and buried under significantly different conditions.

CHAPTER 8

CONCLUSIONS

Examination of stratigraphically equivalent Monterey rocks
subjected to laterally increased temperature and burial depth shows
that:

1. Lithologic characteristics are influenced both by silica
phase and by bulk composition. In terms of silica phase, diatomaceous
rocks are markedly different from all rocks with abundant diagenetic
silica, while opal-CT rocks are lithologically similar to quartz
rocks. In terms of bulk composition, lithologic character is affected
most by the proportion of silica to detrital minerals and, to a lesser
extent, by total silica content and dolomite content.

2. All diagenetic changes occurred independently in different
layers of rock (down to the scale of beds 2 mm or less thick).

3. The timing of silica phase changes in individual beds was
affected by the composition of the bed. In general, opal-CT formed
later, and with greater "order," and quartz (subsequently) formed
earlier as the silica/detrital ratio decreased, even in rocks with
abundant calcite.

4. Lithologic character and physical properties (including
porosity) changed in most rocks only during silica phase transformations
(opal-A to opal-CT and opal-CT to quartz).

5. Opal-CT formed by precipitation of silica dissolved from
diatom frustules, and quartz formed by precipitation of silica

174

dissolved from opal-CT. "Order" in opal-CT changed without appreciable solution or precipitation.

6. Volumetrically significant amounts of silica were not transferred between beds during diagenesis.

7. In general, reduction in porosity resulted from compaction permitted by dissolution during silica phase transformations. Reduction in porosity involved simple cementation or silica addition only in rare instances.

These conclusions show that, under the conditions of deposition and burial found in Monterey rocks along the Santa Barbara coast, most diagenetically altered rocks are equivalent in bulk chemical composition to their unaltered precursors and that most differences between rocks result from primary differences. Exceptions include dolomitic rocks and rare cherts formed partly by replacement. The siliceous rocks studied along the Santa Barbara coast differ, however, from many other siliceous rocks in their high rates of deposition and burial, abundance of organic matter, young age, deposition in a marginal basin, and in that their silica is derived almost entirely from diatom frustules. Each of these characteristics may have had a significant effect on lithologic changes and diagenetic processes.

REFERENCES

American Geological Institute, 1962, Dictionary of geological terms:
    New York, Doubleday, 545 p.

Arnal, R. E., 1976, Miocene paleobathymetric changes of the Santa
    Rosa-Cortes Ridge area, California continental borderland,
    in Howell, D. G., ed., Aspects of the geologic history of the
    California continental borderland: American Association of
    Petroleum Geologists, Pacific Section, Miscellaneous Publication
    24, p. 60-79.

Bailey, E. H., Irwin, W. P., and Jones, D. L., 1964, Franciscan and
    related rocks, and their significance in the geology of western
    California: California Division of Mines and Geology Bulletin
    183, 177 p.

Banks, N. G., 1970, Nature and origin of early and late cherts in
    the Leadville Limestone, Colorado: Geological Society of America
    Bulletin, v. 81, p. 3033-3048.

Barron, J. A., 1976, Revised Miocene and Pliocene diatom biostrati-
    graphy of upper Newport Bay, Newport Beach, California: Marine
    Micropaleontology, v. 1, p. 27-63.

Blatt, H., Middleton, G., and Murray, R., 1972, Origin of sedimentary
    rocks: Englewood Cliffs, N. J., Prentice-Hall, 634 p.

Blow, W. H., 1969, Late middle Eocene to Recent planktonic foraminiferal
    biostratigraphy: International Conference on Planktonic Micro-
    fossils, 1st, Proceedings, v. 1, p. 199-421.

Bramlette, M. N., 1946, The Monterey Formation of California and
    the origin of its siliceous rocks: U.S. Geological Survey
    Professional Paper 212, 57 p.

Bukry, D., 1973, Coccolith and silicoflagellate stratigraphy, Deep
    Sea Drilling Project Leg 18, eastern North Pacific, in Kulm,
    L. D., and von Huene, R., eds., Initial reports of the Deep Sea
    Drilling Project: Washington, D.C., U.S. Government Printing
    Office, v. 18, p. 817-831.

Bukry, D., Brabb, E. E., and Vedder, J. G., 1977, Correlation of
    Tertiary nannoplankton assemblages from the coast and peninsular
    ranges of California: Segundo Congreso Latinoamericano de
    Geologia, Memoria, v. 3, p. 1461-1483.

176

Bush, D. C., and Jenkins, R. E., 1970, Proper hydration of clays for rock property determinations: Journal of Petroleum Technology, v. 22, p. 800-804.

Canfield, C. R., 1939, Subsurface stratigraphy of Santa Maria Valley oil field and adjacent parts of Santa Maria Valley, California: American Association of Petroleum Geologists Bulletin, v. 23, p. 45-81.

Carroll, D., 1970, Clay minerals: a guide to their X-ray identification: Geological Society of America Special Paper 126, 80 p.

Chipping, D. H., 1971, Paleoenvironmental significance of chert in the Franciscan Formation of western California: Geological Society of America Bulletin, v. 82, p. 1707-1712.

Claypool, G. E., Love, A. H., and Maughan, E. K., 1978, Organic geochemistry, incipient metamorphism, and oil generation in black shale members of Phosphoria Formation, western interior United States: American Association of Petroleum Geologists Bulletin, v. 62, p. 98-120.

Corey, W. H., 1965, The paleogeography of the lower Tertiary formations of Santa Barbara County, California, in Western Santa Ynez Mountains, Santa Barbara County, California: Coast Geological Society and Society of Economic Paleontologists and Mineralogists, Pacific Sections, Guidebook, p. 31-37.

Davies, T. A., and Supko, P. R., 1973, Oceanic sediments and their diagenesis: some examples from deep-sea drilling: Journal of Sedimentary Petrology, v. 43, p. 381-390.

Deer, W. A., Howie, R. A., and Zussman, J., 1962, Sheet silicates, v. 3 of Rock-forming minerals: London, Longmans, Green and Co., 270 p.

—————————— 1966, An introduction to the rock-forming minerals: London, Longmans, Green and Co., 528 p.

Dibblee, T. W., Jr., 1950, Geology of southwestern Santa Barbara County, California: California Division of Mines and Geology Bulletin 150, 95 p.

—————————— 1966, Geology of the central Santa Ynez Mountains, Santa Barbara County, California: California Division of Mines and Geology Bulletin 186, 99 p.

Edwards, L. N., 1971, Geology of the Vaqueros and Rincon Formations, Santa Barbara embayment, California: University of California [Santa Barbara] unpublished Ph.D. thesis, 421 p.

Eitel, W., 1957, Structural anomalies in tridymite and cristobalite:
American Ceramic Society Bulletin, v. 36, p. 142-148.

El Wakeel, S. K., and Riley, J. P., 1961, Chemical and mineralogical
studies of deep-sea sediments: Geochimica et Cosmochimica Acta,
v. 25, p. 110-146.

Emery, K. O., and Rittenberg, S. C., 1952, Early diagenesis of
California basin sediments in relation to origin of oil: American
Association of Petroleum Geologists Bulletin, v. 36, p. 735-806.

Ernst, W. G., and Calvert, S. E., 1969, An experimental study of the
recrystallization of porcelanite and its bearing on the origin
of some bedded cherts: American Journal of Science, v. 267-A,
p. 114-133.

Fischer, P. J., 1976, Late Neogene-Quaternary tectonics and depositional
environments of the Santa Barbara Basin, California, in Fritsche,
A. E., and others, eds., Neogene symposium: Society of Economic
Paleontologists and Mineralogists, Pacific Section, p. 33-52.

Flörke, O. W., Jones, J. B., and Segnit, E. R., 1975, Opal-CT
crystals: Neues Jahrbuch Mineralogie Monatshefte, v. 8,
p. 369-377.

Folk, R. L., 1973, Evidence for peritidal deposition of Devonian
Caballos Novaculite, Marathon Basin, Texas: American Association
of Petroleum Geologists Bulletin, v. 57, p. 702-725.

Folk, R. L., and McBride, E. F., 1976, Origin of novaculite members,
pt. I of The Caballos Novaculite revisited: Journal of Sedimen-
tary Petrology, v. 46, p. 659-669.

Fournier, R. O., 1973, Silica in thermal waters: laboratory and field
investigations, in Symposium on hydrogeochemistry and biogeo-
chemistry, v. 1, Hydrogeochemistry: Washington, D.C., Clarke,
p. 122-139.

Frondel, C., 1962, The system of mineralogy (7th ed.): New York,
John Wiley, v. 3, 334 p.

Gibson, T. G., and Towe, K. M., 1971, Eocene volcanism and the origin
of horizon A: Science, v. 172, p. 152-154.

——————————— 1975, Origin of horizon A: Clarification of a viewpoint:
Science, v. 188, p. 1221.

Giger, W., and Schaffner, C., 1979, Hydrocarbon indicators of diagenesis
in Monterey Shale, California [abs.]: Geological Society of
America Abstracts with Programs, v. 11, no. 7, p. 432.

Goldsmith, J. R., and Graf, D. L., 1958, Relation between lattice
    constants and composition of the Ca-Mg carbonates: American
    Mineralogist, v. 43, p. 84-101.

Grant, J., 1951, Quantitative organic microanalysis: London,
    J. & A. Churchill, 342 p.

Greenwood, R., 1973, Cristobalite: its relationship to chert formation
    in selected samples from the Deep Sea Drilling Project: Journal
    of Sedimentary Petrology, v. 43, p. 700-708.

Hallam, A., 1964, Origin of the limestone-shale rhythm in the Blue
    Lias of England: a composite theory: Journal of Geology, v. 72,
    p. 157-169.

Hamilton, E. L., 1976, Variations of density and porosity with depth
    in deep-sea sediments: Journal of Sedimentary Petrology, v. 46,
    p. 280-300.

Hein, J. R., Scholl, D. W., Barron, J. A., Jones, M. G., and Miller, J.,
    1978, Diagenesis of Late Cenozoic diatomaceous deposits and
    formation of the bottom simulating reflector in the southern
    Bering Sea: Sedimentology, v. 25, p. 155-181.

Howell, D. G., 1975, Hypothesis suggesting 700 kilometres of right
    slip in California along northwest oriented faults: Geology,
    v. 3, p. 81-83.

Ingle, J. C., Jr., in press, Cenozoic paleobathymetry and depositional
    history of selected sequences within the southern California
    borderland: Cushman Foundation for Foraminiferal Research,
    Special Publication.

Jennings, C. W., 1959, Santa Maria sheet, geologic map of California:
    California Division of Mines and Geology Map.

Jennings, C. W., and Strand, R. G., 1969, Los Angeles sheet, geologic
    map of California: California Division of Mines and Geology Map.

Johnson, T. C., 1974, The dissolution of siliceous microfossils
    in surface sediments of the eastern tropical Pacific: Deep-Sea
    Research, v. 21, p. 851-864.

Jones, J. B., and Segnit, E. R., 1971, Nomenclature and constituent
    phases, pt. I of The nature of opal: Journal of Geological
    Society of Australia, v. 18, p. 57-68.

———————— 1972, Genesis of cristobalite and tridymite at low
    temperatures: Journal of Geological Society of Australia,
    v. 18, p. 419-422.

Kastner, M., Keene, J. B., and Gieskes, J. M., 1977, Chemical controls on the rate of opal-A to opal-CT transformation--an experimental study, pt. I of Diagenesis of siliceous oozes: Geochimica et Cosmochimica Acta, v. 41, p. 1041-1059.

Keene, J. B., 1975, Cherts and porcellanites from the North Pacific, Deep Sea Drilling Project Leg 32, in Larson, R. L., and others, eds., Initial reports of the Deep Sea Drilling Project: Washington, D.C., U.S. Government Printing Office, v. 32, p. 429-507.

Kleinpell, R. M., 1938, Miocene stratigraphy of California: Tulsa, Okla., American Association of Petroleum Geologists, 450 p.

Klug, H. P., and Alexander, L. E., 1954, X-ray diffraction procedures: New York, John Wiley, 716 p.

Knauth, L. P., and Epstein, S., 1975, Hydrogen and oxygen isotope ratios in silica from the JOIDES Deep Sea Drilling Project: Earth and Planetary Science Letters, v. 25, p. 1-10.

Krauskopf, K. B., 1967, Introduction to geochemistry: New York, McGraw-Hill, 721 p.

Lancelot, Y., 1973, Chert and silica diagenesis in sediments from the central Pacific, in Winterer, E. L., and others, eds., Initial reports of the Deep Sea Drilling Project: Washington, D.C., U.S. Government Printing Office, v. 17, p. 377-405.

Manheim, F. T., and Sayles, F. L., 1974, Composition and origin of interstitial waters of marine sediments, based on deep sea drill cores, in Goldberg, E. D., ed., The sea: New York, John Wiley, p. 527-568.

McBride, E. F., and Thomson, A., 1970, The Caballos Novaculite, Marathon region, Texas: Geological Society of America Special Paper 122, 129 p.

McCulloh, T. H., 1965, A confirmation by gravity measurements of an underground density profile based on core densities: Geophysics, v. 30, p. 1108-1132.

————————— 1967, Mass properties of sedimentary rocks and gravimetric effects of petroleum and natural-gas reservoirs: U.S. Geological Survey Professional Paper 528-A, 50 p.

McCulloh, T. H., and Beyer, L. A., 1979, Geothermal gradients, in Cook, H. E., ed., Geologic studies of the Point Conception deep stratigraphic test well OCS-Cal 78-164 no. 1, outer continental shelf, southern California, United States: U.S. Geological Survey Open-File Report 79-1218, p. 43-48.

Meade, R. H., 1964, Removal of water and rearrangement of particles
    during the compaction of clayey sediments--review: U.S.
    Geological Survey Professional Paper 497-B, 23 p.

Milliman, J. D., 1974, Marine carbonates: New York, Springer-Verlag,
    375 p.

Mitsui, K., and Taguchi, K., 1977, Silica mineral diagenesis in
    Neogene Tertiary shales in the Tempoku district, Hokkaido,
    Japan: Journal of Sedimentary Petrology, v. 47, p. 158-167.

Mizutani, S., 1970, Silica minerals in the early stage of diagenesis:
    Sedimentology, v. 15, p. 419-436.

————————— 1977, Progressive ordering of cristobalitic silica in
    the early stage of diagenesis: Contributions to Mineralogy
    and Petrology, v. 61, p. 129-140.

Murata, K. J., Friedman, I., and Cremer, M., 1972, Geochemistry of
    diagenetic dolomites in Miocene marine formations of California
    and Oregon: U.S. Geological Survey Professional Paper 724-C,
    12 p.

Murata, K. J., Friedman, I., and Gleason, J. D., 1977, Oxygen isotope
    relations between diagenetic silica minerals in Monterey Shale,
    Temblor Range, California: American Journal of Science, v. 277,
    p. 259-272.

Murata, K. J., and Larson, R. R., 1975, Diagenesis of Miocene siliceous
    shales, Temblor Range, California: U.S. Geological Survey
    Journal of Research, v. 3, p. 553-566.

Murata, K. J., and Nakata, J. K., 1974, Cristobalitic stage in the
    diagenesis of diatomaceous shale: Science, v. 184, p. 567-568.

Murata, K. J., and Norman, M. B., II, 1976, An index of crystallinity
    for quartz: American Journal of Science, v. 276, p. 1120-1130.

Pierce, R. L., 1956, Upper Miocene foraminifera and fish from the
    Los Angeles area, California: Journal of Paleontology, v. 30,
    no. 6, p. 1288-1315.

Philippi, G. T., 1965, On the depth, time and mechanism of petroleum
    generation: Geochimica et Cosmochimica Acta, v. 29, p. 1021-1049.

Powell, T. G., Cook, P. J., and McKirdy, D. M., 1975, Organic
    geochemistry of phosphorites: relevance to petroleum genesis:
    American Association of Petroleum Geologists Bulletin, v. 59,
    p. 618-632.

Riedel, W. R., 1959, Siliceous organic remains in pelagic sediments:
    Society of Economic Paleontologists and Mineralogists Special
    Publication 7, p. 80-91.

Robertson, A. H. F., 1977, The origin and diagenesis of cherts from
    Cyprus: Sedimentology, v. 24, p. 11-30.

Scholle, P. A., 1977, Chalk diagenesis and its relation to petroleum
    exploration: oil from chalks, a modern miracle?: American
    Association of Petroleum Geologists Bulletin, v. 61, p. 982-1009.

Schrader, H. J., 1973, Cenozoic diatoms from the northeast Pacific,
    Leg 18, in Kulm, L. D., von Huene, R., and others, eds.,
    Initial reports of the Deep Sea Drilling Project: Washington,
    D.C., U.S. Government Printing Office, v. 18, p. 673-797.

Schultz, L. G., 1964, Quantitative interpretation of mineralogical
    composition from X-ray and chemical data for the Pierre Shale:
    U.S. Geological Survey Professional Paper 391-C, 31 p.

Segnit, E. R., Stevens, T. J., and Jones, J. B., 1965, The role of
    water in opal: Journal of Geological Society of Australia, v. 12,
    p. 211-226.

Shapiro, L., 1975, Rapid analysis of silicate, carbonate, and phosphate
    rocks (rev. ed.): U.S. Geological Survey Bulletin 1401, 76 p.

Stein, C. L., and Kirkpatrick, R. J., 1976, Experimental porcelanite
    recrystallization kinetics: a nucleation and growth model:
    Journal of Sedimentary Petrology, v. 46, p. 430-435.

Steyermark, A., 1951, Quantitative organic microanalysis: Philadelphia,
    Blakiston Co., 389 p.

Stosur, J. J., and David, A., 1976, Petrophysical evaluation of the
    diatomite formation of the Lost Hills field, California: Journal
    of Petroleum Technology, v. 28, p. 1138-1144.

Surdam, R. C., Eugster, H. P., and Mariner, R. H., 1972, Magadi-type
    chert in Jurassic and Eocene to Pleistocene rocks, Wyoming:
    Geological Society of America Bulletin, v. 83, p. 2261-2266.

Taylor, J. C., 1976, Geologic appraisal of the petroleum potential
    of offshore southern California: the borderland compared to
    onshore coastal basins: U.S. Geological Survey Circular 730,
    43 p.

Tissot, B., Durand, B., Espitalié, J., and Combaz, A., 1974, Influence
    of nature and diagenesis of organic matter in formation of
    petroleum: American Association of Petroleum Geologists Bulletin,
    v. 58, p. 499-506.

Tissot, B. P., and Welte, D. H., 1978, Petroleum formation and
    occurrence: New York, Springer-Verlag, 538 p.

U.S. Geological Survey, 1974, Proposed plan of development, Santa Ynez unit, Santa Barbara Channel, off California--final environmental statement: U.S. Geological Survey FES 74-20.

Vedder, J. G., Wagner, H. C., and Schoellhamer, J. E., 1969, Geologic framework of the Santa Barbara Channel region: U.S. Geological Survey Professional Paper 679-A, 11 p.

von Rad, U., Riech, V., and Rösch, H., 1977, Silica diagenesis in continental margin sediments off northwest Africa, in Lancelot, Y., Seibold, E., and others, eds., Initial reports of the Deep Sea Drilling Project: Washington, D.C., U.S. Government Printing Office, v. 41, p. 879-905.

Weaver, C. E., and Pollard, L. D., 1975, The chemistry of clay minerals: New York, Elsevier, 213 p.

Weaver, D. W., 1965, Summary of Tertiary stratigraphy--western Santa Ynez Mountains, in Western Santa Ynez Mountains, Santa Barbara County, California: Coast Geological Society and Society of Economic Paleontologists and Mineralogists, Pacific Sections, Guidebook, p. 16-30.

Weaver, F. M., and Wise, S. W., Jr., 1972, Ultramorphology of deep sea cristobalitic chert: Nature Physical Science, v. 237, p. 56-57.

———————— 1974, Opaline sediments of the southeastern coastal plain and horizon A: biogenic origin: Science, v. 184, p. 899-901.

———————— 1975, Origin of horizon A: Clarification of a viewpoint-- a reply: Science, v. 188, p. 1221-1222.

Wilson, M. J., Russell, J. D., and Tait, J. M., 1974, A new interpreta- tion of the structure of disordered α-cristobalite: Contributions to Mineralogy and Petrology, v. 47, p. 1-6.

Wise, S. W., Jr., and Weaver, F. M., 1974, Chertification of oceanic sediments: International Association of Sedimentologists Special Publication, v. 1, p. 301-326.

Wornhardt, W. W., Jr., 1972, Late Miocene and early Pliocene correla- tions in the California province, in Stinemeyer, E. H., ed., Pacific Coast Miocene Biostratigraphic Symposium: Society of Economic Paleontologists and Mineralogists, Pacific Section, Proceedings, p. 284-333.

Zieglar, D. L., and Spotts, J. H., 1978, Reservoir and source-bed history of Great Valley, California: American Association of Petroleum Geologists Bulletin, v. 62, p. 813-826.

APPENDICES

APPENDIX A

CHEMICAL ANALYSES OF ROCKS

In this appendix, data are presented from those samples extensively
analyzed for elemental abundances. Sample preparation and chemical
methods are first described. Then descriptions and locations of
analyzed samples and chemical data are listed.

Sample Preparation

Samples analyzed for major oxides were prepared in the same
way as were partially analyzed samples (see Appendix B) except that:
(1) 20 to 40 g pieces were used; and (2) trace element analyses and
some analyses for organic carbon were made on sample pieces adjacent
(but carefully matched) to the piece used for oxide analyses, rather
than on powder splits.

Pieces used for trace element analyses were also prepared as
described for partially analyzed samples except that a plattner
mortar was not used for any part of the grinding.

Methods of Chemical Analysis

Twenty-seven samples were analyzed for major oxides, carbonate
carbon, organic carbon, and total sulfur. Major oxides and carbonate
carbon were determined by the U.S.G.S., using rapid rock analysis
(Shapiro, 1975). Skyline Labs analyzed total sulfur in powder splits
of most samples among this suite. Separate (but adjacent) sample

pieces were also analyzed by the U.S.G.S. for organic carbon, after
heating at 110°C for 4 hours, by differences between total carbon
(measured by dry combustion with a Leco apparatus) and carbonate
carbon (the acid-soluble fraction measured by a Leco apparatus after
digestion with phosphoric acid).

Skyline Labs analyzed 20 additional samples for most major oxides
(after heating at 105° to 110°C for 4 hours). Mobil Oil Field Research
Laboratory analyzed splits of many of the same 20 samples for organic
carbon by dry combustion after removal of carbonate carbon.

Trace elements were analyzed by the U.S.G.S. on 49 samples,
including 26 of the 27 samples completely analyzed. Trace element
(as well as major element) contents were determined by semiquantitative
computerized optical emission spectrographic analysis, with a standard
deviation of +50 percent or -32 percent of each value.

Sample Descriptions and Localities

In the following list are given the rock name, dominant silica
phase, member, and section location of samples analyzed for major
oxides or trace elements. Further data on most samples is given in
Appendix G, and elemental analyses of the organic matter in several
samples is listed in Appendix C.

1. GAV-13A-20A. Cherty porcelanite (opal-CT); siliceous member,
Gaviota Beach
2. GAV-13A-32C. Porcelanite (opal-CT); siliceous member,
Gaviota Beach.
3. NAP-13-3. Chert (opal-CT); siliceous member, Naples Beach.
4. NAP-13-4. Porcelanite (opal-CT); siliceous member, Naples
Beach.
5. BLK-6B-2. Porcelanite (quartz); siliceous member, Black
Canyon.

6. BIX-7-6B. Porcelanite (quartz); siliceous member, Quail Canyon.

7. BIX-10-3A. Porcelanite (opal-CT and quartz); siliceous member, Quail Canyon.

8. GAV-13A-33. Siliceous mudstone (opal-CT); siliceous member, Gaviota Beach.

9. BIX-10-11D. Siliceous mudstone (quartz); siliceous member, Quail Canyon.

10. NAP-1-1. Siliceous shale (opal-A and opal-CT); siliceous member, Naples Beach.

11. AUG-7B-5. Calcareous chert (opal-CT); upper calcareous shale member, San Augustine Canyon.

12. AUG-4C-20. Calcareous porcelanite (opal-CT); lower calcareous shale member, San Augustine Canyon.

13. REF-6-6. Calcareous mudstone (opal-CT); lower calcareous shale member, Refugio Beach.

14. WOOD-3-3. Calcareous shale (quartz); lower calcareous shale member, Wood Canyon.

15. BLK-5-2. Calcareous shale (quartz); transition member, Black Canyon.

16. NAP-1-5. Calcareous chert (opal-CT); upper calcareous shale member, Naples Beach.

17. AUG-7B-6. Calcareous shale (opal-CT); upper calcareous shale member, San Augustine Canyon.

18. WOOD-4-2A. Organic shale (quartz); organic shale member, Wood Canyon.

19. REF-6-7. Calcareous mudstone (opal-CT); lower calcareous shale member, Refugio Beach.

20. GAV-13A-31. Dolomite, nodular (opal-CT); siliceous member, Gaviota Beach.

21. AUG-4C-14. Dolomite, laminated and bedded; lower calcareous shale member, San Augustine Canyon.

22. AUG-4C-11. Dolomite, bedded; lower calcareous shale member, San Augustine Canyon.

23. BIX-6-5. Unusual quartz chert (lensoid); upper calcareous shale member, Quail Canyon.

24. DAM-5A-8. Unusual quartz chert (veined core); lower calcareous shale member, Damsite Canyon.

25. AUG-4C-15A. Chert (opal-CT and quartz), with foraminifera tests replaced by quartz; lower calcareous shale member, San Augustine Canyon.

26. SAC-11-2. Siliceous shale (opal-CT); Sisquoc Formation, Sacate Beach.

27. AUG-11-2. Siliceous mudstone (opal-CT); Sisquoc Formation, San Augustine Beach.

28. BUL-4-18. Cherty porcelanite (opal-CT); siliceous member, Bulito Canyon.

29. DAM-8C-8D. Cherty porcelanite (opal-CT); siliceous member, Damsite Canyon.

30. DAM-9B-1. Porcelanite (opal-CT); siliceous member, Damsite Canyon.

31. BUL-4-19. Porcelanite (opal-CT); siliceous member, Bulito Canyon.

32. GAV-13A-30. Porcelanite (opal-CT); siliceous member, Gaviota Beach.

33. BLK-7A-10A. Chert (quartz); siliceous member, Black Canyon.

34. BLK-7A-15. Chert (quartz); siliceous member, Black Canyon.

35. WOOD-10C-1. Porcelanite (opal-CT and quartz); siliceous member, Wood Canyon.

36. BLK-7A-12. Porcelanite (quartz); siliceous member, Black Canyon.

37. BUL-4-23. Porcelanite (opal-CT); siliceous member, Bulito Canyon.

38. BIX-9-1. Porcelanite (opal-CT and quartz); siliceous member, Quail Canyon.

39. BUL-4-22. Porcelanite (opal-CT); siliceous member, Bulito Canyon.

40. WOOD-11-1. Porcelanite (opal-CT and quartz); siliceous member, Wood Canyon.

41. GAT-1-5B. Siliceous mudstone (opal-CT); siliceous member, Gato Canyon.

42. DAM-8C-4A. Siliceous shale (opal-CT and quartz); siliceous member, Damsite Canyon.

43. WOOD-11B-2. Siliceous shale (quartz); siliceous member, Wood Canyon.

44. BIX-7-8B. Siliceous shale (quartz); siliceous member, Quail Canyon.

45. GAT-1-5A. Siliceous mudstone (opal-CT); siliceous member, Gato Canyon.

46. DAM-8C-6. Siliceous mudstone (quartz); siliceous member, Damsite Canyon.

47. GAT-1B-1. Siliceous shale (opal-CT and quartz); siliceous member, Gato Canyon.

48. DAM-6B-9. Organic shale (quartz); organic shale member, Damsite Canyon.

49. NAP-10-5Ch. Calcareous chert (opal-CT), similar to (but not identically matched with) NAP-10-5A and NAP-10-5B; lower calcareous shale member, Naples Beach.

50. NAP-10-5Ca. Calcareous mudstone (opal-CT), located 1 to 2 cm from NAP-10-5Ch (#49); lower calcareous shale member, Naples Beach.

51. REF-6-3R. Dolomitic calcareous mudstone (opal-CT) similar to (but not matched with) REF-6-3; lower calcareous shale member, Refugio Beach.

52. NAP-13-5. Siliceous mudstone (opal-A); siliceous member, Naples Beach.

53. WOOD-3-1. Organic-rich calcareous mudstone, in same bed as WOOD-3-4; lower calcareous shale member, Wood Canyon.

54. AUG-6C-9. Organic shale (opal-CT); organic shale member, San Augustine Canyon.

55. WOOD-5-2. Apatite-rich calcareous shale (quartz); transition member, San Augustine Canyon.

56. WOOD-3-1P. Phosphatic nodule in WOOD-3-1 (#53); lower calcareous shale member, Wood Canyon.

57. BIX-6-4. Dolomite, laminated and bedded; upper calcareous shale member, Quail Canyon.

58. AUG-6C-10A. Dolomite, laminated and bedded; transition member, San Augustine Canyon.

59. AUG-7B-1. Dolomite, bedded; upper calcareous shale member, San Augustine Canyon.

60. BIX-6B-6. Dolomite, bedded; upper calcareous shale member, Quail Canyon.

61. WOOD-3-2. Dolomite; lower calcareous shale member, Wood Canyon.

62. BIX-6B-13. Unusual quartz chert (banded); upper calcareous shale member, Quail Canyon.

63. WOOD-2-4Ch. Unusual quartz chert (lensoid); lower calcareous shale member, Wood Canyon.

64. WOOD-2-4Ca. Calcareous shale 1 to 2 cm from WOOD-2-4Ch(#63); lower calcareous shale member, Wood Canyon.

65. WOOD-9-1Ch. Unusual quartz chert (lensoid); upper calcareous shale member, Wood Canyon.

66. WOOD-9-1Ca. Calcareous shale laterally adjacent to WOOD-9-1Ch (#65); upper calcareous shale member, Wood Canyon.

67. WOOD-8-2. Calcareous chert (quartz); upper calcareous shale member, Wood Canyon.

68. WOOD-9-2. Calcareous dolomitic chert (quartz); upper calcareous shale member, Wood Canyon.

Analyses

Tables A-1 to A-3.   Organic carbon by J. H. Tillman, U.S.G.S., Menlo Park, Calif. Sulfur by Skyline Labs, Inc., Wheat Ridge, Colo. Other analyses by H. Smith, U.S.G.S., Reston, Va.

A-4.   Organic carbon by Mobil Field Research Laboratory, Dallas, Texas. Other analyses by Skyline Labs, Inc., Wheat Ridge, Colo.

A-5 to A-8.   Organic carbon by Mobil Field Research Laboratory, Dallas, Texas (except #54 by J. H. Tillman and #53 by G. E. Claypool, U.S.G.S., Denver, Colo.). Other analyses by J. L. Harris, U.S.G.S., Reston, Va.

A-9 to A-14.   Analyses by J. L. Harris, U.S.G.S, Reston, Va.

Lower limits of detection:

Ag	0.10
B	3.2
Be	0.68
Cd	32
Ce	93
Eu	1.5
Ga	2.2
Gd	6.8
La	10
Li	68
Nb	3.2
Nd	46
Pb	10
Sc	1.0
Sn	6.8
Tb	32
Y	1.5
Zn	22
Zr	4.6

Table A-1

Chemical Compositions of Siliceous (Carbonate-free) Rocks, in % by weight

	#1	#2	#3	#4	#5	#6	#7	#8	#9	#10
SiO_2	89.6	85.6	85.9	75.5	75.7	71.5	76.2	71.1	65.4	63.6
Al_2O_3	3.2	4.1	4.3	6.8	7.9	8.5	9.2	9.2	10.4	11.3
Fe_2O_3	0.80	0.44	0.42	0.95	1.1	1.1	0.79	2.3	2.7	2.1
FeO	0.21	0.29	0.59	0.91	0.29	0.78	0.50	1.2	1.4	1.6
MgO	0.24	0.53	0.34	0.76	0.54	0.59	0.75	0.91	1.3	1.3
CaO	0.16	0.49	0.41	0.56	0.35	0.36	0.29	1.2	0.98	1.2
Na_2O	0.73*	1.0*	0.63*	2.4*	0.89	0.72	0.79	1.1*	1.2	2.0*
K_2O	0.68	1.7	0.68	1.4	1.6	1.3	1.4	2.1	1.9	2.2
H_2O^+	1.9	2.2	1.9	3.0	3.9	4.4	2.7	5.1	5.9	5.2
TiO_2	0.17	0.22	0.22	0.37	0.49	0.57	0.45	0.52	0.59	0.62
P_2O_5	0.07	0.09	0.16	0.21	0.19	0.54	0.23	0.22	0.37	0.42
MnO	0.06	0.02	0.02	0.00	0.01	0.02	0.01	0.04	0.02	0.03
CO_2	0.00	0.05	0.01	0.01	0.06	0.00	0.04	0.00	0.00	0.01
Org. carbon	1.90	2.94	2.08	3.33	4.70	6.60	4.05	3.17	4.52	5.29
Total sulfur	n.d.	n.d.	0.5	0.6	n.d.	1.7	0.25	1.5	1.7	1.3
Total	99.7	99.7	98.2	96.8	97.7	98.7	97.7	99.7	98.4	98.2

n.d. = not determined

Table A-2

Chemical Compositions of Calcareous Rocks and Organic Shales, in % by weight

	#11	#12	#13	#14	#15	#16	#17	#18	#19
SiO_2	70.8	78.3	58.5	50.0	52.0	73.7	52.6	25.3	46.6
Al_2O_3	1.2	1.7	2.2	2.3	3.3	3.4	3.5	5.6	7.1
Fe_2O_3	0.20	0.42	0.41	0.43	0.75	0.44	0.34	1.0	1.3
FeO	0.24	0.53	0.65	0.32	0.40	0.50	0.76	0.61	1.6
MgO	0.12	0.19	0.81	0.27	0.43	0.44	0.44	0.67	1.8
CaO	13.0	5.8	16.3	23.6	20.2	7.0	18.9	30.2	17.6
Na_2O	0.15	0.19	0.78	0.23	0.21	0.78	0.45	0.58	1.2
K_2O	0.23	0.29	0.50	0.37	0.69	0.69	0.59	0.76	1.3
H_2O^+	1.7	2.8	2.0	1.9	2.9	2.2	2.6	4.1	3.2
TiO_2	0.06	0.13	0.15	0.10	0.18	0.20	0.21	0.30	0.42
P_2O_5	0.10	0.14	0.36	0.52	2.0	0.23	1.2	1.8	0.79
MnO	0.00	0.00	0.01	0.01	0.00	0.01	0.01	0.03	0.03
CO_2	9.3	3.8	13.2	16.2	11.8	4.6	12.1	20.5	12.1
Org. carbon	2.07	5.06	2.85	4.48	4.35	4.09	5.67	8.51	4.04
Total sulfur	n.d.	n.d.	0.25	n.d.	n.d.	n.d.	0.65	0.6	0.6
Total	99.2	99.4	99.0	100.7	99.2	98.3	100.0	100.6	99.7

n.d. = not determined

Table A-3

Chemical Compositions of Dolomites, Quartz Cherts, and Other Rocks, in % by weight

	#20	#21	#22	#23	#24	#25	#26	#27
SiO_2	42.9	16.0	5.7	89.5	97.1	94.8	71.1	64.2
Al_2O_3	2.0	1.6	1.6	1.4	0.45	0.98	11.1	12.6
Fe_2O_3	0.92	0.80	0.40	0.40	0.02	0.28	2.7	3.6
FeO	0.53	0.28	0.32	0.12	0.12	0.16	0.88	1.7
MgO	10.7	14.2	16.7	0.28	0.03	0.27	2.0	2.5
CaO	16.8	26.0	31.8	1.9	0.08	0.35	1.2	1.7
Na_2O	0.46	0.22	0.16	0.22	0.00	0.12	1.2	1.5
K_2O	0.51	0.55	0.22	0.14	0.04	0.20	1.6	1.9
H_2O^+	0.94	1.9	0.58	2.0	1.4	0.38	4.0	4.1
TiO_2	0.09	0.14	0.09	0.08	0.01	0.10	0.56	0.64
P_2O_5	0.10	0.10	0.43	0.12	0.04	0.06	0.27	0.35
MnO	0.01	0.01	0.05	0.01	0.01	0.00	0.02	0.03
CO_2	24.5	38.5	40.1	1.4	0.01	0.08	0.02	1.3
Org. carbon	1.25	3.51	1.23	1.88	0.53	1.11	1.00	1.40
Total sulfur	n.d.	n.d.	n.d.	n.d.	n.d.	n.d.	0.6	1.7
Total	101.7	103.8	99.4	99.5	99.8	98.9	98.3	99.2

n.d. = not determined

Table A-4

Partial Chemical Compositions of Siliceous (Carbonate-free) Rocks, in % by weight

	#28	#29	#30	#31	#32	#33	#34	#35	#36	#37
SiO_2	85.5	85.8	81.9	83.7	81.2	76.2	78.8	70.7	71.9	70.9
Al_2O_3	2.5	2.8	4.5	4.7	4.9	4.9	5.3	5.5	5.7	6.0
Fe	0.26	0.52	0.75	0.73	0.71	0.95	1.0	1.3	1.2	1.1
MgO	0.33	0.30	0.41	0.41	0.41	0.36	0.41	0.66	0.53	0.70
Na_2O	0.40	0.58	0.67	0.67	0.67*	0.84	0.81	1.0	0.77	0.98
K_2O	0.51	0.61	0.89	0.99	1.1	1.1	1.1	1.2	1.1	1.3
Total sulfur	n.d.	n.d.	n.d.	0.15	0.3	0.65	0.85	1.2	0.6	0.6
Org. carbon	n.d.	2.02	1.71	3.11	n.d.	3.82	4.77	6.41	7.51	5.75

n.d. = not determined

Table A-4 (cont'd.)

	#38	#39	#40	#41	#42	#43	#44	#45	#46	#47
SiO_2	77.0	78.9	74.0	73.8	69.2	65.9	63.3	72.1	61.0	64.4
Al_2O_3	6.6	7.0	8.3	8.5	8.5	8.9	9.1	9.3	10.6	11.7
Fe	0.56	0.71	0.71	0.69	1.7	1.8	1.4	0.73	2.4	1.1
MgO	0.53	0.60	0.76	0.66	0.81	1.0	0.78	0.71	1.5	1.1
Na_2O	0.86	0.98	1.0	1.3	1.8	1.2	1.0	1.3	1.8	2.0
K_2O	1.3	1.3	1.6	1.7	1.7	1.8	1.7	1.8	2.2	2.3
Total sulfur	1.2	0.6	0.25	0.2	1.5	1.7	1.2	0.4	2.5	0.3
Org. carbon	6.13	4.86	n.d.	2.70	4.55	5.18	7.07	4.00	5.82	n.d.

n.d. = not determined

Table A-5

Semiquantitative Chemical Compositions of Calcareous and
Siliceous (Carbonate-free) Rocks, in % by weight

	#48	#49	#50	#51	#52
SiO_2	24	>73	71	66	66
Al_2O_3	1.9	2.3	3.6	4.0	13
Fe_2O_3	0.62	0.66	1.1	1.7	2.4
MgO	0.58	0.55	1.1	2.0	2.0
CaO	27	6.7	11	9.4	1.2
Na_2O	0.15	0.38	0.58	0.61	2.0
K_2O	0.22	0.33	0.77	0.66	1.6
TiO_2	0.073	0.070	0.16	0.17	0.40
P_2O_5	2.2	0.23	0.41	0.34	0.34
MnO	0.019	0.0084	0.017	0.036	0.035
Org. carbon	n.d.	1.49	n.d.	n.d.	5.35

n.d. = not determined

Table A-6

Semiquantitative Chemical Compositions of Phosphatic and
Organic-rich Rocks, in % by weight

	#53	#54	#55	#56
SiO_2	16	43	13	0.28
Al_2O_3	1.7	8.9	1.3	<0.061
Fe_2O_3	0.60	2.9	2.6	0.16
MgO	0.40	1.1	0.38	0.22
CaO	32	9.9	21	31
Na_2O	0.13	0.53	0.28	0.35
K_2O	0.23	1.0	0.15	0.082
TiO_2	0.068	0.20	0.050	0.018
P_2O_5	1.2	2.5	>23	>23
MnO	0.0097	0.027	0.018	0.0088
Org. carbon	16.0	15.9	n.d.	n.d.

n.d. = not determined

Table A-7

Semiquantitative Chemical Compositions of Dolomites,
in % by weight

	#57	#58	#59	#60	#61
SiO_2	7.1	7.5	4.7	3.4	1.5
Al_2O_3	1.2	0.61	1.5	0.68	<0.61
Fe_2O_3	0.54	0.50	0.62	0.46	0.14
MgO	23	20	20	28	23
CaO	22	25	22	25	24
Na_2O	0.18	0.066	0.12	0.084	0.077
K_2O	0.33	0.12	0.30	0.29	0.092
TiO_2	0.060	0.032	0.075	0.062	<0.011
P_2O_5	0.55	<0.17	<0.17	<0.17	0.32
MnO	0.018	0.067	0.018	0.019	0.037
Org. carbon	n.d.	1.34	n.d.	n.d.	2.48

n.d. = not determined

Table A-8

Semiquantitative Chemical Compositions of Quartz Cherts and Associated Rocks from the Calcareous Members, in % by weight

	#62	#63	#64	#65	#66	#67	#68
SiO_2	>73	>73	>73	>73	>73	>73	66
Al_2O_3	0.81	0.89	1.3	1.1	1.1	3.0	3.4
Fe_2O_3	0.26	0.49	0.63	0.29	0.33	1.6	1.4
MgO	0.37	0.088	0.12	0.14	0.12	0.70	3.3
CaO	0.66	2.2	4.8	1.3	3.5	5.7	4.2
Na_2O	0.069	0.062	0.062	0.11	0.093	0.18	0.28
K_2O	<0.082	<0.082	<0.082	<0.082	<0.082	0.45	0.64
TiO_2	0.028	0.028	0.038	0.025	0.038	0.12	0.12
P_2O_5	<0.17	0.55	0.28	<0.17	0.22	0.46	0.53
MnO	0.0028	0.0031	0.0045	0.0026	0.0036	0.0065	0.014
Org. carbon	1.34	n.d.	n.d.	n.d.	n.d.	n.d.	n.d.

n.d. = not determined

Table A-9

Semiquantitative Trace Element Contents of Siliceous (Carbonate-free) Rocks, in ppm

	#1	#2	#3	#4	#6	#7	#8	#9	#10	#52
Ag	0.43	0.31	0.24	0.52	1.6	0.67	0.58	0.50	0.53	0.53
B	18	25	27	68	49	61	75	65	92	190
Ba	270	260	120	280	320	300	370	310	400	310
Be	<	<	0.81	1.1	1.4	1.2	1.7	1.8	2.2	1.6
Cd	<	<	<	<	<	<	<	<	<	<
Ce	<	<	40	37	32	<	36	68	65	41
Co	2.1	2.3	4.1	4.7	3.5	3.9	6.9	7.4	7.3	7.6
Cr	24	60	31	95	140	100	120	110	150	140
Cu	19	20	27	38	84	33	57	55	59	59
Eu	<	<	<	<	<	<	1.6	2.2	1.8	<
Ga	3.1	4.7	3.2	6.9	7.4	7.9	12	11	15	12
Gd	<	<	<	<	<	<	<	<	<	<
La	<	<	15	12	17	15	17	28	42	22
Li	<	<	<	<	<	<	<	<	<	<
Mn	28	32	88	160	55	54	200	170	310	270
Mo	8.6	18	8.8	16	21	12	11	9.6	20	15
Nb	4.1	3.5	<	4.6	4.1	4.7	6.4	5.3	8.5	4.6
Nd	<	<	<	<	<	<	<	<	<	<
Ni	<	9.6	47	35	45	24	57	75	85	87
Pb	<	<	<	<	<	<	12	<	12	12
Sc	1.7	4.1	3.1	6.7	9.9	10	9.5	12	13	9.7
Sn	<	<	<	<	<	<	<	8.0	7.9	<
Sr	32	43	67	120	100	77	140	150	220	180
Tb	<	<	<	<	<	<	<	<	<	<
V	55	92	64	130	210	130	130	91	210	170
Y	2.0	<	10	10	12	6.4	10	24	38	13
Yb	0.32	0.48	1.4	1.5	2.6	1.3	1.9	2.8	5.7	1.9
Zn	<	<	51	<	<	<	51	96	97	100
Zr	22	33	28	96	59	65	73	87	100	79

< = below level of detection

Table A-10

Semiquantitative Trace Element Contents of Calcareous Rocks, in ppm

	#11	#12	#13	#14	#15	#16	#17	#18	#19
Ag	0.19	0.65	0.41	1.2	1.2	0.48	0.79	2.3	0.24
B	5.6	13	16	7.9	16	27	17	28	52
Ba	160	120	100	110	380	160	250	200	320
Be	<	<	0.78	<	<	0.71	<	<	1.6
Cd	<	<	<	<	<	<	<	<	<
Ce	<	<	<	<	<	<	<	<	<
Co	2.3	1.8	4.5	4.3	2.6	3.5	2.6	6.3	9.7
Cr	15	48	60	77	77	43	67	220	170
Cu	17	23	21	32	53	25	51	74	54
Eu	<	<	<	<	<	<	1.8	<	<
Ga	<	<	3.8	<	3.6	3.8	4.0	5.5	11
Gd	<	<	<	<	<	<	<	<	<
La	<	<	<	<	<	<	<	27	27
Li	<	<	<	<	<	<	<	<	77
Mn	51	43	180	110	93	97	92	290	350
Mo	19	15	6.8	34	6.9	16	13	22	6.8
Nb	<	<	4.4	<	5.6	<	<	4.0	3.9
Nd	<	<	<	<	<	<	<	<	<
Ni	30	36	47	67	36	53	32	71	81
Pb	<	<	<	<	<	<	<	<	<
Sc	1.9	2.7	6.1	4.9	5.0	3.3	5.4	10	15
Sn	<	<	<	10	<	<	<	8.4	8.4
Sr	320	220	510	490	550	260	500	910	630
Tb	<	<	<	<	<	<	<	<	<
V	99	240	73	230	210	100	190	230	130
Y	3.1	5.5	17	16	12	6.3	8.9	32	37
Yb	0.43	1.7	1.8	2.4	2.1	1.1	1.9	3.6	4.6
Zn	35	76	120	200	100	71	93	130	160
Zr	18	22	48	22	52	32	34	88	81

Table A-10 (cont'd.)

	#48	#49	#50	#51
Ag	0.66	0.36	0.62	0.37
B	<	19	25	44
Ba	190	85	200	150
Be	<	<	<	0.82
Cd	<	<	<	<
Ce	<	<	<	<
Co	2.5	3.5	4.4	5.5
Cr	69	23	58	68
Cu	19	17	20	17
Eu	<	<	2.2	<
Ga	<	2.2	2.8	3.9
Gd	<	<	<	<
La	<	<	<	<
Li	<	<	<	<
Mn	150	65	130	280
Mo	7.2	12	12	6.9
Nb	<	<	<	3.7
Nd	<	<	<	<
Ni	32	34	48	50
Pb	<	<	<	<
Sc	4.8	3.1	6.3	6.8
Sn	<	<	<	<
Sr	910	250	460	420
Tb	<	<	<	<
V	58	49	110	100
Y	19	4.4	11	10
Yb	1.1	0.46	1.3	1.5
Zn	140	81	120	57
Zr	33	21	40	49

Table A-11

Semiquantitative Trace Element Contents of Phosphatic and
Organic-rich Rocks, in ppm

	#18	#53	#54	#55	#56
Ag	2.3	1.3	3.6	2.4	0.47
B	28	<	58	11	9.4
Ba	200	30	320	280	830
Be	<	<	<	1.2	1.8
Cd	<	<	<	58	34
Ce	<	<	<	<	98
Co	6.3	3.5	6.4	5.7	2.7
Cr	220	67	220	51	11
Cu	74	22	110	30	3.8
Eu	<	<	<	<	3.9
Ga	5.5	<	8.6	2.2	<
Gd	<	<	10	<	14
La	27	<	26	30	120
Li	<	<	<	<	<
Mn	290	75	210	140	68
Mo	22	29	55	180	4.7
Nb	4.0	<	3.3	<	<
Nd	<	<	<	<	<
Ni	71	88	220	120	27
Pb	<	<	<	<	<
Sc	10	6.0	8.5	6.3	10
Sn	8.4	<	11	<	<
Sr	910	960	500	940	2400
Tb	<	36	<	<	45
V	230	180	310	120	100
Y	32	25	35	26	250
Yb	3.6	1.9	5.4	2.7	14
Zn	130	240	310	230	170
Zr	88	27	66	42	110

Table A-12

Semiquantitative Trace Element Contents of Dolomites, in ppm

	#20	#21	#22	#57	#58	#59	#60	#61
Ag	<	0.92	0.14	0.26	<	0.19	0.25	<
B	5.1	4.7	<	<	<	<	<	<
Ba	380	390	260	380	890	340	86	210
Be	<	<	<	<	<	<	<	<
Cd	<	<	<	<	<	<	<	<
Ce	<	<	<	<	<	<	<	<
Co	2.1	2.8	5.1	2.3	2.3	2.5	2.8	1.8
Cr	19	63	98	37	22	29	21	16
Cu	13	19	13	16	8.9	15	12	4.8
Eu	<	<	<	<	<	<	<	<
Ga	<	3.0	<	<	<	<	<	<
Gd	<	<	<	<	<	<	<	<
La	<	14	<	<	<	<	<	<
Li	<	<	<	<	<	<	<	<
Mn	420	120	930	140	520	140	150	290
Mo	4.5	24	7.3	12	4.5	3.3	5.8	2.5
Nb	<	<	<	<	<	<	<	<
Nd	<	<	<	<	<	<	<	<
Ni	14	41	33	20	12	17	19	18
Pb	<	<	<	<	<	<	<	<
Sc	2.0	5.4	4.8	3.5	2.6	3.5	4.1	<
Sn	<	<	<	<	<	<	<	<
Sr	200	260	370	290	510	250	250	270
Tb	<	<	<	<	<	<	<	<
V	47	210	160	110	130	74	80	56
Y	2.5	9.9	6.0	5.5	5.3	7.2	4.6	6.1
Yb	0.34	1.4	0.77	0.54	0.51	0.47	0.30	0.28
Zn	34	140	130	98	<	<	110	<
Zr	23	30	24	24	47	23	15	8.1

Table A-13

Semiquantitative Trace Element Contents of Quartz Cherts and Associated
Rocks from the Calcareous Members, in ppm

	#23	#24	#62	#63	#64	#65	#66	#67	#68
Ag	0.35	0.11	0.20	0.59	0.51	0.21	0.22	0.68	1.1
B	11	21	34	9.2	8.7	12	7.5	14	18
Ba	87	94	79	31	47	34	49	200	310
Be	<	<	<	<	<	<	<	<	<
Cd	<	<	<	<	<	<	<	<	<
Ce	<	<	<	<	<	<	<	<	<
Co	2.6	1.9	1.9	2.3	1.9	2.1	2.2	2.4	4.2
Cr	17	8.3	10	22	28	11	14	60	63
Cu	26	6.9	16	18	19	17	19	58	38
Eu	<	<	<	<	<	<	<	<	<
Ga	<	<	<	<	<	<	<	2.7	3.3
Gd	<	<	<	<	<	<	<	<	<
La	<	<	<	<	<	<	<	<	<
Li	<	<	<	<	<	<	<	<	<
Mn	33	13	22	24	35	20	28	50	110
Mo	22	8.6	20	15	17	13	17	34	19
Nb	<	<	<	<	<	<	<	<	3.4
Nd	<	<	<	<	<	<	<	<	<
Ni	31	14	21	38	40	24	29	35	59
Pb	<	<	<	<	<	<	<	<	<
Sc	2.5	<	<	1.6	1.8	<	<	4.1	4.6
Sn	<	<	<	<	<	<	<	<	<
Sr	48	5.2	21	37	150	33	140	310	270
Tb	<	<	<	<	<	<	<	<	<
V	80	32	40	140	200	41	86	270	190
Y	2.9	<	2.0	6.5	4.0	2.0	2.2	9.3	8.5
Yb	0.48	0.20	0.28	0.96	1.1	0.24	0.39	2.1	1.7
Zn	28	<	26	140	81	29	43	82	110
Zr	12	<	15	13	21	8.9	13	34	25

Table A-14

Semiquantitative Trace Element Contents
of Miscellaneous Rocks, in ppm

	#25	#27
Ag	0.18	0.16
B	12	130
Ba	50	360
Be	<	1.5
Cd	<	<
Ce	<	62
Co	1.6	8.5
Cr	10	120
Cu	8.3	20
Eu	<	<
Ga	<	14
Gd	<	<
La	<	23
Li	<	<
Mn	9.2	440
Mo	4.0	6.8
Nb	<	5.3
Nd	<	<
Ni	9.4	58
Pb	<	13
Sc	2.1	13
Sn	<	<
Sr	14	200
Tb	<	<
V	32	86
Y	1.9	13
Yb	0.18	2.5
Zn	<	67
Zr	9.9	68

< = below level of detection

APPENDIX B

METHODS USED FOR DETERMINATION OF
MINERAL ABUNDANCE

Mineral abundances in each analyzed sample were determined by
interrelation of partial chemical analysis and X-ray diffraction
(XRD). The method emphasized uniformity, accuracy, and careful
matching of material used in different analyses (including porosity
determinations), rather than high precision. Determinations utilized
analytical constants derived from detailed examination and analysis
of select samples, and checks of the method show considerable accuracy.
Since the determination of analytical constants and the routine
determination of mineral contents involved non-standard procedures,
both are described here in detail.

In this appendix, the term "free silica" is used to indicate
the sum of "silica" (biogenic + diagenetic silica; see p. 19)
+ detrital quartz. All 2θ values refer to Cu Kα radiation.

Analytical Methods

Sample preparation and analytical methods are described here
for all samples except those used for X-ray diffraction analysis of
aluminosilicate minerals. That analysis was performed by Mobil's
Field Research Laboratory (see p. 213).

Sample Preparation

Preparation methods emphasized careful matching and uniformity, and all chemically analyzed samples were prepared in a similar manner by one person (the author).

Samples used for routine determination of mineral abundances were cut on either a dry or free-flowing water saw into 4- to 10-g pieces, matched to adjacent sample pieces used for porosity measurement. Powder pieces were ground initially with a plattner mortar, subsequently with a mullite mortar, and sieved with a brass sieve to 100 mesh. Magnetic fragments from the plattner mortar were carefully removed with a magnet. Powders were split with a rifflesplitter into portions used for analysis of SiO_2 and Al_2O_3 contents, X-ray diffraction analysis, and analysis of organic carbon content. Powders were stored in glass vials with plastic caps.

Preparation methods differed slightly for samples which were more completely chemically analyzed (see Appendix A).

X-ray Diffraction Analysis

X-ray diffraction principles. One basic principle was used from X-ray diffraction theory. The relative peak intensity of any selected diffraction planes of two (or any number of) components in the same powder mixture is proportional to the relative weight (or volume) fraction of the two components (Klug and Alexander, 1954, p. 412). Thus for two components, a constant of proportionality established for one mixture will be applicable to any other mixture as long as the two components are similar in both mixtures and identical methods of preparation and analysis are used.

XRD peak heights—which are commonly used as measures of peak intensity—vary with each mineral structure, its crystallinity and grain size, as well as with grinding methods, slide preparation techniques, and numerous machine characteristics (Klug and Alexander, 1954). When proportionality constants established between minerals in one suite of rocks are applied to samples from other areas or formations, considerable error may result. For this reason, constants of proportionality used in this study were determined on typical Monterey rocks from within the study area. Because clay minerals have many structural variations which affect their diffraction characteristics (Carroll, 1970) and because large opal-CT peaks interfere with the important clay peak at 19.8° 2θ, the abundance of clay was not determined from XRD patterns in this study.

Another XRD principle sometimes applied to quantitative determination of two polymorphs, such as quartz and opal-CT (Ernst and Calvert, 1969), states that absolute peak intensities of any diffraction plane of one polymorph decrease to an exact proportion of volume fraction in a mixture with the second polymorph (Klug and Alexander, 1954). Since the principle does not apply to relative intensities and can only be used for mixtures identical except for differences in polymorph content, the principle was not used in this study and a constant of proportionality between quartz and opal-CT was determined.

X-ray diffraction methods. Initial testing showed little effect on XRD peak intensities from preferred orientation or mesh size, apparently because of the fine grain size and random crystal orientation of minerals, including calcite. Powder splits were therefore ground in a mullite mortar until grittiness disappeared, just

enough water was added to form a paste, and the pastes were smeared
on a glass slide.

Samples were routinely scanned at 2° 2θ per minute between 18°
and 40° 2θ on a single X-ray diffractometer, using Cu Kα radiation.
Although no peak heights were used in the region, most samples were
also scanned from 2° to 18° 2θ in order to check for unusual con-
stituents. Routine scans covered a period of 2 years; samples used
for determination of analytical constants, however, were all scanned
under identical conditions during a 36-hour period.

Measurement of peak intensities. Where specific minerals are
consistent in grain size and crystallinity, XRD peak height quite
accurately approximates peak intensity. For convenience, therefore,
most peak intensities were determined in this study from peak heights.

For opal-CT, however, peak height is not a good indicator of peak
intensity, as peaks sharpen (increase their height-to-width ratio)
during "ordering." Peak intensity of opal-CT was therefore determined
in this study from the area under the principal diffracting peak
near 22° 2θ. Corrections for two small interfering peaks were made
to this value, based on the ratio between the area under each small
peak (quartz at 20.8° 2θ and plagioclase feldspar at 22.0° 2θ)
and the area under the corresponding principal peak (quartz at 26.6°
2θ and plagioclase feldspar near 28.0° 2θ). Values of each ratio
were determined by measurement of peaks on XRD patterns of 25 or
more samples without trace of opal-CT. Where small to moderate
amounts of calcite were present, a correction was also made for a
small calcite peak at 23.0° 2θ which was sometimes present on the
flank of the opal-CT peak. Where large amounts of calcite or dolomite

were present, peak intensity of opal-CT was much reduced, its abun-
dance difficult to measure, and sometimes its actual presence uncertain.
In such cases, insoluble residues were prepared and used to supple-
ment whole-rock XRD analyses. After corrections, opal-CT peak
intensities were converted, by comparison with quartz peak areas,
to equivalent quartz peak heights.

Chemical Analysis

All samples used for routine determination of mineral abundances
were partially chemically analyzed--in all cases for SiO_2 and Al_2O_3
contents, and in many cases for organic carbon contents as well.
All partial chemical analyses were made on 100 mesh powder splits
after drying at 100° to 105°C for 4 hours. SiO_2 and Al_2O_3 were
analyzed by atomic absorption by Skyline Labs at Wheat Ridge,
Colorado. Six blind duplicates show adequate reproducibility
(table B-1). Mobil Research and Development Corporation's Field
Research Laboratory in Dallas, Texas made most organic carbon
analyses by dry combustion after removal of carbonate carbon. Two
blind duplicates indicate excellent reproducibility (table B-2).

Chemical methods used on those samples which were more completely
analyzed are described in Appendix A.

Composition of the Aluminosilicate Fraction

This section examines variation in the composition of the
aluminosilicate fraction. The magnitude of this variation is of
interest because the method used to determine aluminosilicate and
silica contents assumes that the SiO_2 and Al_2O_3 contents of the

Table B-1

Duplicate Analyses of SiO_2 and Al_2O_3

Sample	SiO_2 wt %	Al_2O_3 wt %
1*	69.5	10.6
	70.4	10.6
2*	32.1	4.3
	31.7	4.5
3*	28.8	4.2
	30.9	3.8
4*	15.2	3.8
	15.0	3.6
5**	81.5	3.8
	82.8	4.3
6**	64.6	3.6
	64.0	3.4

*Duplicates analyzed in the same batch.

**Duplicates analyzed in separate batches up
to 1 year apart.

Table B-2

Duplicate Analyses of Organic Carbon

Sample	Organic carbon weight %
1	6.13
	6.06
2	2.98
	2.90

aluminosilicate fraction vary little and do not vary systematically with increasing detrital content.

Variation in the composition of the aluminosilicate fraction is examined first from XRD estimates of mineral abundances in detrital-rich samples. Variation is then more generally examined, in rocks with a complete range of detrital contents, by evaluation of chemical analyses. Finally, the probable effect of variation on aluminosilicate and silica contents is estimated.

X-ray Diffraction Analysis of Aluminosilicate Minerals

Preparation and analysis of samples used to determine aluminosilicate mineral abundances were done by Mobil Research and Development Corporation's Field Research Laboratory, under the supervision of B. E. Felber. Standard X-ray diffraction methods were used.

Samples used for X-ray diffraction analysis of aluminosilicate minerals are somewhat unusual. In the first place, samples are not representative of the range of bulk compositions found in Monterey rocks along the Santa Barbara coast. Samples typify only the more detrital-rich rocks, including both carbonate-free and carbonate-bearing rocks. In addition, portions used by Mobil were not matched with portions used for partial chemical analysis and routine X-ray diffraction. In several cases (as in fig. B-5), however, portions used by Mobil were approximately matched with portions used for more complete chemical analysis.

X-ray Diffraction Data

X-ray diffraction analysis shows that the aluminosilicate fraction contains principally mixed-layer illite-montmorillonite (with

40-60 percent illite layers) and also plagioclase feldspar, K-feldspar, mica, and chlorite. Semiquantitative estimates of relative abundances of these minerals are given in table B-3.

These estimates suggest tentative conclusions about the composition of the aluminosilicate fraction. First, variation is not very great; except for a few mica-rich and chlorite-rich samples, most samples are close to an average composition of 61 percent mixed-layer illite-montmorillonite, 20 percent plagioclase feldspar, 7 percent K-feldspar, and 11 percent mica (fig. B-1). Examination of variations also suggests that abundances of specific minerals do not systematically vary with the SiO_2/Al_2O_3 proportion (fig. B-2).

Chemical Data

Tentative conclusions based on XRD estimates can be evaluated further by examination of chemical analyses, which provide information on samples with a complete range of detrital contents. Exact mineral abundances cannot easily be determined from chemical analyses as most minerals detected by XRD range considerably in chemical composition (table B-4). Most oxides, however, have quite different abundances in different minerals, as shown by proportions of oxides to Al_2O_3 (table B-5). Variation in mineral abundances, therefore, can be broadly evaluated from proportions of Al_2O_3 to the major oxides present in the aluminosilicate fraction.

Are oxide proportions consistent with variations in mineral abundances determined by XRD? Variations of several oxides (CaO, P_2O_5, and H_2O^+) are difficult to evaluate because each of these oxides may be partly present in nonaluminosilicates whose abundance is

Table B-3

Semiquantitative Estimates of Mineral Abundance in the Aluminosilicate Fraction

	1/[3]	2/[3]	Plagioclase feldspar, wt %[3]	K-feldspar wt %[4]	Mica, wt %[3]	Chlorite, wt %[3,5]	Al_2O_3/SiO_2[6]
1	75	0.49	12	4	9	0	0.144
2	55	0.40	18	6	21	0	0.200
3	74	0.60	14	5	7	0	0.147
4	72	0.51	15	5	8	0	0.104
5	73	0.55	14	5	8	0	0.118
6	67	0.51	20	7	6	0	0.086
7	67	0.53	22	7	4	0	0.121
8	71	0.58	15	5	9	0	0.158
9	58	0.40	27	9	6	0	0.089
10	47	0.51	15	5	33	0	0.226
11	55	0.57	30	10	5	0	0.139
12	62	0.57	25	8	5	0	0.182
13	56	0.48	28	9	7	0	0.114
14	55	0.51	25	8	12	0	0.130
15	72	0.40	15	5	8	0	0.167
16	43	0.50	25	8	21	3	0.178
17	52	0.49	15	5	20	8	0.188
18	65	0.40	21	7	7	0	0.220
19	40		16	5	39	0	0.092
20	52	0.40	29	10	9	0	0.090
21	61	0.53	17	6	15	1	0.198
22	42	0.60	12	4	21	21	0.152

[1]Mixed-layer illite-montmorillonite, wt %
[2]Proportion of montmorillonite layers in mixed-layer clay
[3]Analyses under supervision of B. E. Felber of Mobil Field Research Laboratory
[4]Estimated by author
[5]May include minor kaolinite
[6]From chemical analyses
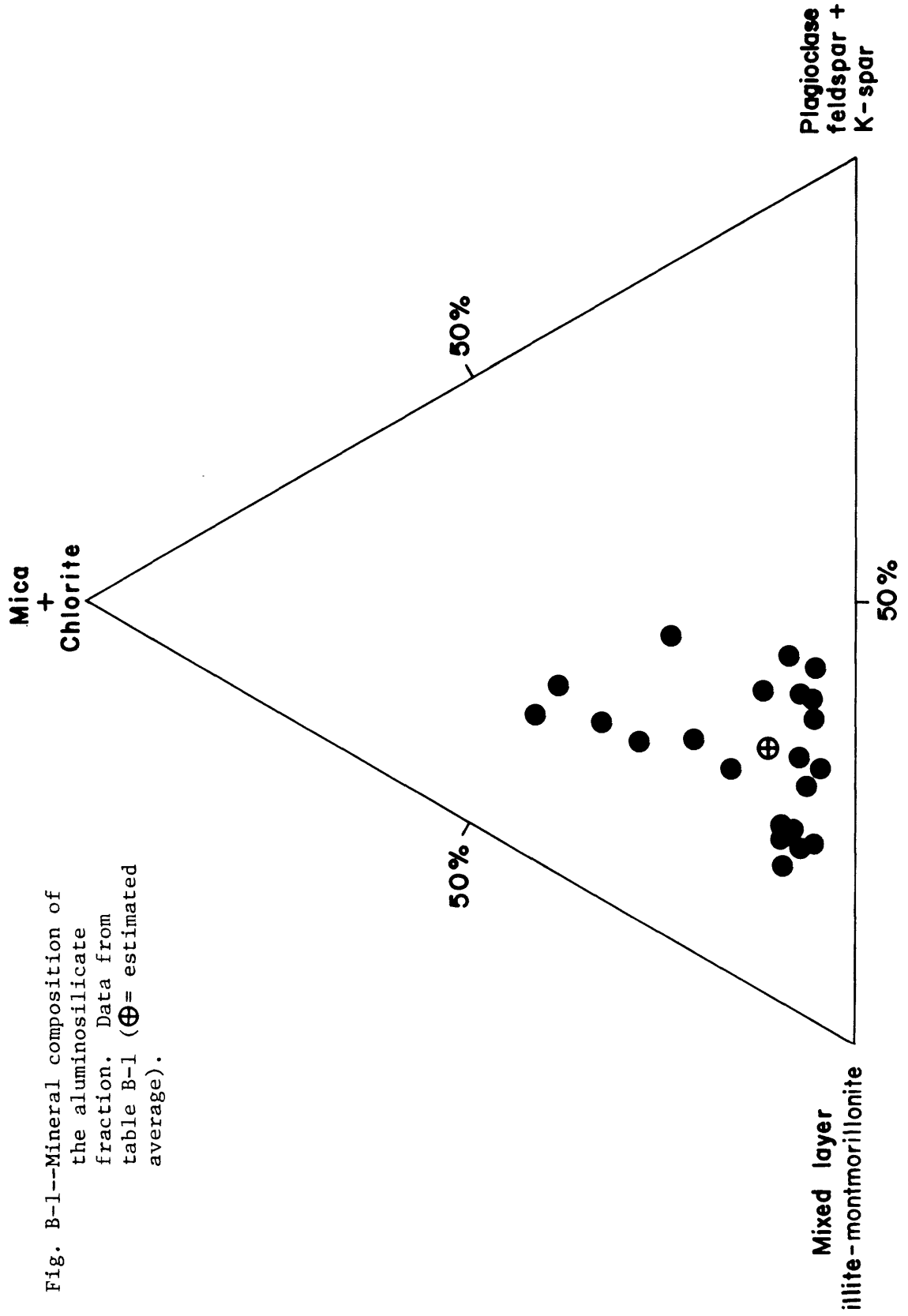
Fig. B-1--Mineral composition of the aluminosilicate fraction. Data from table B-1 ($\oplus$= estimated average).
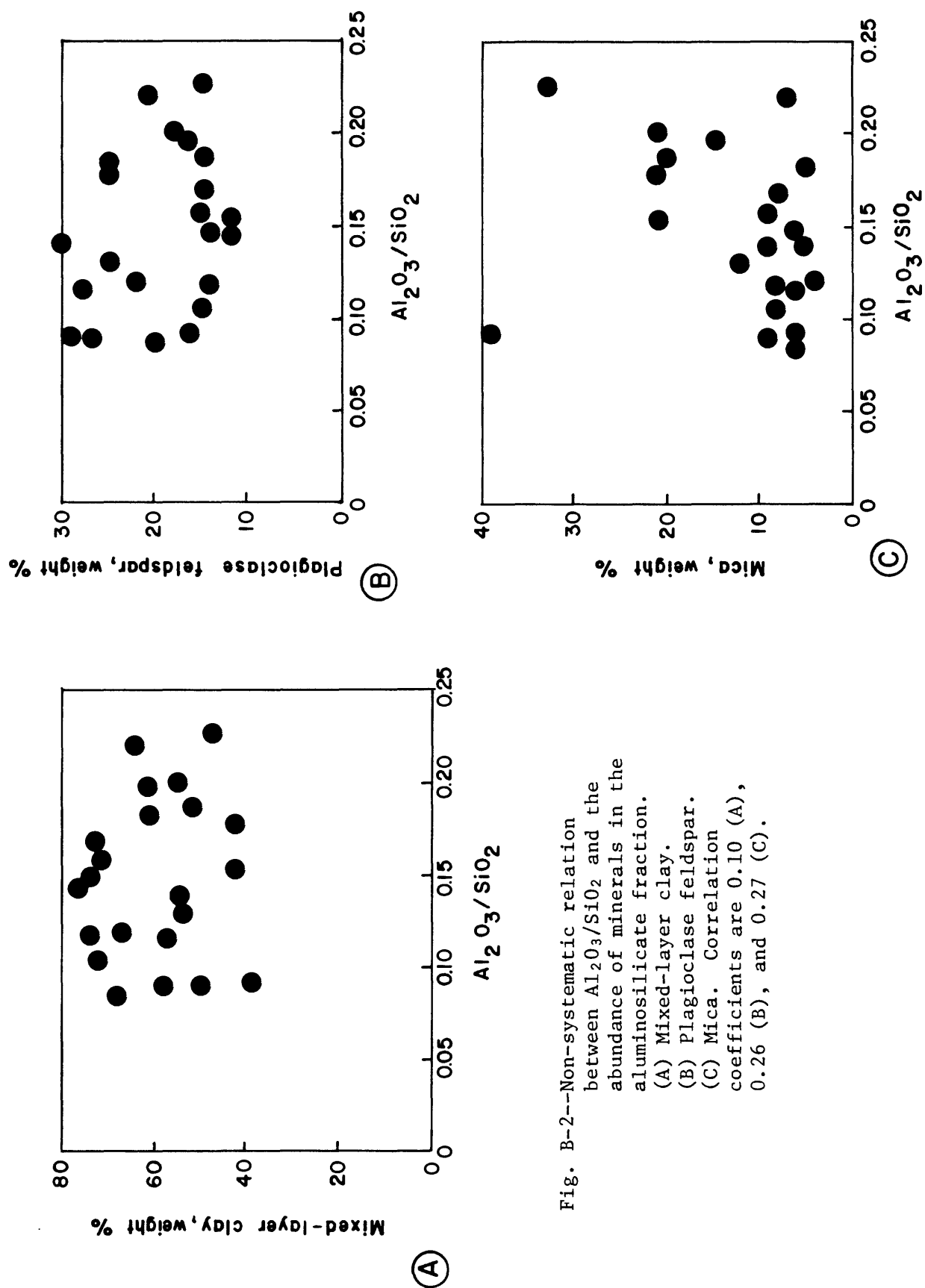
Fig. B-2--Non-systematic relation
between Al_2O_3/SiO_2 and the
abundance of minerals in the
aluminosilicate fraction.
(A) Mixed-layer clay.
(B) Plagioclase feldspar.
(C) Mica. Correlation
coefficients are 0.10 (A),
0.26 (B), and 0.27 (C).

Table B-4

Chemical Composition of Minerals in the Aluminosilicate Fraction

	SiO$_2$	Al$_2$O$_3$	Fe$_2$O$_3$	FeO	MgO	CaO	Na$_2$O	K$_2$O	H$_2$O$^+$	TiO$_2$
Mixed-layer illite-mont.[1]										
Median	54.4	23.9	1.9	0.74	3.0	0.10	0.14	5.6	6.7	0.77
(Range)	(50.9-60.0)	(18.6-34.5)	(0.19-7.5)	(0.00-2.1)	(1.4-4.4)	(0.02-1.5)	(0.00-1.0)	(2.7-9.1)	(5.5-10.8)	(0.22-1.5)
Plagioclase feldspar										
Albite[2]	67.7	20.1	0.04	0.01	0.07	0.40	11.0	0.33	0.36	0.00
Anorthite[3]	44.0	35.6	0.32	0.04	0.00	19.0	0.50	0.02	0.56	0.00
K-feldspar[4]										
Median	64.4	18.9	0.3		0.04	0.16	1.8	13.7	0.1	0.04
(Range)	(63.6-67.3)	(16.7-21.8)	(0.09-2.56)		(0.00-0.14)	(0.03-2.75)	(0.79-7.5)	(3.8-16.1)	(0.01-0.36)	(0.00-0.08)
Mica (illite)[5]										
Median	48.4	30.5	2.7	1.0	1.5	0.26	0.47	7.9	6.2	0.18
(Range)	(45.3-56.9)	(19.0-36.6)	(0.5-5.8)	(0.00-1.9)	(0.00-3.9)	(0.00-1.6)	(0.00-2.0)	(5.3-10.9)	(3.6-8.0)	(0.0-1.2)
Chlorite[6]										
Median	27.0	18.7	3.5	18.2	19.0	0.18	0.1	0.03	11.4	0.3
(Range)	(20.8-31.4)	(17.5-24.4)	(0.1-8.7)	(0-38.0)	(4.2-37.6)	(0-1.0)	(0-0.17)	(0-0.17)	(10.3-13.2)	(0.1-0.88)

[1] Weaver and Pollard (1975), p. 109, 10 analyses
[2] Deer, Howie, and Zussman (1966), p. 324, average of analyses 1 and 2
[3] Deer, Howie, and Zussman (1966), p. 324, average of analyses 7 and 8
[4] Deer, Howie, and Zussman (1966), p. 300-301, 8 analyses (excludes perthites, 1-3, 5-7)
[5] Deer, Howie, and Zussman (1962), p. 218-220, 12 analyses (excludes 2, 14, 15)
[6] Deer, Howie, and Zussman (1966), p. 234-235, 8 analyses

Table B-5

Abundance of Select Oxides, Relative to Al_2O_3, in Minerals in the Aluminosilicate Fraction

	SiO_2/Al_2O_3	Fe/Al_2O_3 x 100	MgO/Al_2O_3 x 100	K_2O/Al_2O_3 x 100	Na_2O/Al_2O_3 x 100	TiO_2/Al_2O_3 x 100
Mixed-layer illite-mont.[1]						
Median	2.2	7.8	12.5	23.8	0.4	2.3
(Range)	(1.5-2.6)	(0.4-33.4)	(4.5-19.0)	(10.3-32.6)	(0-3.0)	(1.0-6.5)
Plagioclase feldspar[1]						
Albite	3.4	0.2	0.3	1.7	55.	0.0
Anorthite	1.2	0.7	0.0	0.1	1.4	0.0
K-feldspar[1]						
Median	3.4	1.2	0.2	61.3	15.6	0.2
(Range)	(2.9-3.9)	(0.3-10.7)	(0-0.6)	(17.2-91.6)	(2.6-42.0)	(0-0.4)
Mica (illite)[1]						
Median	1.6	6.2	6.2	27.5	1.7	0.5
(Range)	(1.3-3.1)	(0.5-19.0)	(0-15.6)	(17.6-35.3)	(0-6.5)	(0-4.4)
Chlorite[1]						
Median	1.3	78.	83.	0.1	0.4	1.5
(Range)	(0.95-1.8)	(0-202)	(24-220)	(0-0.9)	(0-0.9)	(0.5-4.2)
Bulk samples[2]						
Median		20.8	9.4	19.8	13.5	5.5
(Range)		(15.4-41.7)	(6.9-14.2)	(13.7-22.5)	(6.4-20.8)	(4.3-7.6)

[1]Values from published analyses listed in table B-4
[2]Values from this study, analyses 1 to 19 and 28 to 47 in Appendix A. For Na_2O values, excludes beach rocks; for MgO values, excludes dolomite-bearing rocks; for Fe values, excludes slightly bleached samples.

difficult to determine (fig. B-3A,B,C). Even in carbonate-free

rocks, for example, CaO may be present in apatite, which is detectable

petrographically as minute bones or rare nodules. Total CaO contents

in most carbonate-free rocks, however, are too low to form apatite

with all the P_2O_5 present. This relationship suggests that small

amounts of P_2O_5 are not always present as apatite and may in fact

be adsorbed on clays, as in the Pierre Shale (Schultz, 1964).

Apatite contents, and hence apatite-corrected CaO and P_2O_5 contents,

are therefore difficult to determine precisely. Finally, H_2O^+ may

derive from organic matter or from physically adsorbed water in closed

pores as well as from clays. Amounts of H_2O^+ in aluminosilicate

minerals are therefore not precisely determinable.

Iron abundance is also difficult to evaluate in detail (fig. B-3D).

FeO, for example, can be in pyrite; but since sulfur is present in

both pyrite and organic matter, pyrite contents are difficult to

determine precisely. The presence of pyrite also complicates inter-

pretation of Fe_2O_3 because relative amounts of ferric and ferrous

iron cannot be measured reliably due to the reducing effect of the

abundant organic matter (L. Shapiro, pers. commun., 1976). At the

same time, iron contents are so high in chlorite that iron abundance

probably reflects even small differences in chlorite abundance.

Detailed examination of abundances of four other oxides (MgO,

K_2O, Na_2O, and TiO_2) is more clearly informative as these oxides are

present almost entirely in aluminosilicates and also vary in abundance

among different minerals. MgO, for example, is absent in feldspars,

present in moderate amounts in mixed-layer illite-montmorillonite

and mica, and abundant in chlorite. K_2O is present among the feldspars

Fig. B-3--Relation between the abundance of Al_2O_3 and of oxides partly present outside the aluminosilicate fraction. Values on carbonate-free basis; solid lines in (A) and (B) indicate the mean proportion. (A) CaO. (B) P_2O_5. (C) H_2O^+. (D) Fe.
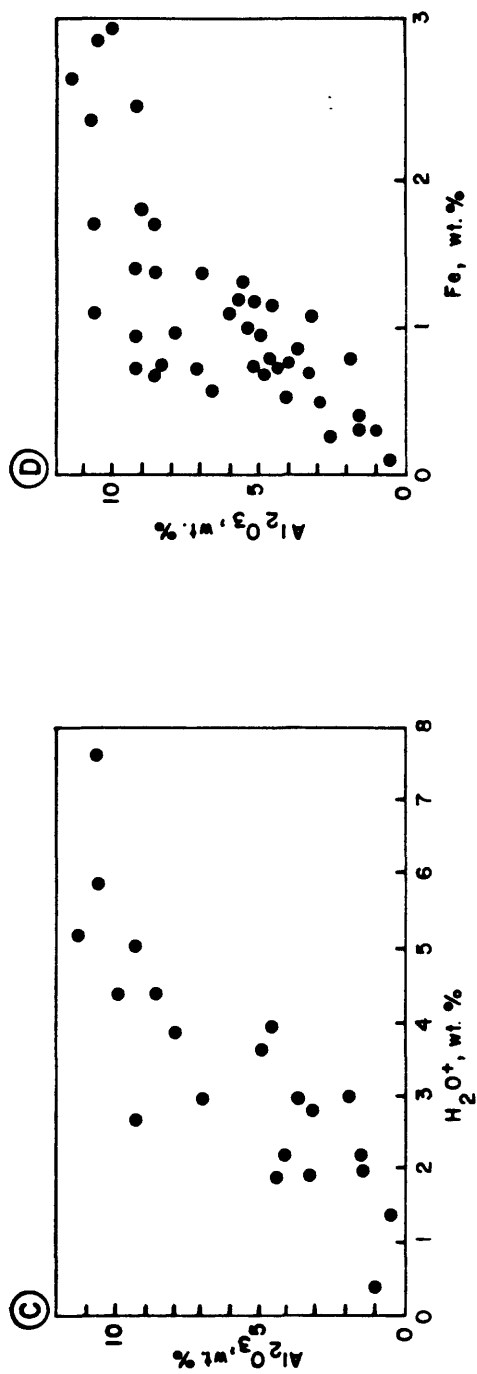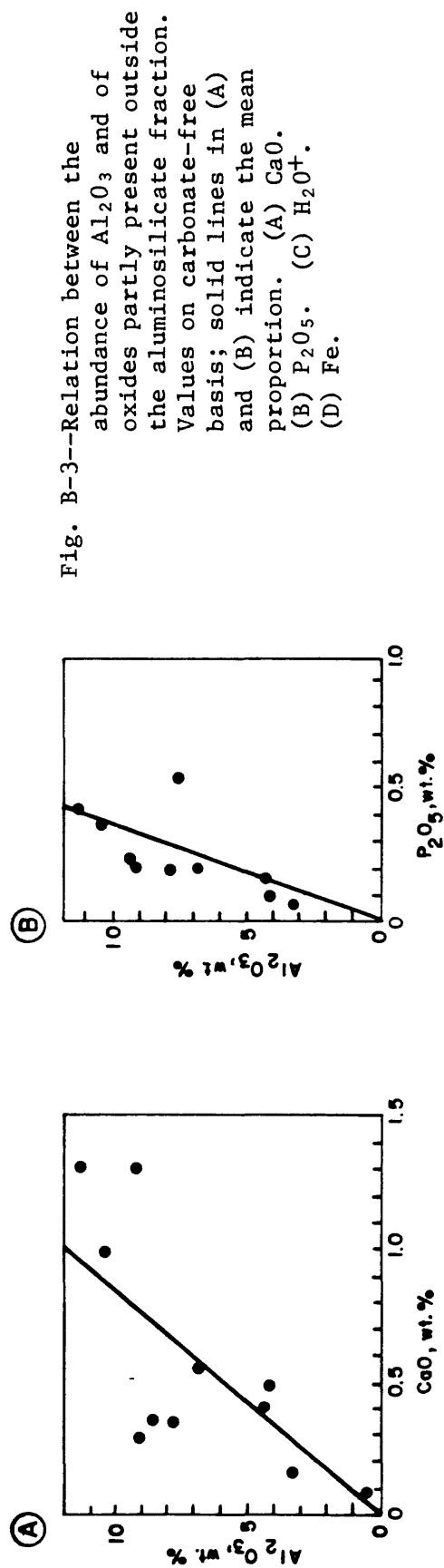
only in K-feldspar and among the clays only in illite and biotite.

Na_2O is present mainly in plagioclase and possibly also in K-feldspar.

TiO_2, virtually absent in feldspar, is usually present in all clays

and could also be in trace amounts of titanium-rich detrital minerals

(which are included here as aluminosilicate minerals).

In view of variations of oxide content in different minerals,

correlations between Al_2O_3 and the oxides MgO, K_2O, Na_2O, TiO_2--

and, to a lesser extent, total iron--suggest that mineral abundances

do not vary greatly (fig. B-4). In general, variations in these

oxide proportions are consistent with variations in mineral abundances

determined by XRD (fig. B-5). Considering this consistency, then,

the fact that relative oxide abundances do not systematically change

with Al_2O_3 (fig. B-4; note distribution of points between dotted

lines) indicates that mineral abundances have a similar range of

proportions in detrital-rich and detrital-poor rocks.

Significance of Variation to Determinations of Components

In this study, determinations of mineral abundances are affected

by the composition of the aluminosilicate fraction mainly in terms

of its average Al_2O_3 and SiO_2 content. In order to evaluate the

importance of mineral variation, then, probable variations in silica

and alumina content resulting from mineral variations were estimated.

The estimate was derived from chemical compositions, based on

median literature values of each mineral (table B-4). Silica and

alumina contents were determined for the average mineral composition

and for samples with extreme abundances of various minerals, as

judged from XRD estimates (table B-3). Results show that errors
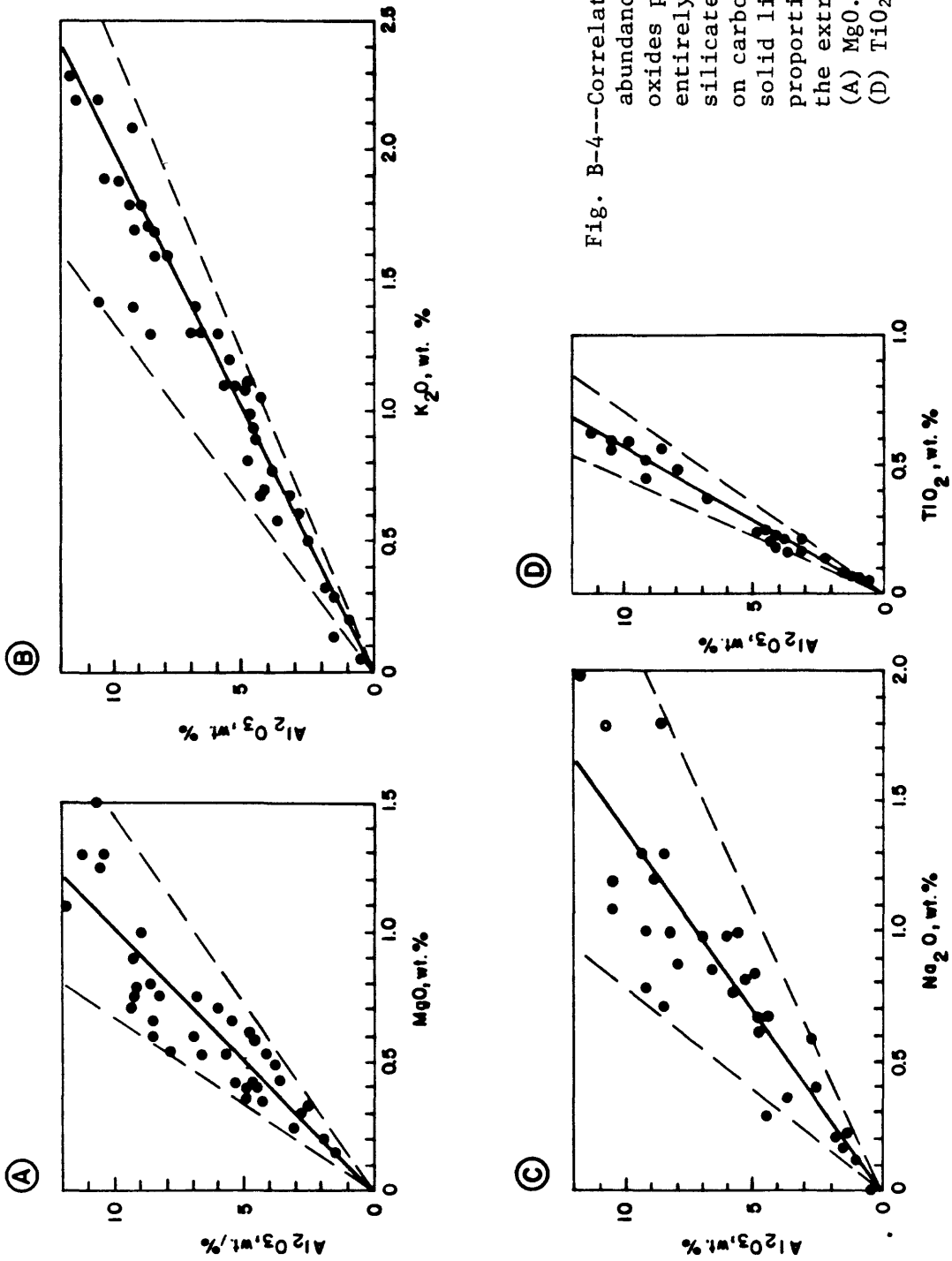
Fig. B-4—Correlation between the abundance of Al_2O_3 and of oxides present almost entirely in the alumino-silicate fraction. Values on carbonate-free basis; solid lines indicate the mean proportions, dashed lines the extreme proportions. (A) MgO. (B) K_2O. (C) Na_2O. (D) TiO_2.

Increasing mica

Increasing mixed-layer clay

Mica + Chlorite

Plagioclase feldspar + K-spar

MgO	Fe	K₂O	TiO₂
11.9	23.2	19.3	5.5
9.9	27.7	22.5	5.6
8.6	-	17.6	-

Mixed layer illite–montmorillonite

Increasing chlorite + mica

Increasing mixed-layer clay

MgO	Fe	K₂O	TiO₂
-	31.2	18.8	5.9
19.8	30.1	15.1	5.1
8.6	19.7	18.3	6.2

Increasing mixed-layer clay

Increasing feldspar

MgO	Mg₂O	K₂O
8.6	10.3	18.3
8.8	12.7	17.6
9.2	16.5	19.7

Fig. B-5--Systematic relation between mineral abundance and relative oxide abundance in the aluminosilicate fraction. o = sample from the Sisquoc Formation.

due to variation are probably not large (table B-6). For most samples
(with 8.0 percent Al_2O_3 or less), errors in calculated values are
less than 2.4 percent aluminosilicate content or 2.3 percent free
silica content.

Determination of Analytical Constants

Determination of analytical constants involved approximations
with sets of samples selected for specific ranges in the abundance of
particular minerals. The method—which was designed to overcome the
usual difficulties in making accurate estimates of aluminosilicate
contents and free silica contents—is applicable only to a suite of
closely associated samples. Important assumptions are that variation
in the aluminosilicate fraction is small and that variations are not
systematically related to the abundance of detrital minerals. For
Monterey rocks along the Santa Barbara coast, both assumptions are
apparently justified. In determining constants, therefore, the
composition of the aluminosilicate fraction was treated as invariant.

Most analytical constants were determined on calcareous rocks.
Calcite is important because it has sharp XRD peaks and because its
true abundance is easily determined by chemical analysis. In this
method, calcite served as an absolute standard.

Outline of Method

Major analytical constants include the abundances of Al_2O_3
and SiO_2 in the aluminosilicate fraction and XRD proportionality
constants for quartz/calcite, opal-CT/calcite, and quartz/opal-CT.

Table B-6

Probable Variation in Oxide Proportions Due to Variation in Composition of the
Aluminosilicate Fraction and Resulting Error in Estimates of Aluminosilicate
Content and of Silica Content. Errors are calculated for
sample with 8.0 percent Al_2O_3.

Sample no.[*]	SiO_2/Al_2O_3	$100/Al_2O_3$	Other oxides/Al_2O_3	Error in aluminosilicate content, wt %	Error in silica content, wt %
1	2.25	4.00	0.75	0.4	0.5
11	2.41	4.13	0.72	0.6	0.8
16	2.22	3.97	0.75	0.6	0.7
19	2.06	3.75	0.69	2.4	2.1
22	2.03	4.08	1.05	0.2	2.3

[*]From table B-3.

Constants were determined by successive estimates. First, limits in the SiO_2/Al_2O_3 value of the aluminosilicate fraction were approximated from literature values. This approximation was applied to calcareous rocks with high SiO_2 and low Al_2O_3 contents, where only a small uncertainty in free silica content was generated by a large uncertainty in the value of SiO_2/Al_2O_3 attributed to aluminosilicates. Good estimates resulted of XRD proportionality constants between calcite and quartz, calcite and opal-CT, and quartz and opal-CT. Actual amounts of free silica could then be closely determined (by reference to calcite) in silica-poor rocks, and amounts of SiO_2 in the aluminosilicate fraction were derived by difference from analyzed SiO_2. Because of low free silica contents and high aluminosilicate contents, only a small uncertainty in aluminosilicate SiO_2 contents was thus generated, and the ratio of SiO_2/Al_2O_3 in the aluminosilicate fraction could be closely approximated. This SiO_2/Al_2O_3 value, combined with the average proportion of other oxides to Al_2O_3, generated an approximation to the proportion of Al_2O_3 in the aluminosilicate fraction. The SiO_2/Al_2O_3 was also used to refine values of XRD proportionality constants.

Literature Approximation of SiO_2/Al_2O_3 in the Aluminosilicate Fraction

Limits of possible values of SiO_2/Al_2O_3 in the aluminosilicate fraction were approximated from semiquantitative estimates of mineral abundances and from mineral analyses in the literature. For each sample in table B-3, the minimum (maximum) value of SiO_2/Al_2O_3 was

calculated from mineral analyses with minimum (maximum) values of SiO_2/Al_2O_3 (table B-7). Results show that the value of SiO_2/Al_2O_3 in the aluminosilicate fraction has a possible range from 1.5 to 3.0.

Calcite Content from Chemical Analyses

Calcite contents were determined from both CaO and CO_2 contents and these values averaged.

CO_2 seems to occur only in calcite and dolomite. Rocks used as standards were pre-selected by XRD for the absence of dolomite, and values of MgO/Al_2O_3, which are similar to values in carbonate-free rocks, confirm its absence. Amounts of calcite from CO_2 contents were therefore determined by assuming a stoichiometric amount of CO_2 at 44.0 percent.

Amounts of calcite from CaO contents were determined after correction for CaO in apatite and in detrital minerals. The correction to CaO for apatite was based on analyses of P_2O_5, corrected for small amounts attributed to clays (fig. B-3B). Calculations were based on 42.4 percent P_2O_5 and 55.5 percent CaO (Deer and others, 1966, p. 506, average of analyses #2 and #5). The small correction to CaO for detrital minerals was based on analyses of siliceous rocks from the siliceous member, in which CO_2 contents average ≤ 0.1 percent. In these rocks, CaO could be present in apatite, but most P_2O_5 is apparently present in clays. All CaO was therefore attributed to aluminosilicates, with CaO/Al_2O_3 equal to 0.084 (fig. B-3A). After these corrections, calcite contents were calculated on the basis of 56.0 percent CaO.

Table B-7

Published Chemical Analyses with Extreme Values of SiO_2/Al_2O_3
for Minerals in the Aluminosilicate Fraction
(For sources, see table B-4.)

	Mixed-layer illite-montmorillonite	Plagioclase feldspar*	K-spar	Mica	Chlorite
Analyses with maximum SiO_2/Al_2O_3:					
SiO_2	57.2	61.8	64.9	58.9	31.4
Al_2O_3	18.9	24.0	16.7	19.1	17.6
SiO_2/Al_2O_3	3.03	2.58	3.88	3.08	1.78
Analyses with minimum SiO_2/Al_2O_3:					
SiO_2	52.0	61.8	63.7	46.6	23.2
Al_2O_3	34.7	24.0	21.8	36.4	24.4
SiO_2/Al_2O_3	1.50	2.58	2.92	1.28	0.95

*Values calculated for 75 percent albite and 25 percent anorthite.

Results of these two calculations show a consistent difference, suggesting that CO_2 analyses are low and/or CaO analyses high. The discrepancy is unrelated to clay or apatite contents, so that it is apparently not due to corrections based on these quantities. The discrepancy is probably due to calibration errors. Additional CO_2 analyses of splits from two of the same powders yielded calcite estimates exactly equalling the average of determinations based on corrected CaO and the first CO_2 analysis. For this reason, averages of calcite determined from corrected CaO and from the initial set of CO_2 analyses were used as actual calcite contents.

First Approximation of Major XRD Proportionality Constants

Quartz/calcite constant. This determination was based on two completely chemically analyzed samples containing little alumina, free silica only as quartz, and carbonate only as calcite. Actual calcite content was determined from chemical analysis. A range of actual quartz contents was calculated from analyzed SiO_2 by subtracting the extreme range of SiO_2 likely to be present in the aluminosilicate fraction.

The first approximation to the proportionality constant between quartz d-$10\bar{1}1$ and calcite d-104 peak heights averages from 1.20 ($SiO_2/Al_2O_3 = 1.5$) to 1.30 ($SiO_2/Al_2O_3 = 3.0$) (table B-8).

Quartz/opal-CT constant. This determination was based on three completely chemically analyzed samples which contain little alumina, minor quartz, free silica mainly as opal-CT, and carbonate only as calcite. The XRD proportionality constant was calculated from the relationships,

Table B-8

First Approximation to the XRD Proportionality
Constant Between Quartz and Calcite

Sample number	1	2
Analyzed values:		
Calcite content, wt %	29.0	38.8
SiO_2 content, wt %	52.0	50.0
Al_2O_3 content, wt %	3.3	2.3
Quartz/calcite, XRD intensity ratio	1.95	1.47
Calculated values for $(SiO_2/Al_2O_3) = 1.5$ in the aluminosilicate fraction:		
SiO_2 in aluminosilicates, wt %	5.0	3.4
Quartz content, wt %	47.0	46.6
Quartz/calcite, wt ratio	1.62	1.20
XRD proportionality constant	1.20	1.22
Calculated values for $(SiO_2/Al_2O_3) = 3.0$ in the aluminosilicate fraction:		
SiO_2 in aluminosilicates, wt %	9.9	6.9
Quartz content, wt %	42.1	43.1
Quartz/calcite, wt ratio	1.45	1.11
XRD proportionality constant	1.34	1.32

$$\frac{S}{C} = \frac{O + Q}{C} = \frac{O/Q + 1}{C/Q} = \frac{\kappa_o(O'/Q') + 1}{\kappa_c(C'/Q')}$$

where in weight percent (primed quantities in XRD intensity):

C = calcite, O = opal-CT, Q = quartz, and S = free silica; and where

κ_c and κ_o are the XRD proportionality constants, respectively,

between quartz and calcite and between quartz and opal-CT. Then,

$$\kappa_o = \frac{\kappa_c(C'/Q')(S/C) - 1}{(O'/Q')} \quad .$$

Solutions were calculated using values of S and κ_c estimated for

SiO_2/Al_2O_3 in the aluminosilicate fraction at the extreme values of

1.5 and 3.0.

The first approximation to the proportionality constant between

intensities of the quartz d-$10\bar{1}1$ and the principal opal-CT peak

averages from 0.826 (SiO_2/Al_2O_3 = 1.5) to 0.875 (SiO_2/Al_2O_3 = 3.0)

(table B-9).

Value of SiO_2/Al_2O_3 in the Aluminosilicate Fraction

Principle of estimate. In rocks where aluminosilicate minerals

are abundant, a large proportion of analyzed SiO_2 is contained in

the aluminosilicate fraction. In samples also containing only small

amounts of free silica, the absolute range in free silica content

(estimated from XRD proportions with calcite) is minimal so that the

absolute range in aluminosilicate SiO_2 (derived by difference between

total SiO_2 and SiO_2 in free silica) is also minimal. The ratio of

SiO_2 to Al_2O_3 in the aluminosilicate fraction can therefore be closely

defined in moderately to highly aluminous calcareous rocks with small

to moderate free silica entirely as opal-CT or quartz.

Table B-9

First Approximation to the XRD Proportionality
Constant Between Quartz and Opal-CT

Sample number	1	2	3
Analyzed values:			
Calcite content, wt %	9.3	22.0	11.1
SiO_2 content, wt %	78.4	70.8	73.7
Al_2O_3 content, wt %	1.7	1.2	3.4
Quartz/calcite, XRD intensity ratio	0.860	0.274	0.448
Opal-CT/quartz, XRD intensity ratio	12.6	15.4	18.8
Calculated values for (SiO_2/Al_2O_3) = 1.5 in the aluminosilicate fraction:			
SiO_2 in aluminosilicates, wt %	2.6	1.8	5.1
SiO_2 in free silica, wt %	75.8	69.0	68.6
XRD proportionality constant	0.823	0.827	0.827
Calculated values for (SiO_2/Al_2O_3) = 3.0 in the aluminosilicate fraction:			
SiO_2 in aluminosilicates, wt %	5.1	3.6	10.2
SiO_2 in free silica, wt %	73.1	67.2	63.6
XRD proportionality constant	0.864	0.876	0.884

<u>Method</u> <u>of</u> <u>estimate</u>. Ideally, calcite content would be determined from chemical analysis. Actual quartz and/or opal-CT content could then be determined from XRD comparison with calcite, this free silica content could be subtracted from total analyzed SiO_2, and the remaining silica could then be attributed to aluminosilicates.

In practice, the ideal method was slightly modified because few detrital-rich samples were chemically analyzed for carbonate carbon. Although actual calcite abundances were therefore unknown, a range of values for the weight ratio of calcite to free silica (quartz and/or opal-CT) could be derived from first approximations to XRD proportionality constants. The method thus needed to be modified only by an additional approximation of the sum of mineral contents.

Analyzed values were first corrected to an organic-free basis. Then for each sample,

$$C + S + A = T$$

where in weight percent (organic-free basis): C = calcite, S = quartz and/or opal-CT, A = aluminosilicate minerals, and the total T is in the range of 95 to 100. (Constituents which decrease the value of T are pyrite, H_2O in closed pores, etc.) The equation can be rewritten as,

$$C + (SiO_2 - \alpha Al_2O_3) + \beta Al_2O_3 = T$$

where in weight percent (organic-free basis): SiO_2 = analyzed SiO_2, Al_2O_3 = analyzed Al_2O_3; and where the unknown constants are:

$\alpha = (SiO_2/Al_2O_3)$ in the aluminosilicate fraction, and $\beta = 100/$(weight percent of the aluminosilicate fraction in Al_2O_3). Rewriting this expression in terms of known quantities produces:

$$SiO_2(1 + C/S) - T = \alpha Al_2O_3(1 + C/S) - \beta Al_2O_3.$$

In the latter equation, which is of the form $z = \alpha x + \beta y$, values

of variables were determined for samples containing at least 3.0 percent

Al_2O_3 and less than four times as much SiO_2 as Al_2O_3. C/S is the

only quantity approximated from literature estimates of α, and two

values of C/S were therefore determined for each sample, using

the extreme limits of α (1.5 and 3.0).

Values of the constants α and β were then estimated by

partitioning with the least squares method, using values of T ranging

from 95 to 100. β is sensitive to fluctuations in the values of T

(solutions to β range from 4.0 to 4.6) but values of α are rela-

tively insensitive (α varies about 0.07 as T ranges from 95 to 100).

For this reason, only α was approximated by this method, and T

was estimated as 100.

Solution then yielded α equal to 1.99 using C/S values

estimated for $\alpha = 1.5$, and α equal to 2.23 using C/S values

estimated for $\alpha = 3.0$ (fig. B-6). Clearly, the approximation rapidly

converges toward $\alpha = 2.1$, and this value was used as the final

estimate of the SiO_2/Al_2O_3 ratio in the aluminosilicate fraction.

Abundance of Al_2O_3 in the Aluminosilicate Fraction

This value was determined from the proportion of major oxides

to Al_2O_3.

$$\beta = \frac{100}{Al_2O_3} = \frac{SiO_2 + Al_2O_3 + M}{Al_2O_3}$$

where each quantity is in weight percent of the aluminosilicate

fraction and M = oxides other than SiO_2 and Al_2O_3. Then,

$$\beta = \frac{SiO_2}{Al_2O_3} + 1 + \frac{M}{Al_2O_3} = \alpha + 1 + \frac{M}{Al_2O_3}.$$

Fig. B-6--Schematic representation of data used to approximate the SiO_2/Al_2O_3 ratio in the aluminosilicate fraction. Each bar represents the total range in values of coefficients for one sample, assuming that SiO_2/Al_2O_3 equals 1.5 (left end of bar) to 3.0 (right end of bar). The right (left) dashed line represents the mean of right (left) end values. Actual solutions were derived from the equations in the text.
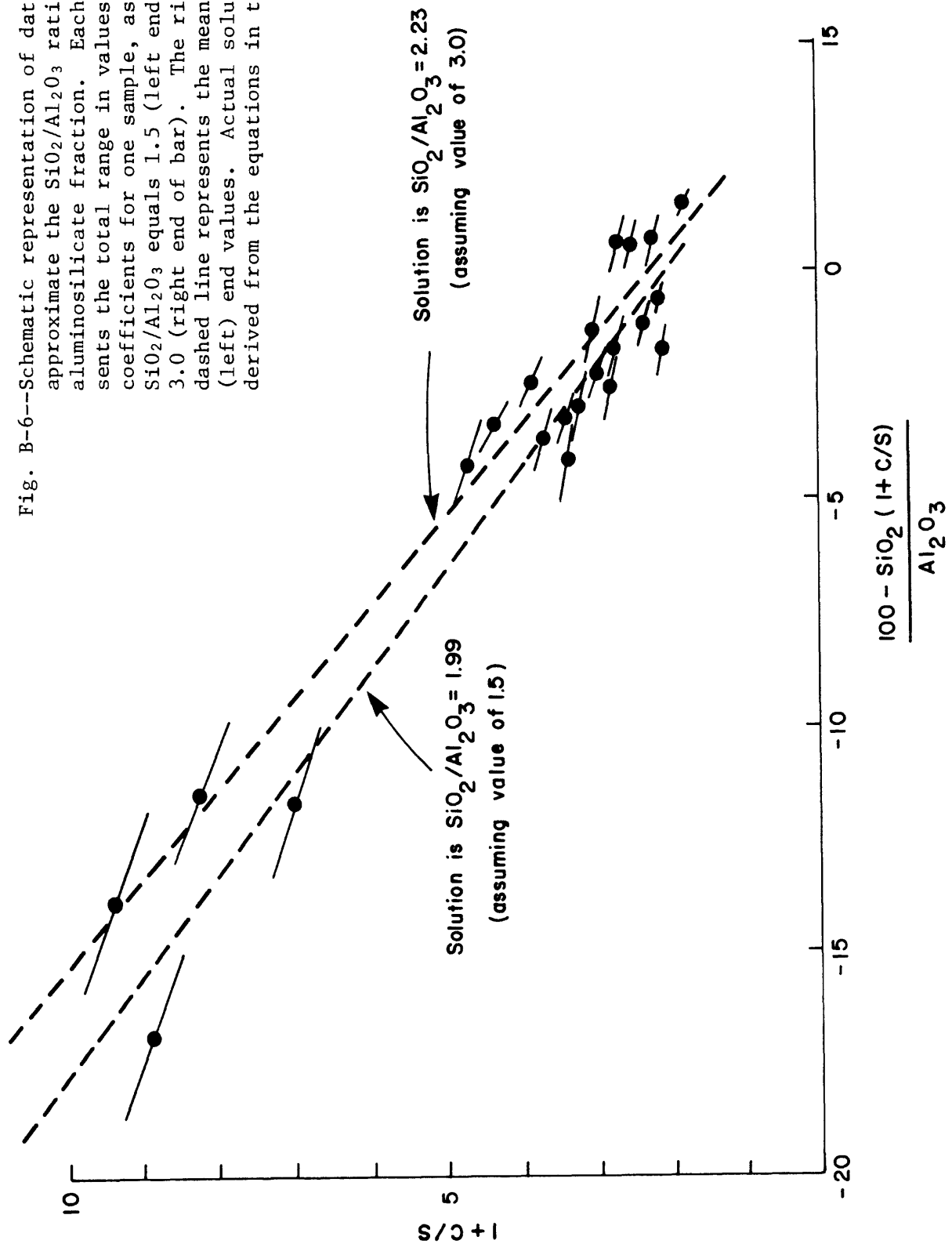
The value of M/Al_2O_3 can be approximated as the sum of average values of the ratio between each major oxide and Al_2O_3 (table B-10). The resulting value of M/Al_2O_3 is 1.1, so that $\beta = 4.2$ and the alumino-silicate fraction contains about 24 percent Al_2O_3.

Final Values of Major XRD Proportionality Constants

With the ratio of SiO_2 to Al_2O_3 in aluminosilicates determined, approximated XRD proportionality constants could be more exactly calculated. The final constants are: 1.26 (quartz/calcite) and 0.85 (quartz/opal-CT).

Other XRD Proportionality Constants

Calcite/apatite constant. This determination was based on three completely analyzed rocks containing calcite and apatite but without dolomite. Calcite and apatite contents were derived from analyzed CaO, P_2O_5, and CO_2, with corrections based on Al_2O_3 (see p. 228).

The proportionality constant between the heights of the calcite d-104 peak and the apatite peak near 32° 2θ averages 1.50 (table B-11). The three values are somewhat scattered, but apatite contents are usually small so that the scatter has little effect on overall accuracy.

Quartz/dolomite constant. The XRD proportionality constant for dolomite was not determined with great accuracy for several reasons. First, dolomite contents are difficult to estimate from analyses due to excess calcium in the structure and also to inconsistencies in CaO and CO_2 analyses (p. 228). Second, dolomite peak height generally varies with composition and ordering, so that a widely applicable XRD constant is probably not determinable. In any case, an accurate XRD constant was not highly important because dolomitic

Table B-10

Average Abundance of Major Oxides in the
Aluminosilicate Fraction

Oxide	Ratio to Al_2O_3	Weight percent
$FeO + Fe_2O_3$	0.20^1	4.7
MgO	0.11^2	2.6
CaO	0.08^2	1.9
Na_2O	0.14^2	3.3
K_2O	0.20^2	4.7
H_2O^+	0.30^3	7.0
TiO_2	0.06^2	1.4
P_2O_5	0.03^2	0.7
Subtotal	1.12	26.3
SiO_2	2.1	50.0
Al_2O_3	1.0	23.8
Total	4.2	100.1

[1]Corrected for pyrite calculated from sulfur analyses
(after subtracting sulfur in organic matter estimated as
equal to 10 percent of organic matter).

[2]Derived from median proportions indicated in tables
B-3 and B-4.

[3]Derived from partitioning, by the least squares
method, between organic matter and aluminosilicates.

Table B-11

Derivation of the XRD Proportionality Constant
Between Calcite and Apatite

Sample number	1	2	3
Calcite/apatite, XRD intensity ratio	17.2	9.7	17.3
Calcite, wt %	47.9	29.0	29.1
Apatite, wt %	3.9	4.5	2.6
Calcite/apatite, wt ratio	12.2	6.41	11.0
XRD proportionality constant	1.41	1.51	1.57

Table B-12

Derivation of the XRD Proportionality Constant
Between Quartz and Dolomite

Sample number	1*	2
Quartz/dolomite, XRD intensity ratio	1.05	0.031
Quartz, wt %	38.7	2.3
Dolomite, wt %	51.4	87.7
Quartz/dolomite, wt ratio	0.753	0.026
XRD proportionality constant	1.40	1.19

*Values for quartz include opal-CT.

rocks were not used in the determination of other analytical constants and dolomite is not present in most diatomaceous rocks.

The XRD proportionality constant between dolomite and quartz (and/or opal-CT) was, however, estimated closely enough to be quite reliable for rocks which are not highly dolomitic. The determination was based on two samples containing minor Al_2O_3, free silica only as opal-CT and/or quartz, and carbonate only as dolomite. Actual free silica contents and partitioning of this quantity between quartz and opal-CT were determined from analyzed SiO_2, Al_2O_3, and the XRD proportionality constant between opal-CT and quartz. Actual dolomite contents were estimated from analyzed CO_2, CaO, and MgO after correction for amounts of CaO in aluminosilicates and apatite (see p. 228) and correction for amounts of MgO in aluminosilicates (fig. B-4A, median value). Amounts of dolomite were then calculated as the sum of $MgCO_3$ (equivalent to corrected MgO) plus $CaCO_3$ (equivalent to the average derived from corrected CaO and from remaining CO_2). The resulting proportionality constant between quartz d-10$\bar{1}$1 and dolomite d-104 peak heights averages 1.30 (table B-12).

Routine Calculation of Mineral Abundances

General Procedure

For routine determinations, actual abundances of free silica, aluminosilicates, and organic matter were based on chemical analyses, and proportions of quartz, opal-CT, calcite, apatite, and dolomite were based on X-ray diffraction (table B-13). In most cases (excepting diatomaceous and highly dolomitic rocks), actual mineral

Table B-13

Analytical Constants Used for Routine Calculation
of Mineral Abundances

Determination	Basis of calculation	Multiplication factor
Relative abundance of:	Intensity of XRD peak near (in deg, 2θ):	
Quartz	26.7	1.00
Opal-CT	22	0.85
Calcite	29.4	1.26
Apatite	32	1.89
Dolomite	31	1.30
Abundance of:		
Aluminosilicate minerals	Al_2O_3	4.2
SiO_2 in aluminosilicate minerals	Al_2O_3	2.1
Organic matter	Organic carbon	1.5*

*See Appendix C.

abundances were calibrated by equating free silica from analyses with the sum of quartz plus opal-CT.

This procedure is fairly sensitive to errors in analytical constants or in determined quantities, and results are easily evaluated by internal consistency. For carbonate-free rocks, amounts of free silica, aluminosilicates, and organic matter must sum close to 100 percent. For carbonate-bearing rocks, determined values are highly interdependent; in order for the sum to be close to 100 percent: (1) SiO_2 and Al_2O_3 analyses must be reasonably accurate to determine actual free silica and aluminosilicate contents; (2) each XRD ratio must be correctly determined to apportion that free silica into quartz and opal-CT and, from those estimates, to determined actual carbonate and apatite contents; and (3) organic carbon must be correctly determined.

Internal consistency shows that the routine calculation procedure generally works well. Sums average 98 percent—the same as the average of analytical totals for carbonate-free rocks (excluding sulfur; samples 1-9, Appendix A). For carbonate-bearing rocks with little (<20 percent) silica, however, small errors in silica contents (or in XRD proportions) are magnified in estimating carbonate by the routine procedure. In these cases, a difference calculation was also made: proportions of mineral contents determined by XRD were normalized to equal 98 percent less the sum of organic matter and aluminosilicate content.

Both procedures were tested on calcareous rocks analyzed for carbonate and organic carbon. Most results compare favorably and are

quite accurate when evaluated by comparison to analyzed calcite
content (table B-14).

Quartz was partitioned into diagenetic and detrital portions
by first calculating the ratio of quartz to aluminosilicates. If
quartz content was less than or equal to one-third the aluminosilicate
content, all quartz was considered detrital (fig. 34). Amounts of
quartz greater than one-third the aluminosilicate content were con-
sidered to be diagenetic. Since the composition of the aluminosilicate
fraction is somewhat variable, partitioning of quartz by this method
is somewhat approximate--particularly for rocks with small amounts of
diagenetic quartz. In most rocks, however, small variations in the
amount of quartz attributed to detrital minerals are insignificant
(e.g., fig. 29).

Modifications for Highly Dolomitic Rocks

Due to imprecision of dolomite's XRD proportionality constant
and to differences in the chemistry or ordering of dolomite, the routine
procedure may lead to inconsistent results (sums much different than
100 percent) in rocks with abundant (>30 percent) dolomite. In these
rocks, carbonate content was therefore determined by difference
(98 percent less the sum of free silica, aluminosilicates, and organic
matter) and apportioned between dolomite and calcite (where present)
by XRD ratios.

Modifications for Diatomaceous Rocks

For diatomaceous rocks, a slightly different procedure was used
because amorphous opal is not easily estimated by XRD, so that the
apportionment of free silica contents into different silica phases

P 245 is followed

was more difficult. In general, quartz contents were estimated from the average ratio of quartz to aluminosilicates in carbonate-free rocks with "disordered" opal-CT (fig. 34). Any opal-CT present was estimated by its XRD proportion with quartz, and amorphous opal was then derived by the difference between total free silica and quartz (+ opal-CT) contents. Since the ratio of quartz to aluminosilicates varies somewhat, quartz contents in diatomaceous rocks--which are based on the median ratio--are somewhat less accurate than in nondiatomaceous rocks.

Results from this method of partitioning free silica were evaluated on calcareous diatomaceous rocks by comparison with results from a second method. In the first method, calcite and apatite contents were derived from XRD peak comparison with quartz contents estimated as just described. In the second method, calcite and apatite contents were calculated by difference (calcite plus apatite set equal to 98 percent less the sum of aluminosilicates, free silica, and organic matter contents) and quartz contents estimated by XRD peak comparison with those quantities. Comparison of the two procedures in calcareous diatomaceous rocks shows that they are reasonably consistent (table B-15).

Table B-15

Comparison of Methods for Estimating Mineral
Abundances in Diatomaceous Rocks

Sample no.	Method*	Estimated mineral abundances		
		Opal-A, wt %	Quartz, wt %	Calcite, wt %
1	1	38	7	16
	2	37	8	18
2	1	18	3	57
	2	18	3	55
3	1	14	12	19
	2	12	13	21
4	1	6	8	28
	2	5	9	32

*as described on p. 245.

APPENDIX C

CHARACTERISTICS OF ORGANIC MATTER

In this appendix, detailed data are presented on the organic

matter in Monterey rocks along the Santa Barbara coast. Sample

preparation and analysis methods are described as well as derivation

of the constant of proportionality used to convert organic carbon

analyses to organic matter contents. Then data and further work

(in progress) on thermal maturity are briefly described. Finally,

tables of sample descriptions and localities, and data on charac-

teristics of the organic matter are presented.

Sample Preparation

Samples were cut with either a dry masonry or a free-flowing

water saw into bulk pieces weighing 20 to 100 g and these pieces

were submitted for analysis. For some samples, pieces used to

characterize organic matter did not exactly match pieces used for

other analyses. In all cases, however, both pieces were visually

similar and nearly adjacent.

Methods of Analysis

Six samples from the central and western part of the area studied

along the Santa Barbara coast were analyzed by the Branch of Oil and

Gas Resources, U.S. Geological Survey, Denver, Colorado, for the

following parameters: (1) organic carbon; (2) carbonate carbon;

(3) bitumen content; (4) total hydrocarbon content; (5) ratio of saturated hydrocarbons to aromatic hydrocarbons; (6) nitrogen, carbon, and hydrogen contents of kerogen concentrate; and (7) color of kerogen concentrate. Saturated hydrocarbon fractions were also analyzed by gas chromatography. All methods of analysis are described in Claypool and others (1978).

Mobil Field Research Laboratory in Dallas, Texas, analyzed 31 additional samples for total organic carbon, prepared kerogen concentrates, and analyzed the concentrates for ash. Elemental analyses were made by Clark Means and Perkins Microanalytical Laboratory in Urbana, Illinois, as follows: (1) carbon and hydrogen content by the Pregl method; (2) oxygen content by a modified Unterzaucher method; (3) nitrogen content by the micro-Dumas method; and (4) sulfur content by the Carius method. The Pregl method is described by Grant (1951) and the other methods by Steyermark (1951).

Derivation of Constant of Proportionality

Organic matter contents were derived by multiplying organic carbon contents by a constant of proportionality equal to 1.5. This constant represents the median value of reciprocals of the carbon fraction, normalized to an ash-free basis, in kerogen concentrates from the 31 samples in which complete elemental analyses were made.

This constant is approximate for two reasons. First, carbon contents of organic matter vary laterally due to thermal diagenesis. The effect of lateral differences is not large, however, as most reciprocals of carbon contents lie within a range of 1.40 to 1.60. For a typical sample with 5 percent organic matter, the corresponding

range of calculated organic matter contents is 7 to 8 percent, or a

1 percent difference. This amount of inaccuracy is negligible because

organic contents are used principally in normalizing mineral composi-

tions (see Appendix B).

The constant of proportionality is also approximate because pyrite

was not removed from kerogen concentrates. Where present, pyrite

produces high sulfur contents and therefore normalized carbon contents

which are erroneously low for organic matter. True organic sulfur

contents are difficult to determine; pyrite sulfur contents cannot

be precisely determined either, because iron is contained in alumino-

silicates as well as pyrite. The magnitude of the effect of pyrite

on the constant of proportionality was therefore estimated by comparison

of total sulfur contents, organic carbon contents, and petrographic

examination. In rocks with little detectable pyrite, the ratio of

organic carbon to sulfur is about 10. Correction of sulfur

contents to this proportion in each kerogen concentrate produces an

average constant of proportionality between organic matter and organic

carbon of about 1.4. Since organic sulfur contents may be higher in

rocks containing pyrite, 1.4 probably represents a minimum for the true

average value of the constant. Pyrite in kerogen concentrates there-

fore caused a maximum of 7 percent error in organic matter determinations.

Thermal Maturity of Organic Matter

Increasing thermal maturity from east to west is indicated by

oxygen/carbon ratios of organic matter in the 31 samples prepared by

Mobil Field Research Laboratory. This is the most important result

from detailed analyses of organic matter and was described earlier (p. 80).

Additional information on thermal maturity derives from analyses

of hydrocarbons in organic matter from Monterey rocks in the central

and western parts of the study area. There, thermal diagenesis

was intermediate between that in Miocene rocks from offshore surface

sampling in the Southern California Borderland (more shallowly buried)

and that in Miocene rocks from the Los Angeles and Ventura Basins (more

deeply buried) (G. E. Claypool, in Taylor, 1976). Sample groups from

offshore and from along the Santa Barbara coast both have similar

ranges of organic carbon, and extractable organic matter in both groups

is generally similar--highly asphaltic, with "hydrocarbon fractions in

which aromatics predominate over saturated hydrocarbons, and branched-

cyclic saturates predominate over straight chain paraffins" (G. E.

Claypool, in Taylor, 1976). Hydrocarbons, however, represent a smaller

proportion of organic matter in offshore surface samples (where hydro-

carbon/carbon ratios range from 0.04-0.077%) than in samples from the

Santa Barbara coast (where most hydrocarbon/carbon ratios range from

1.5-3.4%). One unusual sample from the Santa Barbara coast contains

even more abundant hydrocarbon (13.4% of the bulk sample is soluble

in hot chloroform and 4.0% of the bulk sample is hydrocarbon) and this

sample is a possible source of heavy asphaltic oil. Because overall

thermal characteristics indicate that temperatures along the Santa

Barbara coast probably did not exceed 50° to 70°C, organic matter in

Monterey rocks may therefore yield heavy oil at lower temperatures

than generally assumed (G. E. Claypool, pers. commun., 1976; Powell

and others, 1975; Philippi, 1965).

Further work on the diagenesis and maturity of the organic matter from all parts of the study area has been undertaken. Results confirm the pattern of increasing thermal maturity from east to west and elucidate the detailed chemical changes in the extractable fraction of the organic matter (Giger and Schaffner, 1979).

Tables

Samples in which detailed analyses of organic matter were made are located and described (table C-1). Data from detailed analyses are then presented for the six samples analyzed by the U.S. Geological Survey (table C-2) and for the 31 samples analyzed through Mobil Field Research Laboratory (table C-3).

Table C-1

Sample Descriptions and Localities

No.	Field no.	Description	Member	Section
		Samples analyzed by the U.S.G.S.:		
1	AUG-6C-10B	Dolomite	Transition	San Augustine
2	BIX-7-2	Porcelanite	Siliceous	Quail
3	GAV-10-9	Calcareous dolomitic mudstone	Lo. calc. sh.	Gaviota
4	GAV-19-6	Organic shale	Organic sh.	Gaviota
5	WOOD-3-1	Calcareous organic mudstone	Lo. calc. sh.	Wood
6	WOOD-9-1	Unusual qtz. chert (lensoid)	Up. calc. sh.	Wood
		Samples analyzed through Mobil Field Research Laboratory:		
7	AUG-4C-11	Dolomite	Lo. calc. sh.	San Augustine
8	AUG-4C-13	Phosphatic dolomite	Lo. calc. sh.	San Augustine
9	AUG-4C-25	Organic shale	Lo. calc. sh.	San Augustine
10	AUG-6B-14	Organic shale	Organic sh.	San Augustine
11	AUG-6C-9	Organic shale	Organic sh.	San Augustine
12	AUG-7B-5	Calcareous chert	Up. calc. sh.	San Augustine
13	AUG-7B-15	Calcareous shale	Up. calc. sh.	San Augustine
14	BIX-3-3	Calcareous shale	Lo. calc. sh.	Quail
15	BIX-6B-13	Unusual qtz. chert (banded)	Up. calc. sh.	Quail
16	BIX-7-6B	Porcelanite	Siliceous	Quail
17	BLK-5-2	Calcareous shale	Transition	Black
18	BLK-7A-10	Chert	Siliceous	Black
19	BLK-7A-13	Porcelanite	Siliceous	Black
20	CAP-6R-3	Calcareous chert	Organic sh.	El Capitan
21	CAP-6-4	Organic shale	Organic sh.	El Capitan
22	CAP-6-11	Calcareous mudstone	Lo. calc. sh.	El Capitan
23	DAM-7D-1	Dolomitic shale	Up. calc. sh.	Damsite
24	DAM-7D-3	Dolomitic cherty porcelanite	Up. calc. sh.	Damsite
25	DAM-8C-1	Siliceous mudstone	Siliceous	Damsite
26	DAM-8C-4	Siliceous shale	Siliceous	Damsite
27	DAM-8C-7	Cherty porcelanite	Siliceous	Damsite
28	NAP-1-1	Siliceous shale	Siliceous	Naples
29	NAP-11-5	Organic shale	Organic sh.	Naples
30	NAP-12-6	Calcareous shale	Transition	Naples
31	NAP-13-3	Chert	Siliceous	Naples
32	REF-6-6	Calcareous mudstone	Lo. calc. sh.	Refugio
33	WOOD-3-3	Calcareous shale	Lo. calc. sh.	Wood
34	WOOD-4-2	Organic shale	Organic sh.	Wood
35	WOOD-5-1	Unusual qtz. chert (lensoid)	Transition	Wood
36	WOOD-5-4	Calcareous shale	Transition	Wood
37	WOOD-5-4 dark	Organic shale	Transition	Wood

Table C-2

Characteristics of Organic Matter in Monterey Rocks

Sample no.	Organic carbon, weight %	Carbonate carbon, weight %	Bitumen, ppm	Total HC[1] ppm	S/A[2]	HC/C[3]	N[4]	C[4]	H[4]	H/C[5]	N/C[5]	Color
1	1.9	10.6	1,375	647	0.56	3.41	2.52	60.13	6.55	1.30	0.036	yel-org-brn
2	6.5	<0.1	9,982	1,278	0.1	2.0	2.40	67.41	7.25	1.28	0.031	org-brn
3	3.1	5.1	1,854	461	1.15	1.5	2.97	66.55	7.54	1.35	0.038	yel-org
4	6.4	1.3	5,214	1,128	0.15	1.76	2.46	62.39	7.16	1.37	0.034	yel-org-brn
5	16.0	8.5	134,100	40,000	<0.01	25.0	1.79	67.99	7.43	1.30	0.023	yel-org
6	1.0	<0.1	1,018	159	0.22	1.59	1.32	52.49	6.43	1.46	0.022	yel

[1] Hydrocarbon

[2] Ratio of saturated hydrocarbons (heptane eluate) to aromatic hydrocarbons (benzene eluate)

[3] Ratio of total hydrocarbon to organic carbon x 100

[4] Elemental abundance in kerogen concentrate, in % by weight

[5] Atomic ratios

Table C-3

Elemental Abundances and Elemental Ratios in Kerogen Concentrates

Sample no.	Normalized elemental contents, in weight %					Atomic ratios	
	C	H	O	N	S	H/C	O/C
7	68.07	7.90	10.89	3.15	9.99	1.38	0.120
8	68.95	7.99	10.42	3.11	9.53	1.38	0.113
9	66.02	7.61	7.07	2.72	16.58	1.37	0.080
10	64.17	7.26	7.77	3.07	17.73	1.35	0.090
11	64.67	7.46	9.26	2.72	15.89	1.38	0.108
12	66.18	7.85	7.69	2.46	15.82	1.41	0.087
13	64.15	7.59	9.70	2.71	15.85	1.41	0.114
14	70.64	8.06	8.93	2.28	10.09	1.36	0.095
15	65.04	7.90	5.29	1.37	20.40	1.45	0.061
16	67.31	7.52	12.26	2.73	10.18	1.33	0.137
17	68.91	7.47	11.21	2.42	9.99	1.29	0.122
18	64.79	7.43	8.40	2.41	16.97	1.37	0.097
19	71.51	8.16	7.47	2.84	10.02	1.36	0.078
20	65.73	7.70	12.93	3.44	10.20	1.40	0.148
21	65.24	7.60	12.38	3.14	11.63	1.39	0.143
22	68.83	8.21	12.49	2.66	7.81	1.42	0.136
23	62.37	7.20	8.57	2.01	19.85	1.38	0.103
24	69.69	7.76	5.51	2.64	14.40	1.33	0.059
25	64.77	7.26	11.32	2.68	13.97	1.34	0.131
26	64.66	7.34	11.08	2.24	14.68	1.35	0.129
27	63.60	7.34	8.63	2.90	17.53	1.37	0.102
28	55.24	6.63	22.87	2.44	12.82	1.43	0.311
29	62.79	7.47	16.65	3.95	9.14	1.42	0.199
30	61.63	6.75	16.66	3.28	11.68	1.30	0.203
31	61.16	6.86	16.49	3.51	11.98	1.34	0.202
32	68.11	7.80	13.26	2.52	8.31	1.37	0.146
33	71.42	8.02	10.12	1.84	8.60	1.34	0.106
34	71.51	7.99	7.74	2.33	10.43	1.33	0.081
35	66.25	7.82	7.28	2.05	16.60	1.41	0.083
36	70.76	7.72	7.22	2.10	12.19	1.30	0.077
37	67.50	8.18	8.61	2.11	13.60	1.44	0.096

APPENDIX D

MEASUREMENT OF OPAL-CT D-SPACINGS

In this appendix, methods used for measurement of opal-CT d-spacings
are described. Most measurements used the principal quartz peak for
reference, but this peak turned out to be somewhat unreliable. As a
result, values in many samples were re-determined or corrected by an
empirical relation. Topics are discussed as follows: (1) slide
preparation and X-ray diffraction (XRD) methods; (2) comparison of
standards; (3) adjustments to measurements; and (4) evaluation of
interference from other XRD peaks. All 2θ values refer to Cu Kα
radiation.

Slide Preparation and XRD Methods

D-spacing measurements were made on the same powder splits used
for whole-rock XRD analysis or, in some cases, on insoluble residues
prepared from these splits. Quartz was added to a portion of some
powders as an internal standard, in an amount adjusted so that XRD
peak heights of quartz and opal-CT would be nearly equal. Powders
were then ground until grittiness disappeared, dispersed evenly in
water on a glass slide, and dried. Spacings between quartz d-$10\overline{1}1$
and the principal opal-CT peak near 22° 2θ were then measured at
0.5° (2θ)/min, using counting parameters that maximized sharpness of
the opal-CT peak (peak height > 15 cm above baseline). Scans were
recorded on diffractograms and peak centers measured in the upper part

of each peak (in the area between 80 and 90 percent maximum peak height). The average of an upward and downward scan was used as the d-spacing value. The same methods, quartz standard, and XRD apparatus were all used by Murata and Larson (1975).

In samples with abundant diagenetic quartz, fluorite or halite (both reagent-grade) were used as internal standards. Fluorite, whose principal XRD peak is close to that of plagioclase feldspar, was used only on samples with very small detrital contents. Procedures were identical to those used with quartz standards--except that, when using halite, powders were formed into pastes and smeared on slides. Comparison of the two methods of slide preparation using standard quartz in both cases showed no difference in results. Slides containing all three standards (halite, fluorite, and quartz) were scanned during each period of measurement.

Comparison of Standards

After most d-spacing measurements were made, inconsistencies were discovered between values based on halite or fluorite standards and values using the quartz already present in the rock as a reference. A large number of samples with a wide range of compositions and diagenetic quartz contents were therefore re-measured with a halite standard.

The results of these measurements show that diagenetic quartz differs somewhat in d-$10\overline{1}1$ spacing from standard quartz. By contrast, the d-$10\overline{1}1$ spacing in detrital quartz is similar to that in standard quartz. These relationships show that small, irregularly distributed errors were introduced into the XRD procedure where quartz served as

a reference. In that procedure, standard quartz was added in different amounts, depending on the amount of quartz already present in the sample. As a result, where quartz already present was detrital, the measured d-spacing was the same as if it had been measured using only standard quartz or halite. Where quartz already present was partly diagenetic, however, the measured d-spacing was smaller due to the presence of diagenetic quartz. The maximum effect on opal-CT d-spacings is about 0.01 $\overset{o}{A}$.

The cause of differences in d-$10\overline{1}1$ spacings of quartz was not determined, but may relate to crystal size. XRD characteristics of diagenetic quartz are known to differ somewhat from characteristics of volcanic or metamorphic quartz (Murata and Norman, 1976). Diagenetic quartz has XRD peaks which are broader and less sharp and which show less resolution, particularly at high 2θ angles, suggesting that long-range order is smaller, due mainly to fine crystal size (Murata and Norman, 1976). Peak broadening may cause apparent shifts in d-spacing due to machine responses which are assymetrical with respect to the true peak center (Klug and Alexander, 1954). Thus differences in d-$10\overline{1}1$ spacing among quartz samples of different origin do not necessarily indicate actual differences in the unit cell.

Differences in size of opal-CT crystals could also affect d-spacings of opal-CT, but such differences are probably not the main cause of "ordering" differences. For one thing, the total range of d-spacing differences among opal-CT samples is much greater (about 0.07 $\overset{o}{A}$) than among different types of quartz. Also, other changes in XRD characteristics are associated with different opal-CT d-spacings-- a peak (or bulge) at 20.5° 2θ typifies opal-CT with d-spacings $\geq$ 4.100 $\overset{o}{A}$,

and two peaks at 28.4° and 31.4° 2θ typify opal-CT with d-spacings

≤ 4.060 Å. These differences, particularly the peak at 20.5° 2θ,

are unlikely to be caused merely by differences in crystal size.

Corrections to D-spacing Values

Although many samples were re-measured with standard halite,

this measurement is very time consuming and a correction curve was

used to adjust values in some samples already measured with quartz.

The spacing between the d-10$\overline{1}$1 peak of standard quartz and the d-200

peak of standard halite was measured repeatedly on duplicate slides,

and a median value established. For samples measured with halite and

indigenous quartz, the proportion of diagenetic to total quartz was

calculated, as described in Appendix B, and quartz d-spacings plotted

against the percentage of quartz that is diagenetic (fig. D). For

samples measured only with indigenous quartz as a reference, a corrected

value of quartz d-10$\overline{1}$1, taken from the straight line in figure D,

was then used as the basis for opal-CT d-spacings. For samples measured

with part indigenous quartz and part standard quartz as a reference,

the proportion of diagenetic quartz to total quartz was calculated by

comparison of quartz and opal-CT peak heights in whole-rock XRD slides

and in XRD slides used for d-spacing measurements. In the latter case,

corrections were less reliable and were used mainly when the proportion

of diagenetic quartz was small. Otherwise, samples were re-measured

with halite as a reference.

Corrected values compare well with values based on halite as a

reference (table D). Adjustment therefore produced little variability

in d-spacings.
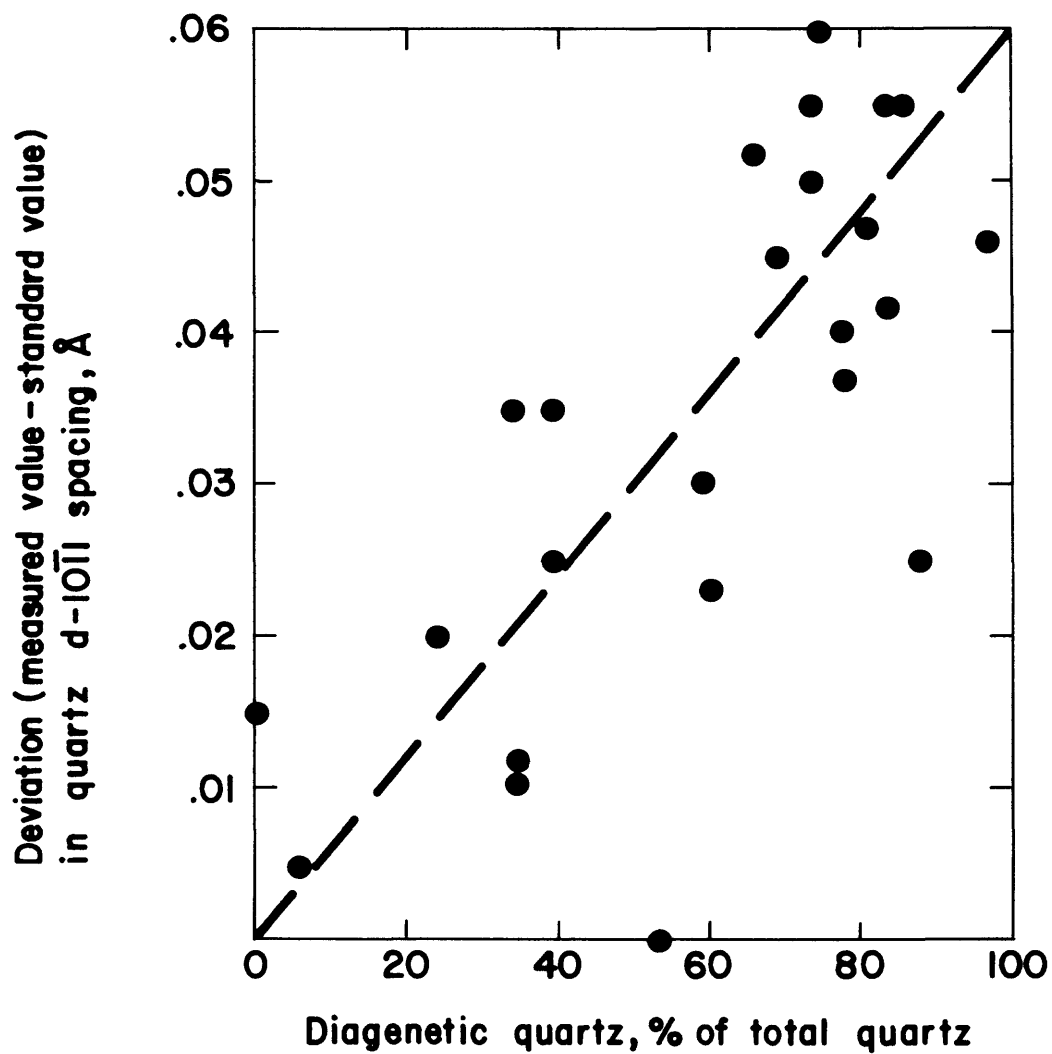
Fig. D—Correlation between quartz d-10$\bar{1}$1 spacing and the percentage of quartz in diagenetic quartz. The halite d-200 peak was used as an internal standard.

Table D

Comparison Between Values of Opal-CT D-spacings Derived
from Measurement with Halite and Corrected Values
Derived from Measurement with Quartz

Sample no.	Opal-CT d-spacing, $\overset{o}{A}$		Difference $\overset{o}{A}$	Diagenetic qtz, % / Total qtz
	Corrected quartz value	Halite value		
1	4.060	4.060	0	64
2	4.058	4.058	0	81
3	4.073	4.070	+0.003	76
4	4.072	4.070	+0.002	74
5	4.061	4.060	+0.001	81
6	4.060	4.060	0	83
7	4.061	4.062	-0.001	69
8	4.066	4.067	-0.001	56
9	4.070	4.070	0	81
10	4.060	4.058	+0.002	86
11	4.073	4.070	+0.003	93
12	4.081	4.081	0	29
13	4.077	4.079	-0.002	0
14	4.084	4.082	+0.002	8
15	4.075	4.075	0	0
16	4.060	4.060	0	0
17	4.059	4.061	-0.002	0
18	4.063	4.062	+0.001	56
19	4.068	4.068	0	32
20	4.061	4.061	0	16
21	4.065	4.063	+0.002	33
22	4.059	4.059	0	55
23	4.079	4.077	+0.002	67
24	4.063	4.061	+0.002	54
25	4.072	4.065	+0.007	48
26	4.068	4.071	-0.003	72
27	4.081	4.074	+0.007	87
28	4.085	4.085	0	0
29	4.077	4.079	-0.002	0
30	4.075	4.079	-0.004	0
31	4.092	4.089	+0.003	0
32	4.072	4.073	-0.001	26

Interference with D-spacing Values from Other XRD Peaks

In samples from the Santa Barbara coast, three XRD peaks may interfere with measurements of d-spacings in opal-CT: (1) calcite d-102 peak at 23.0° 2θ; (2) dolomite d-101 peak at 22.0° 2θ; and (3) a small plagioclase feldspar peak near 22.0° 2θ.

Interference from calcite is easily evaluated because the d-102 peak occurs well away from the center of the opal-CT peak. In samples where the d-102 peak was large, opal-CT d-spacings were measured on insoluble residues of powders.

Interference from dolomite was more difficult to evaluate because the d-101 peak is near the center of peaks in "ordered" opal-CT. Even in highly dolomitic rocks, however, this peak is barely detectable so that interference seems unlikely. In addition, insoluble residues were used for measurements of samples with large amounts of dolomite.

Plagioclase feldspar, on the other hand, does interfere somewhat with measurements of opal-CT d-spacings, and the most highly detrital samples cannot be reliably measured. Precise evaluation of interference is difficult to make with natural samples. As a rule of thumb, samples were measured only if the height of the plagioclase peak at 28.0° 2θ was less than 75 percent of the height of the opal-CT peak at 22.0° 2θ. Comparison of areas under plagioclase peaks shows that the feldspar peak at 22.0° 2θ represents less than 1 percent of the area under the opal-CT peaks of most measured samples and about 2 percent of the area in the most detrital-rich samples measured. Interference is therefore probably negligible in measured samples.

Interference from plagioclase could cause an apparent decrease in d-spacings as detrital content increases, but measured differences in d-spacings related to detrital content are almost certainly real. For one thing, d-spacing differences occur between rocks in which feldspar contents are completely negligible (contributing less than 1 part in 500 to the area under the opal-CT peak). In addition, silica in rocks with high relative detrital contents became completely quartzose earlier than silica in interbedded rocks with less relative detrital content. This diagenetic pattern is consistent with d-spacing differences due to real structural differences in opal-CT rather than to apparent differences from peak interference.

APPENDIX E

MEASUREMENT OF POROSITY AND PERMEABILITY

Porosity Measurements

Method of Preparation and Measurement

Porosity values are derived from measurement of bulk density
and of grain density. Both measurements were made on bulk pieces of
rock, either the same piece or adjacent matching pieces. Pieces
were sawed with a free-flowing water saw or—when soft, friable or
water-sensitive—with a dry masonry saw. Wet-cut samples were air
dried for 4 weeks prior to further processing.

Samples were then heated at 100° to 105°C for 24 hours before
density measurement. Where two pieces were cut for the two density
measurements, only the piece for grain density measurement was heated.
This procedure eliminated possible cracking during heating which would
affect the bulk density measurement. The dry weight of the piece
for bulk density was then calculated from the relative weights of the
two pieces taken prior to heating. After heating, samples were cooled
to room temperature in a desiccator for 30 to 60 min, weighed, and
then stored in a desiccator.

Bulk volume was measured with a vacuum-equipped mercury pycnometer
described by McCulloh (1965). Grain volume was measured with a
Beckman Air Comparison Pycnometer (Model 930), using helium as the
measuring gas. All pieces measured were greater than 10 cc. Bulk

(grain) volume values were reproducible within 0.05 (0.1) cc and variation in bulk (grain) density values due to volume measurement was therefore less than 0.01 (0.02) g/cc.

Defining Porosity in Fine-Grained Rocks for Different Purposes

Porosity values must be viewed with a clear understanding of the limitations of the term "porosity," defined as the percentage volume represented by pore space (or voids). Although simple, this definition is extremely ambiguous when applied to many fine-grained rocks. *In situ*, fluids saturate rocks and sediments, and pores (or voids) are filled. Pore space is frequently equated with water content, but fluid water in pores is not easily differentiated from the many layers of water adsorbed by minerals such as clays and opal-CT. Adsorbed water may more than double grain volume, may not be removable without considerable energy, and probably cannot be replaced by pore fluids (Meade, 1964; Bush and Jenkins, 1970).

For many purposes, therefore, adsorbed water must be considered to be part of the solid rock. Effective porosity may be practically negligible in many rocks (such as shallowly buried clay rocks) which are highly porous under dry conditions. Where porosity values are measured to determine easily replaceable "space"--such as could be filled by migrating hydrocarbons--dry porosity values are clearly misleading. Current practice is to humidify samples under conditions which approximate *in situ* forces on clays, as described by Bush and Jenkins (1970). Humidified values may also be pertinent to study of the character of porosity--especially porosity formed during crystallization of opal-CT, which is highly surface-reactive.

In the present study, porosity values were determined under dry conditions. This method is most appropriate for estimating net compaction, which may be permitted in part by removal of adsorbed water due to overburden pressure. Dry and humidified values of porosity, however, may differ considerably--for opal-CT rocks with 5 to 10 percent adsorbed water by weight, by 7 to 20 porosity percent-- and are not easily compared.

Comments on the Method of Grain Density Measurement

Many techniques for measurement of grain volume (or grain density) are so complex that large numbers of measurements are impractical. Interpolation, extrapolation, or inference of values must be relied upon. Porosity of Monterey rocks, however, cannot be studied in detail without actual measurement of grain densities. Even if based on accurate mineral contents, estimated grain densities will be highly inaccurate because of the large, variable amount of organic matter with low grain density--probably about 1.0 g/cc (Tissot and Welte, 1978). Resulting errors probably range from 4 to 6 porosity percent for rocks with organic contents of about 5 percent and from 7 to 14 porosity percent for rocks with organic contents of 10 percent (table E-1).

In this study, large numbers of grain volume measurements could be made because of the convenience of using bulk (unpowdered) samples. The procedure has several advantages: (1) greater accuracy of matching with pieces used for bulk density measurement; (2) no grinding necessary; (3) no differential loss of material or alteration of material during grinding; (4) ease in handling; and (5) no need to

Table E-1

Error in Porosity Values Due to Inference of Grain Density
Values from Mineral Contents, for Rocks Bearing
Abundant Organic Matter

	Opal-CT rocks				Quartz rocks			
Bulk density, g/cc	1.35	1.45	1.55	1.65	1.90	2.00	2.10	2.20
Inferred grain density, g/cc	2.30	2.30	2.30	2.30	2.65	2.65	2.65	2.65
Estimated porosity, %	41.3	37.0	32.6	28.3	28.3	24.5	20.8	17.0
Including 5 wt % organic matter at 1.0 g/cc:								
Actual grain density, g/cc	2.16	2.16	2.16	2.16	2.45	2.45	2.45	2.45
Actual porosity, %	37.5	32.9	28.2	23.6	22.4	18.3	14.2	10.1
Error in porosity, %	3.8	4.1	4.4	4.7	5.9	6.2	6.6	6.9
Including 10 wt % organic matter at 1.0 g/cc:								
Actual grain density, g/cc	2.04	2.04	2.04	2.04	2.27	2.27	2.27	2.27
Actual porosity, %	33.7	28.7	23.8	18.9	16.5	12.1	7.7	3.3
Error in porosity, %	7.6	8.3	8.8	9.4	11.8	12.4	13.1	13.7

heat the piece used for bulk density measurement and thus elimination of possible cracking or expansion during heating.

The disadvantage in the use of bulk (unpowdered) samples is that they may not be completely penetrable, and the volume of unpenetrated pores is included in the volume of grains. In order to evaluate penetration, measurements were made of one sample (an opal-CT porcelanite) prepared in several different size fractions. Powder (<0.25 mm), granules (0.25-0.5 mm, 0.5-2 mm, 2-4 mm, 4-8 mm) and several bulk pieces as large as 15 cc showed less than 0.02 g/cc difference. This difference is quite small and probably comparable in magnitude to errors produced by greater handling. Penetrability was also indirectly tested by comparison of grain density values for completely chemically analyzed samples. Except for two of the most cherty opal-CT rocks, results are internally consistent, even for dolomites with low (5-10 percent) porosities.

Evaluation of Surface Weathering

Although porosity values of surface rocks are frequently unreliable, values used in this study almost certainly closely represent porosities of fresh unweathered rock. Compared to typical surface exposures, many Monterey exposures along the Santa Barbara coast show relatively little surface alteration. Active coastal erosion, recent canyon downcutting, and low permeability all minimize weathering. Samples for porosity measurement were selected for their especially fresh condition, demonstrated by the presence not only of abundant organic matter (2-24 percent) but also of small amounts of pyrite (as much as 2 percent). The only samples which may be somewhat

affected by surface weathering are diatomaceous rocks from Elwood
Beach, which is not being actively eroded. However, porosities of
all diatomaceous rocks are somewhat increased by rebound when over-
burden is removed (Hamilton, 1976) and are not precisely represen-
tative of values at depth.

Permeability Measurements

Method of Preparation and Measurement

Sample preparation and measurement of permeability values were
both done by Core Laboratories, Inc. in Bakersfield, California.
Each sample was first cored with a diamond core drill to produce a
cylindrical plug approximately 1 in. in diameter and 2.5 in. long.
For humidified values, plugs were placed in a humidity oven at 60°
to 65°C and 40 to 50 percent humidity for 3 days before measurement.
For oven-dried values, plugs were heated at 105°C until water loss
ceased (1-3 days) before measurement.

Standard measurement techniques were used. Plugs mounted in the
test cell were subjected to dry air with a 12 to 15 psi differential
pressure from top to bottom, and flow through the plug was measured.
Permeability values were then calculated from Darcy's law.

Permeability Values

Permeability values are presented in table E-2. These values
were determined on samples also analyzed for mineral abundance and
porosity (table G). Note, however, that although the piece of the
sample used for permeability measurement was similar and close to the
piece used for other analyses, the two pieces were not exactly matched.

Table E-2

Permeability Values

	Oven-dried[1]	Humidified[1]
Siliceous (carbonate-free) rocks		
Opal-A and opal-CT:		
NAP-1-1	0.6	0.5
Opal-CT:		
BUL-4-19	<0.01	<0.01
BUL-4-22	0.04	0.01
DAM-9B-1	0.02	<0.01
GAT-1-5	0.09	0.01
GAT-1B-2	0.04	0.01
GAV-13A-32	0.02	0.01
GAV-13A-33	0.06	0.02
NAP-13-3	0.06	0.01
NAP-13-4	0.07	0.05
Opal-CT and quartz:		
DAM-8C-4[2]	<0.01	<0.01
WOOD-11-3	0.12	0.02
Quartz:		
BIX-7-6	<0.01	<0.01
DAM-8C-6	<0.01	<0.01
Calcareous rocks with >25% silica		
Opal-A:		
NAP-12-6	5.5	1.7

---

[1]Measured parallel to bedding; values in mD.

[2]Permeability of sample also measured perpendicular to bedding; for both oven-dried and humidified conditions, value was <0.01 mD.

Opal-CT:

AUG-4C-26[2]	0.03	0.03
AUG-7B-5	0.07	0.01
AUG-7B-14	0.01	0.01
AUG-7B-15	1.0	0.04
AUG-7B-17	<0.01	<0.01
CAP-6-8	0.01	0.01
NAP-1-5	<0.01	0.01
REF-6-3[2]	<0.01	<0.01
REF-6-5[2]	<0.01	<0.01
REF-6-6[2]	<0.01	<0.01
REF-6-7	<0.01	<0.01

Quartz:

WOOD-3-3	<0.01	<0.01
DAM-7D-1[3]	<0.01	<0.01

Calcareous rocks with <25% silica

Opal-CT:

AUG-6B-15	0.10	0.04
AUG-6B-16	0.20	0.08
AUG-7B-12	0.03	0.01
CAP-6-2	17	4.2
CAP-6-7	0.3	0.1
CAP-6-11	0.29	0.09

Opal-CT and quartz:

AUG-4C-25	0.03	0.02

Dolomites

AUG-4C-11	0.10	0.04
AUG-4C-13	0.30	0.09

[3]Dolomitic shale.

APPENDIX F

STRATIGRAPHIC SECTIONS

In this appendix, field methods are briefly described and general

stratigraphic sections presented. First, however, comments are made

on lateral differences in member thicknesses.

Lateral Differences in Member Thicknesses

For simplicity, figures used in the text of this study schematically

represent members as laterally constant. As previously pointed out,

however, Mohnian strata--which include the siliceous member and upper

strata in the calcareous members--thicken westward. Systematic

thickness changes are also evident in lower strata (of uppermost

Saucesian, Relizian, and Luisian age) which thin westward.

Lateral differences in solid rock thickness (estimated from

porosity values and lithologic distribution) show that original

depositional rates were responsible for both trends (fig. F).

An anomaly in the trends is apparent at Gato and Cojo Canyons, where

all members are unusually thin. Thinning in this area is also apparent

from Dibblee's (1950) mapping, but its cause has not been investigated.

Field Methods

Field characterization of rocks involved a succession of examina-

tion, sampling, analysis, and re-examination. Characterizations

were based on many of the samples listed in Appendix G, and a large
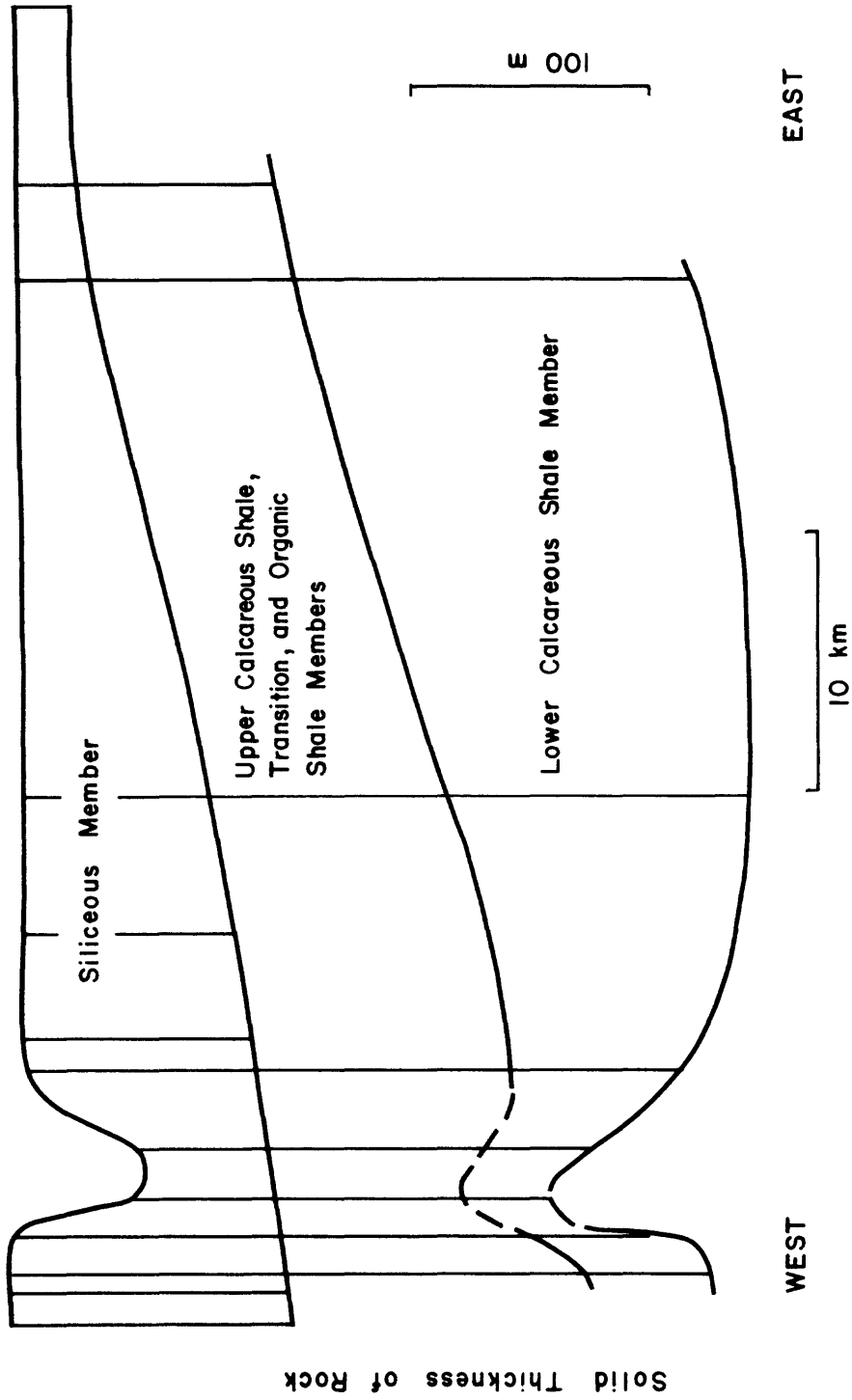
Fig. F—Lateral comparison of solid thickness of rock in members of the Monterey Formation. Values were calculated from stratigraphic measurements and from estimated porosity distribution. (Sections, from left to right: Black, Quail, Wood, Damsite, Cojo, Gato, San Augustine, Agujas, Coyote, Gaviota, El Capitan, Naples, Elwood.)

number of additional samples analyzed only by X-ray diffraction.
After analysis, sample locations--which were exactly recorded by
photographs--were revisited and rocks evaluated in the field for
distinguishing characteristics. These characteristics were then
used extensively in describing and interpreting sections.

Each section was examined at least twice (in some cases, ten
or more times) and measured only after detailed examination. In
most sections, stratigraphic intervals were calculated from level
tape measurements corrected for strike and dip. Measurements included
the position of exposed beds in each member, of each microfossil
locality, and of most lithologic samples. Detailed (foot-by-foot)
descriptions were made of several sections, particularly Damsite,
San Augustine, and Gaviota Canyons. Detailed descriptions were also
made of the upper calcareous shale member at Coyote, Agujas, San
Augustine, Gato, Cojo, Damsite, and Quail Canyons.

Stratigraphic Sections

General section descriptions in the following pages include:
(1) latitude and longitude of the section locality; (2) physical
description of the location of measurement and sampling and strati-
graphic position of prominent features; (3) general stratigraphic
thicknesses of exposed and unexposed intervals in each member; and
(4) comments, including brief remarks on unusual lithologic features
not described in the text. Definitions of member boundaries and
characteristic lithologies in each member were described above (p. 54-
73) and are not elaborated in section descriptions.

Sections are presented in order from east to west as follows: (1) Elwood Beach; (2) Naples Beach; (3) El Capitan Beach; (4) Refugio Beach; (5) Gaviota Beach and Canyon; (6) Coyote Canyon; (7) Agujas Canyon; (8) San Augustine Canyon; (9) Gato Canyon; (10) Cojo Canyon; (11) Damsite Canyon; (12) Wood Canyon; (13) Quail Canyon; and (14) Black Canyon. Most Monterey strata in each of these sections were examined, but only measured parts of sections are described here. Several additional canyons, which were examined and sampled (but not measured), are not described. These include Sacate, Bulito, Wells, and Jalama Canyons.

1. Elwood Beach

Section locality: Dos Pueblos Canyon 7.5' quadrangle; section
    near latitude 34°25.0' N., longitude 119°53.2' W.

Physical description of locality: The section was measured and sampled
    along the base of the beach cliffs. Rocks are generally rather
    weathered, particularly those below the transition member.

    The top of the organic shale member (which is very weathered)
    is exposed about 18 m stratigraphically below (northwest of)
    a prominent dolomite bed near the west end of the paved area.
    The transition member includes the prominent dolomite and opal-CT
    chert beds interbedded with calcareous diatomaceous rocks along
    the paved road. The upper calcareous shale member is opposite
    a small fenced building and its top strata are well exposed in
    the cliff. The siliceous member extends about 19 stratigraphic
    meters beyond (east of) the point where the section crosses the
    paved access road. (This access road is not indicated on the
    1951 quadrangle map.)

Stratigraphic measurements (from the top of the organic shale

member):

Siliceous member   80-148 m

Upper calcareous shale and transition members   0- 80

Comments: A considerable thickness of unmeasured strata is exposed

below the top of the organic shale member, but the base of the

Monterey is apparently faulted out (Dibblee, 1966, pl. 3).

2. Naples Beach

Section locality: Dos Pueblos Canyon 7.5' quadrangle; section between

latitude 34°26.7' N., longitude 119°58.2' W. (base) and latitude

34°26.3' N., longitude 119°57.6' W. (top)

Physical description of locality: The section was measured and sampled

along the base of the beach cliffs. Rocks are generally in very

fresh condition.

The base of the section was placed at a bentonite bed located

a few meters above the lowest exposures on the east side of

Las Varas Canyon. Along the beach southeast of the bentonite,

lower strata in the lower calcareous shale member are exposed

well. In the middle of the member, the section is structurally

deformed, and just west of Dos Pueblos Canyon is an intraforma-

tional breccia illustrated by Bramlette (1946). Near the base

of exposures on the east side of Dos Pueblos Canyon is the

10-ft thick chert bed (laminated calcareous opal-CT chert beds)

mentioned by Kleinpell (1938) at the base of the Luisian.

Stratigraphically above (to the southeast), calcareous diatomaceous

rocks form prominent outcrops. The top of the lower calcareous

shale member, marked by an abrupt break (upward decrease) in resistance to erosion, lies about 35 stratigraphic meters above the 10-ft chert. In beach cliffs farther southeast are exposed the organic shale, transition, and upper calcareous shale member, but differences are not prominent and few resistant beds are present. The siliceous member contains much more numerous resistant beds, some forming prominent dip slopes. The upper boundary of the siliceous member is well exposed but not distinctive.

Stratigraphic measurements:

Siliceous member	385-425 m
Upper calcareous shale and transition members	329-385
Organic shale member	239-329
Lower calcareous shale member	0-239

  (unexposed, intraformational breccia,

  and structurally disturbed zone, 83-193 m)

Comments: Grey vitric tuff beds are present in the upper half of the lower calcareous shale member and throughout the organic shale member. According to an unpublished section made in 1965 by H. D. Gower of the U.S. Geological Survey, vitric tuff represents about 1 percent of the organic shale member, with most beds 1.5 to 5.0 cm thick and the thickest beds 18.0 cm thick.

For thickness of strata below the 10-ft chert bed at the base of the Luisian, Kleinpell's (1938) estimate was used.

3. <u>El</u> <u>Capitan</u> <u>Beach</u>

Section locality: Tajiguas 7.5' quadrangle; section between latitude
34°27.6' N., longitude 120°00.5' W. (base) and latitude 34°27.7' N.,
longitude 120°01.0' W. (top)

Physical description of locality: The section was measured and sampled
along the beach and seawall. Rocks stratigraphically above the
organic shale member are generally rather weathered where exposed
in the beach cliffs, and rocks in the lowest two members are
generally in fresh condition.

The base of the lower calcareous shale member is poorly exposed,
but occurs just west of Cañada de la Destiladera. Disturbed
strata are present in the middle of the member, as in the Naples
Beach section. The top of the member, which is well exposed
but not distinctive, was placed about 30 stratigraphic meters
below a very prominent resistant bed which forms a ledge difficult
to pass at high tide. This resistant bed and adjacent well-
exposed strata are in the organic shale member. Stratigraphically
above (to the west), strata are more weathered and less strikingly
exposed. The base of the transition member was placed about
6 stratigraphic meters below (east of) a deep gully. The base
of the upper calcareous shale member is near the east end of the
seawall, and the top is near a drainage pipe in the middle of
the seawall. The top of the siliceous member is near the west
end of the seawall.

Stratigraphic measurements:

Siliceous member	363-405 m
Upper calcareous shale and transition members	301-363

Organic shale member   200-301 m

Lower calcareous shale member (poorly exposed,   0-200

    0-71 m)

Comments: Most strata in the calcareous members (0-337 m) were

    measured by pacing and may be overestimated.

4. Refugio Beach

Section locality: Tajiguas 7.5' quadrangle; base of section near

    latitude 34°27.7' N., longitude 120°04.4' W.

Physical description of locality: The section was measured and sampled

    along the beach, and rocks are generally in fresh condition.

    The base of the section, which is poorly exposed, was placed

    about 30 m stratigraphically below strata cropping out on the

    rocky point southwest of the public campground. Most samples

    were taken from beds between 15 and 25 m stratigraphically above

    the lowest beds exposed at the rocky point. The remainder of

    the section was not measured and is only partially present.

5. Gaviota Beach and Canyon

Section locality: Gaviota 7.5' quadrangle; section between latitude

    34°28.5' N., longitude 120°13.5' W. (base) and latitude 34°28.2' N.,

    longitude 120°13.7' W. (top)

Physical description of locality: The section was measured and sampled

    mainly on the beach near the pier and in outcrops and roadcuts

    on the west side of the canyon. The base of the section, however,

    was measured and sampled in freeway cuts and exposures on the

    east side of the canyon, using a distinctive dolomite and opal-CT

    chert to correlate across the canyon. Additional samples were

taken from the creek bed and from the cove 0.5 km west of the

pier. Rocks are generally quite weathered except along the beach.

On the northeast side of the freeway, about 0.3 km south of

the turnoff to Gaviota State Beach Park, are exposed the base

(placed at a thin bentonite bed) and a considerable thickness

of lower strata in the lower calcareous shale member. Beds

near the top of the member crop out along a dirt road crossing

the east side of the canyon and along the creek near the junction

of the Hollister road and state park road on the west side of

the canyon. The organic shale member is extensively exposed

(but highly weathered) in cuts along the Hollister road; the

member is much fresher in outcrops along the creek bank, where

the creek cuts into the east side of the canyon approximately

east of the campground. The top of the organic shale member

was placed 15 stratigraphic meters above the base of the outcrop

behind the building which houses the snack bar and public rest-

rooms. In that outcrop are also present the entire transition

member and the base and lower 7 stratigraphic meters of the upper

calcareous shale member. The upper calcareous shale member is

poorly exposed underneath the railroad trestle but well exposed

on the beach 0.5 km west of the pier. Beds in the siliceous

member form prominent outcrops near the entrance to the pier and

immediately to the west of the pier on the beach.

Stratigraphic measurements:

Siliceous member (unexposed top, under water)	258-287 m
Upper calcareous shale member (unexposed	227-258
234-246 m)	

Transition member	205-227 m
Organic shale member	140-205
Unexposed	135-140
Lower calcareous shale member (unexposed	0-135
78-123 m)	

Comments: An intraformational brea conglomerate cuts into the siliceous member just west of the measured section. During low tides, the conglomerate is extensively exposed in a small point just west of the pier and in a rocky point about 0.8 km farther west along the beach. This conglomerate, which is illustrated and described by Bramlette (1946) and Dibblee (1950), contains numerous Monterey clasts, including dolomitic rocks and unusual quartz cherts as well as more typical rocks. Sandstone dikes occur in siliceous rocks just below the conglomerate.

6. Coyote Canyon ("Cañada del Coyote")

Section locality: Sacate 7.5' quadrangle; section between latitude 34°28.6' N., longitude 120°18.0' W. (base of measured portion) and latitude 34°28.5' N., longitude 120°18.0' W. (top)

Physical description of locality: The section was measured and sampled along the dirt road. Rocks are generally rather weathered.

The base of the upper calcareous shale member is marked by an abrupt upward increase in calcareous porcelanites and cherts, and strata in the member are well exposed along the road. The lower boundary of the siliceous member is not distinctive, but numerous sandy beds and lenses (15 cm or more thick) are present between 30 and 60 m above the base. The upper boundary of the siliceous member is poorly exposed and was estimated ±10 m.

Stratigraphic measurements (from the base of the upper calcareous

shale member):

Siliceous member (unexposed 85-106 and   27-154 m

108-118 m)

Upper calcareous shale member (unexposed 18-23 m)   0- 27

Comments: Although not measured, strata below the upper calcareous

shale member are exposed along the road.

In Sacate Canyon (just east of Coyote Canyon), the siliceous

member is much thinner (about 65 m in total thickness), and

uppermost strata are sands and conglomerate lenses.

7. Agujas Canyon ("Cañada de las Agujas")

Section locality: Sacate 7.5' quadrangle; section between latitude

34°28.4' N., longitude 120°20.8' W. (base) and latitude 34°28.1' N.,

longitude 120°20.8' W. (top)

Physical description of locality: The section was measured and

sampled along the creek and in the road (which is not indicated

on the 1953 quadrangle map). Rocks are generally rather weathered.

The upper calcareous shale member is exposed along the creek

bed and in adjacent ledges where the dirt road crosses the creek.

The siliceous member crops out along the road and creek. Upper-

most strata form dip slopes on the south face of the ridge on

the east side of the canyon (near 120 ft elevation at creek level).

Stratigraphic measurements (from the approximate base of the upper

calcareous shale member):

Siliceous member (about half exposed)   27-152 m

Upper calcareous shale member   0- 27

Comments: Stratigraphically below (north of) the measured part

of the section, considerable strata in the lower calcareous

shale and organic shale members are exposed along the road (and

some strata also along the creek).

8. San Augustine Canyon ("Arroyo San Augustin")

Section locality: Sacate 7.5' quadrangle; section between latitude

34°28.4' N., longitude 120°21.6' W. (base) and latitude 34°28.1' N.,

longitude 120°21.5' W. (top)

Physical description of locality: The section was measured along the

dirt road and, south of where the road crosses a saddle, along

the ridge to the southwest. Lithologic samples were taken from

the creek bed and correlated with the road section by reference

to distinctive beds. Generally, rocks are weathered in road

cuts and fresh along the creek.

There are few prominent features in the measured section,

which is quite fully exposed along the road. Unusual quartz

cherts are located between 135 and 150 m in the organic shale

member--four massive black cherts (totalling 2 m thick) and

three opal-CT cherts (totalling 1 m thick) with quartzose cores.

Beds in the upper calcareous shale member and lower part of the

siliceous member crop out mainly in low cuts along the road

and are especially weathered; details in these beds are much

more fully exposed along the creek. Where the road passes through

a small saddle are strata in the middle of the siliceous member.

The top of the member is exposed on the south face of the ridge

southwest of the saddle.

Stratigraphic measurements:

Siliceous member (about half exposed)	243-396 m
Upper calcareous shale member	216-243
Transition member	176-216
Organic shale member	97-176
Lower calcareous shale member (unexposed 0-18 m)	0- 97

9. <u>Gato Canyon</u> ("Cañada del Gato")

Section locality: Point Conception 7.5' quadrangle; section between

latitude 34°28.1' N., longitude 120°23.3' W. (base) and latitude

34°27.9' N., longitude 120°23.3' W. (top)

Physical description of locality: The section was measured and

sampled along the creek and adjacent road (which is not indicated

on the 1953 quadrangle map). Rocks are generally rather weathered,

but several very fresh outcrops are present.

The base of the lower calcareous shale member is poorly exposed,

and lower strata consist of resistant dolomites and occasional

mudstones in the banks of the creek. Upper strata in the member

include thinly layered organic-rich beds exposed along the road.

Uppermost beds in the transition member are exposed on the east

side of the canyon at the base of a prominent cliff. The cliff

consists mainly of beds in the upper calcareous shale member,

which also crops out along the west side of the creek. The base

of the siliceous member is moderately exposed along the road

(on the east side of the creek) and the top of the member is

about 24 stratigraphic meters beyond (south of) the fence between

the Cojo and Hollister Ranches.

Stratigraphic measurements:

Siliceous member	171-252 m
Upper calcareous shale member	155-171
Transition member	148-155
Unexposed	101-148
Lower calcareous shale member (largely	0-101

    unexposed, 0-36 m)

10. <u>Cojo</u> <u>Canyon</u> ("Cañada del Cojo")

Section locality: Point Conception 7.5' quadrangle; section between

    latitude 34°28.3' N., longitude 120°24.8' W. (base) and latitude

    34°28.0' N., longitude 120°24.8' W. (top)

Physical description of locality: The section was sampled along the

    creek and dirt road in the canyon. Rocks are generally rather

    weathered.

    The base of the Monterey was placed at the top of the tuff,

exposed both in the creek and in the road. Little strata in the

overlying lower calcareous shale and organic shale members crop

out, and the thickness of these lower strata are not very

reliable due to folding. The upper calcareous shale member is

exposed in a ridge along the west side of the creek and in an

outcrop along the road containing a massive black quartz chert.

This chert bed was placed about 7 m stratigraphically below the

top of the member. The top of the siliceous member is near the

widening of the canyon floor where the dirt road turns southwest

from the creek (near 140 ft elevation at creek level).

Stratigraphic measurements (from the top of the tuff):

Siliceous member (unexposed 155-183 m)	132-208 m
Upper calcareous shale member	102-132
Transition member (unexposed 92-101 m)	90-102
Unexposed	60- 90
Organic shale member	58- 60
Unexposed	41- 58
Lower calcareous shale member	31- 41
Unexposed	0- 31

Comments: A few sand layers were noted in the lower calcareous

shale member.

11. <u>Damsite</u> <u>Canyon</u>

Section locality: Point Conception 7.5' quadrangle; section between

latitude 34°28.5' N., longitude 120°25.5' W. (base) and latitude

34°28.2' N., longitude 120°25.6' W. (top)

Physical description of locality: The section was sampled mainly

in the creek bottom and measured mainly along the dirt road

(which is not indicated on the 1953 quadrangle map). Rocks are

generally fresh in the creek and rather weathered along the

road.

The base of the Monterey was placed at the top of the tuff,

which is exposed in the creek bed. Strata in the lower calcareous

shale member form outcrops along the road, in the creek (near

320 ft elevation), and on the hillside on the west side of the

canyon. The organic shale is exposed only slightly, in the creek

bed. Upper beds in the transition and most of the upper calcareous

shale member are exposed both in the creek and along the road.

The most prominent and resistant beds in the section (which

form a waterfall 5 m high across the creek, a cliff outcrop

high on the ridge on the west side of the canyon, and a con-

striction of the canyon where the dirt road on the east side

of the canyon trends along strike) are in the upper calcareous

shale member. The top of this member was placed about 5 m

above a folded massive black quartz chert exposed along the road.

The siliceous member crops out less prominently, along the road

and in the creek. The upper boundary of the member (placed

somewhat below 200 ft at creek level) is exposed underneath

an oak tree along the dirt road.

Stratigraphic measurements (from the top of the tuff):

Siliceous member (unexposed 292-306 m)	230-378 m
Upper calcareous shale member	199-230
Transition member (unexposed 183-193 m)	174-199
Unexposed	133-174
Organic shale member	120-133
Unexposed	88-120
Lower calcareous shale member	17- 88
Unexposed	0- 17

12. Wood Canyon

Section locality: Point Conception 7.5' quadrangle; section between

latitude 34°28.8' N., longitude 120°26.4' W. (base) and latitude

34°28.5' N., longitude 120°26.7' W. (top)

Physical description of locality: The section was measured and

sampled along the creek, which is mainly in a steep canyon filled

with brush and flourishing poison oak. In general, rocks along

the creek are fresh.

The tuff and lower strata in the lower calcareous shale member

(near 400 ft elevation) are only moderately exposed along the

creek. The uppermost beds in the lower calcareous shale member

vary in resistance to erosion, forming a series of pools along

the creek. At the top of the member the creek turns abruptly,

trends along strike (about N. 52° W.), and then cuts into the

lower strata of the organic shale member. The transition and

upper calcareous shale members form prominent cliff exposures

and are partly repeated along the creek bottom by undulating

folds. The siliceous member is exposed mainly in the creek

bottom, which is covered by thick brush, and in small ledges.

The canyon widens slightly near the top of the Monterey (placed

near 220 ft elevation).

Stratigraphic measurements (from the top of the tuff):

Siliceous member (about half exposed)	215-376 m
Upper calcareous shale and transition members	149-215
Unexposed	110-149
Organic shale member (unexposed 70-108 m)	61-110
Lower calcareous shale member (unexposed 29-55 m)	8- 61
Unexposed	0- 8

Comments: Tuffaceous sediments and some calcareous sandstones are

present above (and were included with) the tuff, which totals

over 24 m in thickness.

13. <u>Quail</u> <u>Canyon</u>

Section locality: Point Conception 7.5' quadrangle; section between

latitude 34°29.0' N., longitude 120°26.7' W. (base) and latitude

34°28.6' N., longitude 120°27.0' W. (top). This canyon, unnamed

on the 1953 quadrangle map, contains the creek between that in

Wood Canyon (to the southeast) and that originating at Las Animas

Spring (to the northwest).

Physical description of locality: The section was measured and sampled

along the creek, in a steep, rather brushy canyon. Rocks are

generally in fresh condition.

The lowest exposed beds in the upper calcareous shale include

a few lensoid quartz cherts in a small ledge next to the creek.

The creek runs perpendicular to strike in most of the member,

and resistant beds (including massive and banded quartz cherts

as well as opal-CT cherts) create pools along the creek bottom.

The uppermost bed in the upper calcareous shale member (a dolomite)

forms a curved ledge about 1.5 m high across the creek bottom.

An adjacent outcrop 2 to 3 m high on the east side of the creek

contains about 3 stratigraphic meters of dark, platy quartz

porcelanites at the base of the siliceous member. The siliceous

member generally crops out along the creek bottom and in undercut

cliffs along the sides of the creek. The canyon opens up somewhat

near the top of the Monterey (placed, at creek level, near

280 ft elevation).

Stratigraphic measurements (from the approximate base of the upper

calcareous shale member):

Siliceous member (about half exposed)   33-173 m

Upper calcareous shale member   0- 33 m

Comments: The thickness of the siliceous member was estimated from

mapped contacts rather than from taped measurements.

Stratigraphically below (upstream from) the upper calcareous

shale member, the canyon is very brushy and strata generally

crop out sparsely. The lower calcareous shale member and tuff,

however, are exposed along the creek just south of the point

where the canyon widens and the creek changes course (about

400-420 ft elevation).

14. Black Canyon

Section locality: Point Conception 7.5' quadrangle; latitude 34°29.1' N.,

longitude 120°27.6' W. (base of measured portion), latitude

34°28.9' N., longitude 120°27.7' W. (top)

Prominent features in section: The upper part of the section was

measured and sampled on the slopes of the east side of the canyon.

Stratigraphically below the upper part of the siliceous member,

sampling was along the creek. Subsequent building of a dirt

road along the east side of the creek bed exposed the section

more fully.

The base of the siliceous member was placed near an open part

of the creek bottom where a group of water pipes join. Strata

in the member are well exposed, and the upper boundary clearly

marked, along the dirt road.

Stratigraphic measurements (from the top of the upper calcareous

shale member):

Siliceous member (about half exposed)   0-139 m

Comments: Stratigraphically below (north of) the measured part

of the section, parts of the upper calcareous shale and transition

members are exposed along the road. Older strata, however, are

evidently not present due to structural displacement (cf.

Dibblee, 1950).

Near the surface of a marine terrace above the measured

section, on the east side of the canyon, pink and red porcelanites

are present. Clasts of black and red banded cherts are also found

in the creek bottom and near Las Animas Spring (to the east).

APPENDIX G

SAMPLE DATA TABLE

This appendix presents data on those samples for which mineral

abundances were determined. Samples are listed in stratigraphic

sequence (from youngest to oldest) by canyon (in order, from east to

west).

Data columns are explained as follows.

Field no. (column 1): sample field number. Where sample field

numbers differ only by a final latter (e.g., AUG-6B-14A and AUG-6B-14B),

the samples are different parts of the same bed and appear to be

reasonably similar. Where sample field numbers are followed by a

number in parentheses (e.g., AUG-7B-14 (1) and AUG-7B-14 (2)), the

samples are essentially identical and are regarded as duplicates.

Asterisks indicate special rocks, such as unusual quartz cherts and

nodular or relatively pure bedded dolomites.

Strat. pos. (column 2): stratigraphic position, in meters.

The stratigraphic position is measured from the base of the section,

unless otherwise noted. The symbol "c" indicates that the value is

+5 meters.

Mineral abundance (columns 3-10): weight percentages on an

organic-free basis, normalized to 100 percent, determined as described

in Appendix B. "-" means none detected.

Silica component (defined on p. 19):

Op-A (column 3): opal-A

292

Op-CT (column 4): opal-CT

Qtz (column 5): diagenetic quartz

Detrital component (defined on p. 20):

Alum (column 6): aluminosilicate minerals

Qtz (column 7): detrital quartz

Other minerals:

Cal (column 8): calcite

Dol (column 9): dolomite

Ap (column 10): apatite

Org. matter (column 11): organic matter content, in weight percentage, determined as described in Appendix C.

Op-CT d-sp. (column 12): opal-CT d-spacing, in Å. Measurement method described in Appendix D.

Bulk density (column 13): dry bulk density, in g/cc. Measurement method described in Appendix E.

Grain density (column 14): dry grain density, in g/cc. Measurement method described in Appendix E.

Porosity (column 15): dry porosity, in volume percent, derived from values of dry bulk density and dry grain density.

Field no.	Strat. pos.	Silica			Detrital		Other			Org. matter	Op-CT d-sp.	Bulk density	Grain density	Porosity
		Op-A	Op-CT	Qtz	Alum	Qtz	Cal	Dol	Ap					
ELWOOD BEACH SECTION														
Siliceous member														
ELW-1-17A	130[2]	65	–	–	26	9	–	–	–			0.69	2.23	69%
-1-17B	130[2]	53	–	–	35	12	–	–	–			0.83	2.25	63%
-1-16	c 130[2]	55	–	–	34	11	–	–	–			0.80	2.24	64%
-1-15	c 130[2]	36	–	–	48	16	–	–	–					
Transition member														
ELW-1-8	16[2]	–	78	–	8	3	11	–	–		4.118	1.88	2.22	15%
-1-9	16[2]	58	–	1	17	6	18	–	–			0.83	2.24	63%
-1-11A	c 14[2]	48	–	–	18	6	28	–	–			0.87	2.24	61%
-1-11B	c 14[2]	48	–	–	18	6	29	–	–			0.98	2.30	57%
-1-12	c 14[2]	31	–	–	20	7	42	–	–			1.01	2.24	55%
-1-13	c 14[2]	31	–	2	30	10	27	–	–			1.97	2.01	2%
-1-5	12[2]	–	74	1	6	2	16	–	–		4.117	1.00	2.31	57%
-1-6	12[2]	37	–	–	21	7	35	–	–					
Organic shale member														
ELW-2-2	[1]	–	76	1	8	3	12	–	–		4.110	1.85	2.21	16%
-2-4	[1]	–	54	3	4	1	38	–	–		4.116			

[1]Position not measured
[2]Above base of transition member

NAPLES BEACH SECTION

Siliceous member

Sample	No.												
NAP-13-4	393	5	52	–	32	11	–	–	5.0	4.105	1.47	2.29	36%
-13-3	389	–	76	–	19	5	–	–	3.1	4.114	1.83	2.09[3]	12%[3]
-13-5	387[4]	35	–	–	49	16	–	–	8.0		1.29	2.28	43%
-1-1 (1)	[4]	15	14	–	54	18	–	–	7.9		1.39	2.36	41%
(2)											1.40	2.36	41%
-1-2	[4]	23	–	–	58	19	–	–					
-1-3	[4]	5	57	–	28	9	–	–		4.111			
-1-4	[4]	–	76	–	18	6	–	–		4.112			
-1-8		30	15	–	41	14	–	–					

Upper calcareous shale and transition members

Sample	No.												
NAP-13-2	c 367	–	84	–	8	3	6	–		4.116	1.13	2.39	53%
-13-1	c 367	16	–	–	44	15	26	–	9.3		1.86	2.08[3]	11%[3]
-1-5	[4]	–	70	–	16	4	10	–	6.1	4.114	1.80	2.15[3]	16%[3]
-1-7	[4]	–	66	–	21	5	8	–	5.5	4.112			
-12-6	341	44	–	–	25	8	20	2	9.8		0.91	2.22	59%

Organic shale member

Sample	No.												
NAP-12-5	329	16	–	–	42	15	24	3	12.1		1.08	2.29	53%
-11-5	239	8	–	–	34	12	40	6	21.4		1.10	2.17	50%

Lower calcareous shale member

Sample	No.												
NAP-11-4	238	4	–	–	6	2	62	27	4.0		1.75	2.59	33%
-11-2A	c 227	20	–	–	9	3	63	5	9.2				
-11-2B	c 227	25	–	–	10	4	54	4			0.97	2.32	58%
-11-3	206	23	–	–	13	5	49	10					
-11-1	204	–	82	6	5	2	5	–		4.116			

[3] Values low, probably due to enclosed pore space

[4] Samples from exposures 1.5 km east of measured Naples section

Sample	Pos													
NAP-10-8	83	—	16	—	16	5	14	49	—			1.64	2.60	37%
-10-7	68	—	57	3	13	4	23	1	—			1.54	2.33	34%
-10-6	68	—	10	1	27	9	47	5	—	3.4		1.30	2.44	47%
-10-11	62	—	64	—	12	4	18	2	—	7.4	4.101	1.46	2.31	37%
-10-5A	43	—	71	6	7	2	12	2	—	2.2	4.102			
-10-5B	43	—	74	7	7	2	10	—	—	3.5	4.095	1.86	2.27	18%
-10-4	20	—	58	1	13	4	24	—	—	5.6	4.086	1.43	2.31	38%
-10-2	16	—	34	—	20	6	38	2	—			1.31	2.40	46%
-10-3A	14	—	53	—	16	5	22	5	—			1.45	2.34	38%
-10-3B	14	—	53	—	15	5	23	4	—	3.9	4.092	1.42	2.35	40%

EL CAPITAN BEACH SECTION

Siliceous member

Sample	Pos													
CAP-11-1	c 372	—	68	—	25	7	7	—	—		4.092			
-11-2A	c 372	—	73	1	20	7	—	—	—		4.095			
-11-2B	c 372	—	62	3	26	9	—	—	—		4.095			
-11-3	c 372	—	43	—	42	14	—	—	—		4.085			

Upper calcareous shale member

Sample	Pos													
CAP-2-2	333	—	81	—	11	4	5	—	—		4.103	1.73	2.20	21%
-3-1	c 331	—	75	1	12	4	9	—	—		4.101	1.60	2.23	28%
-3-2	c 331	—	57	—	30	6	6	—	2		4.093			
-3-3	c 331	—	36	3	26	8	27	—	—		4.087			
-3-4	c 331	—	55	—	18	4	24[5]	—	—		4.097	1.45	2.31	37%
-2-1	328	—	77	—	17	6	6	—	—		4.100			

Organic shale member

Sample	Pos													
CAP-10-1	c 241	—	12	—	23	6	50	—	9	14.9		1.28	2.25	43%
-10-2	c 241	—	62	6	6	2	24	—	—	6.1	4.105	1.65	2.22	26%
-10-3A	c 241	—	23	—	21	7	43	—	7			1.27	2.21	43%

[5]Present but amount not estimated due to weathered condition

Sample															
CAP-10-3B	c	241	—	20	—	22	7	45	—	6	15.6	4.077	1.23	2.22	44%
-10-4	c	241	—	22	—	22	4	49	—	2			1.41	2.30	39%
-10-5	c	241	—	25	—	13	3	59	—	—	15.5	4.087	1.38	2.32	41%
-6-2		238	—	10	—	25	8	38	—	19			1.24	2.04	39%
-6-1		225	—	3	1	26	9	52	—	10			1.56	2.30	32%
-6-3		207	—	47	9	4	1	46	—	—		4.105	1.88	2.27	17%
-6R-3		207	—	53	—	3	1	34	—	—		4.109	1.30	2.27	43%
-6-4		207	—	5	—	17	4	67	—	7	15.5				
-6-5A		207	—	5	—	24	3	64	—	4	12.4				
-6-5B		207	—	5	—	16	5	69	—	4			1.35	2.30	41%

Lower calcareous shale member

Sample															
CAP-6-7		143	—	22	—	22	5	49	—	2		4.082	1.64	2.43	33%
-6-8		142	—	70	1	14	4	11	—	—	3.3		1.72	2.21	22%
-6R-8		142	—	53	—	23	6	18	—	—	5.1	4.091	1.40	2.30	39%
-6-9		109	—	53	—	19	5	22	2	—	4.4	4.084	1.49	2.33	36%
-6-10		109	—	24	—	20	7	42	7	—	5.5	4.077	1.38	2.40	43%
-6-11		109	—	8	—	36	12	36	9	—	7.4		1.52	2.40	37%
-6-12		106	—	56	—	15	3	20	6	—	3.1	4.092	1.47	2.36	38%

REFUGIO BEACH SECTION

Lower calcareous shale member

Sample															
REF-6-4	[6]		—	11	—	31	9	45	4	—	—	—	1.57	2.44	36%
-6-6 (1)	[6]		—	54	—	10	3	30	3	—	4.3	4.086	1.56	2.35	34%
-6-6 (2)	[6]		—	—	—	—	—	—	—	—	—	—	1.55	2.37	35%
-6-7 (1)	[6]		—	25	—	31	9	31	2	2	6.1	4.065	1.44	2.44	41%
-6-7 (2)	[6]		—	—	—	—	—	—	—	—	—	—	1.46	2.44	40%
-6-11	[6]		—	27	—	39	10	22	3	—	—	4.064	1.47	2.42	39%
-6-8	[6]		—	6	4	41	14	34	—	—	—	—	1.56	2.45	36%
-6-3	[6]		—	33	—	20	6	28	12	—	—	4.077	1.55	2.43	36%

[6]Samples located 30 to 55 m stratigraphically above the base of the lower calcareous shale member

Sample		n												%
REF-6-10	6		60	14	7	2	17	17	–	1.9	4.097	1.94	2.52	23%
-6-5	6		35	–	8	2	55	–	–	2.9	4.085	1.93	2.53	24%

GAVIOTA BEACH AND CANYON SECTION

Siliceous member

Sample		n												%
GAV-13A-31*(1)		287	38	–	9	2	–	51	–			1.59	2.23	29%
-13A-31*(2)		287										1.60	2.23	28%
-13A-20A	c	284	82	–	14	4						1.50	2.36	36%
-13A-20B	c	284	85	1	11	4					4.095	1.51	2.23	32%
-13A-23		282	47	5	36	12					4.081	1.51	2.21	32%
-13A-27A		278	79	1	16	5				4.7	4.091	1.55	2.21	30%
-13A-27B		278	78	–	17	5					4.091	1.39	2.23	37%
-13A-28		277	84	–	12	4				3.0	4.094	1.40	2.23	37%
-13A-32A	c	273	80	–	17	3				4.4		1.51	2.38	36%
-13A-32C	c	273	76	–	18	6				4.8	4.089	1.50	2.25	33%
-13A-33		270	38	5	43	14				2.5	4.072	1.42	2.27	37%
-13A-29		270	83	–	15	3					4.094	1.48	2.26	35%
-13A-30		269	72	2	20	6					4.086	1.49	2.30	35%
-13-2		269	72	–	22	6				3.3	4.087	1.58	2.30	31%
-13-3		268	42	–	45	13				7.1	4.076	1.42	2.26	37%
-12B-8	7		49	–	39	12						1.55	2.24	31%
-12B-10	7		73	–	21	6						1.48	2.27	37%
-12B-11	7		81	–	15	5						1.59	2.24	31%
-12-2	7		65	1	25	9						1.48	2.27	35%
-12-3	7		84	–	12	4						1.59	2.24	29%

Upper calcareous shale member

Sample		n												%
GAV-12-4	8		33	–	42	12	3	10	–	6.2	4.066	1.70	2.39	29%
-12B-1	8		60	–	20	6	12	–	2		4.082	1.50	2.27	34%

[7] Samples from beach exposures 0.25 km west of Gaviota pier, not in measured section

[8] Samples from beach exposures 0.5 km west of Gaviota pier, not in measured section

GAV-12B-2	8	31	–	28	7	2	32	–	4.074	1.65	2.44	33%
-12B-3	8	77	–	17	4	3	–	–	4.088	1.54	2.22	32%
-12B-4	8	38	–	10	2	–	50	–	4.080	1.80	2.42	26%
-12B-5	8	60	–	19	6	15	–	–	4.084	1.44	2.27	36%
-12B-6	8	22	–	28	7	–	–	–	4.070	1.78	2.44	27%
-13B-9	230	69	21	3	1	6	43	–	4.106			

Organic shale member

GAV-19-6	9	5	9	25	8	53	'–	–	9.6	1.41	2.17	35%

Lower calcareous shale member

GAV-10-3	68	61	3	11	4	20	1	–	4.070	1.72	2.44	30%
-10-1	69	–	34	24	8	30	4	–				
-10-7	69	–	16	19	6	53	6	–				
-10-9	70	–	28	17	6	24	26	–				
-17-12	c 35	–	13	35	12	40	–	–		1.95	2.53	23%
-17-11	c 35	–	15	31	10	44	–	–		1.76	2.53	30%
-17-10	29	24	34	11	4	23	–	–		1.74	2.53	31%
-17-9	29	30	17	12	4	34	3	–	4.057			
-17-7	6	39	7	12	4	38	3	–	4.060			

COYOTE CANYON SECTION

Siliceous member

COY-2-2	34[10]	82	–	14	4	–	–	–	4.101			
-2-3	34[10]	83	–	13	4	–	–	–	4.098			
-2-4	34[10]	87	–	10	3	–	–	–	4.101			
-2-5	8[10]	71	–	23	7	–	–	–	4.093			
-2-6	3[10]	86	–	11	3	–	–	–	4.101			
-2-7	3[10]	83	–	13	4	–	–	–	4.102			

[9] Sample from exposure in creek, not in measured section

[10] Above base of siliceous member

BULITO CANYON SECTION

Siliceous member

Sample													
BUL-4-18	1	–	85	–	12	4	–	–		4.096			
-4-19	1	–	74	–	21	5	–	–	4.7	4.088	1.44	2.23	35%
-4-22	1	–	59	–	31	10	–	–	7.3	4.083	1.39	2.23	37%
-4-23	1	–	60	–	30	10	–	–		4.084			
-5-1	1	–	52	–	36	12	–	–	8.6	4.082	1.39	2.24	38%

SAN AUGUSTINE CANYON SECTION

Siliceous member

Sample													
AUG-8C-2	282	–	49	1	38	12	–	–		4.082			
-8B-4	263	–	59	–	33	5	–	–		4.085			
-8B-3	258	–	79	–	15	6	–	3		4.090			
-8B-2	258	–	74	–	21	5	–	–		4.085	1.50	2.26	34%
-8B-1	258	–	85	–	11	4	–	–		4.093			

Upper calcareous shale

Sample													
AUG-7B-16	242	–	70	–	10	4	16	–	4.5	4.094	1.77	2.20	19%
-7B-6	234	–	44	–	16	5	32	2	8.5	4.077	1.62	2.29	29%
-7B-15	234	–	50	–	17	6	25	2		4.078	1.62	2.28	29%
-7B-14 (1)	232	–	64	1	10	4	21	–		4.091			
-7B-14 (2)	232	–	64	12	11	4	21	–	4.4		1.63	2.27	28%
-7B-17	232	–	65	3	4	1	17	–	2.5	4.105	1.92	2.27	15%
-7B-5	232	–	67	–	5	2	23	–	3.1	4.103	1.84	2.27	19%
-7B-12	230	–	24	–	20	6	46	3	9.1	4.071	1.71	2.37	28%
-7B-11	228	–	23	–	25	5	44	2	9.6	4.075	1.68	2.33	28%
-7B-4	228	–	55	1	10	3	30	–	4.1	4.096	1.76	2.29	23%

Transition member

Sample													
AUG-6C-11	198	–	58	12	5	2	23	–	2.0	4.097	1.71	2.30	26%
-6C-10A*	192	–	4	–	3	1	–	93			2.49	2.69	8%

Sample													
Organic shale member													
AUG-6C-9	167	–	16	–	43	14	–	23	5	23.8	4.060	1.54	2.08	26%
-6B-16	167	–	23	–	32	8	–	25	12	11.8	4.061	1.58	2.32	32%
-6B-15	156	–	5	–	18	3	–	66	7	12.2		1.62	2.34	31%
-6B-14A	156	–	–	8	32	11	–	34	15	19.5		1.54	2.31	33%
-6B-14B	156	–	–	4	36	12	–	31	18					
-6B-12	134	–	–	6	19	6	–	59	10	16.4		1.55	2.30	33%
-5C-6	99	–	–	3	12	4	–	79	3	7.1		1.65	2.48	33%
Lower calcareous shale member													
AUG-4C-28	57	–	64	13	5	2	–	16	–	4.8	4.091	1.72	2.30	26%
-4C-27	56	–	65	7	7	2	–	19	–		4.087	1.61	2.26	29%
-4C-21	53	–	61	16	7	2	–	14	–		4.089	1.57	2.18	28%
-4C-20	52	–	74	5	8	3	–	11	–	7.6	4.088	1.58	2.22	29%
-4C-19	52	–	73	5	6	2	–	13	–		4.084	1.74	2.39	27%
-4C-26	52	–	33	2	8	3	–	54	–		4.075			
-4C-17	51	–	32	9	22	7	–	30	–	4.6	4.063			
-4C-25	50	–	5	18	28	9	–	40	–	12.7		1.57	2.20	28%
-4C-24	50	–	10	20	25	8	–	37	–	15.6		1.49	2.17	31%
-4C-15A	43	–	58	36	4	1	–	11	–	17.7	4.087	1.94	2.28	15%
-4C-15B	43	–	57	37	4	1	–	11	–	1.7				
-4C-14*	43	–	–	11	7	2	80	–	–	5.3		2.36	2.61	9%
-4C-13*	42	–	–	5	16	6	67	–	6	4.8		2.14	2.63	19%
-4C-11*	39	–	–	–	7	2	91	–	–	1.8		2.63	2.77	5%
GATO CANYON SECTION													
Siliceous member													
GAT-20-4	247	–	19	5	58	19	–	–	–			1.70	2.45	31%
-1B-1	222	–	20	6	55	18	–	–	–			1.69	2.40	29%

[11] Foraminifera tests replaced by quartz.

Sample														
GAT-1B-2	221	—	42	6	39	13	—	—	—	4.6	4.067	1.66	2.38	30%
-1-5A	217	—	39	4	43	14	—	—	—	6.0	4.065	1.63	2.33	30%
-1-5B	217	—	42	6	40	13	—	—	—	4.0	4.067	1.63	2.36	31%
-1-6	217	—	41	7	39	13	—	—	—	4.7	4.066	1.66	2.33	29%
-2-4	193	—	75	1	18	6	—	—	—		4.080			
-2-9	193	—	73	2	19	6	—	—	—		4.083			
-2-6	192	—	28	8	49	16	—	—	—		4.063			
-2B-5	185	—	69	1	23	7	—	—	—		4.076			
-2B-4	185	—	85	2	10	3	—	—	—		4.089			
-2B-3	184	—	35	3	47	16	—	—	—		4.061			
-2B-2	184	—	81	2	13	4	—	—	—		4.085	1.64	2.24	27%
-3A-2	174	—	80	2	13	4	—	—	—		4.088	1.65	2.26	27%
-3-3	172	—	48	—	39	13	—	—	—		4.065			
-3A-1	171	—	85	5	7	3	—	—	—		4.091			
Upper calcareous shale member														
GAT-3B-7	167	—	70	—	23	7	[12]	—	—		4.072			
-3B-2	166	—	73	—	9	3	—	15	—		4.088			
-3B-3	166	—	21	1	4	1	[12]	73	—					
-3B-8	161	—	79	15	5	2	[12]	—	—		4.098			
-3C-3	155	—	—	16	32	11	3	30	9			1.89	2.30	18%
-3C-1	153	—	—	12	27	9	—	40	13			2.01	2.31	13%
Lower calcareous shale member														
GAT-4-3	96	—	—	9	5	2	82	—	3					
-4-4	95	—	—	10	12	4	69	—	5					
-4-5	92	—	6	3	3	1	80	7	—					
-4-1A	90 [c]	—	21	6	16	5	52	—	—	18.5	4.059	1.61	2.09	23%
-4-1B	90 [c]	—	22	4	14	4	54	—	2					
-4-6A	84	—	8	11	18	6	58	—	—					
-4-6B	84	—	9	10	20	7	55	—	—	11.0	4.052			

[12] Quantity not reliable due to weathered condition

GAT-5-5		74	-	71	4	8	3	14	-	-	3.8	4.084	1.75	2.24	22%
-5-3	c	73	-	77	4	7	2	9	-	-			1.76	2.25	22%
-5-4	c	71	-	-	19	26	9	46	-	-					
-5-2	c	71	-	55	4	11	3	27	-	-		4.075	1.54	2.22	31%
-5-6		70	-	-	12	33	11	38[13]	-	6	18.2				
-6-2	c	55	-	73	10	12	4		-	-					
DAMSITE CANYON SECTION															
Siliceous member															
DAM-9B-1		368	-	66	6	21	7	-	-	-	2.6	4.069	1.77	2.31	23%
-8B-4		308	-	40	11	37	12	-	-	-			1.79	2.42	26%
-8B-3		308	-	38	14	35	12	-	-	-		4.061	1.77	2.39	26%
-8C-4A		308	-	31	14	41	14	-	-	-	6.8		1.91	2.38	20%
-8C-4B		308	-	23	17	45	15	-	-	-					
-8C-3		307	-	13	22	49	16	-	-	-			1.91	2.43	21%
-8C-2A		307	-	17	26	43	14	-	-	-			1.84	2.36	22%
-8C-2B		307	-	16	20	48	16	-	-	-	8.2				
-8C-1A		306	-	-	37	47	16	-	-	-	7.1		1.91	2.45	22%
-8C-1B		306	-	-	35	49	16	-	-	-					
-8C-6		302	-	-	29	53	18	-	-	-	8.7		1.91	2.43	21%
-8C-5		302	-	-	35	49	16	-	-	-			2.00	2.43	18%
-8C-8A		280	-	78	11	8	3	-	-	-		4.079			
-8C-8C		280	-	75	8	13	4	-	-	-		4.078	1.74	2.27	23%
-8C-8D		280	-	75	8	13	4	-	-	-	3.0				
-8C-7A		277	-	71	11	14	5	-	-	-	4.4	4.068	1.58	2.27	30%
-8C-7C		277	-	65	13	17	6	-	-	-					
Upper calcareous shale member															
DAM-7D-1		222	-	-	27	23	8	-	40	3	6.6		2.29	2.52	9%
-7D-2*		221	-	-	7	1	-	-	93	-			2.78	2.79	0.6%

[13]Present but amount not estimated due to weathered condition

Sample		Depth													
DAM-7D-6		221	—	53	22	19	6	—	13	—		4.069			
-7R-6		221	—	70	22	6	2	—	13	—		4.081			
-7D-5		221	—	60	18	15	5	—	2	—		4.067	1.83	2.26	19%
-7D-4		221	—	64	16	12	4	—	5	—	5.7		1.79	2.24	20%
-7D-3		221	—	59	20	12	4	—	5	—					
-7D-7		219	—	24	30	21	7	—	18	—		4.060	1.91	2.34	18%
-7D-9		215	—	—	32	10	3	—	55	—			2.48	2.61	5%

Transition member

Sample		Depth													
DAM-7A-8		195	—	—	22	15	5	9	46	3	6.3		2.33	2.53	8%
-7A-7A		195	—	—	28	11	4	7	45	5			2.40	2.51	4%
-7A-7B		195	—	—	27	14	5	8	44	2	4.0				

Organic shale member

Sample		Depth													
DAM-6B-2	c	133	—	—	10	10	3	57	—	20			1.98	2.72	27%
-6B-8		133	—	—	24	26	9	38	—	3	10.9		1.88	2.39	22%

Lower calcareous shale member

Sample		Depth													
DAM-6-4		53	—	54	39	3	1	4	—	—		4.085			
-5B-6		30	—	55	26	5	2	13	—	—					
-5B-1	c	28	—	41	14	3	1	41	—	—					
-5A-8*	c	25	—	—	97	2	1	—	12	12	0.8		2.55	2.55	0%
-5A-7	c	23	—	—	52	36	12	—	—	—					
-5A-6*	c	23	—	—	4	6	2	—	87	—			2.63	2.79	6%
-5A-5*	c	18	—	—	4	9	3	—	85	—					

WOOD CANYON SECTION

Siliceous member

Sample		Depth													
WOOD-11-1	c	344	—	34	15	38	13	—	—	—	6.4	4.057	1.71	2.45	30%
-11-3	c	340	—	11	33	42	14	—	—	—	5.6		1.71	2.47	31%
-11-4	c	337	—	10	31	44	15	—	—	—					
-11B-2		309	—	—	41	44	15	—	—	—	7.8		1.95	2.44	20%
-11B-1		300	—	19	36	34	11	—	—	—	8.1	4.053	1.60	2.37	33%

Sample	c	Depth													
WOOD-10C-2*		285	–	–	25	13	4	–	58	–	7.9	4.068	2.31	2.55	9%
-10C-1		277	–	40	23	28	9	–	–	–	9.6	4.071	1.68	2.27	26%
-10B-1	c	277	–	61	17	17	6	–	–	–					
-10-2	c	265	–	–	67	25	8	–	–	–					
-10-1	c	265	–	58	10	24	8	–	–	–	3.6	4.066	1.55	2.33	34%
-10-4A		265	–	51	19	23	7	–	–	–		4.067	1.62	2.36	31%
-10-4B		265	–	57	19	18	6	–	–	–		4.071			
-10R-5		264	–	68	20	9	3	–	–	–		4.077			
-10R-7		263	–	5	46	37	12	–	–	–			2.03	2.35	14%
-10-7		263	–	36	32	24	8	–	–	–	9.1	4.063	1.66	2.35	30%
-10-6		263	–	–	54	35	12	–	–	–					
-10-5		263	–	38	29	25	8	–	–	–	9.1	4.067	1.60	2.35	32%

Upper calcareous shale and transition members

Sample	c	Depth													
WOOD-9-3	c	213	–	55	25	8	3	–	9	–			2.17	2.47	12%
-9-9		210	–	–	80	9	3	5	2	–			2.42	2.43	0.3%
-9R-9*	c	210	–	–	83	9	3	3	2	–			2.09	2.34	11%
-9-8	c	208	–	–	41	20	6	28	2	4	9.5		2.54	2.56	1%
-9-7*		206	–	–	52	3	1	7	37	–	2.1				
-8-2	c	198	–	–	63	13	4	20	–	–			2.20	2.35	6%
-8-4		194	–	–	55	14	5	26	–	–	7.9				
-7-4		178	–	32	52	5	2	–	10	–					
-5-3	c	161	–	–	73	18	6	1	–	2			2.16	2.33	7%
-5-4		153	–	–	32	9	3	55	–	–	14.3		1.89	2.33	19%

Organic shale member

Sample	c	Depth													
WOOD-4-6		69	–	–	5	18	6	70	–	–			1.96	2.53	22%
-4-5		69	–	–	6	12	4	76	–	2	8.6		1.84	2.44	25%
-4-1	c	67	–	–	3	16	5	73	–	3	8.6		1.97	2.48	21%
-4-4		66	–	–	6	19	6	63	–	7			1.78	2.41	26%
-4-2A		62	–	–	7	27	9	53	–	4	12.8		–	2.38	–
-4-2E		62	–	–	13	20	7	58	–	3			1.79	2.36	24%
-4-3		61	–	–	8	21	7	60	–	3	12.8		1.75	2.41	27%

Lower calcareous shale member

Sample	c	count												%
WOOD-3-2*		61	—	1	1	—	98	—	3.7			2.59	2.63	2%
-3-4		61	—	27	5	64	2	2	18.2			1.83	1.93	5%
-3-3		58	—	45	10	41	—	—	6.7			2.00	2.42	17%
-2B-6		29	—	61	7	29	—	—	6.8			2.06	2.43	15%
-2B-4*	c	29	—	86	4	7	2	—				2.44	2.47	1%
-2B-5		27	—	60	15	—	20	—				2.05	2.44	16%

QUAIL CANYON SECTION

Siliceous member

Sample	c	count												%
BIX-10-11B (1)		138	—	33	50	17	—	—				1.84	2.44	25%
-10-11B (2)		138	—	33	50	17	—	—				1.81	2.42	25%
-10-11D (1)		138	—	33	50	17	—	6.8				1.83	2.42	25%
-10-11D (2)		138	—	33								1.75	2.42	28%
-10-9	c	138	8	29	47	16	—	—	5.8					
-10-7	c	138	41	8	38	13	—	—	5.0	4.067				
-10-5	c	138	34	10	42	14	—	—	5.9	4.059		1.54	2.34	34%
-10-3A (1)		138	38	8	40	14	—	—	6.1				2.35	
-10-3A (2)		138	52	8	30	10	—	—				1.48	2.33	36%
-10-3B		138	47	12	31	10	—	—				1.43	2.33	39%
-9-1		101	37	31	24	8	—	—	9.2			1.55	2.35	34%
-8-8		54	59	24	13	4	—	—	3.8	4.063				
-8-7		54	57	21	16	5	—	—						
-8-5	c	54	10	35	19	6	—	—		4.070				
-8-4*	c	54	—	49			30	—	11.4			1.97	2.30	14%
-7-7		34	—	56	38	13	—	—						
-7-4		34	—	47	33	11	—	—						
-7-6A		34	—	48	40	13	—	—	9.9			1.98	2.36	16%
-7-6B		34	—	38	39	13	—	—				1.97	2.32	15%
-7-8A		34	—			16	—	—				1.97	2.31	15%
-7-8B		34	—		46		—	—	10.6					

Note: column headers are not printed on this page. Superscript markers (e.g. [10], [12], [1]) are footnote references as printed.

Upper calcareous shale member

Sample												%
BIX-6B-2	29	–	63	28	9	–	–	–	–	–	–	–
-6B-3	29	–	71	22	7	–	–	–	–	–	–	–
-6B-4	27	62	28	7	2	–	–	–	4.070	–	–	–
-6B-6*	25	–	2	4	2	–	92[12]	–	–	2.71	2.76	2%
-6B-7	16	57	33	7	2	–	–	–	4.071	–	–	–
-6B-13*	14	–	92	3	1	–	4[12]	2.0	–	2.50	2.53	1%
-6-6	4	49	38	10	3	–	–	–	4.066	–	–	–
-6-4*	2	–	4	6	2	–	88[12]	–	–	2.50	2.78	10%
-6-5*	2	–	88	6	2	–	4[12]	2.8	–	2.48	2.48	0%

Lower calcareous shale member

Sample												%
BIX-3-3	[1]	–	61	10	3	26	–	9.4	–	2.05	2.36	13%

BLACK CANYON SECTION

Siliceous member

Sample												%
BLK-6B-4	c 67[10]	–	60	30	10	–	–	–	–	–	–	–
-6B-2	c 67[10]	–	52	36	12	–	–	7.1	–	1.91	2.40	20%
-7A-3	53[10]	–	63	28	9	–	–	–	–	–	–	–
-7A-13	50[10]	–	64	27	9	–	–	11.5	–	1.92	2.21	13%
-7A-12	50[10]	–	62	28	9	–	–	11.3	–	1.93	2.20	12%
-7A-11	50[10]	–	64	27	9	–	–	–	–	1.93	2.11	9%
-7A-14B	41[10]	–	84	12	4	–	–	–	–	–	–	–
-7A-14D	41[10]	–	84	12	4	–	–	–	–	–	–	–
-7A-15	41[10]	–	67	25	8	–	–	7.1	–	2.23	2.26	1%
-7A-9	40[10]	–	20	26	9	45	–	–	–	–	–	–
-7A-10A	39[10]	–	68	24	8	–	–	5.7	–	2.48	2.16	13%
-7A-10C	39[10]	–	71	22	7	–	–	–	–	2.30	2.32	1%

Transition member

Sample												%
BLK-5-2 (1)	[1]	–	44	15	5	31	5	6.5	–	2.07	2.49	17%
-5-2 (2)	[1]	–	–	–	5	–	–	–	–	2.07	2.49	17%

APPENDIX H

MICROFOSSIL AGE DETERMINATIONS

This appendix presents the microfossil data used to evaluate
lateral age correlations between lithologic members. Microfossil
identifications and age determinations were made by R. E. Arnal,
J. A. Barron, and R. Z. Poore, all of the U.S. Geological Survey,
Menlo Park, California, and by J. C. Ingle, Jr., of Stanford University,
Stanford, California. Benthonic foraminiferal zones determined by
R. E. Arnal and J. C. Ingle are based on Kleinpell (1938) and on
Pierce (1956), as summarized by Wornhardt (1972). Diatom zones
determined by J. A. Barron are based on Schrader (1973) as modified
by Barron (1976). Planktonic foraminiferal zones determined by
R. Z. Poore are those of Blow (1969) and calcareous nannofossil zones
are those of Bukry (1973).

General geographic and lithostratigraphic relationships between
microfossil samples are illustrated in figure H. In the following
list, samples are arranged geographically (by sections, from east to
west) and described in the numerical order shown in figure H. Data
presented for each sample include exact lithostratigraphic position
within the section, microfossils, age correlations, and the age
assignment used in figure 5.
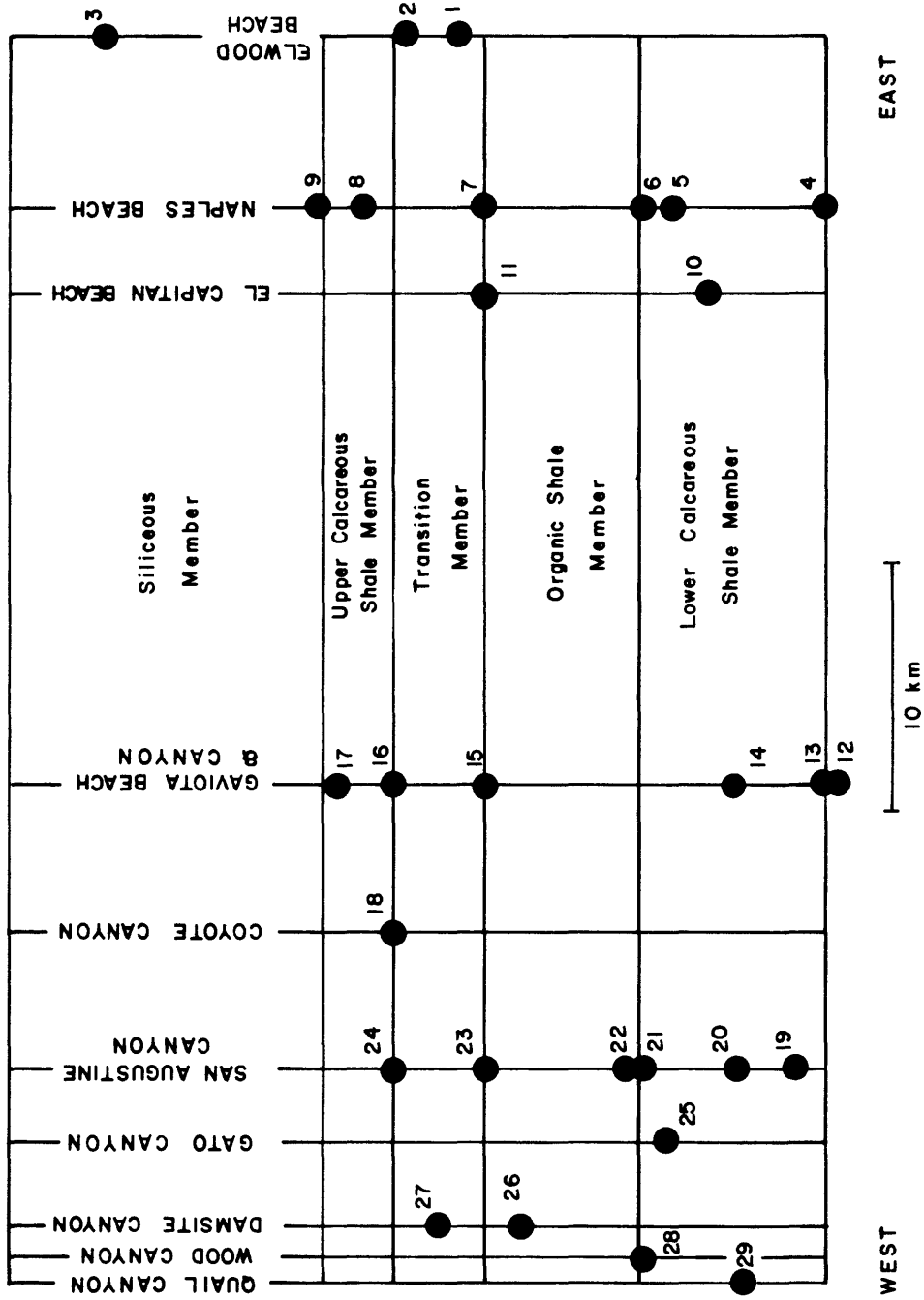
Fig. H—Lateral and lithostratigraphic position of samples used for microfossil age dating. Numerals indicate order of faunal lists in text.

Elwood Beach Section

1. ELW-1-6B

   Lithostratigraphic position: 12 m above the base of the transition member and 68 m below the top of the upper calcareous shale member

   Determinations by J. A. Barron:

   Diatoms include:
   ACTINOCYCLUS ingens Rattray
   ASTEROMPHALUS darwinii Ehrenberg
   DENTICULA hustedtii Simonsen & Kanaya
   DENTICULA hustedtii var.
   HEMIAULUS polymorphus Grunow
   ROUXIA californica Peragallo
   THALASSIONEMA hirosakiensis (Kanaya) Schrader

   Silicoflagellate:
   DISTEPHANUS pseudofibula (Schulz) Bukry

   Age: late Miocene; probably correlates with North Pacific Diatom Zone 13 or 14

   Age assigned in this report: early late Mohnian (probably)

2. ELW-1-22

   Lithostratigraphic position: 43 m below the top of the upper calcareous shale member and 37 m above the base of the transition member

   Determinations by J. A. Barron:

   Diatoms include:
   ACTINOCYCLUS ingens Rattray
   ACTINOPTYCHUS minutus Greville
   ASTEROMPHALUS darwinii Ehrenberg
   NITZSCHIA fossilis (Frenguelli) Kanaya
   ROUXIA californica Peragallo

   Silicoflagellate:
   DISTEPHANUS pseudofibula (Schulz) Bukry

   Age: late Miocene; correlates with North Pacific Diatom Zone 12.

   Age assigned in this report: middle late Mohnian

3. ELW-1-17

   Lithostratigraphic position: 18 m below top of siliceous member
   (which is 68 m thick here)

   Determinations by J. A. Barron:

   Diatoms include:
         ACTINOCYCLUS ingens Rattray
         COSCINODISCUS symbolophorus Grunow
         DENTICULA hustedtii Simonsen & Kanaya
         THALASSIOSIRA antiqua (Grunow) Cleve-Euler
         THALASSIOSIRA cf. *decipiens* (Grunow) Joergensen
         SYNEDRA jouseana Sheshukova-Poretzkaya

   Silicoflagellates:
         DISTEPHANUS speculum (Ehrenberg) Haeckel (long spined)
         DISTEPHANUS crux (Ehrenberg) Haeckel
         MESOCENA circulus (Ehrenberg)

   Age: late Miocene; correlates with North Pacific Diatom
         Zone 11; probably subzone b.

Age assigned in this report: late late Mohnian

Naples Beach Section

4. NAP-10-10

   Lithostratigraphic position: 3 m above base of lower calcareous
   shale member

   Determinations by R. Z. Poore:

   Planktonic foraminifera include:
         GLOBIGERINA praebulloides Blow
         GLOBIGERINA pseudociperoensis Blow
         GLOBOQUADRINA baroemoenensis Leroy
         GLOBOQUADRINA larmeui Akers
         GLOBOQUADRINA venezuelana (Hedberg)
         GLOBOROTALIA cf. *G. continuosa* Blow

   Nannofossils include:
         RETICULOFENESTRA sp.
         RETICULOFENESTRA pseudoumbilica (Gartner) Gartner?
         COCCOLITHUS pelagicus (Wallich) Schiller
       ***CHIASMOLITHUS* sp.
       ***SPHENOLITHUS* cf. *S. obtusus* Bukry
         SPHENOLITHUS heteromorphus Deflandre

SPHENOLITHUS neoabies Bukry & Bramlette
HELICOPONTOSPHAERA kamptneri Hay & Mohler
HELICOPONTOSPHAERA cf. *H. sellii* Bukry & Bramlette
DISCOASTER deflandrei Bramlette & Riedel
DISCOASTER variabilis Martini & Bramlette
DISCOASTER sp.

Age: youngest early Miocene-oldest middle Miocene; most
likely oldest middle Miocene

Comments: Planktonic foraminifera are fairly common but most
specimens are deformed (crushed). My preferred inter-
pretation is to assign this sample to the *SPHENOLITHUS
heteromorphus* Zone (nannoplankton) and thus by correla-
tion foraminifer Zone N9. The sample could, however,
be referable to the *HELICOPONTOSPHAERA ampliapertura*
Zone and be youngest early Miocene.

**reworked taxa

Determinations by R. E. Arnal:

Foraminifera include:
PLECTOFRONDICULARIA miocenica directa
EPISTOMINELLA subperuviana
SUGGRUNDA eckisi
BULIMINELLA curta
BOLIVINA advena
UVIGERINELLA obesa
VIRGULINA californiensis
ROBULUS aff. *simplex*
ROBULUS miocenicus
ROBULUS laimingi

Age: Miocene, late Saucesian or early Relizian

Age assigned in this report: late Saucesian or early Relizian

5. NAP-11-3

Lithostratigraphic position: 33 m below top of lower calcareous
shale member (which is approximately 239 m thick here)

Determinations by J. A. Barron:

Diatoms include:
ACTINOCYCLUS ingens Rattray (common)
DENTICULA lauta Bailey
DENTICULA hyalina of Akiba
SYNEDRA jouseana Sheshukova-Poretzkaya

Silicoflagellate:
     DISTEPHANUS crux (Ehrenberg) Haeckel

Age: early middle Miocene; probably correlates with North
     Pacific Diatom Zone 20-22.

Preservation: moderate

Age assigned in this report: Luisian

6. NAP-11-5

Lithostratigraphic position: at base of organic shale member

Determinations by R. Z. Poore:

Planktonic foraminifera: sample contains rare, nondiagnostic
     planktonic foraminifera

Nannofossils include:
     RETICULOFENESTRA sp.
     DISCOLITHINA sp.
     COCCOLITHUS pelagicus (Wallich) Schiller (s. ampl.)
     SPHENOLITHUS heteromorphus Deflandre
     SPHENOLITHUS neoabies Bukry & Bramlette
     SPHENOLITHUS abies Deflandre
     LITHOSTROMATION sp.
     HELICOPONTOSPHAERA kamptneri Hay & Mohler
     CYCLICARGOLITHUS floridanus (Roth & Hay) Bukry
     CYCLOCOCCOLITHUS macintyrei Bukry & Bramlette
     BRAARUDOSPHAERA bigelowi (Gran & Braarud) Deflandre
     DISCOASTER cf. *D. deflandrei* Bramlette & Riedel
     DISCOASTER variabilis Martini & Bramlette

Age: middle Miocene

Comments: Most likely *SPHENOLITHUS heteromorphus* Zone and
     thus oldest middle Miocene

Determinations by R. E. Arnal:

Foraminifera include:
     VALVULINERIA californica
     BOLIVINA advena striatella
     ANOMALINA salinasensis
     BOLIVINA californica Luisian variant
     EPONIDES keenani
     BOLIVINA dunlapi
     VALVULINERIA araucana?

Age: Miocene, Luisian, possibly late Luisian

Age assigned in this report: Luisian

7.   NAP-12-5

Lithostratigraphic position: at base of transition member

Determinations by J. A. Barron:

Diatoms include:
ACTINOCYCLUS ingens Rattray
DENTICULA hustedtii Simonsen & Kanaya
THALASSIOSIRA excentrica (Ehrenberg) Cleve?
THALASSIOSIRA lineata Jouse

Silicoflagellate:
DISTEPHANUS pseudofibula (Schulz) Bukry

Age: probably early half of late Miocene

Comments: poor preservation

Determinations by R. Z. Poore:

Planktonic foraminifera: none detected

Determinations by R. E. Arnal:

Foraminifera include:
FURKENSOINA californiensis grandis
BOLIVINA sinuata alisoensis (rare)
BULIMINELLA californica
BOLIVINA vaughani
BOLIVINA girardensis
CASSIDULINA barbarana
SUGGRUNDA eckisi
UVIGERINA subperegrina
BOLIVINA barbarana
BOLIVINA sinuata
BOLIVINA bramlettei
BOLIVINA decurtata
MELONIS goudkoffi
UVIGERINA rothwelli
BOLIVINA subadvena spissa

Age: Miocene, late Mohnian, base of BOLIVINA benedictensis
zone, near contact with top of BOLIVINA uvigerinaformis
zone

Age assigned in this report: earliest late Mohnian

8. NAP-13-6

    Lithostratigraphic position: 8 m below top of upper calcareous
    shale member and 48 m above base of transition member

    Determinations by J. A. Barron:

        Diatoms include:
            ACTINOCYCLUS ingens Rattray
            DENTICULA hustedtii Simonsen & Kanaya
            ROUXIA californica Peragallo
            THALASSIOSIRA antiqua (Grunow) Cleve-Euler

        Silicoflagellate:
            DISTEPHANUS pseudofibula (Schulz) Bukry

        Age: late Miocene (middle part); correlates with Barron's
               (1976) subzone a of North Pacific Diatom Zone 11

    Determinations by R. Z. Poore:

        Planktonic foraminifera: none detected

    Determinations by R. E. Arnal:

        Foraminifera include:
            UVIGERINA rothwelli
            BOLIVINA sinuata
            BOLIVINA granti
            BOLIVINA pseudospissa
            BOLIVINA barbarana
            BOLIVINA subadvena spissa

        Age: Miocene, late Mohnian, probably *BOLIVINA granti* zone

    Age assigned in this report: late late Mohnian

9. NAP-13-5

    Lithostratigraphic position: 1.5 m above base of siliceous
    member (which is 40 m thick here)

    Determinations by J. A. Barron:

        Diatoms include:
            ACTINOCYCLUS ingens Rattray
            ASTEROMPHALUS darwinii Ehrenberg
            DENTICULA hustedtii Simonsen & Kanaya
            THALASSIOSIRA antiqua (Grunow) Cleve-Euler
            THALASSIOSIRA lineata Jouse

Silicoflagellate:
  DISTEPHANUS pseudofibula (Schulz) Bukry

Age: late Miocene; correlates with subzone a of North Pacific
      Diatom Zone 11.

Age assigned in this report: late late Mohnian

El Capitan Section

10. CAP-6-6

Lithostratigraphic position: 70 m below top of lower calcareous
shale member (which is 200 m thick here)

Determinations by R. Z. Poore:

    Planktonic foraminifera include:
        GLOBIGERINOIDES quadrilobatus (d Orbigny) (s.l.)
        GLOBIGERINOIDES subquadratus Bronnimann
        GLOBIGERINA praebulloides Blow
        GLOBOROTALIA cf. *G. minutissima* Bolli

    Nannofossils include:
        RETICULOFENESTRA pseudoumbilica (Gartner) Gartner
        COCCOLITHUS pelagicus (Wallich) Schiller (s. ampl.)
        SPHENOLITHUS neoabies Bukry & Bramlette

    Age: middle Miocene

    Comments: Planktonic foraminifera and calcareous nannofossils
               are relatively rare. Sample probably correlative to
               foraminifer Zones N9-N13.

Determinations by R. E. Arnal:

    Foraminifera include:
        SIPHOGENERINA hughesi
        SIPHOGENERINA branneri
        BOLIVINA cuneiformis
        BOLIVINA salinasensis
        UVIGERINELLA californica
        BOLIVINA advena
        BAGGINA cancriformis
        BOLIVINA imbricata
        STILOSTOMELLA advena
        STILOSTOMELLA advena hughesi

    Age: Miocene, early Relizian, *SIPHOGENERINA hughesi* zone

Age assigned in this report: early Relizian

11. CAP-2-7

Lithostratigraphic position: at top of organic shale member

Determinations by R. Z. Poore:

Planktonic foraminifera: none detected

Determinations by R. E. Arnal:

Foraminifera include:
UVIGERINA hootsi
UVIGERINA subperegrina
DENTALINA cf. filiformis
BOLIVINA girardensis?
CASSIDULINA modeloensis
BULIMINA uvigerinaformis

Age: Miocene, early Mohnian, BULIMINA uvigerinaformis zone,
close to contact with overlying BOLIVINA hughesi zone

Age assigned in this report: latest early Mohnian

Gaviota Beach and Canyon Section

12. GAV-17-1

Lithostratigraphic position: 6 m below base of lower calcareous
shale member

Determinations by R. Z. Poore:

Planktonic foraminifera include:
GLOBIGERINA praebulloides Blow
GLOBIGERINA pseudociperoensis Blow
GLOBIGERINA angustiumbilicata Bolli
GLOBOQUADRINA venezuelana (Hedberg)

Nannofossils include:
RETICULOFENESTRA sp.
RETICULOFENESTRA pseudoumbilica (Gartner) Gartner
COCCOLITHUS pelagicus (Wallich) Schiller (s. ampl.)
CYCLICARGOLITHUS floridanus (Roth & Hay) Bukry
HELICOPONTOSPHAERA kamptneri Hay & Mohler
SPHENOLITHUS sp.
DISCOASTER sp. (spp.)

Age: probably oldest middle Miocene

Comments: Planktonic foraminifera and calcareous nannofossils
are fairly common, but poorly preserved.

Determinations by R. E. Arnal:

Foraminifera include:
SIPHOGENERINA transversa
SIPHOGENERINA kleinpelli
VALVULINERIA williami
BOLIVINA advena
BULIMINELLA curta
PLECTOFRONDICULARIA miocenica directa
GLOBIGERINA quadrilatera
BOLIVINA marginata

Age: Miocene, late Saucesian, *UVIGERINELLA obesa* zone

Age assigned in this report: late Saucesian

13. GAV-17-2

Lithostratigraphic position: at base of lower calcareous shale
member

Determinations by R. Z. Poore:

Planktonic foraminifera include:
GLOBIGERINA praebulloides Blow
GLOBIGERINA angustiumbilicata Bolli
GLOBOROTALIA continuosa Blow

Age: middle to late Miocene

Comments: Planktonic foraminifera are rare and poorly preserved.

Determinations by R. E. Arnal:

Foraminifera include:
VALVULINERIA depressa
MELONIS costiferum
BOLIVINA imbricata
BULIMINELLA curta
BOLIVINA advena
BULIMINELLA subfusiformis

Age: Miocene, Relizian or early Luisian

Determinations by J. C. Ingle:

    Foraminifera include:
        SIPHOGENERINA transversa
        VALVULINERIA depressa

    Age: Miocene, uppermost Saucesian

Age assigned in this report: Saucesian-Relizian boundary

14.   GAV-10-8

    Lithostratigraphic position: about 68 m above base of lower
    calcareous shale member (estimated to be 138 m thick)

    Determinations by J. C. Ingle:

        Foraminifera include:
            VALVULINERIA depressa
            ANOMALINA salinasensis
            SIPHOGENERINA branneri

        Age: Miocene, late Relizian

    Age assigned in this report: late Relizian

15.   GAV-13B-21

    Lithostratigraphic position: at base of transition member

    Determinations by R. Z. Poore:

        Planktonic foraminifera: none detected

    Determinations by R. E. Arnal:

        Foraminifera include:
            BULIMINELLA brevior
            BOLIVINA sinuata alisoensis
            BOLIVINA barbarana
            VIRGULINA californiensis grandis
            EPISTOMINELLA (flat of the Mohnian)
            EPISTOMINELLA capitanensis

        Age: Miocene, early Mohnian, *BULIMINA uvigerinaformis* zone

    Age assigned in this report: mid-late early Mohnian

16. GAV-13B-20

Lithostratigraphic position: at base of upper calcareous shale member

Determinations by R. Z. Poore:

Planktonic foraminifera: rare and poorly preserved

Nannofossils include:
COCCOLITHUS pelagicus (Wallich) Schiller (s. ampl.)
CYCLOCOCCOLITHUS macintyrei Bukry & Bramlette
RETICULOFENESTRA pseudoumbilica (Gartner) Gartner
SPHENOLITHUS neoabies Bukry & Bramlette
DISCOASTER broweri Tan Sin Hok (s. ampl.)
DISCOASTER cf. *D. exilis* Martini & Bramlette
DISCOASTER intercalaris Bukry?
DISCOASTER variabilis Martini & Bramlette
LITHOSTROMATION perdurum Deflandre?

Age: middle to late Miocene, most likely middle

Comments: Discoasters are poorly preserved; however, presence of forms close to *D. exilis* and lack of five-rayed forms suggest middle Miocene.

Determinations by R. E. Arnal:

Foraminifera include:
UVIGERINA subperegrina
BOLIVINA sinuata alisoensis
BULIMINELLA subfusiformis
BOLIVINA hughesi parva
BOLIVINA decurtata
UVIGERINA carmeloensis
PULLENIA moorei
UVIGERINA segundoensis

Age: Miocene, early Mohnian, *BULIMINA uvigerinaformis* zone

Age assigned in this report: mid-late early Mohnian

17. GAV-12-4

Lithostratigraphic position: near (within 5 m below) top of upper calcareous shale member (which is 31 m thick here)

Determinations by R. Z. Poore:

Planktonic foraminifera: none detected

Determinations by R. E. Arnal:

Foraminifera include:
      BATHYSIPHON sp.
      CYCLAMMINA or *HAPLOPHRAGMOIDES* sp.
      UVIGERINA subperegrina

Age: Miocene, Mohnian (questionable)

Determinations by J. C. Ingle:

Foraminifera include:
      BOLIVINA sinuata

Age: Miocene, mid-Mohnian

Age assigned in this report: late Mohnian or younger

Coyote Canyon Section

18. COY-3-6

Lithostratigraphic position: at base of upper calcareous shale member

Determinations by R. Z. Poore:

Planktonic foraminifera: none detected

Nannofossils include:
      RETICULOFENESTRA pseudoumbilica (Gartner) Gartner
      COCCOLITHUS pelagicus (Wallich) Schiller (s. ampl.)
      CYCLOCOCCOLITHUS macintyrei Bukry & Bramlette
      SPHENOLITHUS neoabies Bukry & Bramlette
      DISCOLITHINA sp.
      DISCOASTER asymmetricus Gartner
      DISCOASTER brouweri Tan Sin Hok
      DISCOASTER challengeri Bramlette & Riedel
      DISCOASTER interclaris Bukry
      DISCOASTER loeblichii Bukry
      DISCOASTER variabilis Martini & Bramlette

Age: late Miocene

Determinations by R. E. Arnal:

Foraminifera include:
      UVIGERINA hootsi
      DISCORBINELLA valmonteensis
      GYROIDINA multicamerata
      UVIGERINA hannai
      BULIMINA ovata

BOLIVINA barbarana
BOLIVINA girardensis
BOLIVINA parva
BOLIVINA decurtata

Age: Miocene, late Mohnian, *BOLIVINA granti* zone

Age assigned in this report: late late Mohnian

San Augustine Canyon Section

19. AUG-4B-1

Lithostratigraphic position: 18 m above inferred base of lower
calcareous shale member (which is 97 m thick here)

Determinations by R. Z. Poore:

>   Planktonic foraminifera include:
>   *GLOBIGERINA praebulloides* Blow (s.l.)
>   *GLOBIGERINA* cf. *G. euapertura* Jenkins
>   *GLOBIGERINA* cf. *G. pseudociperoensis* Blow
>   *GLOBOQUADRINA* sp.
>   *TURBOROTALITA quinqueloba* (Natland)
>   *GLOBOROTALIA continuosa* Blow
>   *GLOBOROTALIA praescitula* Blow
>   *GLOBOROTALIA* cf. *G. obesa* Bolli
>   *GLOBOTORALOIDES suteri* Bolli

Nannofossils include:
        RETICULOFENESTRA sp.
        SPHENOLITHUS sp.
        COCCOLITHUS pelagicus (Wallich) Schiller (s. ampl.)

Age: early Miocene

Comments: Planktonic foraminifera and calcareous nannofossils
           are poorly preserved. Foraminiferal assemblage suggests
           correlation with Zones 6-9 and thus most likely early
           Miocene.

Determinations by R. E. Arnal:

Foraminifera include:
        SIPHOGENERINA hughesi
        SIPHOGENERINA branneri
        BAGGINA cancriformis
        STILOSTOMELLA advena hughesi
        GLOBIGERINA pseudobulloides
        BOLIVINA imbricata
        BOLIVINA salinasensis
        FURKENSOINA californiensis

Age: Miocene, early Relizian, *SIPHOGENERINA hughesi* zone

Age assigned in this report: early Relizian

20. AUG-4C-17

Lithostratigraphic position: 46 m below top of lower calcareous shale member (which is 97 m thick here)

Determinations by J. C. Ingle:

No faunal list submitted.

Age: Miocene, late Relizian

Age assigned in this report: late Relizian

21. AUG-5B-10

Lithostratigraphic position: at top of lower calcareous shale member

Determinations by R. Z. Poore:

Planktonic foraminifera include:
GLOBIGERINA angustiumbilicata Bolli
GLOBIGERINA praebulloides Blow
GLOBIGERINA woodi connecta Jenkins?
GLOBIGERINITA uvula (Ehrenberg)

Nannofossils include:
HELICOPONTOSPHAERA kamptneri Hay & Mohler
RETICULOFENESTRA sp.
COCCOLITHUS pelagicus (Wallich) Schiller (s. ampl.)
DISCOLITHINA sp.

Age: early to middle Miocene

Comments: Planktonic foraminifera and calcareous nannofossils are poorly preserved.

Determinations by R. E. Arnal:

Foraminifera include:
BAGGINA robusta globosa
SIPHOGENERINA reedi
VALVULINERIA californica robusta
SARACENARIA beali
ANOMALINA salinasensis

BOLIVINA advena
PULLENIA miocenica
UVIGERINELLA californica
BULIMINELLA californica
VALVULINERIA ornata
STILOSTOMELLA advena

Age: Miocene, early Luisian, *SIPHOGENERINA reedi* zone

Age assigned in this report: early Luisian

22. AUG-5C-6

Lithostratigraphic position: 2 m above base of organic shale member (which is 79 m thick here)

Determinations by J. C. Ingle:

No faunal list submitted.

Age: Miocene, early Luisian

Age assigned in this report: early Luisian

23. AUG-6C-13

Lithostratigraphic position: at top of organic shale member

Determinations by R. Z. Poore:

Planktonic foraminifera: very rare and poorly preserved

Determinations by R. E. Arnal:

Foraminifera include:
BULIMINA uvigerinaformis
BOLIVINA sinuata alisoensis
UVIGERINA hootsi
UVIGERINA foxenensis
UVIGERINA subperegrina
BULIMINELLA brevior
BOLIVINA californica
EPISTOMINELLA capitanensis
EPISTOMINELLA (flat of the Mohnian)
BOLIVINA cf. *minuta*
STILOSTOMELLA advena
BOLIVINA interjuncta
BOLIVINA barbarana
BOLIVINA pseudospissa

BOLIVINA decurtata
BOLIVINA hughesi

Age: Miocene, early Mohnian, *BULIMINA uvigerinaformis* zone

Age assigned in this report: mid-late early Mohnian

24. AUG-6B-17

Lithostratigraphic position: at top of transition member

Determinations by R. Z. Poore:

Planktonic foraminifera: very rare and poorly preserved

Nannofossils include:
RETICULOFENESTRA pseudoumbilica (Gartner) Gartner
CYCLOCOCCOLITHUS macintyrei Bukry & Bramlette
COCCOLITHUS pelagicus (Wallich) Schiller (s. ampl.)

Age: middle Miocene or younger

Comments: Calcareous nannofossils are poorly preserved.

Determinations by R. E. Arnal:

Foraminifera include:
BOLIVINA barbara
BOLIVINA pseudospissa
BOLIVINA girardensis
UVIGERINA subperegrina
DISCORBINELLA valmonteensis
BOLIVINA interjuncta
BULIMINA ovata

Age: Miocene, late Mohnian, *BOLIVINA benedictensis* zone

Age assigned in this report: early late Mohnian

Gato Canyon Section

25. GAT-4-3

Lithostratigraphic position: 96 m above inferred base of lower calcareous shale member and near top of this member (probably about 10 m below top)

Determinations by R. Z. Poore:

Planktonic foraminifera include:
GLOBIGERINA praebulloides Blow (s.1.)
GLOBIGERINA cf. *G. euapertura* Jenkins
GLOBOQUADRINA sp.
TURBOROTALITA sp.
GLOBOROTALIA minutissima Bolli
GLOBIGERINOIDES subquadratus Bronnimann

Nannofossils include:
COCCOLITHUS pelagicus (Wallich) Schiller (s. ampl.)
SPHENOLITHUS cf. *S. moriformis* (Bronnimann & Stradner)
    Bramlette & Wikoxon
SPHENOLITHUS neoabies Bukry & Bramlette?

Age: early to middle Miocene

Comments: Planktonic foraminifera are common but poorly
        preserved. Calcareous nannofossils are also poorly
        preserved. Foraminiferal Zones N6-N13.

Determinations by R. E. Arnal:

Foraminifera include:
BOLIVINA advena ornata
BOLIVINA advena striatella
BAGGINA robusta globosa
VALVULINERIA californica appressa
ANOMALINA salinasensis
PULLENIA miocenica
SIPHOGENERINA reedi
SIPHOGENERINA branneri
SIPHOGENERINA kleinpelli
BOLIVINA californica (Luisian variant)
BOLIVINA advena striatella
VALVULINERIA californica obesa
BOLIVINA salinasensis
GLOBIGERINA pseudobulloides
BULIMINELLA curta
VALVULINERIA depressa

Age: Miocene, early Luisian, *SIPHOGENERINA reedi* zone

Age assigned in this report: early Luisian

Damsite Canyon Section

26. DAM-6B-6

Lithostratigraphic position: in organic shale member (estimated
to be 23 m below top of this member, which is estimated to be
67 m thick here)

Determinations by R. Z. Poore:

    Planktonic foraminifera: sample contains very few, crushed, nondiagnostic planktonic foraminifera

Determinations by R. E. Arnal:

    Foraminifera include:
        BOLIVINA californica
        BOLIVINA advena
        BOLIVINA advena striatella
        VALVULINERIA californica obesa
        ANOMALINA salinasensis
        ROBULUS smileyi
        SARACENARIA beali
        BAGGINA robusta
        CASSIDULINA williami
        BOLIVINA californica (Luisian variant)

    Age: Miocene, probably Luisian, possibly upper Relizian

Age assigned in this report: Luisian (probably)

27. DAM-7A-5

Lithostratigraphic position: 25 m below top of transition member (estimated to be 41 m thick here)

Determinations by R. Z. Poore:

    Planktonic foraminifera: none detected

Determinations by R. E. Arnal:

    Foraminifera include:
        BOLIVINA pseudospissa
        BULIMINA uvigerinaformis
        BOLIVINA decurtata
        BOLIVINA barbarana
        UVIGERINA hootsi
        BOLIVINA woodringi
        FURKENSOINA californiensis
        BOLIVINA woodringi
        EPISTOMINELLA subperuviana
        BULIMINA ovata

    Age: Miocene, early Mohnian, *BULIMINA uvigerinaformis* zone

Age assigned in this report: mid-late early Mohnian

Wood Canyon Section

28. WOOD-4-3

Lithostratigraphic position: at base of organic shale member

Determinations by R. Z. Poore:

Planktonic foraminifera: sample contains very few, poorly
preserved, nondiagnostic planktonic foraminifera

Determinations by R. E. Arnal:

Foraminifera include:
BOLIVINA salinasensis
NODOSARIA longiscata
UVIGERINELLA californica perparva
UVIGERINELLA californica
VALVULINERIA depressa
VALVULINERIA californica appressa
PULLENIA miocenica
BAGGINA californica
VALVULINERIA miocenica
UVIGERINELLA nudocostata

Age: Miocene, Luisian

Age assigned in this report: Luisian

Quail Canyon Section

29. BIX-3-4

Lithostratigraphic position: 15 m above base of lower calcareous
shale member (estimated to be 40 m thick here)

Determinations by R. Z. Poore:

Planktonic foraminifera include:
GLOBIGERINA pseudociperoensis Blow
GLOBIGERINA praebulloides Blow (s.l.)
GLOBIGERINA cf. *G. angustiumbilicata* Bolli
GLOBOQUADRINA cf. *G. baroemoenensis* Leroy
GLOBIGERINOIDES quadrilobatus (d Orbigny) (s.l.)
GLOBIGERINOIDES sicanus de Stefani?
GLOBOROTALIA praescitula Blow
GLOBOROTALIA peripheroronda Blow & Banner
TURBOROTALITA sp.

Nannofossils include:
HELICOPONTOSPHAERA kamptneri Hay & Mohler
COCCOLITHUS pelagicus (Wallich) Schiller (s. ampl.)
RETICULOFENESTRA sp.
DISCOLITHINA sp.
CYCLICARGOLITHUS floridanus (Roth & Hay) Bukry
SPHENOLITHUS heteromorphus Deflandre
SPHENOLITHUS spp.
DISCOASTER deflandrei Bramlette & Riedel

Age: early to middle Miocene, most likely early

Comments: Planktonic foraminifera are common, but most
specimens are deformed (crushed). My preferred inter-
pretation is to assign this sample to foraminiferal
Zone N8 and the *HELICOPONTOSPHAERA ampliapertura* Zone
(nannofossil) and thus consider it as youngest early
Miocene. It is possible, however, that the sample repre-
sents oldest middle Miocene.

Determinations by R. E. Arnal:

Foraminifera include:
ANOMALINA salinasensis
BAGGINA cancriformis
BOLIVINA advena striatella
VALVULINERIA depressa
VALVULINERIA ornata
UVIGERINELLA californica
BOLIVINA californica
VALVULINERIA californica appressa
MELONIS pizarrensis
VALVULINERIA californica obesa
UVIGERINELLA nudocostata
BAGGINA californica robusta
BOLIVINA californica (Luisian variant)

Age: Miocene, lowermost Luisian, *SIPHOGENERINA reedi* zone

Age assigned in this report: lowermost Luisian